学位論文

金野 幸吉

目次

1. 主論文

   General Relativistic Approach to Electromagnetic Fields and Deformation of Magnetized Stars
   (磁場を持つ星の電磁場と変形に対しての一般相対論的な解析)
   金野 幸吉

2. 公表論文

   (1) Deformation of Relativistic Magnetized Stars
   Kohkichi Konno, Tomohiro Obata, Yasufumi Kojima
   Astronomy and Astrophysics, **352**(1999) 211-216

   (2) Flattening Modulus of A Neutron Star by Rotation and Magnetic Field
   Kohkichi Konno, Tomohiro Obata, Yasufumi Kojima
   Astronomy and Astrophysics, **356**(2000) 234-237

   (3) General Relativistic Modification of a Pulsar Electromagnetic Field
   Kohkichi Konno, Yasufumi Kojima
   Progress of Theoretical Physics, **104**(2000) 1117-1127

3. 参考論文

   (1) General Relativistic Effects of Gravity in Quantum Mechanics
   — A Case of Ultra-Relativistic, Spin 1/2 Particles —
   Kohkichi Konno, Masumi Kasai
   Progress of Theoretical Physics, **100**(1998) 1145-1157

   (2) Asymmetry in Microlensing-Induced Light Curves
   Kohkichi Konno, Yasufumi Kojima
   Progress of Theoretical Physics, **101**(1999) 885-901

主論文

GENERAL RELATIVISTIC APPROACH TO ELECTROMAGNETIC FIELDS AND DEFORMATION OF MAGNETIZED STARS

By

Kohkichi Konno

A Dissertation Submitted in
Partial Fulfillment of the
Requirements for the Degree of

Doctor of Science

in
Physics

at

Hiroshima University
January, 2001

GENERAL RELATIVISTIC APPROACH TO ELECTROMAGNETIC FIELDS AND DEFORMATION OF MAGNETIZED STARS

By

Kohkichi Konno

Hiroshima University, January, 2001

Under the Supervision of Professor Yasufumi Kojima

Abstract

Recent observations suggest that soft-gamma repeaters and anomalous X-ray pulsars belong to new classes of neutron stars with very strong magnetic fields. Associated with this discovery, there is growing interest in the subjects concerning ultra-magnetized neutron stars, i.e. magnetars. Motivated by the recent observational situation, we study the equilibrium configurations of magnetized stars in the context of general relativity. For this purpose, we first investigate stellar electromagnetic fields in a general relativistic framework. Next, we consider the stellar deformation induced by magnetic stress. In particular, based on the perturbation method, we formulate the magnetic deformation of a star endowed with a dipole magnetic field. We further estimate ellipticity for several stellar models. We find the general relativistic modifications of field strength and ellipticity, which are characterized by factors.

Acknowledgments

It is my great pleasure to thank my supervisor Yasufumi Kojima for many useful discussions and enlightening suggestions. He led me to a field in physics of neutron stars. I believe that if there were not his support, I could not accomplish this work. I also express my gratitude to Masumi Kasai for his invaluable instruction and continuous encouragement. He was my previous supervisor when I belonged to Department of Physics at Hirosaki University. I learned many things about physics under him. I would also like to thank Hideki Asada for many stimulating comments and conversations, and Toshifumi Futamase for continuous encouragement. I greatly benefited from a seminar with T. Futamase when I was an undergraduate at Hirosaki University.

I am indebted to Masayasu Hosonuma for giving me a numerical code for relativistic rotating stars and many fruitful discussions, which were very helpful particularly at the early stage of this work. I also wish to thank Tomohiro Obata for useful discussions. A large part of this work was done in collaboration with him.

I am grateful to all the people of Astrophysics Group and Theoretical Particle Physics Group at Hiroshima University. I wish to express my thanks to Kazuhiro Yamamoto, Hiroyuki Kawamura, Masaaki Morita, Jun Ogura, Michihiro Hori, Hiroaki Nishioka, Tsukasa Murata, Hironori Miguchi and Taku Shirai for conversations on various topics from physics to non-scientific issues. I also appreciate the assistance of the office workers belonging to Department of Physics at Hiroshima University, especially Hideko Masuda and Yuko Tsutsui.

I would like to thank Japan Society for the Promotion of Science (JSPS) for financial support during the third year of the doctor course at Hiroshima University.

Finally, I am very grateful to my parents for their continuous support and encouragement.

Contents

List of Figures

List of Tables

Chapter 1

Introduction

1.1 Brief history of neutron stars

The possibility of the existence of neutron stars was postulated soon after the discovery of the neutrons by Chadwick in 1932. In 1934, Baade and Zwicky proposed the idea of neutron stars. Linking supernovae with the collapse of ordinary stars to neutron stars tentatively, they suggested that there is a bound state with very higher density and smaller radius than ordinary stars. The first theoretical models for neutron stars were developed by Oppenheimer and Volkoff [1] in 1939. In these models, an ideal gas of free neutrons was assumed as the ingredients of neutron stars. However, they did not become the focus of attention of physicists and astronomers. This is because the thermal radiation from neutron stars would be too faint to observe owing to astronomical distances.

This situation among physicists and astronomers was dramatically changed by the accidental observational discovery of pulsars by Hewish and Bell [2] in 1967. Pulsars are objects emitting pulses of radiation at short and remarkably regular intervals. Their pulse periods range from milliseconds to several seconds. The most famous pulsar is the Crab Pulsar, which is at the heart of the Crab Nebula. According to Chinese historical records, this remnant of a supernova occurred in 1054 AD. This pulsar has a period of 33ms and is steadily slowing down.

The observed period of pulsars supported the fact that they can be identified with neutron stars. The principal argument to identify pulsars with neutron stars can be understood by considering the characteristic periods of oscillation and rotation of a star. First, we consider the probability of stellar oscillation as the origin of pulses. The characteristic period of oscillation is proportional to $(G\overline{\rho})^{-1/2}$, i.e. $t \sim (G\overline{\rho})^{-1/2}$, where $\overline{\rho}$ is the average density. Hence, in the case of white dwarfs with $M \sim M_\odot$ and $R \sim 10^4$km, we derive $t_{\rm WD}^{\rm (Oscillation)} \sim 100$s. On the other hand, we have $t_{\rm NS}^{\rm (Oscillation)} \sim 1$ms in the case of neutron stars with $M \sim M_\odot$ and $R \sim 10$km. Therefore, the oscillation models of white dwarfs cannot explain the shorter periods of pulsars, while those of neutron stars cannot produce the somewhat longer periods. Next, we discuss the possibility of rotation. In this case, we have to bear in mind that matter will be thrown off the star if the rotational velocity is very quick. From this consideration, we can derive the maximum angular velocity, which is usually called the Keplarian angular velocity $\Omega_{\rm K}$. The maximum value can be derived by equating the gravitational attraction to the centrifugal force at the stellar surface. The result is given by $\Omega_{\rm K} = (GM/R^3)^{1/2}$ or $t_{\rm min} = 2\pi(R^3/(GM))^{1/2}$. Hence, we derive $t_{\rm min\ WD} \sim 10$s for white dwarfs and $t_{\rm min\ NS} \sim 1$ms for neutron stars. Therefore, pulsars such as the Crab Pulsar can be explained only by a rotating neutron star. We note that the possibility of rapid rotation is a direct consequence of the high density of neutron stars.

Many theoretical studies have been done with intense vigor since the discovery of neutron stars. This circumstance about theoretical works was further enhanced by the discovery of pulsating, compact X-ray sources by the Uhuru satellite [3–5] in 1971. It seems that these are neutron stars in close binary systems, and X-ray is emitted from the accreting gas from their normal companion stars. The latter consequence can be extrapolated by the fact that their X-ray luminosity was much larger than that of the so-called rotation-powered pulsars like the Crab Pulsar. Furthermore, the fact that they showed a long-term overall spin-up behavior strongly supports the evidence of accretion.

In recent years, various aspects of neutron stars have been disclosed with the growing number of pulsars, including new types of these objects, which are mentioned later.

1.2 Physics of neutron stars

The subjects concerning neutron stars involve a wide range of physics. This would be seen by considering various features of neutron stars actually. In order to show this point clearly, we now review some aspects of neutron stars concretely (see also Refs. [6–8]).

First, let us review the formation and structure of neutron stars. A star with a very large mass $\gtrsim 10M_\odot$ is expected to evolve through all the stages of nuclear burning. After any available nuclear energy is exhausted, the gravitational contraction of the central core occurs. Initially, this contraction can be controlled by the pressure of degenerate electron gas in the core. However, associated with the creation of more iron in the surrounding shell, the core can no longer be supported by the degenerate pressure. In this contraction, two energy absorbing processes, the photo-disintegration of atomic nuclei and the capture of electrons via inverse beta decay, are further added and ultimately lead to an uncontrolled collapse. In the former, kinetic energy is used to unbind atomic nuclei, and in the latter the kinetic energy of degenerate electrons is converted into the kinetic energy of electron neutrinos which escape from the core. The time-scale of the collapse of the core is given by the free-fall time $t_{\rm FF} \sim (G\rho)^{-1/2}$. At a density of $\rho \sim 10^9$g cm^{-3}, we derive $t_{\rm FF} \sim$ 1ms. Therefore, the collapse is very rapid. Associated with the free fall, a large amount of gravitational energy is liberated within this time-scale. The collapse of the core is not opposed until a density comparable to the density of nuclear matter is reached. After the nuclear density is reached, the core is expected to resist compression due to nuclear forces and rebound falling matter. This produce an explosion called a supernova.

A neutron star can be left behind after the supernova explosion. In fact, it is believed that neutron stars are created in a significant fraction of supernova explosions. A newly-born neutron star initially has a temperature between 10^{11} to 10^{12}K. However, it rapidly cools due to neutrino emission and reaches a temperature of the order of 10^9K in a day. Its temperature further comes down to 10^8K in many years. Although these temperatures are very high compared with the solar standards, they are low if we consider the standards set by the high densities inside a neutron star. This is also stated that the temperature inside a neutron star is lower than the Fermi temperature. Namely, electrons, protons and above all neutrons are degenerate inside a neutron star. Therefore, some state variable, e.g., pressure depends on only one variable, e.g., density inside a neutron star, since the temperature can be regarded as zero.

Owing to the electron capture during the collapse, the core is made of neutron-rich nuclei. When the density exceeds 4×10^{11}g cm^{-3}, a new phenomenon occurs in such a core, that is, neutrons drip from neutron-rich nuclei. This phenomenon is called neutron drip. At high densities, since the normal beta-decay mode $n \longrightarrow p + e^- + \overline{\nu}_e$ is blocked by the Pauli exclusion principle, neutrons can survive in a neutron star without decaying. Hence, neutrons are the dominant constituent of neutron stars. At higher densities around 10^{15}g cm^{-3}, the core further becomes energetically possible to produce pions, muons and hyperons. At higher densities still, it seems that quarks come into play. In order to understand the structure of neutron stars, we have to know the equations of state (EOS) of neutron stars. Therefore, we need the knowledge of nuclear physics and high-energy particle physics.

A neutron star is also a luminous source with a very wide range of radiation from the radio to the γ-ray range. Hence, as another aspect of neutron stars, we now consider the radiation from them. There are two important energy sources which can produce radiation. One is the rotational energy of a star in the presence of a strong magnetic field. When a magnetized star rotates, an electric field, whose strength is proportional to the rotational velocity, is induced. This electric field acts on the surface electrons and protons of a neutron star. Since the electric force can become much larger than the gravitational force at the surface, the electric charges would eventually be ripped off the surface. Thus, the magnetosphere filled with a plasma is built [9]. The electric field also contributes the acceleration of charged particles which are seeds of radiation. The accelerated particles move along the curved magnetic field lines and therefore emit curvature radiation photons. These emitted photons may be subject to magnetic pair production in the strong field. The repetition of these processes leads to a cascade, which would produce some part of radiation. The other source is the gravitational potential energy of matter that is captured by the star and accreted onto its surface. Accreting X-ray pulsars are classified into this type. If a neutron star is in a binary system, then such matter is available enough. In this case, some large part of the energy is converted into heat and subsequently into radiation.

Furthermore, neutron stars can become gravitational radiation sources. We can consider coalescing binary neutron stars and oscillating neutron stars to be the plausible sources of gravitational waves. The signals from them may be detected by the new generation of gravitational-wave interferometers (LIGO, VIRGO, GEO600 and TAMA300). Therefore, at present, gravitational waves are investigated by many astrophysicists with intense vigor, in relation with the detection.

As seen above, the subjects about neutron stars include various fields in modern physics. This situation would further be excited by the appearance of new classes of neutron stars called soft-gamma repeaters (SGRs) and anomalous X-ray pulsars (AXPs). These objects are mentioned in the next section.

1.3 New classes of neutron stars

The steady spin-down of most pulsars is explained by the magnetic dipole radiation from the rotating, magnetized stars. Indeed, the analysis of the Crab Pulsar based on dipole radiation is almost consistent with the Chinese historical records. This success gives strong evidence that pulsars have magnetic fields, especially dipole magnetic fields. The magnetic field strength can be determined by the period and period derivative of a pulsars. From the measurements of these quantities, we know that neutron stars have strong magnetic field within a range 10^8-10^{13}G. However, very recently, the new classes of objects such as SGRs and AXPs appeared with great surprise. This is because the observations of periods indicated that these objects are the neutron stars with very strong magnetic fields within a range 10^{14}-10^{15}G (see Ref. [10] for the effect of a pulsar wind on the spin-down). Therefore, these seems to be *magnetars* [11–17]. This terminology is used for the star whose magnetic energy is dominant over the rotational energy, or the star whose radiation energy is mainly supplied by the magnetic energy. The discovery of the strong magnetic fields in excess of $B_{\rm cr} \sim 10^{13}$G raised the upper limit of a pulsar magnetic field by a factor of 10^2. In such a strong magnetic field, quantum electrodynamics with external fields should be taken into account seriously. Hence, elementary processes in these strong fields would have quite different features from those in ordinary circumstances (see Ref. [18] for detail discussion). Thus, these new objects may promote a new branch concerning neutron stars at the beginning of this twenty-first century. We now give a brief review of the observations of SGRs and AXPs (see also Ref. [19]).

1.3.1 Soft-gamma repeaters

Some of SGRs have already be known since twenty years ago. However, it is very recently that the various features of these objects are revealed.

SGRs are transient sources of high-energy photons. They emit sporadic and short bursts of soft γ-rays during periods of activity. The time scale of the bursts is typically ~ 0.1s, and the luminosity is characterized by 10^{39}-10^{41}erg s^{-1}. It is very interesting that these recurrent bursts and earthquakes share four distinctive statistical properties: power-law energy distributions, log-symmetric waiting time distributions, strong positive correlations between waiting times of successive events, and weak or no correlations between intensities and waiting times [20]. This fact suggests that SGR events are induced by star-quakes. Therefore, crust-quakes due to magnetic stress [15] seem to be a plausible explanation for the bursts.

SGRs are also persistent X-ray sources of luminosity 10^{35}-10^{36}erg s^{-1}. In addition, the periodicity for some SGRs and the association with supernova remnants were reported. These would give evidence that SGRs are neutron stars. There are so far four known SGRs, SGR 0525–66 [21–29], SGR 1900+14 [30–54], SGR 1806–20 [32, 55–70], SGR 1627–41 [71–76], and one possible candidate SGR 1801–23 [77]. In the following, we briefly review each object.

SGR 0525–66

SGR 0525–66 was discovered by a giant burst on March 5, 1979 [21–24]. The time profile of the burst consists of an initial, narrow structure-less pulse and a pulsating tail part. Associated with the discovery of this burst, the periodicity of 8.1s was found in the pulsating stage [21,22]. Furthermore, the association with the supernova remnant N49 in the Large Magellanic Cloud

(LMC) was suggested [21, 22, 25, 26]. If it is true, the luminosity of isotropic radiation in the initial impulse would be $\sim 5 \times 10^{44}$erg s^{-1}, and that at the pulsating stage would be $\sim 3.6 \times 10^{42}$erg s^{-1} [22]. After the giant burst and subsequent weak recurrent bursts, some weak bursts were observed in 1981 and 1982 [27]. In recent years, X-ray observations of SGR 0525–66 were done, which gave a X-ray luminosity of 10^{36}erg s^{-1} [28]. However, some observations showed the negative conclusion that there is no evidence for the association with the supernova remnant N49 in the LMC [29].

SGR 1900+14

SGR 1900+14 was discovered by three bursts on March 24, 25 and 26, 1979 [30]. However, this object had been quiet for thirteen years since these bursts. In 1992, some weak recurrent bursts were detected [31]. Recently, after the detection of one quiescent X-ray source [33, 38, 39], the clear periodicity of 5.16s [33, 39, 40] and the period derivative of 1.1×10^{-10}s s^{-1} [40] were founded from this source. These leads to the magnetic field strength for magnetars. The luminosity of X-ray emission are within a range 10^{35}-10^{36}erg s^{-1} [40]. The association with the supernova remnant G42.8+0.6 in our galaxy was also suggested [33, 38].

On August 27, 1998, a giant burst occurred at the location of SGR 1900+14 [48]. This burst was very similar to that of SGR 0525–66 on March 5, 1979. The time profile of this burst had a tail 300s long, which also showed a clear periodicity of 5.16s [48]. Furthermore, it is very interesting to notice that the average spin-down rate became ~ 2.6 times larger than that before the giant burst [45].

SGR 1806–20

This object was also found fortuitously by short bursts in 1979 [55]. The association with the supernova remnant G10.0–0.3 in our galaxy was indicated by Kulkarni and Frail [59]. From X-ray observations, a quiescent X-ray source having a luminosity of 3×10^{35}erg s^{-1} was identified with SGR 1806–20 [61]. Furthermore, a period of 5.47s and a period derivative of 8.3×10^{-11}s s^{-1} were detected [66] in the quiescent X-ray emission. These results also give a very strong magnetic field in excess of 10^{13}G.

SGR 1627–41

SGR 1627–41 was found very recently [71]. This object has a persistent X-ray source of a luminosity 7-9 $\times 10^{34}$erg s^{-1} and shows weak evidence for the periodicity of 6.41s [71].

AXP	Period [s]	Period derivative [s s^{-1}]
4U 0142+61	8.69	2×10^{-12}
1E 2259+586	6.98	6×10^{-13}
1E 1048.1–5937	6.44	2×10^{-11}
1RXS J170849.0–400910	11.0	2×10^{-11}
1E 1841–045	11.8	4×10^{-11}
AX J1845–0258	7.0	—
RX J0720.4–3125	8.4	2.6×10^{-12}

Table 1.1: The periods and period derivatives of known AXPs.

However, this period was not derived in other observations [76]. SGR 1627–41 also seems to be associated with the supernova remnant G337.0–0.1 in our galaxy [71].

SGR 1801–23

Soft bursts from SGR 1801–23 were observed twice in the direction of the Galactic center on Jun 29, 1997 [77]. Their time histories and energy spectra were consistent with those of other SGRs. However, there are no other bursts from this object to date. Therefore, we do not have any other information about SGR 1801–23 at present.

1.3.2 Anomalous X-ray pulsars

AXPs constitute a separate group of neutron stars, but have many similarities to SGRs. AXPs do not emit any bursts like SGRs. In general, AXPs are characterized by the following: (i) a narrow spin period distribution compared with the other X-ray pulsars, (ii) soft X-ray spectra, (iii) a relatively low luminosity of the order of $\sim 10^{35}$erg s^{-1}, (iv) almost constant flux, (v) a stable spin period evolution, and (vi) the association with supernova remnants. There are seven known AXPs: 4U 0142+61 [78–82], 1E 2259+586 [80, 83–86], 1E 1048.1–5937 [80, 82, 86–89], 1RXS J170849.0–400910 [90, 91], 1E 1841–045 [92], AX J1845–0258 (J1845.0–0300) [93–95], and RX J0720.4–3125 [96]. The periods and period derivatives of these AXPs takes very similar values to those of SGRs. Hence, we find the magnetic field strength of magnetars again. These values are summarized in Table 1.1.

1.4 Subjects dealt with in this paper

Most stars have spherically symmetric structure. However, they are subject to the effects of rotation and a stellar magnetic field, which both lead to deformation of a star. It is well known that the rotational effect produces flattening of a star with respect to the rotational axis. If we consider a dipole magnetic field, then this also gives the same effect with respect to the magnetic axis. In most cases, these effects are very small, and therefore can be treated as perturbations to a spherically symmetric star. As seen in the last section, there exist neutron stars with very strong magnetic fields, although the relation between SGRs and AXPs is not yet clear. For these ultra-magnetized stars, the magnetic effect is dominant over the rotational effect. Hence, such a star is deformed mainly by the magnetic stress. The magnetic field strength of magnetars is much stronger than that of typical pulsars. However, this magnetic field strength can also be treated in a perturbative approach. Incidentally, stellar deformation may shows an observable effect. In fact, the irregular spin-down [84, 85, 88, 89] observed for two AXPs, 1E 1048.1–5937 and 1E 2259+586, can be interpreted as an effect arising from stellar magnetic deformation, which is called radiative precession [97, 98]. As discussed by Melatos [97, 98], this effect is given by the coupling between precession due to magnetic deformation and an oscillating component of electromagnetic torque. Thus, magnetic deformation plays a significant role for some kind of stars. Therefore, it is important to evaluate the deformation of magnetized stars seriously. In this paper, we study magnetic deformation of a star in the context of general relativity.

The quadrupole deformation of Newtonian stars due to a dipole magnetic field was discussed by Chandrasekhar and Fermi [99] and Ferraro [100]. In their papers, the incompressible fluid body with a dipole magnetic field is assumed. This kind of deformation was discussed also in relation to gravitational radiation [101, 102]. The general relativistic approach by Bonazzola et al. [103], Bocquet et al. [104], and Bonazzola and Gourgoulhon [105] appeared recently. However, their approach is fully numerical. Hence, their physical interpretation is not easy. In this paper, we develop a more analytic treatment using the perturbation method (see also Ref. [106]). Our formulation is regarded as a general relativistic version of Refs. [99, 100]. In our method, we can easily include realistic EOS and construct relativistic magnetized stars. Furthermore, this method gives simple calculations of ellipticity of deformed stars etc, and makes the results transparent for physical interpretation.

For the purpose of the formulation of relativistic magnetized stars, we first take a non-rotating, spherically symmetric star as a background. Second, we consider a stellar magnetic field, which is regarded as a perturbation, in the context of general relativity. We restrict the discussion of stellar magnetic deformation to non-rotating, i.e. static cases. We then take into account only axisymmetric, poloidal magnetic fields produced by long-lived toroidal electric currents, because toroidal magnetic fields would break the symmetric property (see also Ref. [104] and reference therein). Furthermore, we assume a perfectly conducting interior. Since we now consider non-rotating configurations, this implies that the electric field inside the stars must vanish. Hence, there is no electric charge inside the stars. Furthermore, the surface charge should be absent, since the total charge should vanish in astrophysical situations. Otherwise, the electromagnetic field itself would have the angular momentum due to the non-vanishing electric field produced by the charge [107–109]. This is not a purely static case. From this discussion, we can write the four-current as $J_\mu = (0, 0, 0, J_\phi)$ [104]. Here, the current distribution J_ϕ is introduced as the first-order quantity with respect to the perturbation. The corresponding magnetic field is solved from the Maxwell equation. We investigate deformation of stars due to the resulting magnetic stress, which arises as the second-order correction to the background. This perturbation method is very similar to that of slowly rotating, relativistic stars developed by Hartle [110], in which rotation is regarded as a small parameter. Our formalism can be applied to any configurations of the magnetic fields. However, we restrict our discussion to dipole magnetic fields because dipole fields are important in many astrophysical situations.

As mentioned previously, the configurations of pulsars are affected by both rotation and a stellar magnetic field. Therefore, it is important to further compare both effects for various pulsars. In general, the rotational axis of pulsars does not aligned with the axis of the dipole magnetic field. The general relativistic treatment for this case is a complicated task, because the situation is not stationary. However, in this paper, we assume that the rotational effect decouples from the magnetic effect. Thus we compare both effects by considering the deformation arising from each perturbation separately (see also Ref. [111]); the rotational deformation is provided by the formulation by Hartle [110], and the magnetic deformation is given by our formulation [106] mentioned above. This estimate is important to judge which effect dominates in rotating, magnetized stars, whose rotation rate and magnetic field strength are within a wide range. We note that if both effects are comparable, our estimate breaks down, and therefore sophisticated numerical codes are required.

When the deformed star rotates on the axis which does not coincide with the magnetic axis, the star precesses inevitably. The above-mentioned wobbles in the spin-down of the two AXPs also arise from precession probably due to the stellar magnetic deformation. These deformed, precessing objects are analyzed by solving the Euler equation of motion in the form $I_{ij} d\Omega^j/dt - \varepsilon_{ijk} I^{jl} \Omega^k \Omega_l = N_i$, where I_{ij} is the inertia tensor, Ω^i is the angular velocity, and N_i is the torque acting on the object. When we take into account the electromagnetic torque by a rotating magnetic dipole [112, 113], the radiative precession [97, 98] can actually be found for a magnetically deformed star. Furthermore, since such a star emits gravitational waves, we can consider the gravitational radiation reaction torque [114,115]. The gravitational backreaction damps the wobbles on a time-scale proportional to $[(I_z - I_x)^2 / I_x]^{-1}$ for wobbling, axisymmetric rigid bodies (see Refs. [114,115] for detailed discussion), where I_i is the principal moments of inertia. Thus, the moments of inertia play a significant role in the analyses of pulsar precession. The estimates of the moments of inertia have been done in the context of Newtonian gravity so far, but neutron stars are fully general relativistic objects. Therefore, we further discuss the principal moments of inertia of magnetically deformed stars in the context of general relativity.

1.5 Plan of this paper

This paper is organized as follows. We first describe non-rotating, spherically symmetric stars, as background in Chapter 2. This becomes the basic part in our formulation of magnetized stars. We deal with several polytropic stellar models in the context of both Newtonian gravity and general relativity. Next, we review the rotational flattening of stars using the perturbation method in Chapter 3. It is very useful to see this approach in order to develop the formulation of magnetized stars. In Chapter 4, we study the electromagnetic fields of pulsars following Refs. [116, 117]. We discuss not only dipole magnetic fields, but also induced electric fields in the cases of aligned dipole rotators, which is needed to define the moment of inertia of magnetically deformed stars with respect to the symmetric axis. In Chapter 5, we formulate magnetic deformation of stars, assuming non-rotating configurations. Furthermore, we compare the magnetic effect with the rotational effect on stellar deformation for various pulsars. Using the results of stellar deformation, we further investigate the moments of inertia of the stars in the context of general relativity in Chapter 6. Finally, we give summary and conclusion. in Chapter 7. We use units in which $c = G = 1$ in most places.

Chapter 2

Non-Rotating Stars

In this chapter, we review the formulation and solutions for non-rotating, spherically symmetric stars, which become background in the perturbation method. We discuss such stars in the context of both Newtonian gravity and general relativity (see also standard texts [6,8,118,119]). In this discussion, we adopt polytropic stellar models. First, we discuss Newtonian stars in §2.1. Second, we consider the general relativistic versions in §2.2.

2.1 Newtonian stars

2.1.1 Formulation

We now consider a spherically symmetric star which is in hydrostatic equilibrium. The basic equations governing such a star are

$$0 = \nabla\Phi + \frac{1}{\rho}\nabla p, \tag{2.1}$$

$$\nabla^2\Phi = 4\pi\rho, \tag{2.2}$$

where p and ρ denote pressure and density respectively, and Φ denotes gravitational potential. From the spherical symmetry, Eqs. (2.1) and (2.2) reduce to

$$0 = \frac{d\Phi(r)}{dr} + \frac{1}{\rho(r)}\frac{dp(r)}{dr}, \tag{2.3}$$

$$\frac{1}{r^2}\frac{d}{dr}\left(r^2\frac{d\Phi(r)}{dr}\right) = 4\pi\rho(r). \tag{2.4}$$

If we consider main sequence stars like the sun, the above equations should be supplemented with the equations concerning power generated in the stars (see, e.g., Ref. [8]). However, our discussion is intended for neutron stars, which have no power generation and lower temperature than Fermi temperature. Therefore, it is sufficient to consider Eqs. (2.1) and (2.2) only.

The above equations (2.3) and (2.4) is combined to give the second-order differential equation

$$\frac{1}{r^2}\frac{d}{dr}\left(\frac{r^2}{\rho}\frac{dp}{dr}\right) = -4\pi\rho. \tag{2.5}$$

This equation involves two unknown functions p and ρ. Hence, we need another relation between the pressure and the density, which is given by an equation of state (EOS). By assuming such a relation, the equations can be reduced to a differential equation consisting of one unknown function. We can finally obtain the structure of a star by solving the differential equation.

We now adopt polytropic stellar models. A polytropic model with index n is specified by the following relation between pressure and density,

$$p = K\rho^{1+1/n}, \tag{2.6}$$

where K is a constant. Using this, we have the differential equation for ρ,

$$\frac{1}{r^2}\frac{d}{dr}\left[\frac{r^2}{\rho}\frac{d}{dr}\left(K\rho^{1+1/n}\right)\right] = -4\pi\rho. \tag{2.7}$$

Normalized equations

Let us now introduce the normalized quantities of the density, the pressure and the radial coordinate as

$$\rho = \rho_{\rm c}\tilde{\rho}, \tag{2.8}$$

$$p = p_{\rm c}\tilde{p}, \tag{2.9}$$

$$r = r_*\tilde{r}, \tag{2.10}$$

where $\rho_{\rm c}$ and $p_{\rm c}$ are the values of density and pressure at the stellar center respectively, and r_* is given by

$$r_* = \sqrt{\frac{p_{\rm c}}{4\pi\rho_{\rm c}^2}}. \tag{2.11}$$

Using the normalized quantities, we derive the equation,

$$\frac{1}{\tilde{r}^2}\frac{d}{d\tilde{r}}\left(\frac{\tilde{r}^2}{\tilde{\rho}}\frac{d}{d\tilde{r}}\tilde{\rho}^{1+1/n}\right) = -\tilde{\rho}. \tag{2.12}$$

Furthermore, it is convenient to introduce the function Θ defined as

$$\tilde{\rho} = \Theta^n. \tag{2.13}$$

Using this function, Eq. (2.12) reduces to

$$(1+n)\frac{d^2\Theta}{d\tilde{r}^2}+\frac{2(1+n)}{\tilde{r}}\frac{d\Theta}{d\tilde{r}}+\Theta^n=0. \tag{2.14}$$

This differential equation must be solved by imposing two boundary conditions. Such conditions are expressed as

$$\Theta|_{\tilde{r}=0} = 1, \tag{2.15}$$

$$\left.\frac{d\Theta}{d\tilde{r}}\right|_{\tilde{r}=0} = 0, \tag{2.16}$$

where the second condition follows immediately from the substitution of Eq. (2.6) into Eqs. (2.3) and (2.4). Once we obtain the solution for Θ, we can calculate the solution for density and pressure from the relation

$$\rho = \rho_{\mathrm{c}}\Theta^n, \tag{2.17}$$

$$p = p_{\mathrm{c}}\Theta^{1+n}. \tag{2.18}$$

Furthermore, from Eq. (2.3), the gravitational potential Φ can be written as

$$\Phi=\Phi_*\tilde{\Phi}=\Phi_*\left[-\left(n+1\right)\Theta+c_{1\Phi}\right], \tag{2.19}$$

where Φ_* is defined by $\Phi_*=p_{\mathrm{c}}/\rho_{\mathrm{c}}$, and $c_{1\Phi}$ is a constant. This internal potential must be connected smoothly with the exterior solution given by

$$\Phi=\Phi_*\frac{c_{2\Phi}}{\tilde{r}}, \tag{2.20}$$

where $c_{2\Phi}$ is a constant fixed by the junction conditions. Therefore, Eq. (2.14) governs stellar structure in polytropic models. In the next subsection, we discuss the analytic and numerical solutions for several polytropic indices.

2.1.2 Solutions for stellar configurations

We can find analytic solutions for several polytropic indices. Such solutions are summarized as follows:

- $n=0$

$$\Theta = 1-\frac{\tilde{r}^2}{6}, \tag{2.21}$$

$$\tilde{\rho} = 1, \tag{2.22}$$

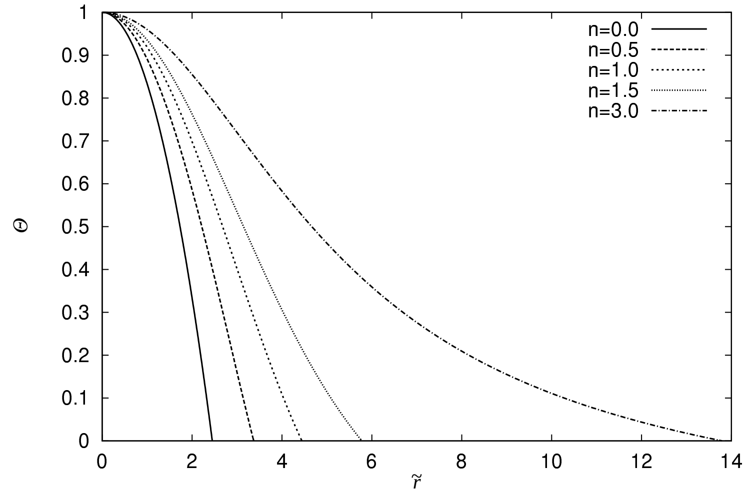

Figure 2.1: The function $\Theta(\tilde{r})$ for several polytropic stellar models. The polytropic index is denoted by n.

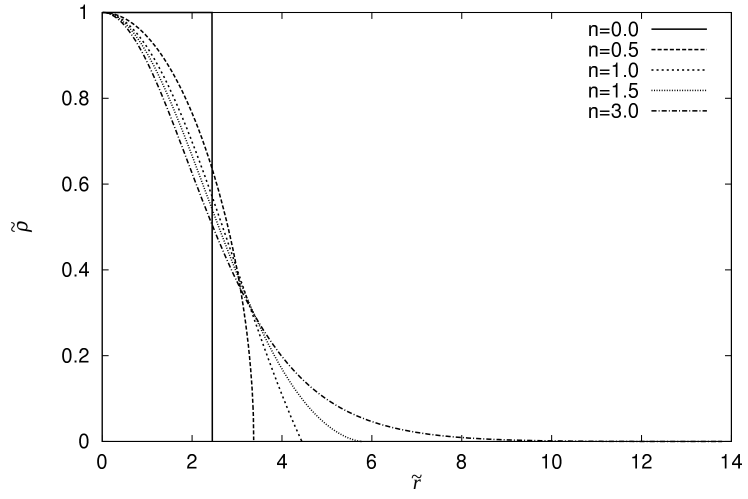

Figure 2.2: The density $\tilde{\rho}$ plotted as a function of $\tilde{r}$ for several polytropic stellar models.

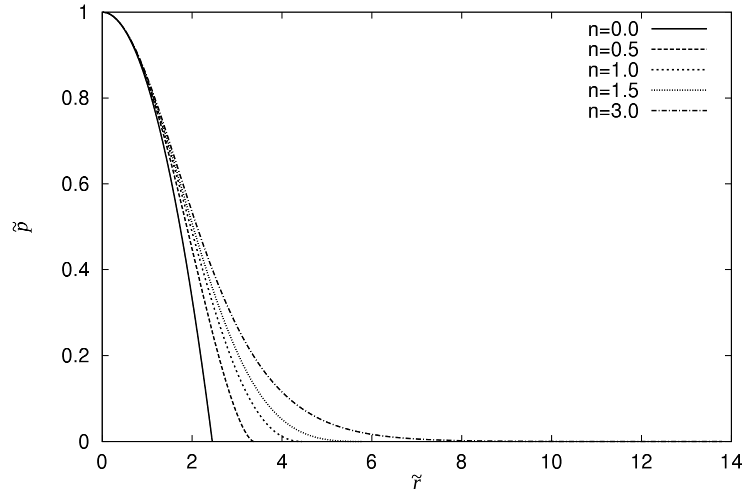

Figure 2.3: The pressure $\tilde{p}$ plotted as a function of $\tilde{r}$ for several polytropic stellar models.

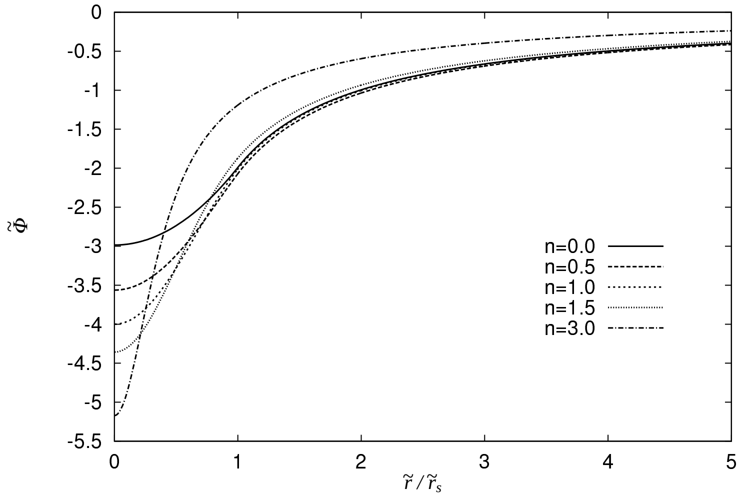

Figure 2.4: The potential $\tilde{\Phi}$ plotted as a function of $\tilde{r}$ for several polytropic stellar models.

$$\tilde{p} = 1 - \frac{\tilde{r}^2}{6}, \tag{2.23}$$

$$\tilde{\Phi} = \begin{cases} \frac{\tilde{r}^2}{6} - 3 & (\tilde{r} < \tilde{r}_{\rm s}) \\ -\frac{2\sqrt{6}}{\tilde{r}} & (\tilde{r} > \tilde{r}_{\rm s}) \end{cases}, \tag{2.24}$$

$$\tilde{r}_{\rm s} = \sqrt{6}, \tag{2.25}$$

$$\frac{\rho_{\rm c}}{\bar{\rho}} = 1, \tag{2.26}$$

- $n = 1$

$$\Theta = \frac{\sqrt{2}}{\tilde{r}} \sin\left(\frac{\tilde{r}}{\sqrt{2}}\right), \tag{2.27}$$

$$\tilde{\rho} = \frac{\sqrt{2}}{\tilde{r}} \sin\left(\frac{\tilde{r}}{\sqrt{2}}\right), \tag{2.28}$$

$$\tilde{p} = \frac{2}{\tilde{r}^2} \sin^2\left(\frac{\tilde{r}}{\sqrt{2}}\right), \tag{2.29}$$

$$\tilde{\Phi} = \begin{cases} -\frac{2\sqrt{2}}{\tilde{r}} \sin\left(\frac{\tilde{r}}{\sqrt{2}}\right) - 2 & (\tilde{r} < \tilde{r}_{\rm s}) \\ -\frac{2\sqrt{2}\pi}{\tilde{r}} & (\tilde{r} > \tilde{r}_{\rm s}) \end{cases}, \tag{2.30}$$

$$\tilde{r}_{\rm s} = \sqrt{2}\pi, \tag{2.31}$$

$$\frac{\rho_{\rm c}}{\bar{\rho}} = \frac{\pi^2}{3}, \tag{2.32}$$

- $n = 5$

$$\Theta = \left(1 + \frac{\tilde{r}^2}{18}\right)^{-1/2}, \tag{2.33}$$

$$\tilde{\rho} = \left(1 + \frac{\tilde{r}^2}{18}\right)^{-5/2}, \tag{2.34}$$

$$\tilde{p} = \left(1 + \frac{\tilde{r}^2}{18}\right)^{-3}, \tag{2.35}$$

$$\tilde{r}_{\rm s} \to \infty, \tag{2.36}$$

$$\frac{\rho_{\rm c}}{\bar{\rho}} \to \infty. \tag{2.37}$$

Here, $\tilde{r}_{\rm s}$ corresponds to the stellar radius R, i.e. $R = r_* \tilde{r}_{\rm s}$, and $\bar{\rho}$ denotes the average density as, using the total mass M,

$$\bar{\rho} \equiv \left(\frac{4\pi}{3} R^3\right)^{-1} M. \tag{2.38}$$

The total mass can be derived by integrating the following equation for the mass function $m(r)$,

$$\frac{dm}{dr} = 4\pi r^2 \rho. \tag{2.39}$$

After using the boundary condition

$$m|_{r=0} = 0, \tag{2.40}$$

we can derive the total mass $M = m(R)$. Equation (2.39) can also be written in the normalized form

$$\frac{d\tilde{m}}{d\tilde{r}} = \tilde{r}^2 \tilde{\rho}. \tag{2.41}$$

The normalized mass function $\tilde{m}$ is defined as

$$m = m_* \tilde{m}, \tag{2.42}$$

where m_* is given by

$$m_* = \sqrt{\frac{p_{\rm c}^3}{4\pi \rho_{\rm c}^4}}. \tag{2.43}$$

Using the above quantity, the ratio of the central density to the average density is derived in the form

$$\frac{\rho_{\rm c}}{\bar{\rho}} = \frac{4\pi R^3 \rho_{\rm c}}{3M} = \frac{\tilde{r}_{\rm s}^3}{3\tilde{m}(\tilde{r}_{\rm s})}. \tag{2.44}$$

From the analytic solution (2.22), we see that the case of $n = 0$ corresponds to an incompressible fluid body. Furthermore, from Eq. (2.36), we can see that the stellar radius becomes infinity as n approaches to 5. In this case, the ratio of the central density to the average density also diverges. Therefore, it seems that plausible models for stars are described by polytropic indices in a range $0 < n < 5$.

The solutions for the other polytropic indices can be obtained by numerical calculations. Figures 2.1, 2.2, 2.3 and 2.4 display the numerical results of Θ, $\tilde{\rho}$, $\tilde{p}$ and $\tilde{\Phi}$, respectively, for $n = 0,\ 0.5,\ 1,\ 1.5$ and 3. These are plotted as a function of $\tilde{r}$. In Table 2.1, we further show the numerical values of the radius $\tilde{r}_{\rm s}$ and the ratio of the central density to the average density $\rho_{\rm c}/\bar{\rho}$, together with the analytic results. From this table, we find that the stellar radius $\tilde{r}_{\rm s}$ and the ratio $\rho_{\rm c}/\bar{\rho}$ become larger with the polytropic index n.

2.2 General relativistic stars

2.2.1 Formulation

Next, we deal with non-rotating, general relativistic stars. As in the last section, we assume that the equilibrium configurations have spherical symmetry. The spherically symmetric spacetime can be described by the line element

$$ds^2 = -e^{\nu(r)} dt^2 + e^{\lambda(r)} dr^2 + r^2 \left(d\theta^2 + \sin^2\theta d\phi^2 \right). \tag{2.45}$$

n	$\tilde{r}_{\rm s}$ (analytic)	$\tilde{r}_{\rm s}$ (numerical)	$\rho_{\rm c}/\bar{\rho}$ (analytic)	$\rho_{\rm c}/\bar{\rho}$ (numerical)
0.	$\sqrt{6}$	2.4495	1	1.0000
0.5	—	3.3714	—	1.8351
1.	$\sqrt{2}\pi$	4.4428	$\pi^2/3$	3.2897
1.5	—	5.7770	—	5.9903
3.	—	13.793	—	54.175
5.	∞	—	∞	—

Table 2.1: The stellar radius $\tilde{r}_{\rm s}$ and the ratio of the central density to the average density $\rho_{\rm c}/\bar{\rho}$ derived for polytropic models.

It is sometimes useful to use the following function instead of the function λ,

$$m = \frac{r}{2}\left(1 - e^{-\lambda}\right). \tag{2.46}$$

This function is the general relativistic version of the mass function Eq. (2.42) as will be seen below.

The stress-energy tensor of a star consisting of perfect fluid is given by

$$T^{\mu}_{\ \nu} = (\rho + p)\, u^{\mu} u_{\nu} + p\delta^{\mu}_{\ \nu}, \tag{2.47}$$

where the four-velocity u^{μ} is written in the form

$$u^{\mu} = \left(e^{-\nu/2}, 0, 0, 0\right). \tag{2.48}$$

The equations which govern stellar structure can be obtained from the Einstein equation

$$G^{\mu}_{\ \nu} = 8\pi T^{\mu}_{\ \nu} \tag{2.49}$$

and the equation of motion

$$T^{\mu}_{\ \nu;\mu} = 0. \tag{2.50}$$

First, from the (t,t)-component of Eq. (2.49), we obtain

$$\frac{dm}{dr} = 4\pi r^2 \rho. \tag{2.51}$$

This equation exactly has the same form as Eq. (2.39) in the form. Hence, this is the reason why m is called the mass function. Second, the following equation can be obtained from (r,r)-component of Eq. (2.49),

$$\frac{d\nu}{dr} = \frac{2m + 8\pi r^3 p}{r(r-2m)}. \tag{2.52}$$

Third, the r-component of Eq. (2.50) reduces to the equation

$$\frac{dp}{dr} = -\frac{1}{2}(\rho + p)\frac{d\nu}{dr}. \tag{2.53}$$

Using Eq. (2.52), we derive the equation

$$\frac{dp}{dr} = -\frac{(\rho + p)(m + 4\pi r^3 p)}{r(r - 2m)}. \tag{2.54}$$

This equation is called the Tolman-Oppenheimer-Volkoff equation (see, e.g., Refs. [1,118–120]). In addition to Eqs. (2.51), (2.52) and (2.54), we have an EOS

$$p = p(\rho). \tag{2.55}$$

These give four equations for the four unknown functions ν, m, ρ and p. Therefore, stellar structure is governed by these equations.

Normalized equations

As in the last section, it is convenient to introduce the normalized quantities $\tilde{r}$, $\tilde{m}$, $\tilde{\rho}$ and $\tilde{p}$. Using these, Eqs. (2.51), (2.52) and (2.54) reduce, respectively, to

$$\frac{d\tilde{m}}{d\tilde{r}} = \tilde{r}^2\tilde{\rho}, \tag{2.56}$$

$$\frac{d\nu}{d\tilde{r}} = \frac{2\zeta(\tilde{m} + \zeta\tilde{r}^3\tilde{p})}{\tilde{r}\,(\tilde{r} - 2\zeta\tilde{m})}. \tag{2.57}$$

$$\frac{d\tilde{p}}{d\tilde{r}} = -\frac{(\tilde{\rho} + \zeta\tilde{p})(\tilde{m} + \zeta\tilde{r}^3\tilde{p})}{\tilde{r}(\tilde{r} - 2\zeta\tilde{m})}, \tag{2.58}$$

where ζ is the parameter defined by

$$\zeta \equiv \frac{p_c}{\rho_c}. \tag{2.59}$$

Note that this parameter can be related with the general relativistic factor M/R in the way

$$\frac{M}{R} = \frac{m_*\tilde{m}(\tilde{r}_s)}{r_*\tilde{r}_s} = \zeta\frac{\tilde{m}(\tilde{r}_s)}{\tilde{r}_s}. \tag{2.60}$$

We now use the polytropic EOS (2.6) again, which is described by Θ. Using the function Θ, we have

$$\frac{d\tilde{m}}{d\tilde{r}} = \tilde{r}^2\Theta^n, \tag{2.61}$$

$$\frac{d\nu}{d\tilde{r}} = \frac{2\zeta(\tilde{m} + \zeta\tilde{r}^3\Theta^{n+1})}{\tilde{r}\,(\tilde{r} - 2\zeta\tilde{m})}. \tag{2.62}$$

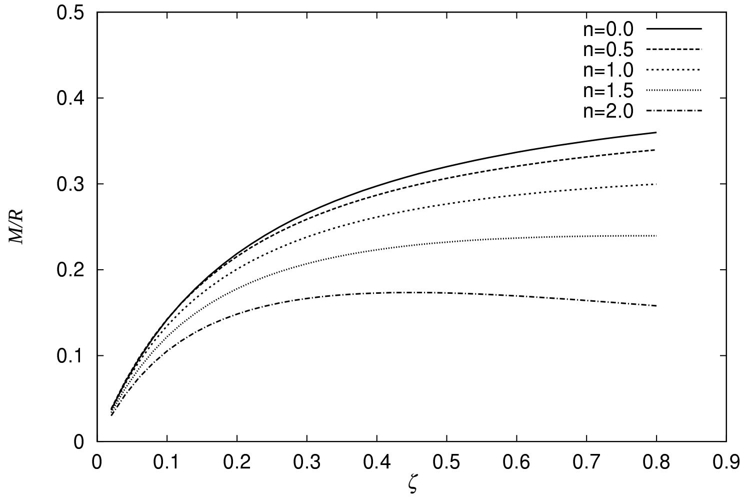

Figure 2.5: The general relativistic factor M/R plotted as a function of ζ. The polytropic index is denoted by n.

$$\frac{d\Theta}{d\tilde{r}} = -\frac{(1+\zeta\Theta)\left(\tilde{m}+\zeta\tilde{r}^3\Theta^{n+1}\right)}{(n+1)\tilde{r}(\tilde{r}-2\zeta\tilde{m})}. \tag{2.63}$$

These differential equations govern polytropic stellar models in the context of general relativity. Equations (2.61), (2.62) and (2.63) should be solved using the boundary conditions

$$\tilde{m}|_{\tilde{r}=0} = 0, \quad \nu|_{\tilde{r}=0} = \text{const}, \quad \Theta|_{\tilde{r}=0} = 1. \tag{2.64}$$

Furthermore, we have to impose the junction condition in which the interior solution is connected with the exterior solution smoothly.

2.2.2 Solutions for stellar configurations

Exterior solution

First, let us discuss the stellar exterior solution which is asymptotically flat at infinity. The outside of the star is assumed to be a vacuum, i.e. $\rho = p = \Theta = 0$. In this case, from Eq. (2.61), we derive

$$\tilde{m} = \text{const} \equiv \frac{M}{m_*}. \tag{2.65}$$

This result is equivalent to

$$e^{\lambda} = \left(1-\frac{2M}{r}\right)^{-1}. \tag{2.66}$$

Substituting Eq. (2.65) into Eq. (2.62) and integrating the equation, we derive

$$\nu = \ln\left(1-\frac{2M}{r}\right). \tag{2.67}$$

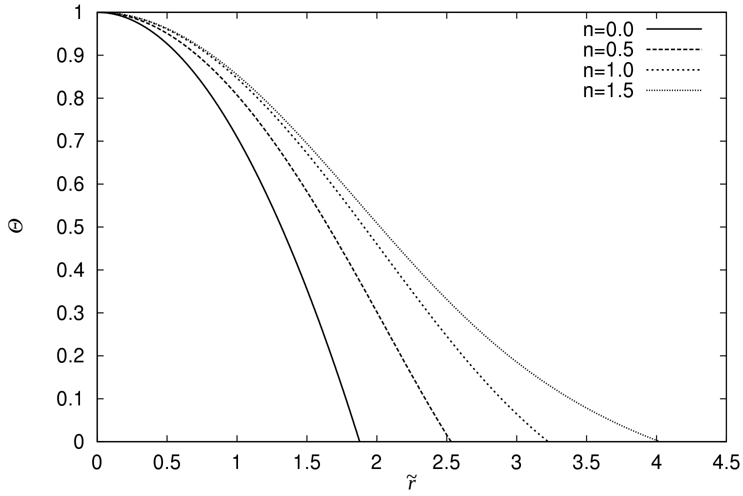

Figure 2.6: Radial dependence of Θ for polytropic stellar models with $M/R = 0.2$.

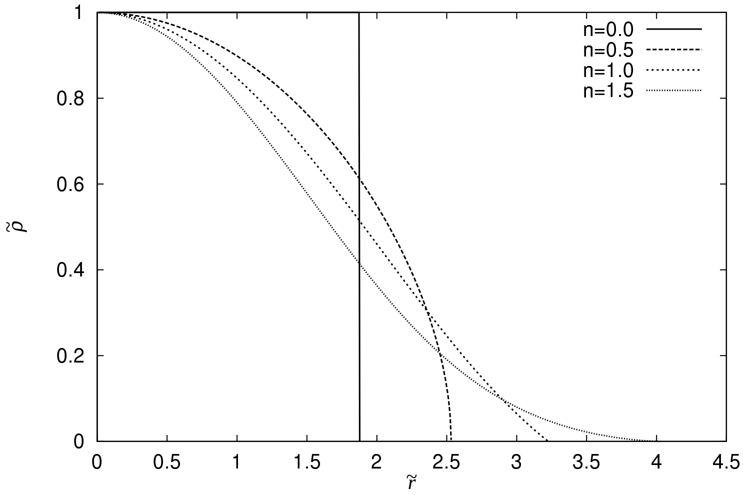

Figure 2.7: Radial dependence of $\tilde{\rho}$ for polytropic stellar models with $M/R = 0.2$.

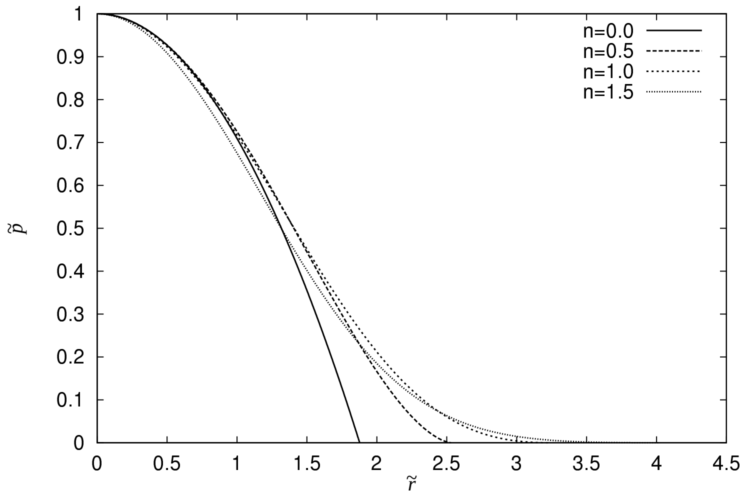

Figure 2.8: Radial dependence of $\tilde{p}$ for polytropic stellar models with $M/R = 0.2$.

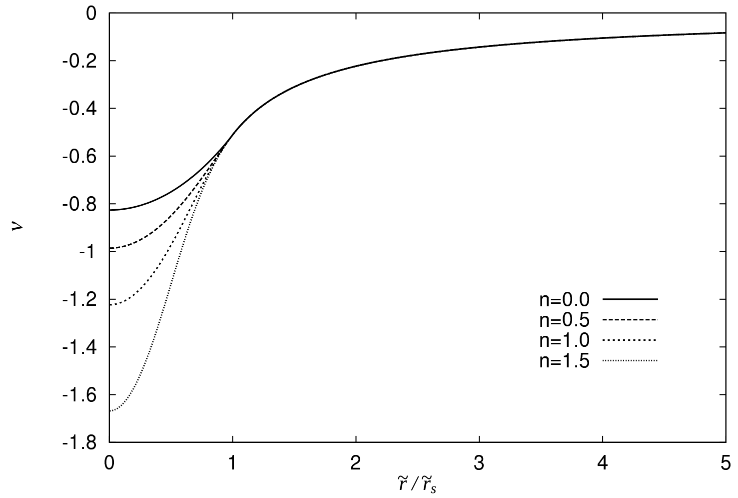

Figure 2.9: Radial dependence of ν for polytropic stellar models with $M/R = 0.2$.

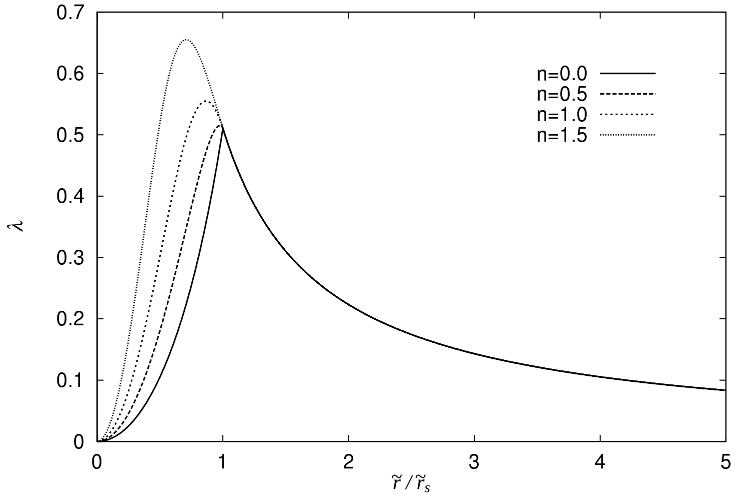

Figure 2.10: Radial dependence of λ for polytropic stellar models with $M/R = 0.2$.

Therefore, we obtain the line element

$$ds^2 = -\left(1 - \frac{2M}{r}\right) dt^2 + \left(1 - \frac{2M}{r}\right)^{-1} dr^2 + r^2 \left(d\theta^2 + \sin^2\theta d\phi^2\right). \tag{2.68}$$

This is the well-known Schwarzschild metric.

Interior solutions

Next, we discuss interior solutions. It is somewhat difficult to seek analytic solutions for stellar structure in the general relativistic case unlike the Newtonian case. However, we can find the analytic solution for the case of $n = 0$. In this case, the integration of Eq. (2.61) gives

$$\tilde{m} = \frac{1}{3}\tilde{r}^3. \tag{2.69}$$

Using this result, from Eq. (2.63), we derive the equation

$$\frac{d\Theta}{(1+\zeta\Theta)(1+3\zeta\Theta)} = -\frac{\tilde{r}d\tilde{r}}{3 - 2\zeta\tilde{r}^2}. \tag{2.70}$$

This is easily integrated as

$$\frac{1+3\zeta\Theta}{1+\zeta\Theta} = \frac{1+3\zeta}{1+\zeta}\left(1 - \frac{2\zeta\tilde{m}}{\tilde{r}}\right)^{\frac{1}{2}}. \tag{2.71}$$

Hence, we obtain

$$\Theta = \frac{-(1+\zeta) + (1+3\zeta)\left(1 - \frac{2\zeta\tilde{m}}{\tilde{r}}\right)^{\frac{1}{2}}}{\zeta\left[3(1+\zeta) - (1+3\zeta)\left(1 - \frac{2\zeta\tilde{m}}{\tilde{r}}\right)^{\frac{1}{2}}\right]}. \tag{2.72}$$

If we take the limit $\Theta \to 0$, which corresponds to $\tilde{r} \to \tilde{r}_\mathrm{s}$, in Eq. (2.71), then we can derive

$$\tilde{r}_\mathrm{s} = \left\{ \frac{3}{2\zeta} \left[1 - \left(\frac{1+\zeta}{1+3\zeta} \right)^2 \right] \right\}^{\frac{1}{2}} \tag{2.73}$$

or

$$\zeta = \frac{1 - \left(1 - \frac{2M}{R}\right)^{\frac{1}{2}}}{3\left(1 - \frac{2M}{R}\right)^{\frac{1}{2}} - 1}. \tag{2.74}$$

From this result, we can find that ζ diverges, which means $p_\mathrm{c} \to \infty$, as M/R approaches to 4/9. Therefore, there cannot exist the star whose radius is smaller than $9M/4$. The metric function ν can be obtained by integrating the following equation derived from Eq. (2.62),

$$\frac{d\nu}{d\tilde{r}} = \frac{8\zeta\tilde{r}}{3} \frac{(1+3\zeta)\left(1 - \frac{2\zeta}{3}\tilde{r}^2\right)^{-\frac{1}{2}}}{3(1+\zeta) - (1+3\zeta)\left(1 - \frac{2\zeta}{3}\tilde{r}^2\right)^{\frac{1}{2}}}. \tag{2.75}$$

The integration gives

$$e^\nu = \left[\frac{3}{2}\left(1 - \frac{2M}{R}\right)^{\frac{1}{2}} - \frac{1}{2}\left(1 - \frac{2Mr^2}{R^3}\right)^{\frac{1}{2}} \right]^2, \tag{2.76}$$

where the junction condition at the surface has been used.

The other solutions can be obtained by numerical integration (see also Ref. [121]). In their calculations, ζ plays an important role, because this parameter specifies the general relativistic factor M/R through the relation (2.60). Figure 2.5 displays the relations between M/R and ζ for several polytropic models. From this figure, we can find that the values of M/R become smaller as n becomes large for fixed ζ. Furthermore, we can find that there exits an attainable, maximum value of M/R for the stellar model of $n = 2$. Thus, we cannot construct a stellar model with $M/R = 0.2$ for the case of $n \gtrsim 2$.

Figure 2.6, 2.7, 2.8, 2.9 and 2.10 display radial dependence of Θ, $\tilde{\rho}$, $\tilde{p}$, ν and λ, respectively, for polytropic stellar models with $M/R = 0.2$. From the comparison with the Newtonian cases, we find that $\tilde{r}_\mathrm{s}$ becomes small slightly owing to the general relativistic effect for the fixed polytropic index.

Chapter 3

Rotating Stars

In this chapter, we deal with rotating configurations of stars. Stellar rotation causes centrifugal force and therefore induces the rotational flattening of stars. We now discuss the deformation of stars due to rotation. We assume that stars rotate with uniform angular velocity Ω. The rotational effect can be treated as a perturbation. This is because rotational energy is much smaller than gravitational energy in most cases. The characteristic small parameter ε_Ω is given by the square root of the ratio of the rotational energy $\sim MR^2\Omega^2$ to the gravitational energy $\sim M^2/R$, i.e. $\varepsilon_\Omega \sim \sqrt{R^3\Omega^2/M}$.

In a similar way as the last chapter, Newtonian stars (see also Refs. [122–124]) and general relativistic stars (see also Refs. [110, 125]) are discussed in §3.1 and §3.2, respectively.

3.1 Newtonian stars

3.1.1 Formulation

In the case of rotating stars, the basic equations are written in the forms

$$0 = \nabla\Phi + \frac{1}{\rho}\nabla p + \boldsymbol{\Omega} \times (\boldsymbol{\Omega} \times \boldsymbol{r}), \tag{3.1}$$

$$\nabla^2\Phi = 4\pi\rho. \tag{3.2}$$

The last term in Eq. (3.1) is a second-order quantity in ε_Ω and can be expressed as

$$\boldsymbol{\Omega} \times (\boldsymbol{\Omega} \times \boldsymbol{r}) = \left[-\frac{2}{3}r\Omega^2 + \frac{2}{3}r\Omega^2 P_2(\cos\theta)\right]\boldsymbol{e}_r + \frac{1}{3}r\Omega^2\frac{dP_2(\cos\theta)}{d\theta}\boldsymbol{e}_\theta, \tag{3.3}$$

where P_l is the Legendre polynomial of order l.

We can now expand ρ, p and Φ as

$$\begin{aligned}
\rho &= \rho^{(0)}(r) + \left[\rho_0^{(2)}(r) + \rho_2^{(2)}(r)P_2\right], && (3.4)\\
p &= p^{(0)}(r) + \left[p_0^{(2)}(r) + p_2^{(2)}(r)P_2\right], && (3.5)\\
\Phi &= \Phi^{(0)}(r) + \left[\Phi_0^{(2)}(r) + \Phi_2^{(2)}(r)P_2\right], && (3.6)
\end{aligned}$$

where the superscripts "(0)" and "(2)" here denote zeroth and second order in ε_Ω, respectively. The zeroth-order quantities $\rho^{(0)}$, $p^{(0)}$ and $\Phi^{(0)}$ have been discussed in the last chapter. We shall abbreviate "(0)" in most places hereafter.

Multiplying Eq. (3.1) by $\boldsymbol{e}_r$ or $\boldsymbol{e}_\theta$, we obtain

$$\begin{aligned}
\frac{d\Phi_0^{(2)}}{dr} + \frac{\rho_0^{(2)}}{\rho}\frac{d\Phi}{dr} + \frac{1}{\rho}\frac{dp_0^{(2)}}{dr} - \frac{2}{3}r\Omega^2 &= 0, && (3.7)\\
\frac{d\Phi_2^{(2)}}{dr} + \frac{\rho_2^{(2)}}{\rho}\frac{d\Phi}{dr} + \frac{1}{\rho}\frac{dp_2^{(2)}}{dr} + \frac{2}{3}r\Omega^2 &= 0, && (3.8)
\end{aligned}$$

and

$$\Phi_2^{(2)} + \frac{p_2^{(2)}}{\rho} + \frac{1}{3}r^2\Omega^2 = 0, \tag{3.9}$$

Here we have used the expression

$$\nabla = \boldsymbol{e}_r\frac{\partial}{\partial r} + \boldsymbol{e}_\theta\frac{1}{r}\frac{\partial}{\partial\theta} + \boldsymbol{e}_\phi\frac{1}{r\sin\theta}\frac{\partial}{\partial\phi}. \tag{3.10}$$

Equations (3.7) and (3.8) can easily be integrated using the relations

$$\begin{aligned}
\frac{d\Phi}{dr} &= -\frac{1}{\rho}\frac{dp}{dr}, && (3.11)\\
\rho_0^{(2)} &= \frac{d\rho}{dp}p_0^{(2)}, && (3.12)\\
\rho_2^{(2)} &= \frac{d\rho}{dp}p_2^{(2)}. && (3.13)
\end{aligned}$$

One of the integrated forms is Eq. (3.9), and the other is

$$\Phi_0^{(2)} + \frac{p_0^{(2)}}{\rho} - \frac{1}{3}r^2\Omega^2 = \text{const.} \tag{3.14}$$

Furthermore, from Eq. (3.2), we obtain

$$\begin{aligned}
\frac{1}{r^2}\frac{d}{dr}\left(r^2\frac{d\Phi_0^{(2)}}{dr}\right) &= 4\pi\rho_0^{(2)}, && (3.15)\\
\frac{1}{r^2}\frac{d}{dr}\left(r^2\frac{d\Phi_2^{(2)}}{dr}\right) - \frac{6}{r^2}\Phi_2^{(2)} &= 4\pi\rho_2^{(2)}, && (3.16)
\end{aligned}$$

where we have used the formulas

$$\nabla^2 = \frac{1}{r^2}\frac{\partial}{\partial r}\left(r^2\frac{\partial}{\partial r}\right) + \frac{1}{r^2\sin\theta}\frac{\partial}{\partial\theta}\left(\sin\theta\frac{\partial}{\partial\theta}\right) + \frac{1}{r^2\sin^2\theta}\frac{\partial^2}{\partial\phi^2}, \tag{3.17}$$

$$\frac{1}{\sin\theta}\frac{d}{d\theta}\left(\sin\theta\frac{dP_l}{d\theta}\right) = -l(l+1)P_l. \tag{3.18}$$

Outside the star, we have to solve Eqs. (3.15) and (3.16) with $\rho_0^{(2)} = \rho_2^{(2)} = 0$, assuming the potentials to vanish at infinity. Inside the star, it is useful to introduce $\delta P_0^{(2)}$ and $\delta P_2^{(2)}$ defined as

$$\delta P_0^{(2)} = \frac{p_0^{(2)}}{\rho}, \tag{3.19}$$

$$\delta P_2^{(2)} = \frac{p_2^{(2)}}{\rho}. \tag{3.20}$$

Using Eqs. (3.9) and (3.14), we can derive the differential equations for $\delta P_0^{(2)}$ and $\delta P_2^{(2)}$,

$$\frac{d^2}{dr^2}\delta P_0^{(2)} + \frac{2}{r}\frac{d}{dr}\delta P_0^{(2)} + 4\pi\frac{\rho'}{p'}\rho\delta P_0^{(2)} = 2\Omega^2, \tag{3.21}$$

$$\frac{d^2}{dr^2}\delta P_2^{(2)} + \frac{2}{r}\frac{d}{dr}\delta P_2^{(2)} + \left(4\pi\frac{\rho'}{p'}\rho - \frac{6}{r^2}\right)\delta P_2^{(2)} = 0, \tag{3.22}$$

where the prime here denotes differentiation with respect to r. Hence, Eq. (3.21) and (3.22) should be solved inside the star, using boundary conditions at the stellar center. Thereby we can derive the internal potentials $\Phi_0^{(2)}$ and $\Phi_2^{(2)}$ through the relations (3.9) and (3.14). The potentials must be connected at the stellar surface, by imposing the junction conditions mentioned below. Consequently, Eqs. (3.9), (3.14), (3.15), (3.16), (3.21) and (3.22) govern the deformed star by rotation.

Junction conditions

We now discuss the junction conditions about the potentials. Here some remark concerning the junction conditions should be mentioned (see also Ref. [123]). Let us express internal and external gravitational potentials by $\Phi_{\rm in}$ and $\Phi_{\rm ext}$, respectively. These can be written, showing order explicitly, as

$$\Phi_{\rm in} = \Phi_{\rm in}^{(0)} + \Phi_{\rm in}^{(2)}, \tag{3.23}$$

$$\Phi_{\rm ext} = \Phi_{\rm ext}^{(0)} + \Phi_{\rm ext}^{(2)}. \tag{3.24}$$

Furthermore, we express the boundary surface by ξ. This can also be expanded as

$$\xi = \xi^{(0)} + \xi^{(2)}. \tag{3.25}$$

Here, $\xi^{(0)}$ is simply given by $\xi^{(0)} = R$, while $\xi^{(2)}$ can be written as

$$\xi^{(2)} = \xi_0^{(2)} + \xi_2^{(2)} P_2 = -\left(\frac{1}{\rho}\frac{dp}{dr}\right)^{-1} \left(\delta P_0^{(2)} + \delta P_2^{(2)} P_2\right). \tag{3.26}$$

Using these quantities, we have

$$\begin{aligned}
\Phi_{\rm in}\big|_{\xi} &= \Phi_{\rm in}^{(0)}\Big|_{\xi^{(0)}} + \left(\Phi_{\rm in}^{\prime(0)}\Big|_{\xi^{(0)}} \xi^{(2)} + \Phi_{\rm in}^{(2)}\Big|_{\xi^{(0)}}\right), & (3.27)\\
\Phi'_{\rm in}\big|_{\xi} &= \Phi_{\rm in}^{\prime(0)}\Big|_{\xi^{(0)}} + \left(\Phi_{\rm in}^{\prime\prime(0)}\Big|_{\xi^{(0)}} \xi^{(2)} + \Phi_{\rm in}^{\prime(2)}\Big|_{\xi^{(0)}}\right), & (3.28)\\
\Phi_{\rm ext}\big|_{\xi} &= \Phi_{\rm ext}^{(0)}\Big|_{\xi^{(0)}} + \left(\Phi_{\rm ext}^{\prime(0)}\Big|_{\xi^{(0)}} \xi^{(2)} + \Phi_{\rm ext}^{(2)}\Big|_{\xi^{(0)}}\right), & (3.29)\\
\Phi'_{\rm ext}\big|_{\xi} &= \Phi_{\rm ext}^{\prime(0)}\Big|_{\xi^{(0)}} + \left(\Phi_{\rm ext}^{\prime\prime(0)}\Big|_{\xi^{(0)}} \xi^{(2)} + \Phi_{\rm ext}^{\prime(2)}\Big|_{\xi^{(0)}}\right). & (3.30)
\end{aligned}$$

Hence, boundary conditions are now expressed as

$$\begin{aligned}
\left(\Phi_{\rm in}^{(0)} - \Phi_{\rm ext}^{(0)}\right)\Big|_{\xi^{(0)}} &= 0, & (3.31)\\
\left(\Phi_{\rm in}^{\prime(0)} - \Phi_{\rm ext}^{\prime(0)}\right)\Big|_{\xi^{(0)}} &= 0, & (3.32)\\
\left(\Phi_{\rm in}^{(2)} - \Phi_{\rm ext}^{(2)}\right)\Big|_{\xi^{(0)}} &= 0, & (3.33)
\end{aligned}$$

$$\left[\left(\Phi_{\rm in}^{\prime\prime(0)} - \Phi_{\rm ext}^{\prime\prime(0)}\right)\Big|_{\xi^{(0)}}\right] \xi^{(2)} + \left(\Phi_{\rm in}^{\prime(2)} - \Phi_{\rm ext}^{\prime(2)}\right)\Big|_{\xi^{(0)}} = 0. \tag{3.34}$$

From Eq. (2.4), we can derive

$$\frac{d^2}{dr^2}\left(\Phi_{\rm in}^{(0)} - \Phi_{\rm ext}^{(0)}\right)\Bigg|_{\xi^{(0)}} = -\frac{2}{r}\frac{d}{dr}\left(\Phi_{\rm in}^{(0)} - \Phi_{\rm ext}^{(0)}\right)\Bigg|_{\xi^{(0)}} + 4\pi\rho^{(0)}\Big|_{\xi^{(0)}}. \tag{3.35}$$

Thus, the left-hand side of Eq. (3.35) vanishes except for the case of $n = 0$. Therefore, in the cases of $n \neq 0$, we can use the junction condition

$$\left(\Phi_{\rm in}^{\prime(2)} - \Phi_{\rm ext}^{\prime(2)}\right)\Big|_{\xi^{(0)}} = 0. \tag{3.36}$$

However, in the case of $n = 0$, we have to use the condition (3.34) instead of Eq. (3.36).

Normalized equations

In the remaining part of this subsection, we consider the normalized forms of the equations mentioned above. In addition to $\tilde{r}$, $\tilde{\rho}$, $\tilde{p}$ and $\tilde{\Phi}$, we use the dimensionless quantities $\tilde{\Omega}$, $\delta\tilde{P}_0^{(2)}$ and $\delta\tilde{P}_2^{(2)}$ defined as

$$\begin{aligned}
\Omega &= \Omega_* \tilde{\Omega}, & (3.37)\\
\delta P_0^{(2)} &= \delta P_* \delta\tilde{P}_0^{(2)}, & (3.38)\\
\delta P_2^{(2)} &= \delta P_* \delta\tilde{P}_2^{(2)}, & (3.39)
\end{aligned}$$

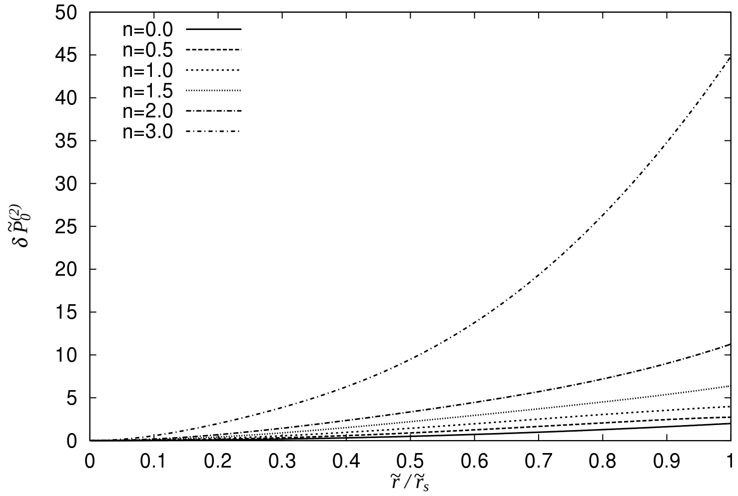

Figure 3.1: The function $\delta\tilde{P}_0^{(2)}$ plotted with respect to $\tilde{r}$.

where

$$\Omega_* = \sqrt{4\pi\rho_c}, \tag{3.40}$$

$$\delta P_* = \frac{p_c}{\rho_c}. \tag{3.41}$$

Equations (3.9) and (3.14) are then written as

$$\tilde{\Phi}_0^{(2)} = -\delta\tilde{P}_0^{(2)} + \frac{1}{3}\tilde{r}^2\tilde{\Omega}^2 + \mathrm{const}, \tag{3.42}$$

$$\tilde{\Phi}_2^{(2)} = -\delta\tilde{P}_2^{(2)} - \frac{1}{3}\tilde{r}^2\tilde{\Omega}^2. \tag{3.43}$$

Furthermore, Eqs. (3.21) and (3.22) are written as

$$\frac{d^2}{d\tilde{r}^2}\delta\tilde{P}_0^{(2)} + \frac{2}{\tilde{r}}\frac{d}{d\tilde{r}}\delta\tilde{P}_0^{(2)} + \frac{\tilde{\rho}'}{\tilde{p}'}\tilde{\rho}\delta\tilde{P}_0^{(2)} = 2\tilde{\Omega}^2, \tag{3.44}$$

$$\frac{d^2}{d\tilde{r}^2}\delta\tilde{P}_2^{(2)} + \frac{2}{\tilde{r}}\frac{d}{d\tilde{r}}\delta\tilde{P}_2^{(2)} + \left(\frac{\tilde{\rho}'}{\tilde{p}'}\tilde{\rho} - \frac{6}{\tilde{r}^2}\right)\delta\tilde{P}_2^{(2)} = 0, \tag{3.45}$$

where the prime with respect to normalized functions denotes differentiation with respect to $\tilde{r}$.

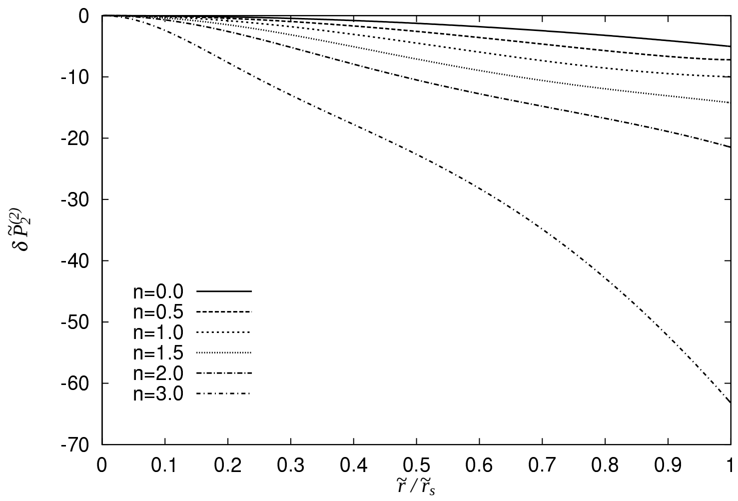

Figure 3.2: The function $\delta\tilde{P}_2^{(2)}$ plotted with respect to $\tilde{r}$.

3.1.2 Solutions for stellar configurations

Exterior solution

First, we consider the outside of the star. The gravitational potential terms $\Phi_0^{(2)}$ and $\Phi_2^{(2)}$ obey the following equations derived from Eqs. (3.15) and (3.16),

$$\frac{1}{r^2}\frac{d}{dr}\left(r^2\frac{d\Phi_0^{(2)}}{dr}\right) = 0, \tag{3.46}$$

$$\frac{1}{r^2}\frac{d}{dr}\left(r^2\frac{d\Phi_2^{(2)}}{dr}\right) - \frac{6}{r^2}\Phi_2^{(2)} = 0. \tag{3.47}$$

The solution which vanishes at infinity is given by

$$\tilde{\Phi}_0^{(2)} = \frac{c_{1\Phi}}{\tilde{r}}, \tag{3.48}$$

$$\tilde{\Phi}_2^{(2)} = \frac{d_{1\Phi}}{\tilde{r}^3}, \tag{3.49}$$

where $c_{1\Phi}$ and $d_{1\Phi}$ are constants. This exterior solution must be connected with an interior solution, using the junction conditions mentioned previously.

Interior solutions

Next, we discuss interior solutions. For $n = 0$, we can easily obtain the analytic expressions of $\delta\tilde{P}_0^{(2)}$ and $\delta\tilde{P}_2^{(2)}$. From Eqs. (3.44) and (3.45), we obtain the following solution which vanishes at the stellar center,

$$\begin{aligned}\delta\tilde{P}_0^{(2)} &= \frac{1}{3}\tilde{r}^2\tilde{\Omega}^2, && (3.50)\\ \delta\tilde{P}_2^{(2)} &= d_{2\Phi}\tilde{r}^2, && (3.51)\end{aligned}$$

where $d_{2\Phi}$ is a constant. From these expressions, we derive

$$\begin{aligned}\tilde{\Phi}_0^{(2)} &= c_{2\Phi}, && (3.52)\\ \tilde{\Phi}_2^{(2)} &= -\left(d_{2\Phi}+\frac{1}{3}\tilde{\Omega}^2\right)\tilde{r}^2 && (3.53)\end{aligned}$$

where we have used Eqs. (3.42) and (3.43). In this case, we have

$$\tilde{\Phi}_{\rm in}^{\prime\prime(0)} - \tilde{\Phi}_{\rm ext}^{\prime\prime(0)} = 1, \qquad (3.54)$$

$$\left(\frac{1}{\tilde{\rho}}\frac{d\tilde{p}}{d\tilde{r}}\right)^{-1} = -\frac{\sqrt{6}}{2}, \qquad (3.55)$$

$$\tilde{\xi}_0^{(2)} = \sqrt{6}\tilde{\Omega}^2, \quad \tilde{\xi}_2^{(2)} = 3\sqrt{6}d_{2\Phi}. \qquad (3.56)$$

Using these results, from the junction conditions (3.33) and (3.34), we derive the equations

$$\begin{aligned}\frac{c_{1\Phi}}{\sqrt{6}} - c_{2\Phi} &= 0, && (3.57)\\ \frac{c_{1\Phi}}{6} &= -\sqrt{6}\tilde{\Omega}^2, && (3.58)\end{aligned}$$

$$\begin{aligned}\frac{d_{1\Phi}}{6} + 6\sqrt{6}d_{2\Phi} &= -2\sqrt{6}\tilde{\Omega}^2, && (3.59)\\ \frac{d_{1\Phi}}{12} + \sqrt{6}d_{2\Phi} &= \frac{2\sqrt{6}}{3}\tilde{\Omega}^2. && (3.60)\end{aligned}$$

Therefore, we obtain

$$\begin{aligned}c_{1\Phi} &= -6\sqrt{6}\tilde{\Omega}^2, && (3.61)\\ c_{2\Phi} &= -6\tilde{\Omega}^2, && (3.62)\end{aligned}$$

$$\begin{aligned}d_{1\Phi} &= 18\sqrt{6}\tilde{\Omega}^2, && (3.63)\\ d_{2\Phi} &= -\frac{5}{6}\tilde{\Omega}^2. && (3.64)\end{aligned}$$

Consequently, we have

$$\delta\tilde{P}_0^{(2)} = \frac{1}{3}\tilde{r}^2\tilde{\Omega}^2, \qquad (3.65)$$

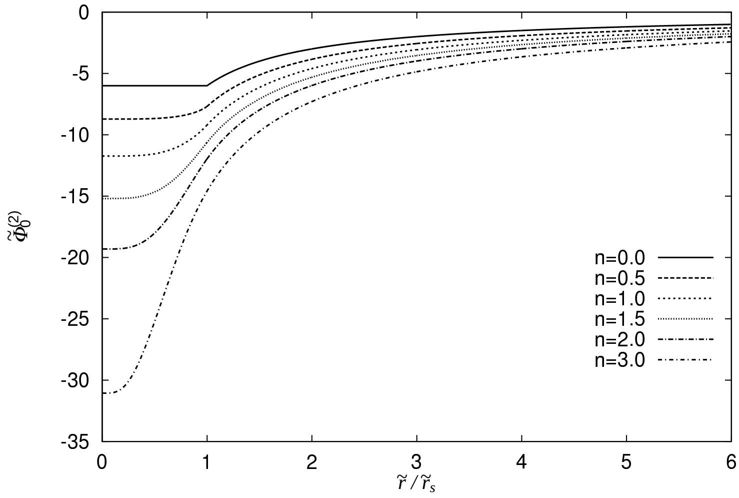

Figure 3.3: The potential $\tilde{\Phi}_0^{(2)}$ plotted as a function of $\tilde{r}$.

$$\delta\tilde{P}_2^{(2)} = -\frac{5}{6}\tilde{r}^2\tilde{\Omega}^2, \tag{3.66}$$

$$\tilde{\Phi}_0^{(2)} = \begin{cases} -6\tilde{\Omega}^2 & (\tilde{r} < \tilde{r}_{\rm s}) \\ -\frac{6\sqrt{6}}{\tilde{r}}\tilde{\Omega}^2 & (\tilde{r} > \tilde{r}_{\rm s}) \end{cases}, \tag{3.67}$$

$$\tilde{\Phi}_2^{(2)} = \begin{cases} \frac{1}{2}\tilde{\Omega}^2\tilde{r}^2 & (\tilde{r} < \tilde{r}_{\rm s}) \\ \frac{18\sqrt{6}}{\tilde{r}^3}\tilde{\Omega}^2 & (\tilde{r} > \tilde{r}_{\rm s}) \end{cases}, \tag{3.68}$$

$$\tilde{\xi}^{(2)} = \sqrt{6}\left(\tilde{\Omega}^2 - \frac{5}{2}\tilde{\Omega}^2 P_2\right). \tag{3.69}$$

Taking into account the last result (3.69), we can find the value of ellipticity as

$$\text{ellipticity} \equiv -\frac{3}{2}\frac{\xi_2^{(2)}}{R} = \frac{15}{4}\tilde{\Omega}^2 = \frac{5}{4}\frac{R^3\Omega^2}{M}, \tag{3.70}$$

where ellipticity is defined by the difference between the equatorial radius and the polar radius.

The other solutions can be obtained by numerical calculations. In general, the potentials can be written as

$$\tilde{\Phi}_0^{(2)} = \begin{cases} \frac{c_{1\Phi}}{\tilde{r}} & (\tilde{r} > \tilde{r}_{\rm s}) \\ -\delta\tilde{P}_0^{(2)} + \frac{1}{3}\tilde{r}^2\tilde{\Omega}^2 + c_{2\Phi} & (\tilde{r} < \tilde{r}_{\rm s}) \end{cases}, \tag{3.71}$$

$$\tilde{\Phi}_2^{(2)} = \begin{cases} \frac{d_{1\Phi}}{\tilde{r}^3} & (\tilde{r} > \tilde{r}_{\rm s}) \\ -d_{2\Phi}\delta\tilde{P}_2^{(2)\dagger} - \frac{1}{3}\tilde{r}^2\tilde{\Omega}^2 & (\tilde{r} < \tilde{r}_{\rm s}) \end{cases}, \tag{3.72}$$

where $c_{1\Phi}$, $c_{2\Phi}$, $d_{1\Phi}$ and $d_{2\Phi}$ are constants, and $\delta\tilde{P}_2^{(2)} = d_{2\Phi}\delta\tilde{P}_2^{(2)\dagger}$. From the junction conditions (3.33) and (3.34), we derive

$$-\frac{c_{1\Phi}}{\tilde{r}_{\rm s}} + c_{2\Phi} = \delta\tilde{P}_0^{(2)}(\tilde{r}_{\rm s}) - \frac{1}{3}\tilde{r}_{\rm s}^2\tilde{\Omega}^2, \tag{3.73}$$

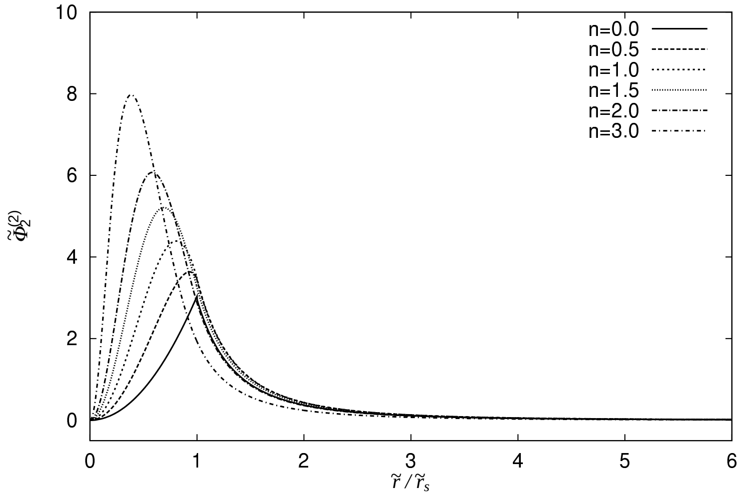

Figure 3.4: The potential $\tilde{\Phi}_2^{(2)}$ plotted as a function of $\tilde{r}$.

$$\frac{c_{1\Phi}}{\tilde{r}_s^2} = \delta\tilde{P}_0^{\prime(2)}(\tilde{r}_s) - \frac{2}{3}\tilde{r}_s\tilde{\Omega}^2 - \tilde{\xi}_0^{(2)}A, \tag{3.74}$$

$$\frac{d_{1\Phi}}{\tilde{r}_s^3} + \delta\tilde{P}_2^{(2)\dagger}(\tilde{r}_s)d_{2\Phi} = -\frac{1}{3}\tilde{r}_s^2\tilde{\Omega}^2, \tag{3.75}$$

$$\frac{3}{\tilde{r}_s^4}d_{1\Phi} + \left[-\delta\tilde{P}_2^{\prime(2)\dagger}(\tilde{r}_s) + \tilde{\xi}_2^{(2)\dagger}A\right]d_{2\Phi} = \frac{2}{3}\tilde{r}_s\tilde{\Omega}^2, \tag{3.76}$$

where

$$\xi_0^{(2)} = -\left(\frac{1}{\rho}\frac{dp}{dr}\right)^{-1}\delta P_0^{(2)}\Bigg|_{\xi^{(0)}}, \tag{3.77}$$

$$\xi_2^{(2)\dagger} = -\left(\frac{1}{\rho}\frac{dp}{dr}\right)^{-1}\delta P_2^{(2)\dagger}\Bigg|_{\xi^{(0)}}, \tag{3.78}$$

$$A = \left(\tilde{\Phi}_{\rm in}^{\prime\prime(0)} - \tilde{\Phi}_{\rm ext}^{\prime\prime(0)}\right)\Big|_{\xi^{(0)}}. \tag{3.79}$$

Therefore, we obtain

$$c_{1\Phi} = \tilde{r}_s^2\left[\delta\tilde{P}_0^{\prime(2)}(\tilde{r}_s) - \frac{2}{3}\tilde{r}_s\tilde{\Omega}^2 - \tilde{\xi}_0^{(2)}A\right], \tag{3.80}$$

$$c_{2\Phi} = \delta\tilde{P}_0^{(2)}(\tilde{r}_s) + \tilde{r}_s\delta\tilde{P}_0^{\prime(2)}(\tilde{r}_s) - \tilde{r}_s^2\tilde{\Omega}^2 - \tilde{r}_s\tilde{\xi}_0^{(2)}A, \tag{3.81}$$

$$d_{1\Phi} = \frac{\tilde{r}_s^5\left[2\delta\tilde{P}_2^{(2)\dagger}(\tilde{r}_s) - \tilde{r}_s\delta\tilde{P}_2^{\prime(2)\dagger}(\tilde{r}_s) + \tilde{r}_s\tilde{\xi}_2^{(2)\dagger}A\right]\tilde{\Omega}^2}{3\left[3\delta\tilde{P}_2^{(2)\dagger}(\tilde{r}_s) + \tilde{r}_s\delta\tilde{P}_2^{\prime(2)\dagger}(\tilde{r}_s) - \tilde{r}_s\tilde{\xi}_2^{(2)\dagger}A\right]}, \tag{3.82}$$

$$d_{2\Phi} = -\frac{5\tilde{r}_s^2\tilde{\Omega}^2}{3\left[3\delta\tilde{P}_2^{(2)\dagger}(\tilde{r}_s) + \tilde{r}_s\delta\tilde{P}_2^{\prime(2)\dagger}(\tilde{r}_s) - \tilde{r}_s\tilde{\xi}_2^{(2)\dagger}A\right]}. \tag{3.83}$$

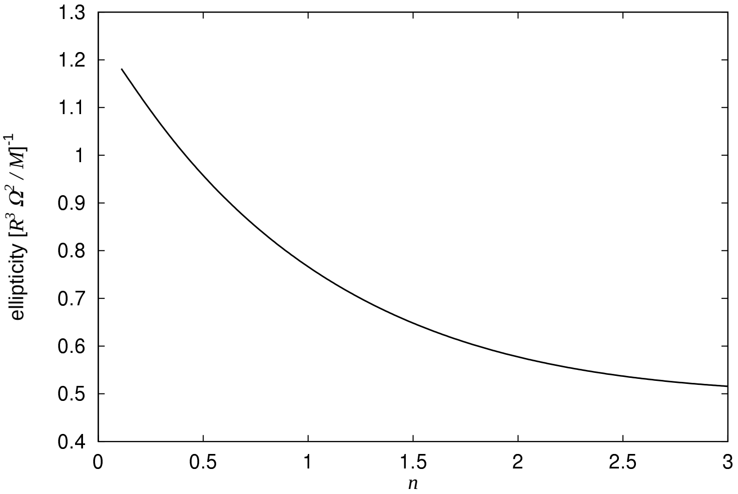

Figure 3.5: Dependence of ellipticity on the polytropic index n.

Using these expressions, we can obtain solutions for $\delta P_0^{(2)}$, $\delta P_2^{(2)}$, $\Phi_0^{(0)}$ and $\Phi_2^{(0)}$ numerically. We show these functions for several polytropic models in Figs. 3.1, 3.2, 3.3 and 3.4.

The ellipticity of the star can be derived in the same way as Eq. (3.70),

$$\text{ellipticity} = -\frac{3}{2}\frac{\xi_2^{(2)}}{R} = -\frac{3}{2}\frac{\tilde{\xi}_2^{(2)}\tilde{m}(\tilde{r}_{\rm s})}{\tilde{r}_{\rm s}^4\tilde{\Omega}^2}\frac{R^3\Omega^2}{M}. \tag{3.84}$$

We show dependence of ellipticity on the polytropic index n in Fig. 3.5. We find that the value of ellipticity becomes small as the polytropic index n becomes large for fixed $R^3\Omega^2/M$.

3.2 General relativistic stars

3.2.1 Formulation

Next, we discuss rotating, general relativistic stars. The basic procedure is almost the same as in the Newtonian case. However, a different point from the Newtonian case arises in the general relativistic case. In the context of general relativity, rotating objects induce dragging of inertial frames. Hence, there is some change about stellar deformation from the Newtonian case, owing to this effect. We investigate stellar deformation, in particular concentrating on the general relativistic effect.

Frame dragging

First, we consider frame dragging due to a rotating, spherically symmetric star. We now assume that the star slowly rotates with uniform angular velocity Ω. The metric can be written in the form

$$ds^2 = -e^{\nu}[dt - \omega(r)d\phi]^2 + e^{\lambda}dr^2 + r^2\left(d\theta^2 + \sin^2\theta d\phi^2\right), \tag{3.85}$$

where the function ω is of the same order as Ω and causes frame dragging. The equation which ω obeys can be obtained from the (t,ϕ)-component of the Einstein equation Eq. (2.49),

$$\frac{d^2}{dr^2}\varpi + \left(\frac{4}{r} - \frac{\mathcal{J}'}{\mathcal{J}}\right)\frac{d}{dr}\varpi + \frac{4\mathcal{J}'}{r\mathcal{J}}\varpi = 0, \tag{3.86}$$

where ϖ and $\mathcal{J}$ are defined, respectively, as

$$\begin{aligned} \varpi &= \Omega - \omega, & (3.87) \\ \mathcal{J} &= e^{-\frac{\nu+\lambda}{2}}. & (3.88) \end{aligned}$$

Here, Ω is written as

$$\Omega = \frac{d\phi}{dt} = \frac{\frac{d\phi}{d\tau}}{\frac{dt}{d\tau}} = \frac{u^{\phi}}{u^{t}}, \tag{3.89}$$

where u^{μ} denotes four-velocity of fluid.

Outside the star, the solution for ϖ can easily be derived. Since we have $\nu' + \lambda' = 0$ outside the star, we find

$$\varpi = \Omega - \frac{2J}{r^3}. \tag{3.90}$$

Here, J corresponds to the angular momentum of the star [126]. This exterior solution must be connected smoothly with an interior solution, which is obtained later.

Stellar deformation

Now, we formulate a relativistic star deformed by rotation. The space-time can be described by the line element [110]

$$\begin{aligned} ds^2 &= -e^{\nu}\left[1 + 2\left(h_0(r) + h_2(r)P_2\right)\right]dt^2 + e^{\lambda}\left[1 + \frac{2e^{\lambda}}{r}\left(m_0(r) + m_2(r)P_2\right)\right]dr^2 \\ &\quad + r^2\left(1 + 2k_2(r)\right)\left[d\theta^2 + \sin^2\theta\left(d\phi - \omega dt\right)^2\right], \end{aligned} \tag{3.91}$$

where h_0, h_2, m_0, m_2 and k_2 are functions of second order in ε_{Ω}.

The stress-energy tensor of the star made of perfect fluid has the form

$$T^{\mu}_{\ \nu} = (\rho + p)\, u^{\mu}u_{\nu} + p\delta^{\mu}_{\ \nu}, \tag{3.92}$$

where the density ρ and the pressure p are expanded in the same way as in the Newtonian case,

$$\begin{aligned} \rho &= \rho^{(0)} + \left[\rho_0^{(2)} + \rho_2^{(2)} P_2\right], && (3.93) \\ p &= p^{(0)} + \left[p_0^{(2)} + p_2^{(2)} P_2\right]. && (3.94) \end{aligned}$$

Up to second order in ε_Ω, the non-vanishing components of four-velocity have the forms

$$\begin{aligned} u^t &= e^{-\frac{\nu}{2}} \left[1 - (h_0 + h_2 P_2)\right] + \frac{1}{2} e^{-\frac{3}{2}\nu} r^2 \sin^2\theta \varpi^2, && (3.95) \\ u^\phi &= \Omega u^t. && (3.96) \end{aligned}$$

The basic equations of equilibrium configurations can be obtained from the Einstein equation (2.49) and the equation of motion (2.50) using the above quantities. First, from Eq. (2.50), we obtain the equations

$$\begin{aligned} \frac{1}{\rho + p} \frac{dp_0^{(2)}}{dr} &= -\frac{\nu'}{2(\rho + p)} \left(\frac{\rho'}{p'} + 1\right) p_0^{(2)} - \frac{dh_0}{dr} + \frac{d}{dr}\left(\frac{1}{3} r^2 e^{-\nu} \varpi^2\right), && (3.97) \\ \frac{1}{\rho + p} \frac{dp_2^{(2)}}{dr} &= -\frac{\nu'}{2(\rho + p)} \left(\frac{\rho'}{p'} + 1\right) p_2^{(2)} - \frac{dh_2}{dr} - \frac{d}{dr}\left(\frac{1}{3} r^2 e^{-\nu} \varpi^2\right), && (3.98) \end{aligned}$$

$$\frac{p_2^{(2)}}{\rho + p} = -h_2 - \frac{1}{3} r^2 e^{-\nu} \varpi^2, \tag{3.99}$$

where the superscript "(0)" is abbreviated. When we recall Eq. (2.53), Eqs. (3.97) and (3.98) are integrated to give Eq. (3.99) and

$$\frac{p_0^{(2)}}{\rho + p} = -h_0 + \frac{1}{3} r^2 e^{-\nu} \varpi^2 + \text{const.} \tag{3.100}$$

As in the Newtonian case, it is useful to introduce $\delta P_0^{(2)}$ and $\delta P_2^{(2)}$ defined by

$$\begin{aligned} \delta P_0^{(2)} &= \frac{p_0^{(2)}}{\rho + p}, && (3.101) \\ \delta P_2^{(2)} &= \frac{p_2^{(2)}}{\rho + p}. && (3.102) \end{aligned}$$

Using these quantities, we have

$$\begin{aligned} \delta P_0^{(2)} &= -h_0 + \frac{1}{3} r^2 e^{-\nu} \varpi^2 + \text{const}, && (3.103) \\ \delta P_2^{(2)} &= -h_2 - \frac{1}{3} r^2 e^{-\nu} \varpi^2. && (3.104) \end{aligned}$$

These relations correspond to Eq. (3.9) and (3.14) in the Newtonian case.

Furthermore, we can obtain the following equations from Eq. (2.49),

$$\begin{aligned}\frac{dm_0}{dr} &= 4\pi r^2\left(\rho+p\right)\frac{\rho'}{p'}\delta P_0^{(2)}\\ &\quad +\frac{1}{12}r^4e^{-(\nu+\lambda)}\varpi'^2+\frac{1}{3}r^3\left(\nu'+\lambda'\right)e^{-(\nu+\lambda)}\varpi^2,\end{aligned}\tag{3.105}$$

$$\begin{aligned}\frac{d\delta P_0^{(2)}}{dr} &= -\left(\frac{1}{r^2}+\frac{\nu'}{r}\right)e^{\lambda}m_0-4\pi r\left(\rho+p\right)e^{\lambda}\delta P_0^{(2)}+\frac{2}{3}re^{-\nu}\varpi^2\\ &\quad -\frac{1}{3}r^2\nu'e^{-\nu}\varpi^2+\frac{2}{3}r^2e^{-\nu}\varpi\varpi'+\frac{1}{12}r^3e^{-\nu}\varpi'^2,\end{aligned}\tag{3.106}$$

$$\frac{d}{dr}\left(h_2+k_2\right) = \left(\frac{1}{r}-\frac{\nu'}{2}\right)h_2+\frac{e^{\lambda}}{r}\left(\frac{1}{r}+\frac{\nu'}{2}\right)m_2,\tag{3.107}$$

$$h_2+\frac{e^{\lambda}}{r}m_2 = \frac{1}{6}r^4e^{-(\nu+\lambda)}\varpi'^2-\frac{1}{3}r^3\left(e^{-(\nu+\lambda)}\right)'\varpi^2,\tag{3.108}$$

$$\begin{aligned}\frac{dh_2}{dr}+\left(\frac{r\nu'}{2}+1\right)\frac{dk_2}{dr} &= 4\pi re^{\lambda}\left(\rho+p\right)\delta P_0^{(2)}+\left(\frac{1}{r^2}+\frac{\nu'}{r}\right)e^{\lambda}m_2\\ &\quad +\frac{3}{r}e^{\lambda}h_2+\frac{2}{r}e^{\lambda}k_2+\frac{1}{12}r^3e^{-\nu}\varpi'^2.\end{aligned}\tag{3.109}$$

Here, it is convenient to introduce the function υ_2 defined as

$$\upsilon_2 \equiv h_2+k_2.\tag{3.110}$$

Using this, from Eqs. (3.107), (3.108) and (3.109), we obtain a couple of equations

$$\frac{d\upsilon_2}{dr} = -\nu'h_2+\left(\frac{1}{r}+\frac{\nu'}{2}\right)\left[\frac{1}{6}r^4e^{-(\nu+\lambda)}\varpi'^2+\frac{1}{3}r^3\left(\nu'+\lambda'\right)e^{-(\nu+\lambda)}\varpi^2\right],\tag{3.111}$$

$$\begin{aligned}\frac{dh_2}{dr} &= -\frac{4e^{\lambda}}{r^2\nu'}\upsilon_2+\left[8\pi\frac{e^{\lambda}}{\nu'}\left(\rho+p\right)+\frac{2}{r^2\nu'}\left(1-e^{\lambda}\right)-\nu'\right]h_2\\ &\quad +\frac{1}{6}\left(\frac{r\nu'}{2}-\frac{e^{\lambda}}{r\nu'}\right)r^3e^{-(\nu+\lambda)}\varpi'^2+\frac{1}{3}\left(\frac{r\nu'}{2}+\frac{e^{\lambda}}{r\nu'}\right)r^2\left(\nu'+\lambda'\right)e^{-(\nu+\lambda)}\varpi^2.\end{aligned}\tag{3.112}$$

Therefore, we have to solve two sets of equations (3.105)-(3.106) and (3.111)-(3.112) for the four unknown functions m_0, $\delta P_0^{(2)}$, υ_2 and k_2. The other functions, i.e. h_0, $\delta P_2^{(2)}$, m_2 and k_2 can be derived from Eqs. (3.103), (3.104), (3.108) and (3.110), respectively. However, outside the star, we have the following equations in place of the set of equations (3.105)-(3.106),

$$\frac{dm_0}{dr} = \frac{1}{12}r^4\varpi'^2,\tag{3.113}$$

$$\frac{dh_0}{dr} = \frac{1}{(r-2M)^2}m_0-\frac{r^4}{12(r-2M)}\varpi'^2,\tag{3.114}$$

since $\delta P_0^{(2)}$ is meaningless in this case.

Boundary and junction conditions

Solutions for the metric functions can be obtained by imposing boundary and junction conditions. These are summarized as follows:

- $r \to \infty$

$$\begin{aligned} h_0, h_2 &\to 0, && (3.115) \\ m_0, m_2 &\to \text{finite}, && (3.116) \\ k_2, \omega &\to \frac{1}{r^\alpha} \quad (\alpha \geq 3)\,, && (3.117) \end{aligned}$$

- $r = R$

$$\begin{aligned} g_{\mu\nu}|_{-\xi} &= g_{\mu\nu}|_{+\xi} \quad (\mu, \nu = t, r, \theta, \phi)\,, && (3.118) \\ g_{ab,r}|_{-\xi} &= g_{ab,r}|_{+\xi} \quad (a, b = t, \theta, \phi)\,, && (3.119) \end{aligned}$$

- $r \to 0$

$$\begin{aligned} \omega, h_0, \delta P_0^{(2)} &\to \text{finite}, && (3.120) \\ m_0, m_2, h_2, v_2 &\to 0. && (3.121) \end{aligned}$$

The conditions for the limit $r \to 0$ can be seen by taking Taylor expansions about the stellar center.

Concerning the conditions (3.118) and (3.119), a similar situation to the Newtonian case arises when $n = 0$. This stems from the fact that ν'' and λ' are discontinuous in the case of $n = 0$. Now, we have

$$\begin{aligned} g_{rr}|_\xi &= e^\lambda\Big|_{\xi^{(0)}} + \left[\lambda' e^\lambda\Big|_{\xi^{(0)}} \xi^{(2)} + \frac{2e^{2\lambda}}{r} m\Bigg|_{\xi^{(0)}}\right], && (3.122) \\ g_{tt,r}|_\xi &= \nu' e^\nu|_{\xi^{(0)}} + \left[\left(\nu'' + \nu'^2\right) e^\nu\Big|_{\xi^{(0)}} \xi^{(2)} + 2e^\nu \left(\nu' h + h'\right)|_{\xi^{(0)}}\right], && (3.123) \end{aligned}$$

where m and h are given by

$$\begin{aligned} m &= m_0 + m_2 P_2, && (3.124) \\ h &= h_0 + h_2 P_2. && (3.125) \end{aligned}$$

Hence, from the conditions (3.118) and (3.119), we derive

$$\left(\lambda'_{\text{in}} - \lambda'_{\text{ext}}\right)|_{\xi^{(0)}} \xi_a^{(2)} + \frac{2e^\lambda}{r} \left(m_{a\,\text{in}} - m_{a\,\text{ext}}\right)\Bigg|_{\xi^{(0)}} = 0, \quad (3.126)$$

$$\left(\nu''_{\text{in}} - \nu''_{\text{ext}}\right)|_{\xi^{(0)}} \xi_a^{(2)} + 2\left(h'_{a\,\text{in}} - h'_{a\,\text{ext}}\right)|_{\xi^{(0)}} = 0, \quad (3.127)$$

where a takes 0 or 2. In the general relativistic case, $\xi_0^{(2)}$ and $\xi_2^{(2)}$ are given, respectively, by

$$\xi_0^{(2)} = -\left(\frac{1}{\rho+p}\frac{dp}{dr}\right)^{-1}\delta P_0^{(2)}, \tag{3.128}$$

$$\xi_2^{(2)} = -\left(\frac{1}{\rho+p}\frac{dp}{dr}\right)^{-1}\delta P_2^{(2)}. \tag{3.129}$$

From Eqs. (3.126) and (3.127), in the case of $n=0$, we see that m_0 and m_2 are discontinuous, and that h_0 and h_2 are not smooth at the surface. On the other hand, in the cases of $n \neq 0$, the metric functions m_0 and m_2 are connected continuously, and h_0 and h_2 are connected smoothly at the surface along with ω and k_2.

Normalized equations

Next, we consider the normalization of the above equations. Note that the metric functions h_0, h_2 and k_2 are dimensionless, while m_0 and m_2 have the same dimension as mass. Hence, we normalize m_0 and m_2 as

$$m_0 = m_*\tilde{m}_0, \quad m_2 = m_*\tilde{m}_2. \tag{3.130}$$

Furthermore, we can write

$$\varpi = \Omega_*\tilde{\varpi}. \tag{3.131}$$

Using these quantities, we derive

$$\begin{aligned}\frac{d\tilde{m}_0}{d\tilde{r}} &= \tilde{r}^2\left(\tilde{\rho}+\zeta\tilde{p}\right)\frac{\tilde{\rho}'}{\tilde{p}'}\delta\tilde{P}_0^{(2)} \\ &\quad +\frac{1}{12}\tilde{r}^4 e^{-(\nu+\lambda)}\tilde{\varpi}'^2+\frac{1}{3}\tilde{r}^3\left(\nu'+\lambda'\right)e^{-(\nu+\lambda)}\tilde{\varpi}^2, \end{aligned}\tag{3.132}$$

$$\begin{aligned}\frac{d\delta\tilde{P}_0^{(2)}}{d\tilde{r}} &= -\left(\frac{1}{\tilde{r}^2}+\frac{\nu'}{\tilde{r}}\right)e^{\lambda}\tilde{m}_0-\zeta\tilde{r}\left(\tilde{\rho}+\tilde{p}\right)e^{\lambda}\delta\tilde{P}_0^{(2)}+\frac{2}{3}\tilde{r}e^{-\nu}\tilde{\varpi}^2 \\ &\quad -\frac{1}{3}\tilde{r}^2\nu' e^{-\nu}\tilde{\varpi}^2+\frac{2}{3}\tilde{r}^2 e^{-\nu}\tilde{\varpi}\tilde{\varpi}'+\frac{1}{12}\tilde{r}^3 e^{-\nu}\tilde{\varpi}'^2, \end{aligned}\tag{3.133}$$

$$\frac{dv_2}{d\tilde{r}} = -\nu' h_2+\zeta\left(\frac{1}{\tilde{r}}+\frac{\nu'}{2}\right)\left[\frac{1}{6}\tilde{r}^4 e^{-(\nu+\lambda)}\tilde{\varpi}'^2+\frac{1}{3}\tilde{r}^3\left(\nu'+\lambda'\right)e^{-(\nu+\lambda)}\tilde{\varpi}^2\right], \tag{3.134}$$

$$\begin{aligned}\frac{dh_2}{d\tilde{r}} &= -\frac{4e^{\lambda}}{\tilde{r}^2\nu'}v_2+\left[2\zeta\frac{e^{\lambda}}{\nu'}\left(\tilde{\rho}+\zeta\tilde{p}\right)+\frac{2}{\tilde{r}^2\nu'}\left(1-e^{\lambda}\right)-\nu'\right]h_2 \\ &\quad +\frac{\zeta}{6}\left(\frac{\tilde{r}\nu'}{2}-\frac{e^{\lambda}}{\tilde{r}\nu'}\right)\tilde{r}^3 e^{-(\nu+\lambda)}\tilde{\varpi}'^2+\frac{\zeta}{3}\left(\frac{\tilde{r}\nu'}{2}+\frac{e^{\lambda}}{\tilde{r}\nu'}\right)\tilde{r}^2\left(\nu'+\lambda'\right)e^{-(\nu+\lambda)}\tilde{\varpi}^2, \end{aligned}\tag{3.135}$$

$$\zeta\delta\tilde{P}_0^{(2)} = -h_0+\frac{\zeta}{3}\tilde{r}^2 e^{-\nu}\tilde{\varpi}^2+\text{const}, \tag{3.136}$$

$$\zeta\delta\tilde{P}_2^{(2)} = -h_2-\frac{\zeta}{3}\tilde{r}^2 e^{-\nu}\tilde{\varpi}^2, \tag{3.137}$$

$$\zeta \tilde{m}_2 = \tilde{r} e^{-\lambda} \left[-h_2 + \frac{\zeta}{6} \tilde{r}^4 e^{-(\nu+\lambda)} \tilde{\varpi}'^2 + \frac{\zeta}{3} \tilde{r}^3 \left(\nu' + \lambda' \right) e^{-(\nu+\lambda)} \tilde{\varpi}^2 \right]. \tag{3.138}$$

Furthermore, outside the stars, we have

$$\frac{d\tilde{m}_0}{d\tilde{r}} = \frac{1}{12} \tilde{r}^4 \tilde{\varpi}'^2, \tag{3.139}$$

$$\frac{dh_0}{d\tilde{r}} = \frac{\zeta}{(\tilde{r} - 2\zeta \tilde{M})^2} \tilde{m}_0 - \frac{\zeta \tilde{r}^4}{12(\tilde{r} - 2\zeta \tilde{M})} \tilde{\varpi}'^2. \tag{3.140}$$

The junction conditions are written as

$$\left(\lambda'_{\text{in}} - \lambda'_{\text{ext}}\right)\big|_{\tilde{\xi}^{(0)}} \tilde{\xi}_a^{(2)} + \frac{2\zeta e^{\lambda}}{\tilde{r}} \left(\tilde{m}_{a\,\text{in}} - \tilde{m}_{a\,\text{ext}} \right)\Big|_{\tilde{\xi}^{(0)}} = 0, \tag{3.141}$$

$$\left(\nu''_{\text{in}} - \nu''_{\text{ext}}\right)\big|_{\tilde{\xi}^{(0)}} \tilde{\xi}_a^{(2)} + 2\left(h'_{a\,\text{in}} - h'_{a\,\text{ext}} \right)\big|_{\tilde{\xi}^{(0)}} = 0. \tag{3.142}$$

Moreover, we have

$$\tilde{\xi}_0^{(2)} = -\left(\frac{1}{\tilde{\rho} + \zeta \tilde{p}} \frac{d\tilde{p}}{d\tilde{r}} \right)^{-1} \delta \tilde{P}_0^{(2)}, \tag{3.143}$$

$$\tilde{\xi}_2^{(2)} = -\left(\frac{1}{\tilde{\rho} + \zeta \tilde{p}} \frac{d\tilde{p}}{d\tilde{r}} \right)^{-1} \delta \tilde{P}_2^{(2)}. \tag{3.144}$$

In these normalized equations, the prime denotes differentiation with respect to $\tilde{r}$.

3.2.2 Solutions for stellar configurations

The first-order function ϖ and the moment of inertia

First, we have to derive solutions for ϖ, which are needed to find the second-order quantities in ε_Ω. In Fig. 3.6, we show numerical interior solutions for ϖ connected with the exterior solution (3.90). These have been obtained for several polytropic stellar models with $M/R = 0.2$. The values of the angular momentum J and the angular velocity Ω can be obtained by using the relations

$$J = \frac{1}{6} R^4 \varpi'(R), \tag{3.145}$$

$$\Omega = \varpi(R) + \frac{1}{3} R \varpi'(R). \tag{3.146}$$

Once we know J from the solutions for ω, we can derive the values of the moment of inertia I of the spherically symmetric star with respect to the rotation axis in the way

$$I = \frac{J}{\Omega} = \sqrt{\frac{p_{\text{c}}^3}{(4\pi \rho_{\text{c}}^2)^3}} \frac{\tilde{J}}{\tilde{\Omega}} = \frac{m_* r_*^2}{\zeta} \frac{\tilde{J}}{\tilde{\Omega}} = \frac{\tilde{J}/\tilde{\Omega}}{\zeta \tilde{m}(\tilde{r}_{\text{s}}) \tilde{r}_{\text{s}}^2} M R^2. \tag{3.147}$$

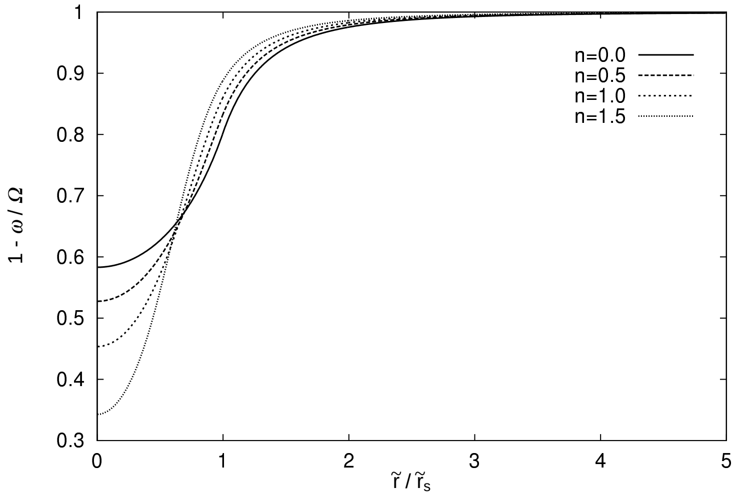

Figure 3.6: The function ϖ normalized by Ω, which is plotted as a function of $\tilde{r}$ for stellar models with $M/R = 0.2$.

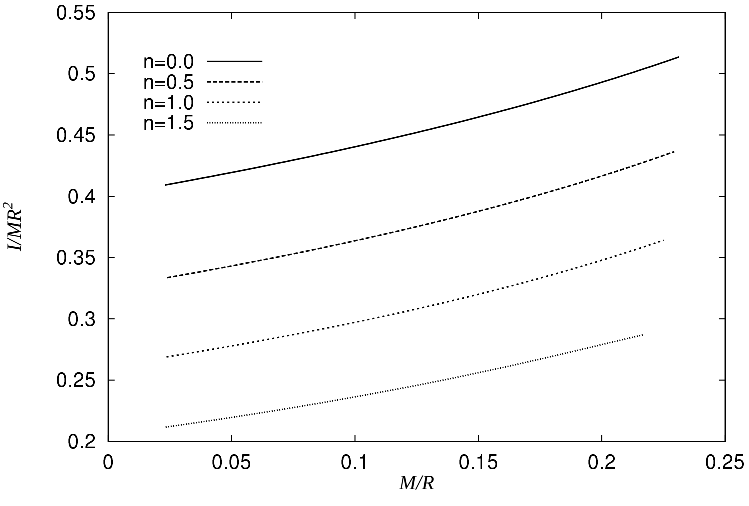

Figure 3.7: The moment of inertia I, which is plotted as a function of M/R and normalized by MR^2.

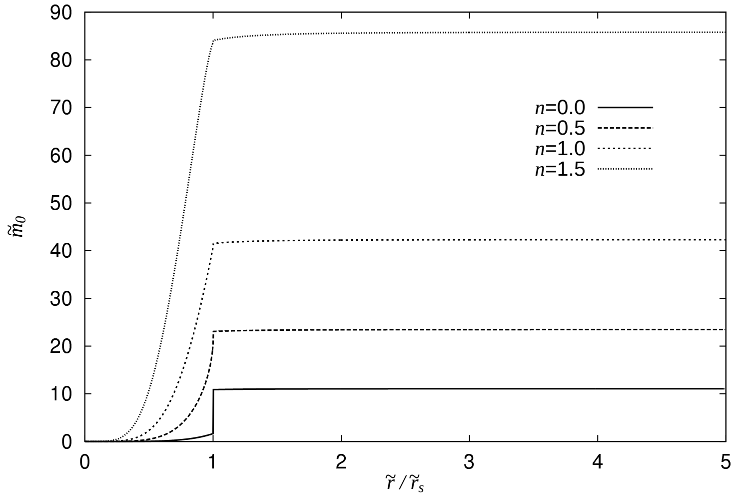

Figure 3.8: The function $\tilde{m}_0(\tilde{r})$ under the boundary condition $\delta P_0^{(2)}(0) = 0$. Stellar models with $M/R = 0.2$ are adopted here.

Here, J has been normalized as

$$J = J_* \tilde{J}, \quad J_* = \sqrt{\frac{p_c^3}{16\pi^2 \rho_c^5}}. \tag{3.148}$$

Figure 3.7 displays the moment of inertia I as a function of M/R. From this figure, we can find that the values of the moment of inertia become large with the general relativistic factor M/R for each polytropic index n.

The functions m_0, $\delta P_0^{(2)}$ and h_0

Now, we discuss the second-order functions in ε_Ω. The exterior solution for $\tilde{m}_0$ and $\tilde{h}_0$ can be obtained from Eqs. (3.139) and (3.140) as

$$\tilde{m}_0 = -\frac{\tilde{J}^2}{\tilde{r}^3} + c_{\rm m}, \tag{3.149}$$

$$h_0 = \frac{\zeta \tilde{J}^2}{\tilde{r}^3 \left(\tilde{r} - 2\zeta \tilde{m}(\tilde{r}_{\rm s})\right)} - \frac{\zeta c_{\rm m}}{\tilde{r} - 2\zeta \tilde{m}(\tilde{r}_{\rm s})}, \tag{3.150}$$

where we have here imposed the condition in which h_0 must vanish at infinity. The remaining constant $c_{\rm m}$ corresponds to mass shift and should be fixed by the junction condition at the stellar surface.

In Figs. 3.8, 3.9 and 3.10, we show numerical results for $\tilde{m}_0$, $\delta\tilde{P}_0^{(2)}$ and h_0. These have been obtained by using the condition in which $\delta P_0^{(2)}$ vanishes at the stellar center. The imposition

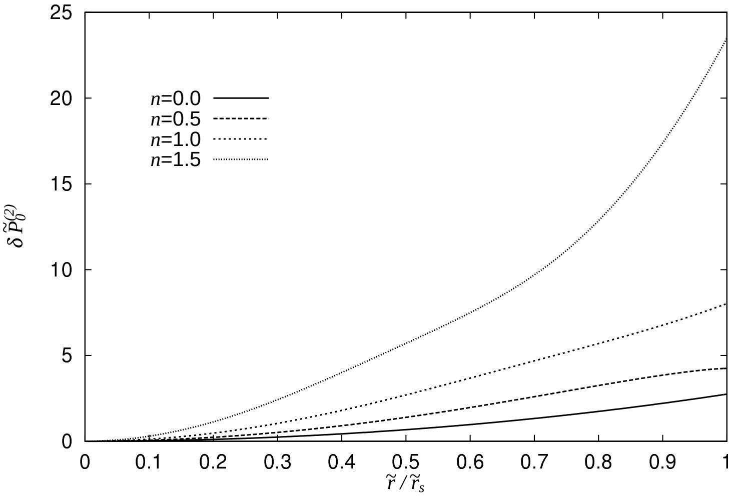

Figure 3.9: The function $\delta\tilde{P}_0^{(2)}(\tilde{r})$ under the boundary condition $\delta P_0^{(2)}(0) = 0$. Stellar models with $M/R = 0.2$ are adopted here.

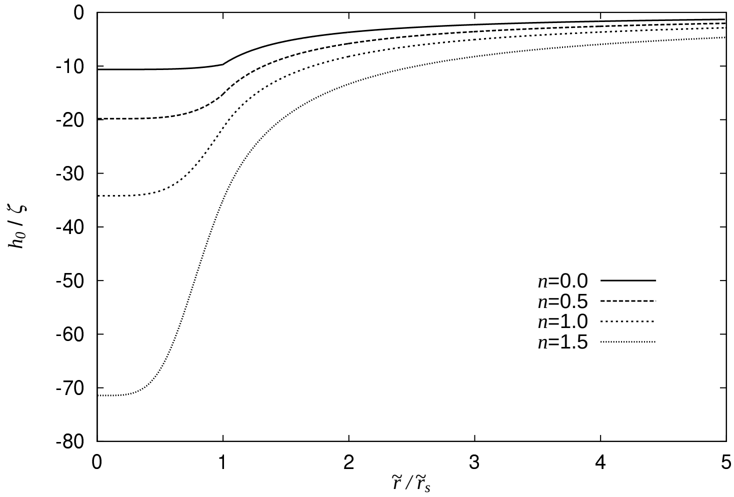

Figure 3.10: The function $h_0(\tilde{r})$ under the boundary condition $\delta P_0^{(2)}(0) = 0$. Stellar models with $M/R = 0.2$ are adopted here.

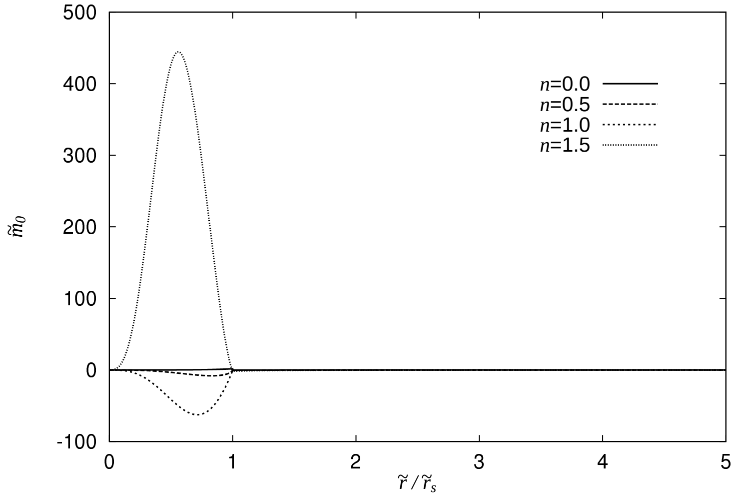

Figure 3.11: The function $\tilde{m}_0(\tilde{r})$ in the case of vanishing mass shift. Stellar models with $M/R = 0.2$ are adopted here.

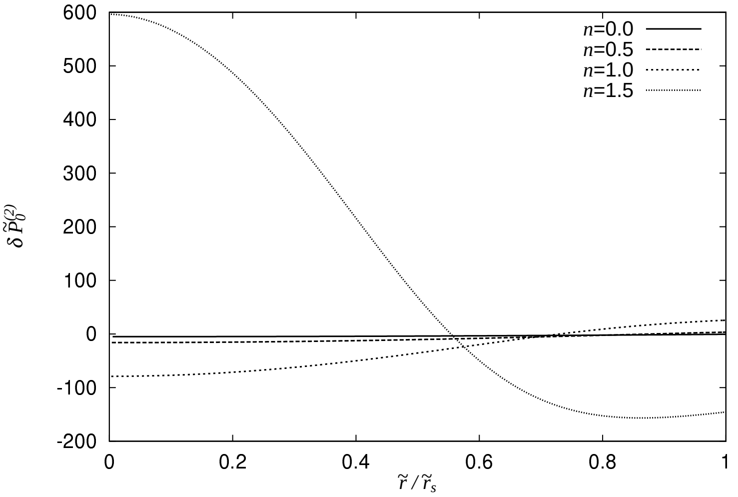

Figure 3.12: The function $\delta\tilde{P}_0^{(2)}(\tilde{r})$ in the case of vanishing mass shift. Stellar models with $M/R = 0.2$ are adopted here.

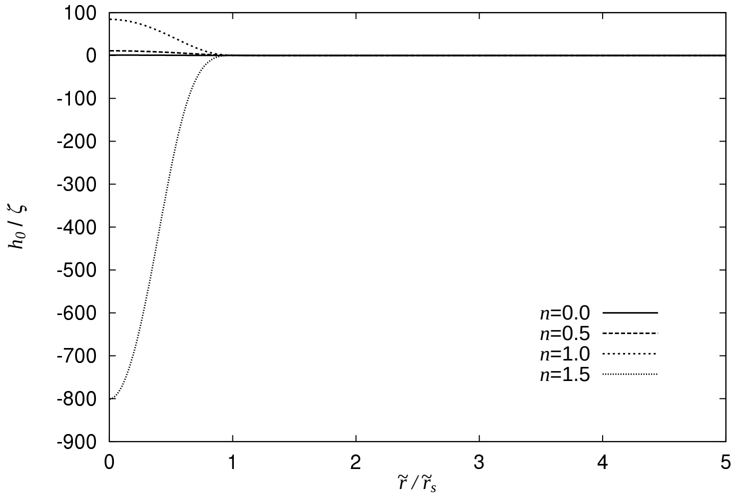

Figure 3.13: The function $h_0(\tilde{r})$ in the case of vanishing mass shift. Stellar models with $M/R = 0.2$ are adopted here.

of this condition corresponds to seeing the sequences of stars with the same central density. In this case, the mass shift c_m is determined at the stellar surface in the way

$$c_\mathrm{m} = \tilde{m}_{0\mathrm{s}} + \frac{\tilde{J}^2}{\tilde{r}_\mathrm{s}^3} + \frac{\tilde{r} e^{-\lambda}}{2\zeta} A_\lambda \tilde{\xi}_0^{(2)}, \tag{3.151}$$

where $\tilde{m}_{0\mathrm{s}}$ is the surface value of $\tilde{m}_0$, which can be derived by numerical integration from the stellar center, and A_λ is defined as

$$A_\lambda = (\lambda'_\mathrm{in} - \lambda'_\mathrm{ext})|_{\xi^{(0)}} \,. \tag{3.152}$$

We further note that h_0/ζ exactly corresponds to $\tilde{\Phi}_0^{(2)}$ in the Newtonian case (see Fig. 3.3).

Furthermore, we show the other numerical results for $\tilde{m}_0$, $\delta\tilde{P}_0^{(2)}$ and h_0 in Figs. 3.11, 3.12 and 3.13. These have been obtained in the case of vanishing mass shift, i.e. $c_\mathrm{m} = 0$. In this case, an interior solution can be written as

$$\tilde{m}_0 = c_0 \tilde{m}_{0\mathrm{H}} + \tilde{m}_{0\mathrm{P}}, \tag{3.153}$$

$$\delta\tilde{P}_0^{(2)} = c_0 \delta\tilde{P}_{0\mathrm{H}}^{(2)} + \delta\tilde{P}_{0\mathrm{P}}^{(2)}, \tag{3.154}$$

where the subscripts 'H' and 'P' denote homogeneous and particular solutions respectively, and c_0 is a constant. We can also express $\tilde{\xi}_0^{(2)}$ as

$$\tilde{\xi}_0^{(2)} = c_0 \tilde{\xi}_{0\mathrm{H}}^{(2)} + \tilde{\xi}_{0\mathrm{P}}^{(2)}, \tag{3.155}$$

where

$$\tilde{\xi}_{0\mathrm{H}}^{(2)} = -\left(\frac{1}{\tilde{\rho} + \zeta\tilde{p}} \frac{d\tilde{p}}{d\tilde{r}}\right)^{-1} \delta\tilde{P}_{0\mathrm{H}}^{(2)}, \tag{3.156}$$

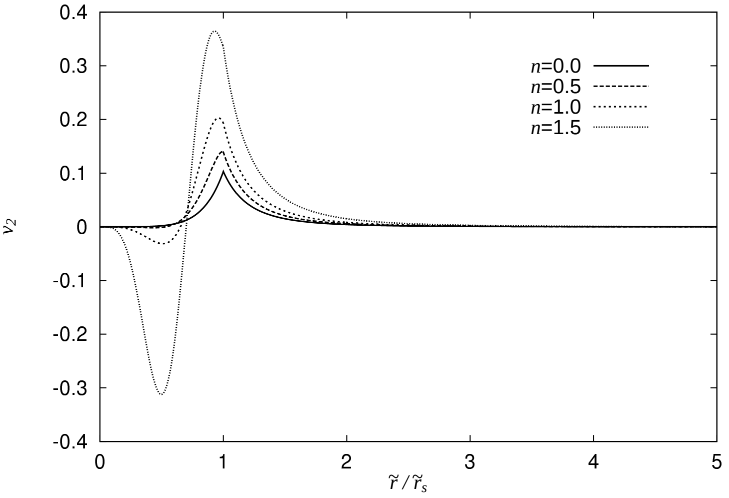

Figure 3.14: The function $v_2(\tilde{r})$ obtained for stellar models with $M/R = 0.2$.

$$\tilde{\xi}^{(2)}_{0\mathrm{P}} = -\left(\frac{1}{\tilde{\rho}+\zeta\tilde{p}}\frac{d\tilde{p}}{d\tilde{r}}\right)^{-1}\delta\tilde{P}^{(2)}_{0\mathrm{P}}. \tag{3.157}$$

Considering the junction conditions, we derive c_0 in the form

$$c_0 = -\frac{\frac{\tilde{J}^2}{\tilde{r}_\mathrm{s}^3} + \tilde{m}_{0\mathrm{Ps}} + \frac{\tilde{r}_\mathrm{s}e^{-\lambda}}{2\zeta}A_\lambda\tilde{\xi}^{(2)}_{0\mathrm{P}}}{\tilde{m}_{0\mathrm{Hs}} + \frac{\tilde{r}_\mathrm{s}e^{-\lambda}}{2\zeta}A_\lambda\tilde{\xi}^{(2)}_{0\mathrm{H}}}. \tag{3.158}$$

In these calculations, we adopted polytropic stellar models with $M/R = 0.2$.

The functions v_2, h_2, k_2, m_2 and $\delta P^{(2)}_2$

Next, we discuss v_2 and h_2. Here, it is useful to introduce the new variable z

$$z = \frac{r}{M} - 1 = \frac{\tilde{r}}{\zeta\tilde{m}(\tilde{r}_\mathrm{s})} - 1. \tag{3.159}$$

Using this variable, Eq. (3.134) and (3.135) can be written outside the star as

$$\frac{dv_2}{dz} = -\frac{2}{z^2-1} + \frac{6\tilde{J}^2}{\zeta^3\tilde{m}(\tilde{r}_\mathrm{s})^4}\frac{z}{(z-1)(z+1)^5}, \tag{3.160}$$

$$\frac{dh_2}{dz} = -2v_2 - \frac{2z}{z^2-1}h_2 - \frac{3\tilde{J}^2}{\zeta^3\tilde{m}(\tilde{r}_\mathrm{s})^4}\frac{z^2-3}{(z-1)(z+1)^5}. \tag{3.161}$$

From these equations, we can derive the second-order differential equation for h_2 in the form

$$\frac{d^2h_2}{dz^2} - \frac{2z}{1-z^2}\frac{dh_2}{dz} + \left(\frac{6}{1-z^2} - \frac{4}{(1-z^2)^2}\right)h_2 = -\frac{12\tilde{J}^2}{\zeta^3\tilde{m}(\tilde{r}_\mathrm{s})^4}\frac{z^2+3z-3}{(z-1)^2(z+1)^6}. \tag{3.162}$$

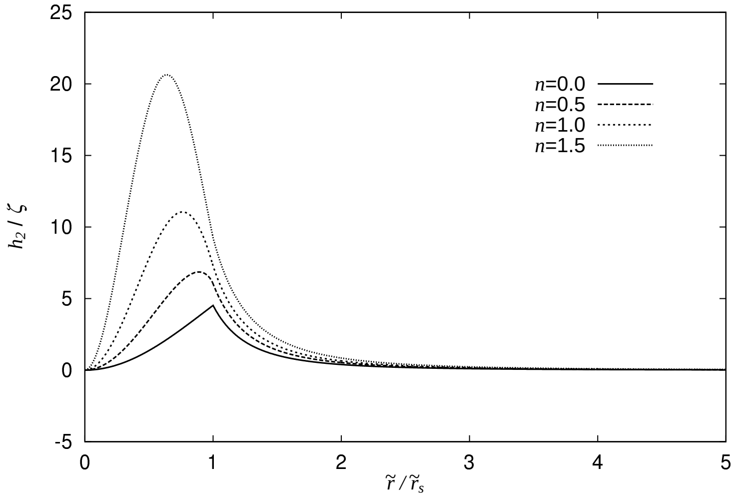

Figure 3.15: The function $h_2(\tilde{r})$ obtained for stellar models with $M/R = 0.2$.

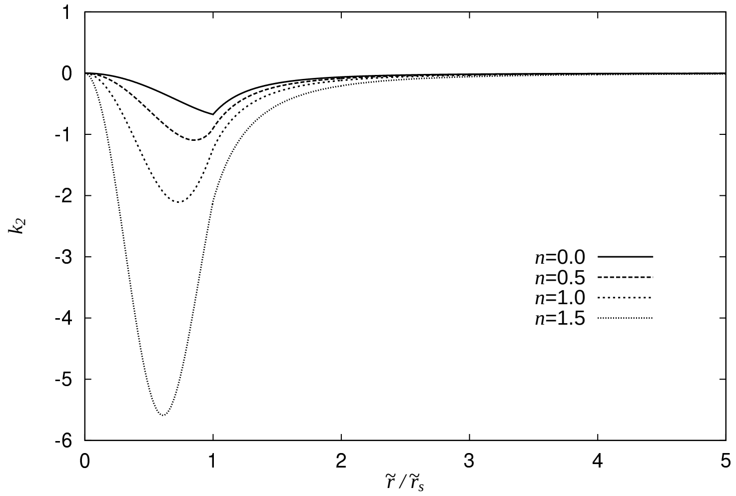

Figure 3.16: The function $k_2(\tilde{r})$ obtained for stellar models with $M/R = 0.2$.

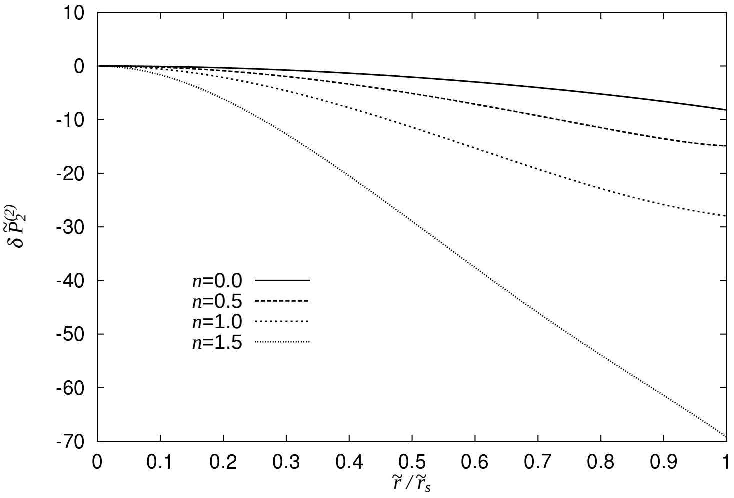

Figure 3.17: The function $\delta P_2^{(2)}(\tilde{r})$ obtained for stellar models with $M/R = 0.2$.

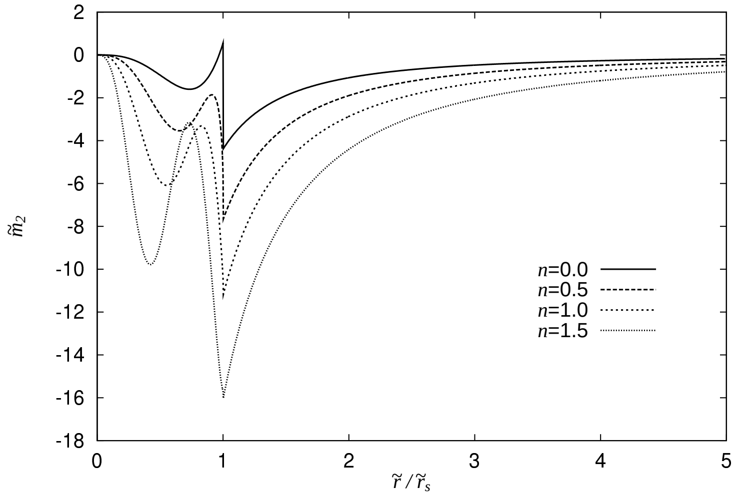

Figure 3.18: The function $m_2(\tilde{r})$ obtained for stellar models with $M/R = 0.2$.

Solutions for the homogeneous equation are given by the associated Legendre functions

$$\begin{aligned} P_2^2(z) &= 3\left(1-z^2\right), && (3.163)\\ Q_2^2(z) &= \frac{3}{2}\left(z^2-1\right)\ln\left(\frac{z+1}{z-1}\right)-\frac{3z^3-5z}{z^2-1}. && (3.164) \end{aligned}$$

Hence, the general solution that vanishes at infinity can be written as

$$h_2 = c_1 Q_2^2 + \frac{\tilde{J}^2}{\zeta^3 \tilde{m}(\tilde{r}_{\rm s})^4}\frac{z+2}{(z+1)^4}, \tag{3.165}$$

where c_1 is a constant. In a similar way, homogeneous solutions for v_2 can be expressed in terms of the associated Legendre functions

$$\begin{aligned} P_2^1 &= 3z\sqrt{z^2-1}, && (3.166)\\ Q_2^1 &= \sqrt{z^2-1}\left[\frac{3z^2-2}{z^2-1}-\frac{3}{2}z\ln\left(\frac{z+1}{z-1}\right)\right]. && (3.167) \end{aligned}$$

The solution for v_2 that vanishes at infinity can be derived as

$$v_2 = \frac{2c_1}{\sqrt{z^2-1}}Q_2^1 + \frac{\tilde{J}^2}{\zeta^3 \tilde{m}(\tilde{r}_{\rm s})^4}\frac{1}{(z+1)^4}. \tag{3.168}$$

The constant c_1 must be fixed by the junction condition.

Let us now write the above exterior solution as

$$\begin{aligned} v_2 &= c_1 u_1(z) + u_2(z), && (3.169)\\ h_2 &= c_1 w_1(z) + w_2(z). && (3.170) \end{aligned}$$

An interior solution can be expressed as

$$\begin{aligned} v_2 &= c_2 v_{2\,\rm H} + v_{2\,\rm P}, && (3.171)\\ h_2 &= c_2 h_{2\,\rm H} + h_{2\,\rm P}, && (3.172) \end{aligned}$$

where c_2 is a constant. Then, the continuous conditions require

$$\begin{aligned} c_1 &= \frac{v_{2\,\rm P}h_{2\,\rm H} - v_{2\,\rm H}h_{2\,\rm P} - u_2 h_{2\,\rm H} + w_2 v_{2\,\rm H}}{h_{2\,\rm H}u_1 - v_{2\,\rm H}w_1}, && (3.173)\\ c_2 &= \frac{-v_{2\,\rm P}w_1 + h_{2\,\rm P}u_1 + u_2 w_1 - u_1 w_2}{-h_{2\,\rm H}u_1 + v_{2\,\rm H}w_1}. && (3.174) \end{aligned}$$

Here, we use the surface values for the functions in these expressions. Figures 3.14 and 3.15 display the functions v_2 and h_2, respectively, with respect to $\tilde{r}$. Here, h_2/ζ corresponds to $\tilde{\Phi}_2^{(2)}$ in the Newtonian case (see Fig. 3.4). These have been obtained for stellar models with $M/R = 0.2$. Furthermore, we show k_2, $\delta\tilde{P}_2^{(2)}$ and $\tilde{m}_2$ derived from Eqs. (3.110), (3.137) and (3.138) in Figs. 3.16, 3.17 and 3.18.

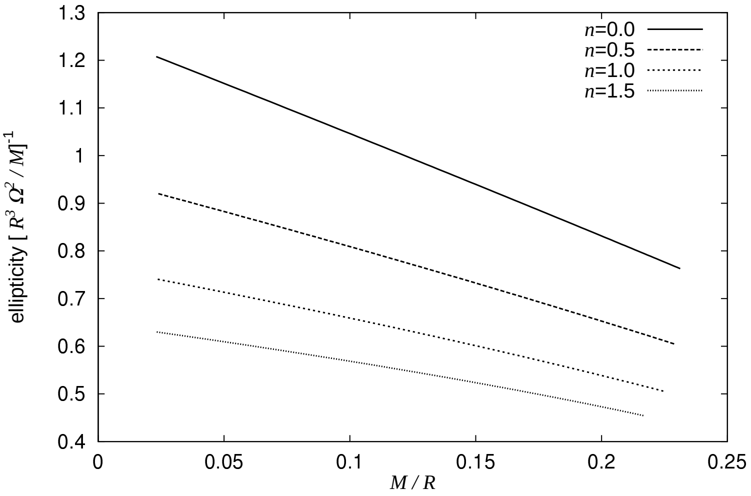

Figure 3.19: Ellipticity plotted as a function of M/R, which is obtained for polytropic stellar models.

3.2.3 Ellipticity

Ellipticity is now defined in the same way as in the Newtonian case. However, the expression of ellipticity has the somewhat different form [125]

$$\text{ellipticity} = -\frac{3}{2}\left(\frac{\xi_2^{(2)}}{r_\mathrm{s}} + k_2(r_\mathrm{s})\right), \tag{3.175}$$

where k_2 arises due to a definition of the radius, that is, the circumferential radius. Figure 3.19 display the values of ellipticity as a function of M/R for several polytropic stellar models. From this figure, we can see that the ellipticity becomes small as the general relativistic factor M/R becomes large for fixed $R^3\Omega^2/M$ in each model.

Chapter 4

Stellar Electromagnetic Fields

In this chapter, we discuss stellar electromagnetic fields (see also Refs. [6, 7, 127]). We here restrict our discussion to axisymmetric, poloidal magnetic fields. In particular, we are interested in dipole magnetic fields, because these play significant roles in many astrophysical situations. The magnetic fields are assumed to be weak, i.e. $B \sim O(\varepsilon_B)$, and therefore we neglect the backreaction to stellar structure in this chapter. We also consider electric fields induced by stellar rotation. In this discussion, we assume slow, uniform rotation of angular velocity $\Omega \sim O(\varepsilon_\Omega)$. The discussion in Minkowski space-time is reviewed in §4.1. The treatment in the context of general relativity is given in §4.2.

4.1 Minkowskian cases

4.1.1 Dipole magnetic fields

The equations governing magnetic fields are given by the Maxwell equation,

$$\begin{aligned} \nabla \cdot \boldsymbol{B} &= 0, & (4.1) \\ \nabla \times \boldsymbol{B} &= 4\pi \boldsymbol{J}, & (4.2) \end{aligned}$$

where $\boldsymbol{J}$ is electric current. It is conventional to introduce the vector potential $\boldsymbol{A}$ defined as

$$\boldsymbol{B} = -\nabla \times \boldsymbol{A}. \tag{4.3}$$

Using this quantity, Eq. (4.1) is automatically satisfied, while Eq. (4.2) reduces to

$$\nabla \times (\nabla \times \boldsymbol{A}) = -4\pi \boldsymbol{J}. \tag{4.4}$$

In general, poloidal magnetic fields are written as

$$\boldsymbol{A} = A_{(\phi)}\boldsymbol{e}_\phi = A_\phi \boldsymbol{d\phi}, \tag{4.5}$$

where $A_{(\phi)}$ is related with A_ϕ in the way

$$A_{(\phi)} = \frac{A_\phi}{r\sin\theta}. \tag{4.6}$$

The electric current $\boldsymbol{J}$ is also written as

$$\boldsymbol{J} = J_{(\phi)}\boldsymbol{e}_\phi = J_\phi \boldsymbol{d\phi}. \tag{4.7}$$

Since we consider axisymmetric cases, A_ϕ and J_ϕ are independent of the coordinate ϕ. The equation for A_ϕ can be obtained from Eq. (4.4) in the form

$$\frac{\partial^2 A_\phi}{\partial r^2} + \frac{1}{r^2}\frac{\partial^2 A_\phi}{\partial\theta^2} - \frac{1}{r^2}\cot\theta\frac{\partial A_\phi}{\partial\theta} = -4\pi J_\phi. \tag{4.8}$$

The potential A_ϕ and the current J_ϕ can now be expanded as

$$\begin{aligned} A_\phi &= \sum_{l=1}^{\infty} a_{\phi l}(r)\sin\theta\frac{dP_l}{d\theta}, && (4.9)\\ J_\phi &= \sum_{l=1}^{\infty} j_{\phi l}(r)\sin\theta\frac{dP_l}{d\theta}. && (4.10)\end{aligned}$$

Here, we note that dipole magnetic fields correspond to $l = 1$. The equation for the radial part is obtained from Eq. (4.8) in the form

$$\frac{d^2 a_{\phi l}}{dr^2} - \frac{l(l+1)}{r^2}a_{\phi l} = -4\pi j_{\phi l}, \tag{4.11}$$

where we have used the formula

$$\frac{1}{\sin\theta}\frac{d}{d\theta}\left(\sin\theta\frac{dP_l}{d\theta}\right) + l(l+1)P_l = 0. \tag{4.12}$$

By solving Eq. (4.11), we can obtain the configurations of magnetic fields through the expression

$$\begin{aligned} \boldsymbol{B} &= \left(\frac{\cot\theta}{r}A_{(\phi)} + \frac{1}{r}\frac{\partial A_{(\phi)}}{\partial\theta}\right)\boldsymbol{e}_r + \left(-\frac{1}{r}A_{(\phi)} - \frac{\partial A_{(\phi)}}{\partial r}\right)\boldsymbol{e}_\theta \\ &= \frac{1}{r^2\sin\theta}\frac{\partial A_\phi}{\partial\theta}\boldsymbol{e}_r - \frac{1}{r\sin\theta}\frac{\partial A_\phi}{\partial r}\boldsymbol{e}_\theta. && (4.13)\end{aligned}$$

In the case of a dipole magnetic field, we have

$$\boldsymbol{B} = -\frac{2a_{\phi 1}}{r^2}\cos\theta\boldsymbol{e}_r + \frac{a'_{\phi 1}}{r}\sin\theta\boldsymbol{e}_\theta. \tag{4.14}$$

Normalized forms

Now, we show the normalization of the above-mentioned quantities. The magnetic field strength B, the magnetic dipole moment μ, the potential $a_{\phi 1}$ and the current $j_{\phi 1}$ are normalized as follows:

$$\begin{aligned} B &= B_* \tilde{B}, \quad B_* = \sqrt{4\pi p_{\mathrm{c}}}, & (4.15) \\ \mu &= \mu_* \tilde{\mu}, \quad \mu_* = r_*^3 \sqrt{4\pi p_{\mathrm{c}}}, & (4.16) \\ a_{\phi 1} &= a_{\phi *} \tilde{a}_{\phi 1}, \quad a_{\phi *} = r_*^2 \sqrt{4\pi p_{\mathrm{c}}}, & (4.17) \\ j_{\phi 1} &= j_{\phi *} \tilde{j}_{\phi 1}, \quad j_{\phi *} = \sqrt{\frac{p_{\mathrm{c}}}{4\pi}}. & (4.18) \end{aligned}$$

Using these quantities, Eq. (4.11) is written as

$$\frac{d^2 \tilde{a}_{\phi l}}{d\tilde{r}^2} - \frac{l(l+1)}{\tilde{r}^2} \tilde{a}_{\phi l} = -\tilde{j}_{\phi l}. \tag{4.19}$$

In the following, we discuss the solution for a dipole field.

Exterior solution

First, we consider the exterior solution which vanishes at infinity. Setting $j_{\phi l} = 0$ in Eq. (4.11), we derive the solution

$$a_{\phi l} \propto \frac{1}{r^l}. \tag{4.20}$$

In the case of a dipole magnetic field, we have

$$a_{\phi 1} = -\frac{\mu}{r}, \tag{4.21}$$

where μ is the magnetic dipole moment. Using Eq. (4.13), we obtain the magnetic configuration

$$\boldsymbol{B} = \frac{2\mu}{r^3} \cos\theta \boldsymbol{e}_r + \frac{\mu}{r^3} \sin\theta \boldsymbol{e}_\theta. \tag{4.22}$$

The magnetic dipole moment μ must be fixed by the junction to an interior solution, which is discussed below.

Interior solutions

Next, we consider interior solutions. For this purpose, we need to have the current distribution $j_{\phi 1}$. It is significant to notice that the current distribution is not arbitrary, but restricted by an integrability condition [100, 128]. This condition can be written as

$$j_{\phi 1} = c_j r^2 \rho, \tag{4.23}$$

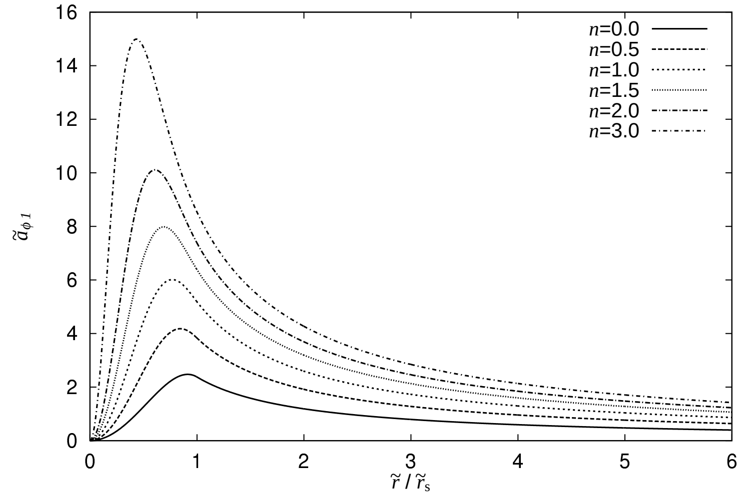

Figure 4.1: The potential $\tilde{a}_{\phi 1}$ plotted as a function of $\tilde{r}$. The polytropic index is denoted by n.

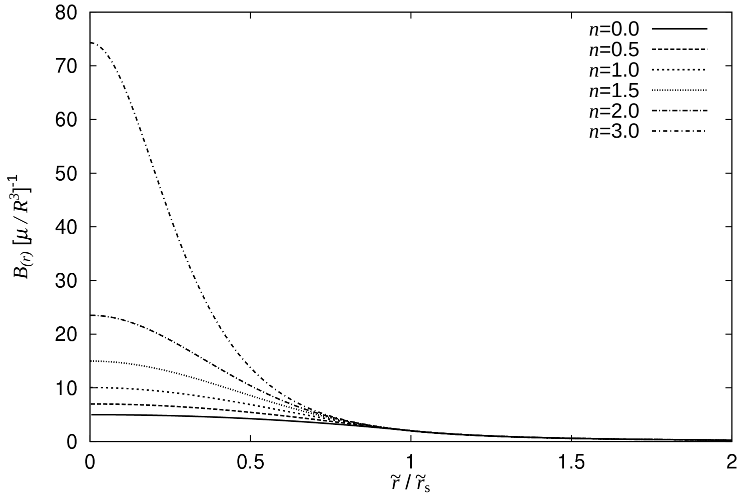

Figure 4.2: The r-component of the magnetic fields $B_{(r)}$ on the symmetry axis ($\theta = 0$), which is plotted as a function of $\tilde{r}$. The field strength is normalized by the typical value μ/R^3.

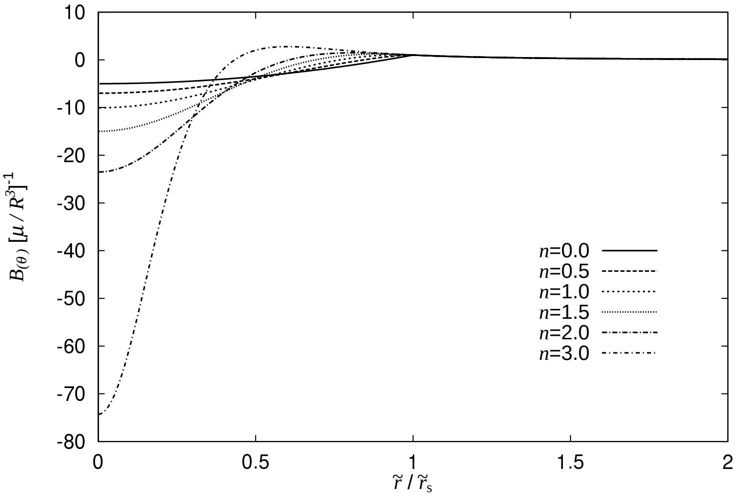

Figure 4.3: The θ-component of the magnetic fields $B_{(\theta)}$ on the equatorial plane ($\theta = \pi/2$), which is plotted as a function of $\tilde{r}$. The field strength is normalized by the typical value μ/R^3.

where c_j is a constant. This is normalized as

$$\tilde{j}_{\phi 1} = \tilde{c}_j \tilde{r}^2 \tilde{\rho}, \tag{4.24}$$

where $c_j = \tilde{c}_j / r_*$. This restriction can be obtained by considering the equilibrium configurations of the stars endowed with a dipole magnetic field (see Chapter 5 for more detailed discussion). After assuming a current distribution which satisfies Eq. (4.23), we can obtain a solution by solving the differential equation (4.11). In this paper, we adopt the current which exists in the whole area of the star.

In the case of incompressible fluid, i.e. $n = 0$, we can derive an analytic interior solution. Since $\rho = \text{const}$, from Eqs. (4.19) and (4.24), we derive the interior solution

$$\tilde{a}_{\phi 1} = c_a \tilde{r}^2 - \frac{1}{10} \tilde{c}_j \tilde{r}^4, \tag{4.25}$$

which is regular at the stellar center. Here, c_a is a constant fixed by the junction at the stellar surface.

In general, the junction conditions for $a_{\phi 1}$ are expressed by

$$a_{\phi 1}\big|_{-R} = a_{\phi 1}\big|_{+R}, \tag{4.26}$$

$$\left.\frac{da_{\phi 1}}{dr}\right|_{-R} = \left.\frac{da_{\phi 1}}{dr}\right|_{+R}. \tag{4.27}$$

In the case of $n = 0$, from Eq. (4.21) and (4.25), we derive

$$c_a = \frac{1}{6} \tilde{c}_j \tilde{r}_s^2, \tag{4.28}$$

$$\tilde{\mu} \ = \ -\frac{1}{15}\tilde{c}_j\tilde{r}_{\rm s}^5. \tag{4.29}$$

Namely, we have

$$\tilde{a}_{\phi 1} = \begin{cases} \frac{\tilde{c}_j}{15}\frac{\tilde{r}_{\rm s}^5}{\tilde{r}} & (\tilde{r} > \tilde{r}_{\rm s}) \\ \frac{\tilde{c}_j}{6}\tilde{r}_{\rm s}^2\tilde{r}^2 - \frac{\tilde{c}_j}{10}\tilde{r}^4 & (\tilde{r} < \tilde{r}_{\rm s}) \end{cases} . \tag{4.30}$$

In the other cases, the constants c_a and μ can be derived in the forms

$$c_a \ = \ -\frac{1}{3\tilde{r}_{\rm s}^2}\left[\tilde{a}_{\phi p}(\tilde{r}_{\rm s}) + \tilde{r}_{\rm s}\tilde{a}'_{\phi p}(\tilde{r}_{\rm s})\right], \tag{4.31}$$

$$\tilde{\mu}_a \ = \ \frac{\tilde{r}_{\rm s}^2}{3}\left[-2\tilde{a}_{\phi p}(\tilde{r}_{\rm s}) + \tilde{r}_{\rm s}\tilde{a}'_{\phi p}(\tilde{r}_{\rm s})\right], \tag{4.32}$$

where $a_{\phi p}$ denotes the particular solution for $a_{\phi 1}$.

Numerical solutions

We show numerical solutions for $a_{\phi 1}$, $B_{(r)}$ and $B_{(\theta)}$ in Figs. 4.1, 4.2 and 4.3, respectively. The magnetic field strength is normalized by the typical surface field strength μ/R^3. The results in Fig. 4.1 corresponds to the choice of $\tilde{c}_j = 1$.

4.1.2 Induced electric fields

Next, we discuss the electric field induced by rotation of the star which has a dipole magnetic field. The electric field can be described by the Maxwell equation,

$$\nabla\cdot\boldsymbol{E} \ = \ -4\pi J_t, \tag{4.33}$$

$$\nabla\times\boldsymbol{E} \ = \ 0, \tag{4.34}$$

where J_t is related with the electric charge $\rho_{\rm e}$ as $J_t = -\rho_{\rm e}$. It is useful to introduce the potential A_t defined as

$$\boldsymbol{E} = \nabla A_t, \tag{4.35}$$

where A_t is related with the usual scalar potential φ in the form $A_t = -\varphi$. This ensures Eq. (4.34), while Eq. (4.33) gives the equation for A_t,

$$\frac{\partial^2 A_t}{\partial r^2} + \frac{2}{r}\frac{\partial A_t}{\partial r} + \frac{1}{r^2}\frac{\partial^2 A_t}{\partial\theta^2} + \frac{\cot\theta}{r^2}\frac{\partial A_t}{\partial\theta} = -4\pi J_t. \tag{4.36}$$

We now expand A_t and J_t as

$$A_t \ = \ \sum_{l=0}^{\infty} a_{tl}(r)P_l, \tag{4.37}$$

$$J_t \ = \ \sum_{l=0}^{\infty} j_{tl}(r)P_l. \tag{4.38}$$

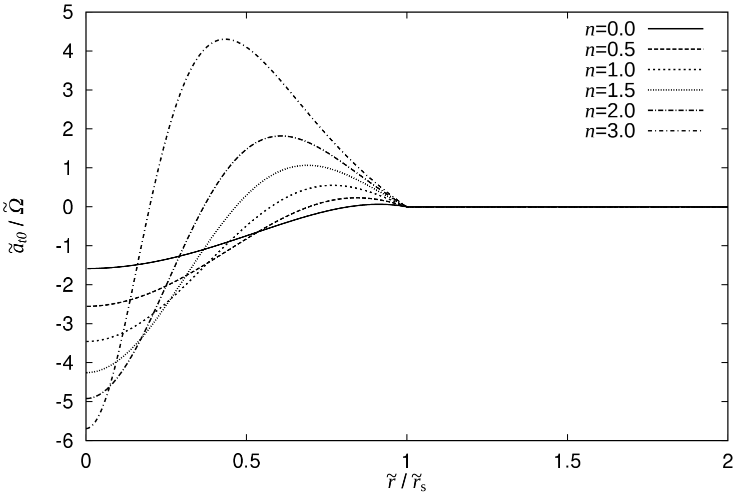

Figure 4.4: The potential $\tilde{a}_{t0}$ as a function of $\tilde{r}$.

Note that the symmetry with respect to the equatorial plane requires

$$a_{tl} = 0 \quad (l : \text{odd}), \tag{4.39}$$

$$j_{tl} = 0 \quad (l : \text{odd}). \tag{4.40}$$

Using Eqs. (4.37) and (4.38), we obtain the equation

$$\frac{d^2 a_{tl}}{dr^2} + \frac{2}{r}\frac{da_{tl}}{dr} - \frac{l(l+1)}{r^2} a_{tl} = -4\pi j_{tl}. \tag{4.41}$$

This equation governs stellar electric fields. In the normalized form, this reduces to

$$\frac{d^2 \tilde{a}_{tl}}{d\tilde{r}^2} + \frac{2}{\tilde{r}}\frac{d\tilde{a}_{tl}}{d\tilde{r}} - \frac{l(l+1)}{\tilde{r}^2} \tilde{a}_{tl} = -\tilde{j}_{tl}, \tag{4.42}$$

where we have used the normalization

$$a_{tl} = a_{t*}\tilde{a}_{tl}, \quad a_{t*} = \Omega_* a_{\phi *} = \left(\frac{p_c}{\rho_c}\right)^{\frac{3}{2}}, \tag{4.43}$$

$$j_{tl} = j_{t*}\tilde{j}_{tl}, \quad j_{t*} = \Omega_* j_{\phi *} = \sqrt{\rho_c p_c}, \tag{4.44}$$

and Eqs. (4.15)–(4.18).

Solutions

A perfectly conducting interior is usually assumed, because the time scale of the magnetic decay of neutron stars is much longer than the other time scales. We also adopt this reasonable assumption in this paper. The generalized Ohm's law is written as

$$\boldsymbol{J} = \sigma \left(\boldsymbol{E} + \boldsymbol{v} \times \boldsymbol{B}\right), \tag{4.45}$$

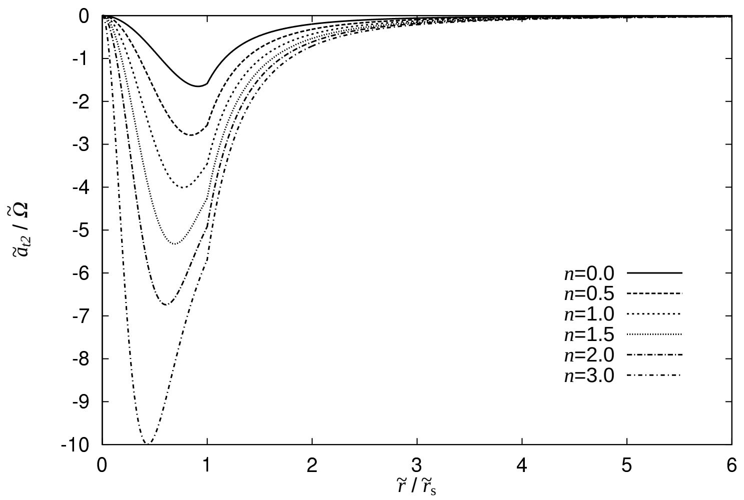

Figure 4.5: The potential $\tilde{a}_{t2}$ as a function of $\tilde{r}$.

where σ is conductivity, and we have used the slow rotation approximation. Hence, in the case of a perfect conductor, i.e. $\sigma \to \infty$, we derive

$$\boldsymbol{E} + \boldsymbol{v} \times \boldsymbol{B} = 0. \tag{4.46}$$

Using the potential functions A_t and $\boldsymbol{A}$, this relation is written in the form

$$A_t + \Omega A_\phi = c_A, \tag{4.47}$$

where c_A is a constant of integration. In particular, in the case of a dipole field, we have

$$a_{t0} = \frac{2}{3}\Omega a_{\phi 1} + c_A, \tag{4.48}$$

$$a_{t2} = -\frac{2}{3}\Omega a_{\phi 1}, \tag{4.49}$$

$$a_{tl} = 0 \quad (l \neq 0, 2). \tag{4.50}$$

Therefore, monopole and quadrupole electric fields are excited due to the rotation of a dipole magnetic field. In this way, inside the star, we can derive the configurations of the electric field by not solving the Maxwell equation, but considering the assumption of a perfect conductor. Furthermore, we can obtain the induced charge configuration using Eqs. (4.11) and (4.41) as follows:

$$j_{t0} = \frac{2}{3}\Omega j_{\phi 1} - \frac{\Omega}{3\pi r}\frac{da_{\phi 1}}{dr} - \frac{\Omega}{3\pi r^2}a_{\phi 1}, \tag{4.51}$$

$$j_{t2} = -\frac{2}{3}\Omega j_{\phi 1} + \frac{\Omega}{3\pi r}\frac{da_{\phi 1}}{dr} - \frac{2\Omega}{3\pi r^2}a_{\phi 1}. \tag{4.52}$$

In the normalized forms, we derive

$$\begin{aligned}\tilde{j}_{t0} &= \left(\frac{2}{3}\tilde{j}_{\phi 1} - \frac{4}{3\tilde{r}}\frac{d\tilde{a}_{\phi 1}}{d\tilde{r}} - \frac{4}{3\tilde{r}^2}\tilde{a}_{\phi 1}\right)\tilde{\Omega}, \quad (4.53)\\ \tilde{j}_{t2} &= \left(-\frac{2}{3}\tilde{j}_{\phi 1} + \frac{4}{3\tilde{r}}\frac{d\tilde{a}_{\phi 1}}{d\tilde{r}} - \frac{8}{3\tilde{r}^2}\tilde{a}_{\phi 1}\right)\tilde{\Omega}. \quad (4.54)\end{aligned}$$

Outside the star, from Eq. (4.41), we derive the general expression of the exterior solution,

$$a_{tl} \propto \frac{1}{r^{l+1}}. \quad (4.55)$$

Considering the junction to the above-mentioned interior solution, we obtain the exterior solution

$$\begin{aligned}a_{t2} &= \frac{2\Omega\mu R^2}{3r^3}, \quad (4.56)\\ a_{tl} &= 0 \quad (l \neq 2). \quad (4.57)\end{aligned}$$

Here, the vanishing monopole part corresponds to the assumption that the total charge equals to zero.

Consequently, we obtain the solution

$$\begin{aligned}a_{t0} &= \begin{cases} \frac{2\Omega}{3}a_{\phi 1} + \frac{2\Omega\mu}{3R} & (r \leq R) \\ 0 & (r \geq R) \end{cases}, \quad (4.58)\\ a_{t2} &= \begin{cases} -\frac{2}{3}\Omega a_{\phi 1} & (r \leq R) \\ \frac{2}{3}\frac{\Omega\mu R^2}{r^3} & (r \geq R) \end{cases}. \quad (4.59)\end{aligned}$$

Note that a_{t0} and a_{t2} need not be connected smoothly at the surface, owing to induced surface charge. The electric field components are now given by

$$\boldsymbol{E} = \begin{cases} \frac{2}{3}\Omega a'_{\phi 1}(1 - P_2)\,\boldsymbol{e}_r + \frac{2\Omega a_{\phi 1}}{r}\sin\theta\cos\theta\boldsymbol{e}_\theta & (r \leq R) \\ -\frac{2\Omega\mu R^2}{r^4}P_2\boldsymbol{e}_r - \frac{2\Omega\mu R^2}{r^4}\sin\theta\cos\theta\boldsymbol{e}_\theta & (r \geq R) \end{cases}. \quad (4.60)$$

The exterior field is characterized by the quadrupole moment $Q = \Omega\mu R^2/3$.

Numerical results

We show the numerical solutions for a_{t0} and a_{t2} in Figs. 4.4 and 4.5, respectively. These functions are normalized by $\tilde{\Omega}$. Furthermore, we show the components of the electric field in Fig. 4.6, 4.7, 4.8, 4.9, 4.10 and 4.11. We have adopted the stellar models of $n = 0, 1, 3$. In these figures, θ denotes the angle of the radial direction from the symmetry axis.

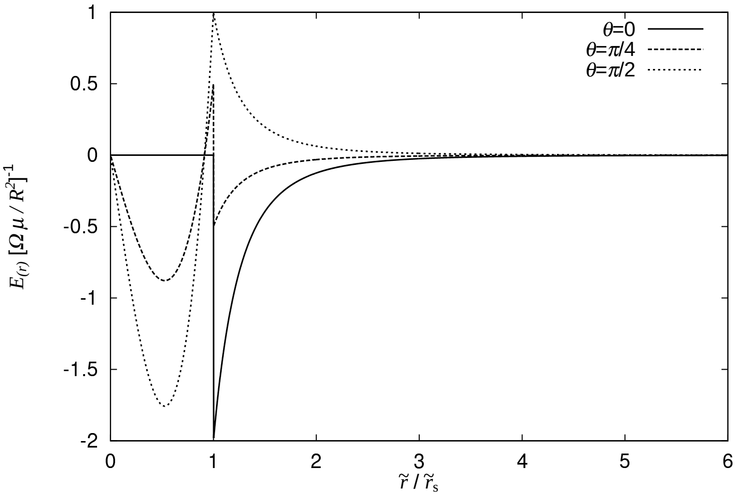

Figure 4.6: The r-component of the electric field $E_{(r)}$ for the stellar model of $n = 0$. The field strength is normalized by the typical value $\Omega\mu/R^2$ and plotted as a function of $\tilde{r}$.

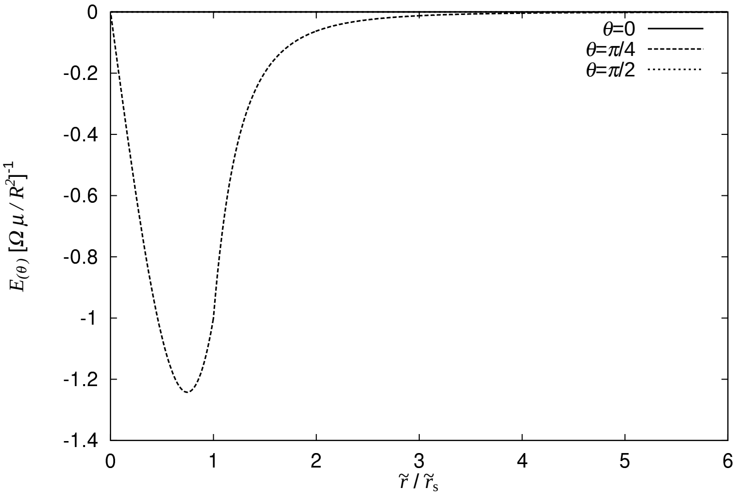

Figure 4.7: The θ-component of the electric field $E_{(\theta)}$ for the stellar model of $n = 0$. The field strength is normalized by the typical value $\Omega\mu/R^2$ and plotted as a function of $\tilde{r}$.

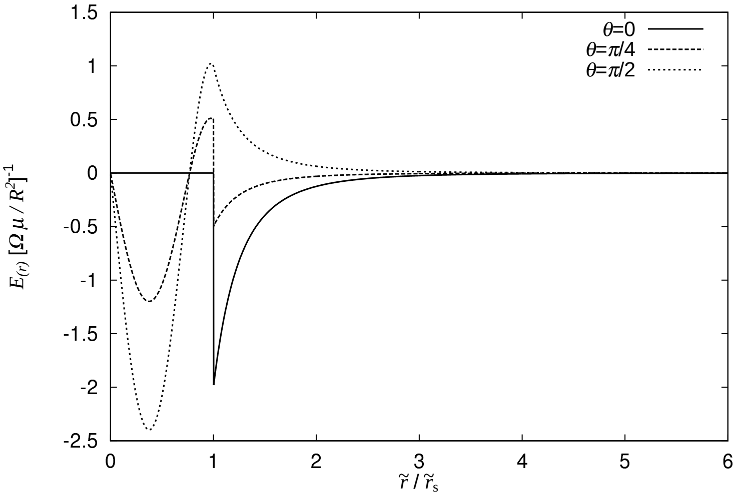

Figure 4.8: The r-component of the electric field $E_{(r)}$ for the stellar model of $n = 1$. The field strength is normalized by the typical value $\Omega\mu/R^2$ and plotted as a function of $\tilde{r}$.

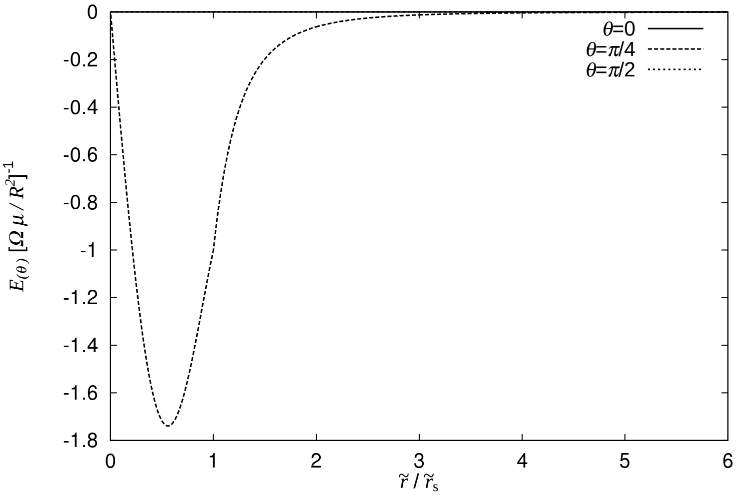

Figure 4.9: The θ-component of the electric field $E_{(\theta)}$ for the stellar model of $n = 1$. The field strength is normalized by the typical value $\Omega\mu/R^2$ and plotted as a function of $\tilde{r}$.

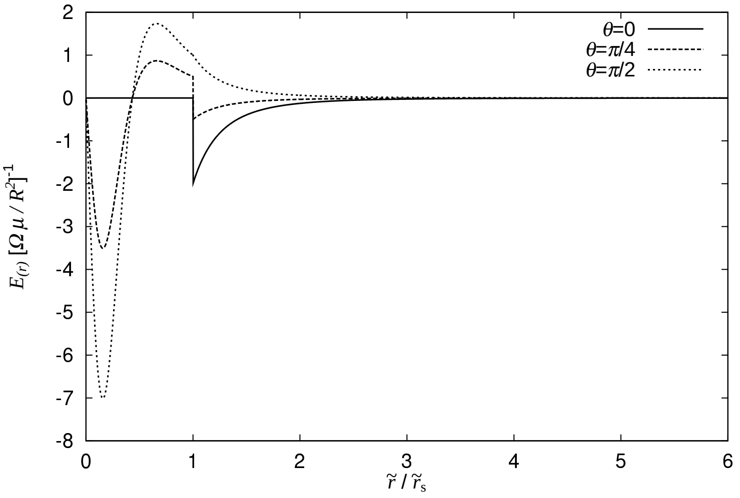

Figure 4.10: The r-component of the electric field $E_{(r)}$ for the stellar model of $n = 3$. The field strength is normalized by the typical value $\Omega\mu/R^2$ and plotted as a function of $\tilde{r}$.

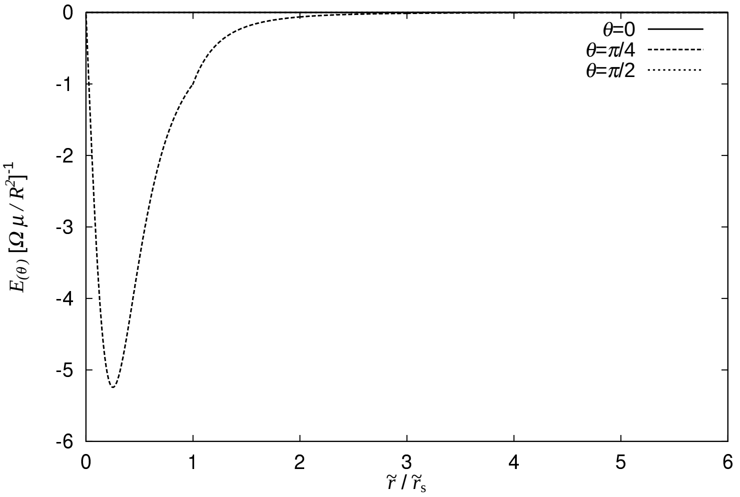

Figure 4.11: The θ-component of the electric field $E_{(\theta)}$ for the stellar model of $n = 3$. The field strength is normalized by the typical value $\Omega\mu/R^2$ and plotted as a function of $\tilde{r}$.

4.2 General relativistic cases

4.2.1 Dipole magnetic fields

We now deal with a stellar dipole magnetic field in the context of general relativity. The magnetic field obeys the Maxwell equation

$$F_{\mu\ ;\nu}^{\ \nu} = 4\pi J_\mu, \tag{4.61}$$

where $F_{\mu\nu}$ is the Faraday tensor, and J_μ is four-current. We now introduce the four-potential A_μ defined as

$$F_{\mu\nu} = A_{\nu,\mu} - A_{\mu,\nu}. \tag{4.62}$$

The poloidal magnetic field can be described by

$$\begin{aligned} A_\mu &= (0,0,0,A_\phi)\,, && (4.63)\\ J_\mu &= (0,0,0,J_\phi)\,, && (4.64)\end{aligned}$$

where A_ϕ and J_ϕ are expanded as Eqs. (4.9) and (4.10), respectively, again. From Eq. (4.61), the equation for A_ϕ is derived in the form

$$e^{-\lambda}\frac{\partial^2 A_\phi}{\partial r^2} + \frac{1}{2}\left(\nu' - \lambda'\right) e^{-\lambda}\frac{\partial A_\phi}{\partial r} + \frac{1}{r^2}\frac{\partial^2 A_\phi}{\partial \theta^2} - \frac{1}{r^2}\cot\theta\frac{\partial A_\phi}{\partial \theta} = -4\pi J_\phi. \tag{4.65}$$

This is the general relativistic version of Eq. (4.8). Furthermore, the equations for the radial parts of A_ϕ can be written in the form

$$e^{-\lambda}\frac{d^2 a_{\phi l}}{dr^2} + \frac{1}{2}\left(\nu' - \lambda'\right) e^{-\lambda}\frac{d a_{\phi l}}{dr} - \frac{l(l+1)}{r^2}a_{\phi l} = -4\pi j_{\phi l}. \tag{4.66}$$

This equation is also written in the normalized form

$$e^{-\lambda}\frac{d^2 \tilde{a}_{\phi l}}{d\tilde{r}^2} + \frac{1}{2}\left(\nu' - \lambda'\right) e^{-\lambda}\frac{d \tilde{a}_{\phi l}}{d\tilde{r}} - \frac{l(l+1)}{\tilde{r}^2}\tilde{a}_{\phi l} = -\tilde{j}_{\phi l}, \tag{4.67}$$

where the prime here denotes differentiation with respect to $\tilde{r}$, and we have used Eqs. (4.15)–(4.18).

In local inertial frames, electric and magnetic fields are now defined as

$$F_{(\mu)(\nu)} = \begin{pmatrix} 0 & -E_{(r)} & -E_{(\theta)} & -E_{(\phi)} \\ E_{(r)} & 0 & B_{(\phi)} & -B_{(\theta)} \\ E_{(\theta)} & -B_{(\phi)} & 0 & B_{(r)} \\ E_{(\phi)} & B_{(\theta)} & -B_{(r)} & 0 \end{pmatrix}, \tag{4.68}$$

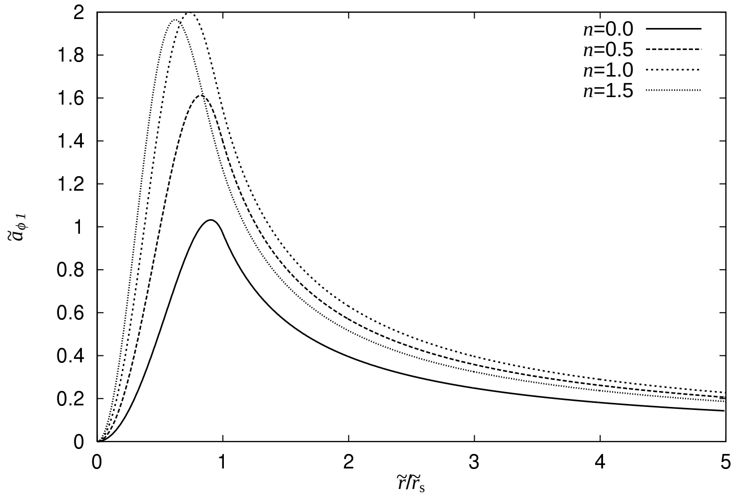

Figure 4.12: The potential $\tilde{a}_{\phi 1}$ as a function of $\tilde{r}$. We adopted polytropic stellar models with $M/R = 0.2$.

where $F_{(\mu)(\nu)}$ is derived from $F_{(\mu)(\nu)} = e^{\lambda}_{(\mu)} e^{\sigma}_{(\nu)} F_{\lambda\sigma}$ using the tetrad $e^{\lambda}_{(\mu)}$. Hence, we derive the general expression of the dipole magnetic field in the form

$$\begin{aligned} \boldsymbol{B} &= \frac{1}{r^2 \sin\theta}\frac{\partial A_\phi}{\partial \theta}\boldsymbol{e}_r - \frac{e^{-\frac{\lambda}{2}}}{r\sin\theta}\frac{\partial A_\phi}{\partial r}\boldsymbol{e}_\theta && (4.69) \\ &= -\frac{2a_{\phi 1}}{r^2}\cos\theta \boldsymbol{e}_r + \frac{e^{-\frac{\lambda}{2}} a'_{\phi 1}}{r}\sin\theta \boldsymbol{e}_\theta. && (4.70) \end{aligned}$$

Once we obtain the solution for $a_{\phi 1}$, we can find the configuration of the dipole field from the above expression.

Exterior solution

We now discuss the exterior solution which vanishes at infinity. Such a solution can be obtained in the form [129–131]

$$a_{\phi l} \propto \left(\frac{2M}{r}\right)^l \psi_l(r), \tag{4.71}$$

where ψ_l can be expressed by the hyper-geometric function,

$$\begin{aligned} \psi_l &= {}_2F_1\left(l, l+2, 2(l+1); \frac{2M}{r}\right) && (4.72) \\ &= \frac{(2l+1)!}{(l-1)!(l+1)!}\sum_{n=0}^{\infty}\frac{(n+l-1)!(n+l+1)!}{(n+2l+1)!n!}\left(\frac{2M}{r}\right)^n. && (4.73) \end{aligned}$$

Hence, we can write the dipole field as

$$a_{\phi 1} = \frac{3\mu}{8M^3} r^2 \left[\ln\left(1 - \frac{2M}{r}\right) + \frac{2M}{r} + \frac{2M^2}{r^2}\right], \tag{4.74}$$

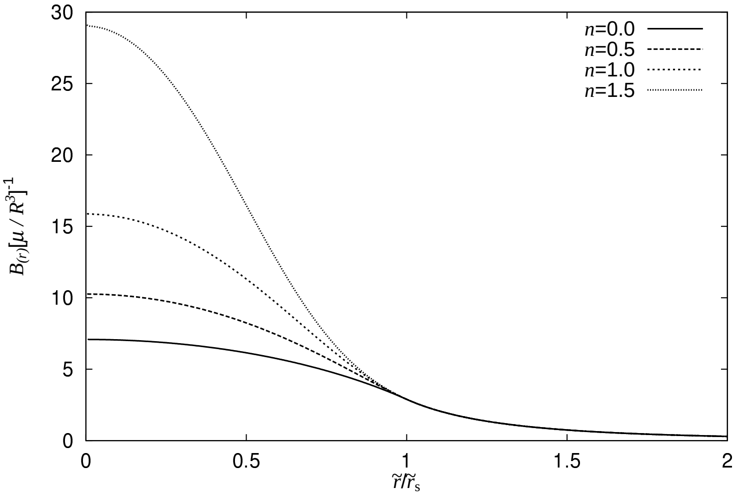

Figure 4.13: The magnetic field component $B_{(r)}$ on the symmetry axis, which is plotted as a function of $\tilde{r}$. The magnetic field strength is normalized by the typical value μ/R^3. We adopted polytropic stellar models with $M/R = 0.2$.

where μ is the magnetic dipole moment with respect to an observer at infinity. Note that this expression reduces to the Newtonian expression at large r. Using the normalized quantities, this equation can be written as

$$\tilde{a}_{\phi 1} = \frac{3\tilde{\mu}}{8\zeta^3 \tilde{m}(\tilde{r}_{\rm s})^3}\tilde{r}^2 \left[\ln\left(1 - \frac{2\zeta\tilde{m}(\tilde{r}_{\rm s})}{\tilde{r}}\right) + \frac{2\zeta\tilde{m}(\tilde{r}_{\rm s})}{\tilde{r}} + \frac{2\zeta^2\tilde{m}(\tilde{r}_{\rm s})^2}{\tilde{r}^2}\right]. \tag{4.75}$$

In the local frames, the components of the dipole magnetic field are given by

$$B_{(r)} = -\frac{3\mu}{4M^3}\left[\ln\left(1 - \frac{2M}{r}\right) + \frac{2M}{r} + \frac{2M^2}{r^2}\right]\cos\theta, \tag{4.76}$$

$$B_{(\theta)} = \frac{3\mu}{4M^3}\left[\sqrt{1 - \frac{2M}{r}}\ln\left(1 - \frac{2M}{r}\right) + \frac{2M(r-M)}{r\sqrt{r(r-2M)}}\right]\sin\theta. \tag{4.77}$$

At large r, we can re-derive the expression (4.22) in Minkowski space-time.

Interior solutions

Next, we discuss interior solutions. As in the case of Minkowski space-time, electric current $j_{\phi 1}$ must satisfies the integrability condition (see Ref. [103] or Chapter 5 for detailed discussion)

$$j_{\phi 1} = c_j r^2 \left(\rho + p\right). \tag{4.78}$$

In the normalized form, we have

$$\tilde{j}_{\phi 1} = \tilde{c}_j \tilde{r}^2 \left(\tilde{\rho} + \zeta\tilde{p}\right), \tag{4.79}$$

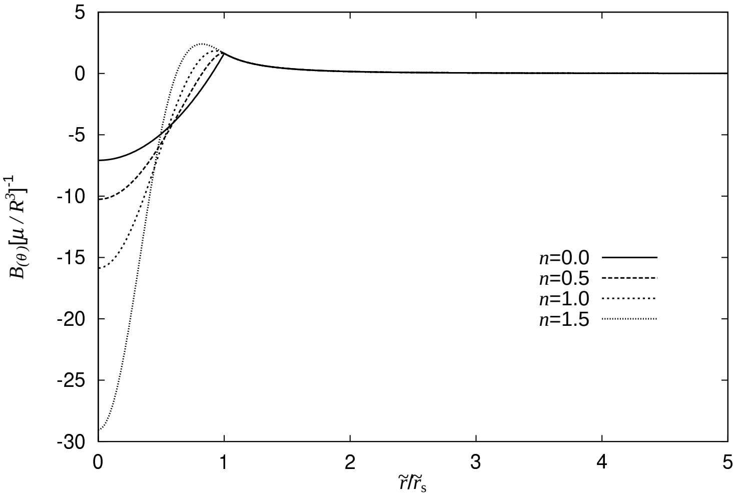

Figure 4.14: The magnetic field component $B_{(\theta)}$ on the equatorial plane, which is plotted as a function of $\tilde{r}$. The magnetic field strength is normalized by the typical value μ/R^3. We adopted polytropic stellar models with $M/R = 0.2$.

where $c_j = \tilde{c}_j/r_*$. Interior solutions can be obtained by solving Eq. (4.66) numerically under this restriction.

Numerical results

We show the numerical solutions of $\tilde{a}_\phi$ for several polytropic stellar models in Fig. 4.12. These results correspond to the choice of $\tilde{c}_j = 1$. Furthermore, Figs. 4.13 and 4.14 display the magnetic field components in local frames. In these figures, we adopted polytropic stellar models with $M/R = 0.2$. From the comparison with the Newtonian case, we can find that the magnetic field strength at the stellar center becomes large due to the general relativistic effect. In the case of $M/R = 0.2$, the increment is about 50% of the Newtonian values. As an example, in the case of $n = 1$, we show the comparison of the magnetic field strength between the Newtonian and the general relativistic calculations in Figs. 4.15 and 4.16.

4.2.2 Induced electric fields

Next, we consider the electric field induced by stellar rotation in the context of general relativity. The electric field can be expressed by the t-component of four-potential A_t, which is a quantity of order $\varepsilon_\Omega \varepsilon_B$. The potential function A_t obeys the following differential equation

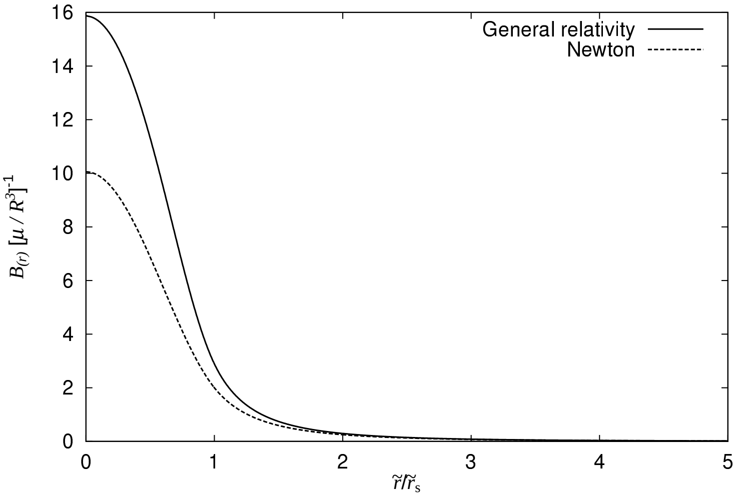

Figure 4.15: Comparison of the magnetic field component $B_{(r)}$ between the Newtonian and the general relativistic calculations in the case of $n = 1$.

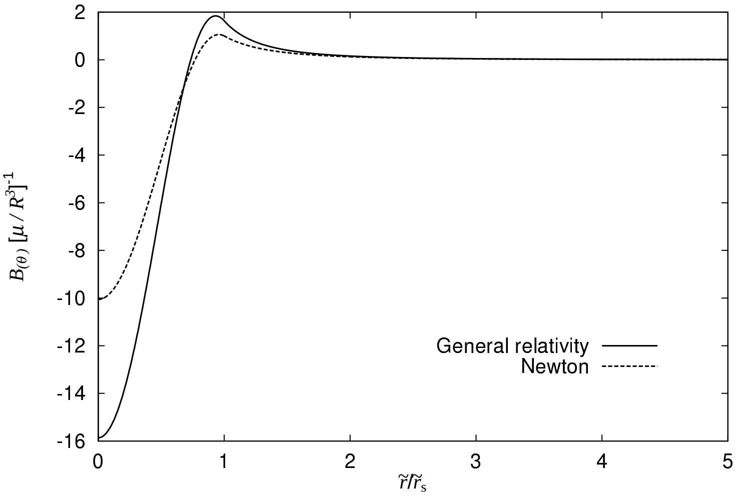

Figure 4.16: Comparison of the magnetic field component $B_{(\theta)}$ between the Newtonian and the general relativistic calculations in the case of $n = 1$.

derived from the Maxwell equation,

$$\begin{aligned}
&e^{-\lambda}\frac{\partial^2 A_t}{\partial r^2} - \left(\frac{\nu' + \lambda'}{2} - \frac{2}{r}\right) e^{-\lambda}\frac{\partial A_t}{\partial r} + \frac{1}{r^2}\frac{\partial^2 A_t}{\partial \theta^2} + \frac{\cot\theta}{r^2}\frac{\partial A_t}{\partial \theta} \\
&= -4\pi J_t + \left[\left(\nu' - \frac{2}{r}\right)\omega - \omega'\right] e^{-\lambda}\frac{\partial A_\phi}{\partial r} - \frac{2}{r^2}\cot\theta\,\omega\frac{\partial A_\phi}{\partial \theta}. \qquad (4.80)
\end{aligned}$$

This equation is the general relativistic version of Eq. (4.36). Using the expansion (4.37) and (4.38) again, we obtain the equations

- $l < 2$

$$\begin{aligned}
&e^{-\lambda}\frac{d^2 a_{tl}}{dr^2} - \left(\frac{\nu' + \lambda'}{2} - \frac{2}{r}\right) e^{-\lambda}\frac{d a_{tl}}{dr} - \frac{l(l+1)}{r^2}a_{tl} \\
&= -4\pi j_{tl} - \frac{(l+1)(l+2)}{2l+3}\left[\left(\nu' - \frac{2}{r}\right)\omega - \omega'\right] e^{-\lambda}a'_{\phi\, l+1} + \frac{2(l+1)^2(l+2)}{(2l+3)r^2}\omega a_{\phi\, l+1}, \qquad (4.81)
\end{aligned}$$

- $l \geq 2$

$$\begin{aligned}
&e^{-\lambda}\frac{d^2 a_{tl}}{dr^2} - \left(\frac{\nu' + \lambda'}{2} - \frac{2}{r}\right) e^{-\lambda}\frac{d a_{tl}}{dr} - \frac{l(l+1)}{r^2}a_{tl} \\
&= -4\pi j_{tl} - \frac{(l+1)(l+2)}{2l+3}\left[\left(\nu' - \frac{2}{r}\right)\omega - \omega'\right] e^{-\lambda}a'_{\phi\, l+1} + \frac{2(l+1)^2(l+2)}{(2l+3)r^2}\omega a_{\phi\, l+1} \\
&+\frac{l(l-1)}{2l-1}\left[\left(\nu' - \frac{2}{r}\right)\omega - \omega'\right] e^{-\lambda}a'_{\phi\, l-1} + \frac{2l^2(l-1)}{(2l-1)r^2}\omega a_{\phi\, l-1}. \qquad (4.82)
\end{aligned}$$

When we deal with a dipole magnetic field, it is sufficient to consider the monopole and quadrupole parts only. The differential equations for these are given by

$$\begin{aligned}
&e^{-\lambda}\frac{d^2 a_{t0}}{dr^2} - \left(\frac{\nu' + \lambda'}{2} - \frac{2}{r}\right) e^{-\lambda}\frac{d a_{t0}}{dr} \\
&= -4\pi j_{t0} - \frac{2}{3}\left[\left(\nu' - \frac{2}{r}\right)\omega - \omega'\right] e^{-\lambda}a'_{\phi 1} + \frac{4}{3r^2}\omega a_{\phi 1}, \qquad (4.83) \\
&e^{-\lambda}\frac{d^2 a_{t2}}{dr^2} - \left(\frac{\nu' + \lambda'}{2} - \frac{2}{r}\right) e^{-\lambda}\frac{d a_{t2}}{dr} - \frac{6}{r^2}a_{t2} \\
&= -4\pi j_{t2} + \frac{2}{3}\left[\left(\nu' - \frac{2}{r}\right)\omega - \omega'\right] e^{-\lambda}a'_{\phi 1} + \frac{8}{3r^2}\omega a_{\phi 1}. \qquad (4.84)
\end{aligned}$$

These are also written in the normalized forms

$$\begin{aligned}
&e^{-\lambda}\frac{d^2 \tilde{a}_{t0}}{d\tilde{r}^2} - \left(\frac{\nu' + \lambda'}{2} - \frac{2}{\tilde{r}}\right) e^{-\lambda}\frac{d \tilde{a}_{t0}}{d\tilde{r}} \\
&= -\tilde{j}_{t0} - \frac{2}{3}\left[\left(\nu' - \frac{2}{\tilde{r}}\right)\tilde{\omega} - \tilde{\omega}'\right] e^{-\lambda}\tilde{a}'_{\phi 1} + \frac{4}{3\tilde{r}^2}\tilde{\omega}\tilde{a}_{\phi 1}, \qquad (4.85) \\
&e^{-\lambda}\frac{d^2 \tilde{a}_{t2}}{d\tilde{r}^2} - \left(\frac{\nu' + \lambda'}{2} - \frac{2}{\tilde{r}}\right) e^{-\lambda}\frac{d \tilde{a}_{t2}}{d\tilde{r}} - \frac{6}{\tilde{r}^2}\tilde{a}_{t2} \\
&= -\tilde{j}_{t2} + \frac{2}{3}\left[\left(\nu' - \frac{2}{\tilde{r}}\right)\tilde{\omega} - \tilde{\omega}'\right] e^{-\lambda}\tilde{a}'_{\phi 1} + \frac{8}{3\tilde{r}^2}\tilde{\omega}\tilde{a}_{\phi 1}. \qquad (4.86)
\end{aligned}$$

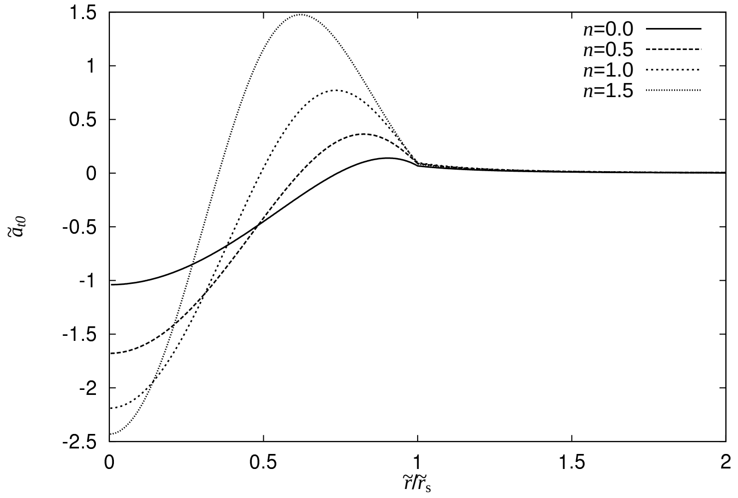

Figure 4.17: The potential $\tilde{a}_{t0}$ plotted as a function of $\tilde{r}$ for polytropic stellar models with $M/R = 0.2$.

The last terms on the right-hand sides in these equations denote the coupling between the magnetic field and frame dragging.

Solutions

We now adopt the assumption of a perfectly conducting interior again. This condition is expressed by

$$0 = F_{\mu\nu}u^{\nu} = u^t\left(0, \frac{\partial A_t}{\partial r} + \Omega\frac{\partial A_\phi}{\partial r}, \frac{\partial A_t}{\partial \theta} + \Omega\frac{\partial A_\phi}{\partial \theta}, 0\right). \tag{4.87}$$

Hence, we derive the same relation as in the Minkowskian case,

$$A_t = -\Omega A_\phi + c_A, \tag{4.88}$$

where c_A is a constant. Therefore, the interior solution can be derived by using the numerical solution for $a_{\phi 1}$ in the same forms as Eqs. (4.48)–(4.50). Furthermore, using Eqs. (4.83) and (4.84), we can obtain the interior charge distribution in the forms

$$j_{t0} = \frac{2}{3}\Omega j_{\phi 1} + \frac{1}{6\pi}\left[\left(\nu' - \frac{2}{r}\right)\varpi + \varpi'\right]e^{-\lambda}a'_{\phi 1} - \frac{1}{3\pi r^2}\varpi a_{\phi 1}, \tag{4.89}$$

$$j_{t2} = -\frac{2}{3}\Omega j_{\phi 1} - \frac{1}{6\pi}\left[\left(\nu' - \frac{2}{r}\right)\varpi + \varpi'\right]e^{-\lambda}a'_{\phi 1} - \frac{2}{3\pi r^2}\varpi a_{\phi 1}, \tag{4.90}$$

or in the normalized forms

$$\tilde{j}_{t0} = \frac{2}{3}\tilde{\Omega}\tilde{j}_{\phi 1} + \frac{2}{3}\left[\left(\nu' - \frac{2}{\tilde{r}}\right)\tilde{\varpi} + \tilde{\varpi}'\right]e^{-\lambda}\tilde{a}'_{\phi 1} - \frac{4}{3\tilde{r}^2}\tilde{\varpi}\tilde{a}_{\phi 1}, \tag{4.91}$$

$$\tilde{j}_{t2} = -\frac{2}{3}\tilde{\Omega}\tilde{j}_{\phi 1} - \frac{2}{3}\left[\left(\nu' - \frac{2}{\tilde{r}}\right)\tilde{\varpi} + \tilde{\varpi}'\right]e^{-\lambda}\tilde{a}'_{\phi 1} - \frac{8}{3\tilde{r}^2}\tilde{\varpi}\tilde{a}_{\phi 1}. \tag{4.92}$$

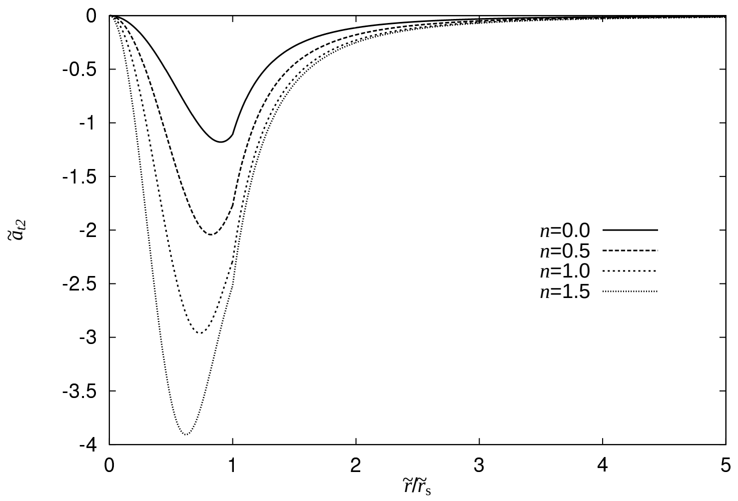

Figure 4.18: The potential $\tilde{a}_{t2}$ plotted as a function of $\tilde{r}$ for polytropic stellar models with $M/R = 0.2$.

The exterior solution for a_{t0} and a_{t2} can be obtained by using Eqs. (2.68), (3.90) and (4.74). The homogeneous solutions of Eqs. (4.83) and (4.84) are given by, respectively,

$$\begin{aligned} a_{t0\,\mathrm{H}} &= \text{const} \quad \text{or} \quad \frac{1}{r}, && (4.93)\\ a_{t2\,\mathrm{H}} &= \frac{1}{M^2}(r-M)(r-2M) \\ &\quad \text{or} \quad \frac{2}{Mr}\left(3r^2-6Mr+M^2\right)+\frac{3}{M^2}\left(r^2-3Mr+2M^2\right)\ln\left(1-\frac{2M}{r}\right). && (4.94)\end{aligned}$$

Hence, the solution which vanishes at infinity is obtained as

$$\begin{aligned} a_{t0} &= \frac{J\mu}{2M^3r^2}(3r-M)+\frac{J\mu}{4M^4r}(3r-4M)\ln\left(1-\frac{2M}{r}\right), && (4.95)\\ a_{t2} &= c_{a_{t2}}\left[\frac{2}{Mr}\left(3r^2-6Mr+M^2\right)+\frac{3}{M^2}\left(r^2-3Mr+2M^2\right)\ln\left(1-\frac{2M}{r}\right)\right] \\ &\quad -\frac{J\mu}{M^5r^2}\left(12r^3-24Mr^2+4M^2r+M^3\right) \\ &\quad -\frac{J\mu}{2M^6r^2}\left(12r^3-36Mr^2+24M^2r+M^3\right)\ln\left(1-\frac{2M}{r}\right), && (4.96)\end{aligned}$$

where we have assumed that the total charge of the star is zero. The constant $c_{a_{t2}}$ is fixed by the junction condition at the stellar surface in the form

$$\begin{aligned} c_{a_{t2}} &= \left\{\frac{J\mu}{M^5R^2}\left(12R^3-24MR^2+4M^2R+M^3\right)\right. \\ &\quad +\frac{J\mu}{2M^6R}\left(12R^3-36MR^2+24M^2R+M^3\right)\ln\left(1-\frac{2M}{R}\right) \\ &\quad \left.-\frac{\mu\Omega}{4M^3}\left[2MR+2M^2+R^2\ln\left(1-\frac{2M}{R}\right)\right]\right\} \\ &\quad \Big/\left[\frac{2}{MR}\left(3R^2-6MR+M^2\right)+\frac{3}{M^2}\left(R^2-3MR+2M^2\right)\ln\left(1-\frac{2M}{R}\right)\right]. && (4.97)\end{aligned}$$

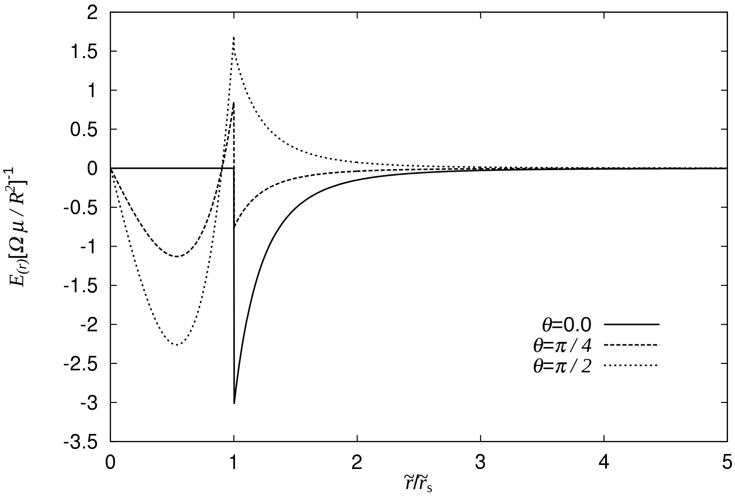

Figure 4.19: The electric field component $E_{(r)}$ in the case of the polytropic stellar model of $n = 0$ and $M/R = 0.2$. The field strength is normalized by the typical value $\Omega\mu/R^2$ and plotted as a function of $\tilde{r}$.

The exterior electric field in local frames is now expressed by

$$\begin{aligned}
E_{(r)} &= \frac{1}{2M^6r^3}\left\{c_{a_{t2}}\left[4M^5r\left(6r^2-3Mr-M^2\right)+6M^4r^3\left(2r-3M\right)\ln\left(1-\frac{2M}{r}\right)\right]\right.\\
&\qquad -2J\mu M\left(24r^3-12Mr^2-4M^2r-3M^3\right)\\
&\qquad \left. -3J\mu r\left(8r^3-12Mr^2-M^3\right)\ln\left(1-\frac{2M}{r}\right)\right\}P_2,\\
E_{(\theta)} &= -\frac{3}{M^6r^3\sqrt{r(r-2M)}}\\
&\quad \times\left\{c_{a_{t2}}\left[2M^5r^2\left(3r^2-6Mr+M^2\right)+3M^4r^3\left(r^2-3Mr+2M^2\right)\ln\left(1-\frac{2M}{r}\right)\right]\right.\\
&\quad -J\mu M\left(12r^4-24Mr^3+4M^2r^2-M^4\right)\\
&\quad \left. -6J\mu r^3\left(r^2-3Mr+2M^2\right)\ln\left(1-\frac{2M}{r}\right)\right\}\sin\theta\cos\theta, \qquad (4.98)
\end{aligned}$$

while the interior solution is given by

$$E_{(r)} = e^{-\frac{\lambda+\nu}{2}}\varpi a'_{\phi1}\sin^2\theta, \qquad (4.99)$$

$$E_{(\theta)} = \frac{2e^{-\frac{\nu}{2}}}{r}\varpi a_{\phi1}\sin\theta\cos\theta. \qquad (4.100)$$

Note that $E_{(r)}$ can become discontinuous at the stellar surface, owing to induced surface electric charge.

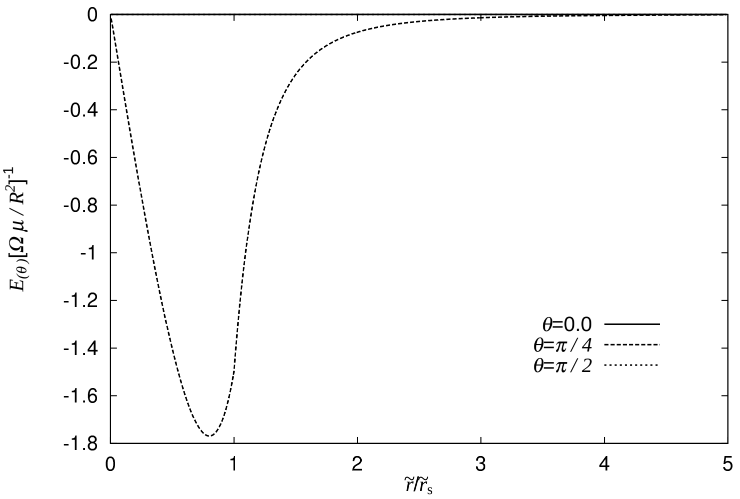

Figure 4.20: The electric field component $E_{(\theta)}$ in the case of the polytropic stellar model of $n = 0$ and $M/R = 0.2$. The field strength is normalized by the typical value $\Omega\mu/R^2$ and plotted as a function of $\tilde{r}$.

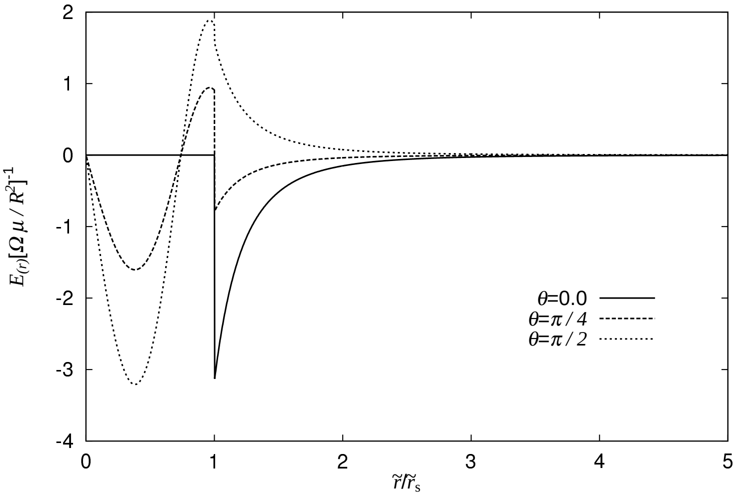

Figure 4.21: The electric field component $E_{(r)}$ in the case of the polytropic stellar model of $n = 1$ and $M/R = 0.2$. The field strength is normalized by the typical value $\Omega\mu/R^2$ and plotted as a function of $\tilde{r}$.

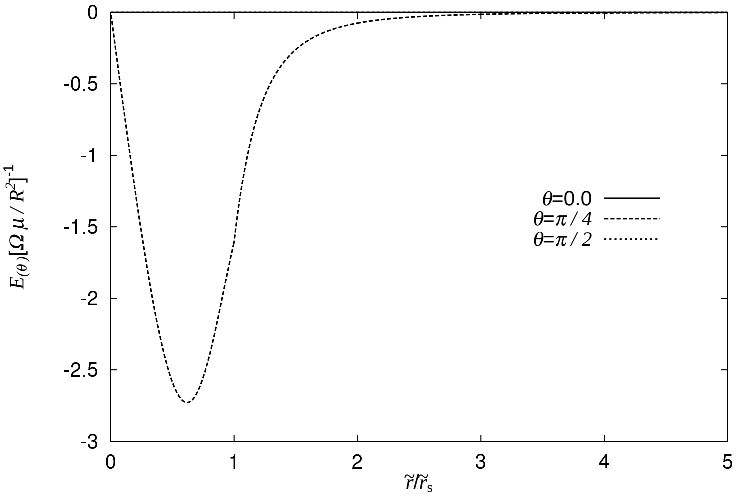

Figure 4.22: The electric field component $E_{(\theta)}$ in the case of the polytropic stellar model of $n = 1$ and $M/R = 0.2$. The field strength is normalized by the typical value $\Omega\mu/R^2$ and plotted as a function of $\tilde{r}$.

Numerical results

First, we show the numerical solutions of a_{t0} and a_{t2} in Figs. 4.17 and 4.18, respectively. Furthermore, Figs. 4.19, 4.20, 4.21 and 4.22 display the electric field component in local frames. In these figures, we adopted polytropic stellar models $(n = 0, 1)$ with $M/R = 0.2$. The comparison with the Newtonian calculations is shown in Fig. 4.23, 4.24, 4.25 and 4.26 explicitly. From these figures, we can find that the electric field strength in the context of general relativity is about 1.5 times larger than that by the Newtonian calculations. This consequence gives the very interesting effect of general relativity, because the enhancement of the electric field strength leads to higher energy radiation from pulsars.

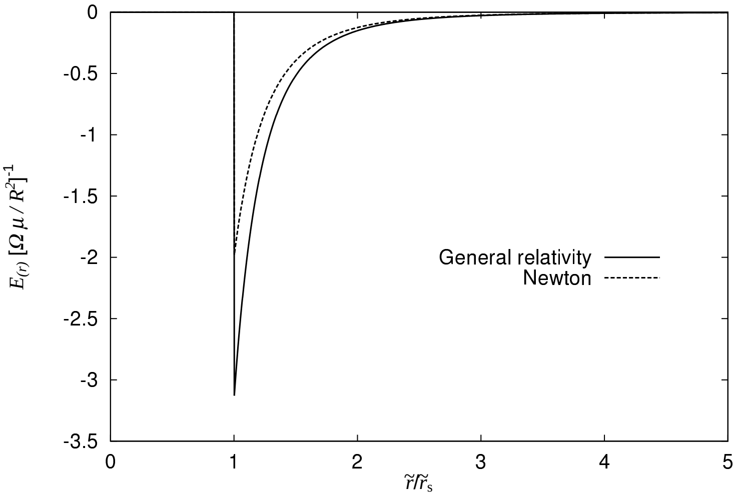

Figure 4.23: Comparison of the electric field $E_{(r)}$ between the Newtonian and the general relativistic calculations for $\theta = 0$. We adopted the polytropic stellar model of $n = 1$.

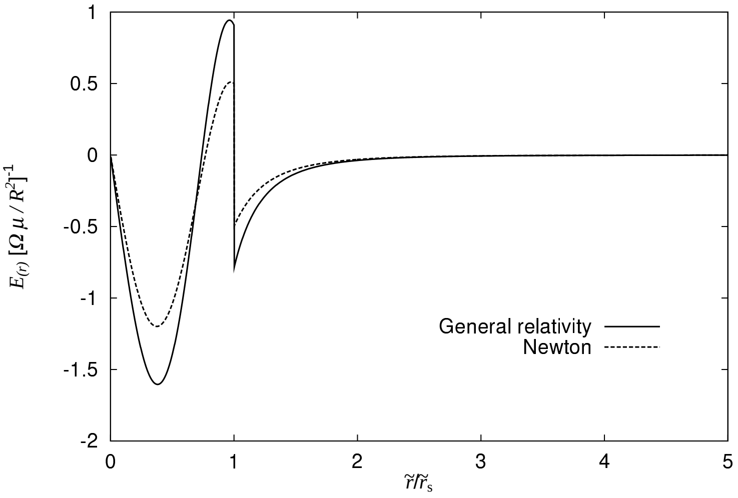

Figure 4.24: Comparison of the electric field $E_{(r)}$ between the Newtonian and the general relativistic calculations for $\theta = \pi/4$. We adopted the polytropic stellar model of $n = 1$.

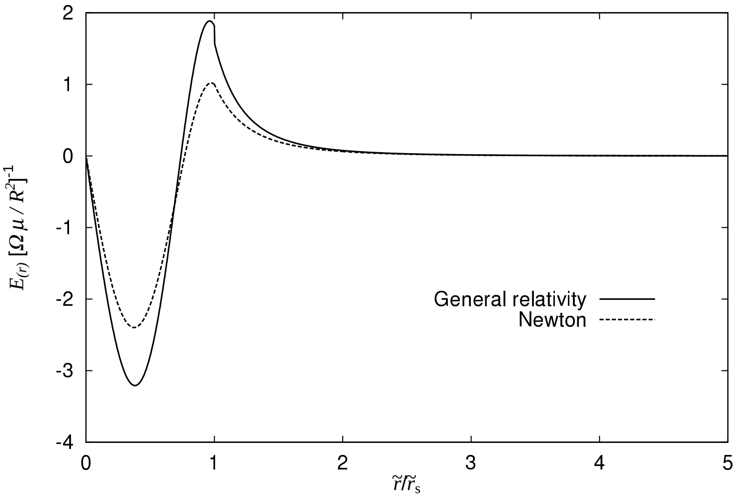

Figure 4.25: Comparison of the electric field $E_{(r)}$ between the Newtonian and the general relativistic calculations for $\theta = \pi/2$. We adopted the polytropic stellar model of $n = 1$.

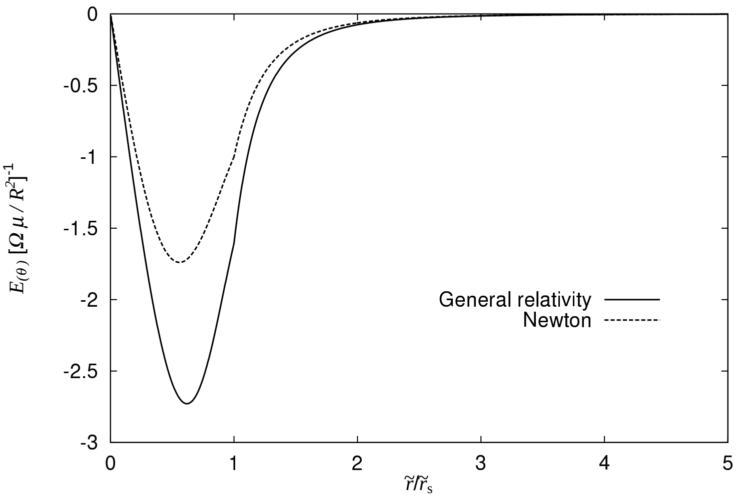

Figure 4.26: Comparison of the electric field $E_{(\theta)}$ between the Newtonian and the general relativistic calculations for $\theta = \pi/4$. We adopted the polytropic stellar model of $n = 1$.

Chapter 5

Stellar Magnetic Deformation

In this chapter, we discuss the magnetic deformation of stars. We consider a dipole magnetic field only as a stellar magnetic field, which can be treated as perturbation. The stellar magnetic deformation arises as a second-order effect in ε_B. Neglecting the rotation of the star, we formulate the quadrupole deformation due to a dipole magnetic field. The Newtonian case is dealt with in §5.1, while the general relativistic case is discussed in §5.2.

5.1 Newtonian stars

5.1.1 Formulation

The structure of the star endowed with a magnetic field is governed by the following equations

$$0 = \nabla\Phi + \frac{1}{\rho}\nabla p - \frac{1}{\rho}\boldsymbol{J}\times\boldsymbol{B}, \tag{5.1}$$

$$\nabla^2\Phi = 4\pi\rho, \tag{5.2}$$

$$\nabla\cdot\boldsymbol{B} = 0, \tag{5.3}$$

$$\nabla\times\boldsymbol{B} = 4\pi\boldsymbol{J}. \tag{5.4}$$

Equations (5.3) and (5.4) have been solved in the last chapter. Using Eq. (5.4), we can write Eq. (5.1) as

$$0 = \nabla\Phi + \frac{1}{\rho}\nabla p - \frac{1}{4\pi\rho}\left(\nabla\times\boldsymbol{B}\right)\times\boldsymbol{B}. \tag{5.5}$$

Here, we have

$$\frac{1}{4\pi}\left(\nabla\times\boldsymbol{B}\right)\times\boldsymbol{B} = \left(\frac{2}{3r^2}a'_{\phi1}j_{\phi1} - \frac{2}{3r^2}a'_{\phi1}j_{\phi1}P_2\right)\boldsymbol{e}_r - \frac{2}{3r^3}a_{\phi1}j_{\phi1}\frac{dP_2}{d\theta}\boldsymbol{e}_\theta, \tag{5.6}$$

where we assumed a dipole magnetic field and used the expansions (4.9) and (4.10) for A_ϕ and J_ϕ.

In the same way as in the rotational case, we expand ρ, p and Φ as follows:

$$\begin{aligned}
\rho &= \rho^{(0)}(r) + \left[\rho_0^{(2)}(r) + \rho_2^{(2)}(r)P_2\right], && (5.7)\\
p &= p^{(0)}(r) + \left[p_0^{(2)}(r) + p_2^{(2)}(r)P_2\right], && (5.8)\\
\Phi &= \Phi^{(0)}(r) + \left[\Phi_0^{(2)}(r) + \Phi_2^{(2)}(r)P_2\right], && (5.9)
\end{aligned}$$

where the superscripts '(0)' and '(2)' here denote the zeroth-order and second-order quantities in ε_B. In most parts, we abbreviate the superscript of the background quantities.

Using the above expansions, from Eq. (5.1), we derive

$$\begin{aligned}
\frac{d\Phi_0^{(2)}}{dr} + \frac{\rho_0^{(2)}}{\rho}\frac{d\Phi}{dr} + \frac{1}{\rho}\frac{dp_0^{(2)}}{dr} - \frac{2}{3r^2\rho}a'_{\phi1}j_{\phi1} &= 0, && (5.10)\\
\frac{d\Phi_2^{(2)}}{dr} + \frac{\rho_2^{(2)}}{\rho}\frac{d\Phi}{dr} + \frac{1}{\rho}\frac{dp_2^{(2)}}{dr} + \frac{2}{3r^2\rho}a'_{\phi1}j_{\phi1} &= 0, && (5.11)
\end{aligned}$$

and

$$\Phi_2^{(2)} + \frac{p_2^{(2)}}{\rho} + \frac{2}{3r^2\rho}a_{\phi1}j_{\phi1} = 0. \tag{5.12}$$

In order for Eqs. (5.10) and (5.11) to be integrated as in the rotational case, the following relation must be satisfied [100, 128],

$$\frac{j_{\phi1}}{r^2\rho} = c_j = \text{const.} \tag{5.13}$$

This integrability condition restricts the current distribution. When Eq. (5.13) is satisfied, Eq. (5.12) can be derived from Eq. (5.11) actually. Hence, Eqs. (5.11) and (5.12) are consistent with this integrability condition. Furthermore, from Eq. (5.10), we can derive

$$\Phi_0^{(2)} + \frac{p_0^{(2)}}{\rho} - \frac{2}{3r^2\rho}a_{\phi1}j_{\phi1} = \text{const.} \tag{5.14}$$

Here, it is useful to introduce $\delta P_0^{(2)}$ and $\delta P_2^{(2)}$ defined as

$$\begin{aligned}
\delta P_0^{(2)} &= \frac{p_0^{(2)}}{\rho}, && (5.15)\\
\delta P_2^{(2)} &= \frac{p_2^{(2)}}{\rho}. && (5.16)
\end{aligned}$$

Using these quantities, we have

$$\begin{aligned}
\Phi_0^{(2)} &= -\delta P_0^{(2)} + \frac{2}{3r^2\rho}a_{\phi1}j_{\phi1} + \text{const}, && (5.17)\\
\Phi_2^{(2)} &= -\delta P_2^{(2)} - \frac{2}{3r^2\rho}a_{\phi1}j_{\phi1}. && (5.18)
\end{aligned}$$

From the Poisson equation (5.2), we derive the equations

$$\begin{aligned} \frac{1}{r^2}\frac{d}{dr}\left(r^2\frac{d\Phi_0^{(2)}}{dr}\right) &= 4\pi\rho_0^{(2)}, & (5.19)\\ \frac{1}{r^2}\frac{d}{dr}\left(r^2\frac{d\Phi_2^{(2)}}{dr}\right)-\frac{6}{r^2}\Phi_2^{(2)} &= 4\pi\rho_2^{(2)}. & (5.20)\end{aligned}$$

Substituting Eqs. (5.17) and (5.18) into these equations, we obtain

$$\frac{d^2}{dr^2}\delta P_0^{(2)}+\frac{2}{r}\frac{d}{dr}\delta P_0^{(2)}+4\pi\frac{\rho'}{p'}\rho\delta P_0^{(2)}=\frac{2}{3}\left(\frac{2}{r}a'_{\phi 1}+\frac{2}{r^2}a_{\phi 1}-4\pi j_{\phi 1}\right)\frac{j_{\phi 1}}{r^2\rho}, \quad (5.21)$$

$$\frac{d^2}{dr^2}\delta P_2^{(2)}+\frac{2}{r}\frac{d}{dr}\delta P_2^{(2)}+\left(4\pi\frac{\rho'}{p'}\rho-\frac{6}{r^2}\right)\delta P_2^{(2)}=-\frac{2}{3}\left(\frac{2}{r}a'_{\phi 1}-\frac{4}{r^2}a_{\phi 1}-4\pi j_{\phi 1}\right)\frac{j_{\phi 1}}{r^2\rho}. \quad (5.22)$$

These equations should be solved inside the star. Once we obtain the solution for $\delta P_0^{(2)}$ and $\delta P_2^{(2)}$, we can derive the potential $\Phi_0^{(2)}$ and $\Phi_2^{(2)}$ from Eqs. (5.17) and (5.18). The derived interior solution for $\Phi_0^{(2)}$ and $\Phi_2^{(2)}$ must be connected with the exterior solution which vanishes at infinity. As the junction conditions, Eqs. (3.33) and (3.34) should be used again.

Normalized equations

Now, we write down the normalized equations of the above-mentioned equations. Equations (5.17) and (5.18) reduce, respectively, to

$$\begin{aligned} \tilde{\Phi}_0^{(2)} &= -\delta\tilde{P}_0^{(2)}+\frac{2}{3\tilde{r}^2\tilde{\rho}}\tilde{a}_{\phi 1}\tilde{j}_{\phi 1}+\mathrm{const}, & (5.23)\\ \tilde{\Phi}_2^{(2)} &= -\delta\tilde{P}_2^{(2)}-\frac{2}{3\tilde{r}^2\rho}\tilde{a}_{\phi 1}\tilde{j}_{\phi 1}. & (5.24)\end{aligned}$$

Furthermore, from Eqs. (5.21) and (5.22), we derive

$$\frac{d^2}{d\tilde{r}^2}\delta\tilde{P}_0^{(2)}+\frac{2}{\tilde{r}}\frac{d}{d\tilde{r}}\delta\tilde{P}_0^{(2)}+\frac{\tilde{\rho}'}{\tilde{p}'}\tilde{\rho}\delta\tilde{P}_0^{(2)}=\frac{2}{3}\left(\frac{2}{\tilde{r}}\tilde{a}'_{\phi 1}+\frac{2}{\tilde{r}^2}\tilde{a}_{\phi 1}-\tilde{j}_{\phi 1}\right)\frac{\tilde{j}_{\phi 1}}{\tilde{r}^2\tilde{\rho}}, \quad (5.25)$$

$$\frac{d^2}{d\tilde{r}^2}\delta\tilde{P}_2^{(2)}+\frac{2}{\tilde{r}}\frac{d}{d\tilde{r}}\delta\tilde{P}_2^{(2)}+\left(\frac{\tilde{\rho}'}{\tilde{p}'}\tilde{\rho}-\frac{6}{\tilde{r}^2}\right)\delta\tilde{P}_2^{(2)}=-\frac{2}{3}\left(\frac{2}{\tilde{r}}\tilde{a}'_{\phi 1}-\frac{4}{\tilde{r}^2}\tilde{a}_{\phi 1}-\tilde{j}_{\phi 1}\right)\frac{\tilde{j}_{\phi 1}}{\tilde{r}^2\tilde{\rho}}. \quad (5.26)$$

These are very useful in numerical integration.

5.1.2 Solutions for stellar configurations

Exterior solution

The exterior solution for $\Phi_0^{(2)}$ and $\Phi_2^{(2)}$ takes the same forms as in the case of rotational flattening,

$$\tilde{\Phi}_0^{(2)} = \frac{c_{1\Phi}}{\tilde{r}}, \quad (5.27)$$

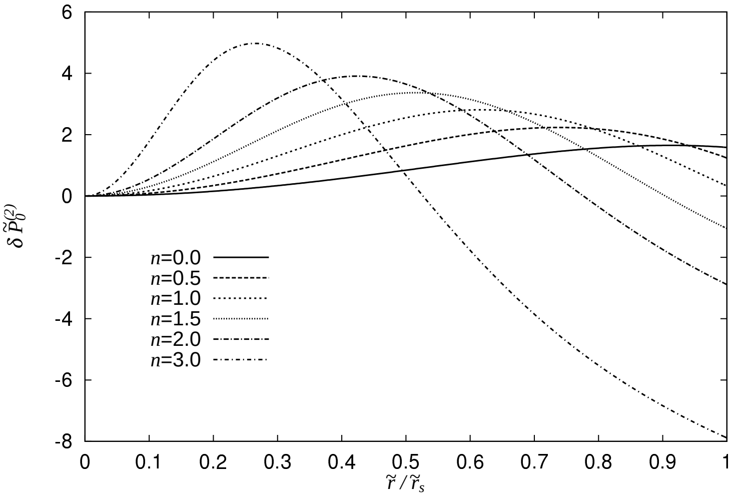

Figure 5.1: The function $\delta\tilde{P}_0^{(2)}$ with respect to $\tilde{r}$ for several polytropic stellar models.

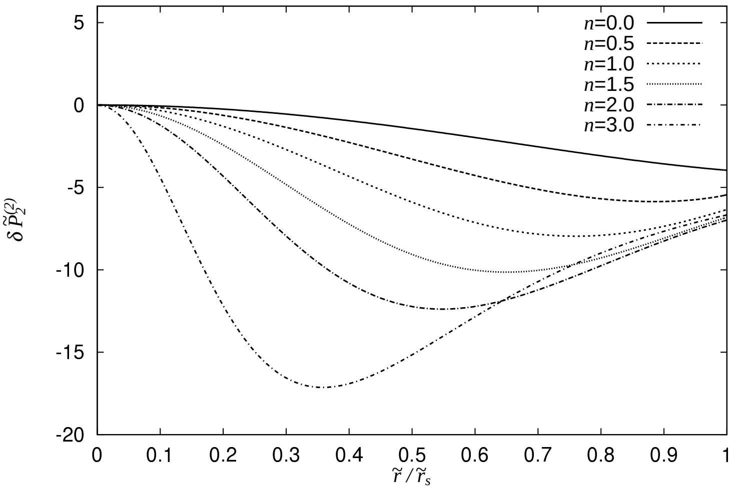

Figure 5.2: The function $\delta\tilde{P}_2^{(2)}$ with respect to $\tilde{r}$ for several polytropic stellar models.

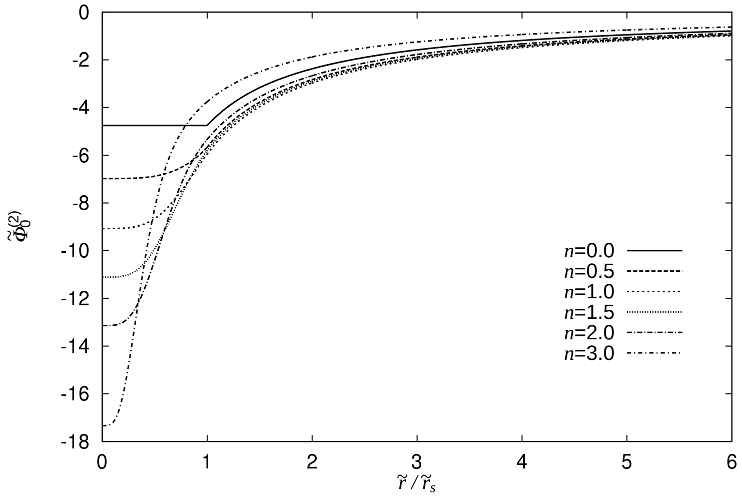

Figure 5.3: The potential $\tilde{\Phi}_0^{(2)}$ plotted as a function of $\tilde{r}$ for several polytropic stellar models.

$$\tilde{\Phi}_2^{(2)} = \frac{d_{1\Phi}}{\tilde{r}^3}, \tag{5.28}$$

where $c_{1\Phi}$ and $d_{1\Phi}$ are constants fixed by the junction with the interior solution at the stellar surface.

Interior solutions

First, we consider the interior solution in the case of an incompressible fluid body, i.e. $n = 0$. In this case, using the solution for the dipole magnetic field given by Eq. (4.30), we derive the differential equations

$$\frac{d^2}{d\tilde{r}^2}\delta\tilde{P}_0^{(2)} + \frac{2}{\tilde{r}}\frac{d}{d\tilde{r}}\delta\tilde{P}_0^{(2)} = -\frac{4}{3}\tilde{c}_j^2\left(\tilde{r}^2 - 3\right), \tag{5.29}$$

$$\frac{d^2}{d\tilde{r}^2}\delta\tilde{P}_2^{(2)} + \frac{2}{\tilde{r}}\frac{d}{d\tilde{r}}\delta\tilde{P}_2^{(2)} - \frac{6}{\tilde{r}^2}\delta\tilde{P}_2^{(2)} = \frac{14}{15}\tilde{c}_j^2\tilde{r}^2. \tag{5.30}$$

Hence, we can obtain the interior solution for $\delta\tilde{P}_0^{(2)}$ and $\delta\tilde{P}_2^{(2)}$ which vanishes at the stellar center in the forms

$$\delta\tilde{P}_0^{(2)} = -\frac{1}{15}\tilde{c}_j^2\tilde{r}^2\left(\tilde{r}^2 - 10\right), \tag{5.31}$$

$$\delta\tilde{P}_2^{(2)} = d_{2\Phi}\tilde{r}^2 + \frac{1}{15}\tilde{c}_j^2\tilde{r}^4, \tag{5.32}$$

where $d_{2\Phi}$ is a constant. From these results, we also derive

$$\tilde{\Phi}_0^{(2)} = c_{2\Phi}, \tag{5.33}$$

$$\tilde{\Phi}_2^{(2)} = -\left(d_{2\Phi} + \frac{2}{3}\tilde{c}_j^2\right)\tilde{r}^2, \tag{5.34}$$

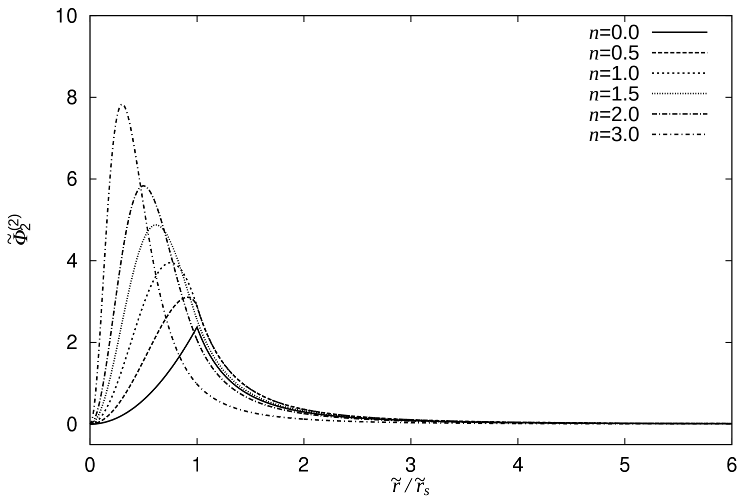

Figure 5.4: The potential $\tilde{\Phi}_2^{(2)}$ plotted as a function of $\tilde{r}$ for several polytropic stellar models.

where $c_{2\Phi}$ is a constant. This interior solution should be connected with the exterior solution given by Eqs. (5.27) and (5.28) under the junction conditions, i.e. Eqs. (3.33) and (3.34). In the current case, we have

$$\tilde{\Phi}''^{(0)}_{\text{in}} - \tilde{\Phi}''^{(0)}_{\text{ext}} = 1, \tag{5.35}$$

$$\left(\frac{1}{\tilde{\rho}}\frac{d\tilde{p}}{d\tilde{r}}\right)^{-1} = -\frac{\sqrt{6}}{2}, \tag{5.36}$$

$$\tilde{\xi}_0^{(2)} = \frac{4\sqrt{6}}{5}\tilde{c}_j^2, \quad \tilde{\xi}_2^{(2)} = 3\sqrt{6}d_{2\Phi} + \frac{6\sqrt{6}}{5}\tilde{c}_j^2. \tag{5.37}$$

Hence, from the junction conditions, we obtain the algebraic equations

$$\frac{c_{1\Phi}}{\sqrt{6}} - c_{2\Phi} = 0, \tag{5.38}$$

$$\frac{c_{1\Phi}}{6} = -\frac{4\sqrt{6}}{5}\tilde{c}_j^2, \tag{5.39}$$

$$\frac{d_{1\Phi}}{6\sqrt{6}} + 6d_{2\Phi} = -4\tilde{c}_j^2, \tag{5.40}$$

$$\frac{d_{1\Phi}}{12} + \sqrt{6}d_{2\Phi} = \frac{2\sqrt{6}}{15}\tilde{c}_j^2. \tag{5.41}$$

The solution is given by

$$c_{1\Phi} = -\frac{24\sqrt{6}}{5}\tilde{c}_j^2, \tag{5.42}$$

$$c_{2\Phi} = -\frac{24}{5}\tilde{c}_j^2, \tag{5.43}$$

$$\begin{aligned} d_{1\Phi} &= \frac{72\sqrt{6}}{5}\tilde{c}_j^2, && (5.44) \\ d_{2\Phi} &= -\frac{16}{15}\tilde{c}_j^2. && (5.45) \end{aligned}$$

Consequently, we obtain

$$\begin{aligned} \delta\tilde{P}_0^{(2)} &= -\frac{1}{15}\tilde{c}_j^2\tilde{r}^2\left(\tilde{r}^2-10\right), && (5.46) \\ \delta\tilde{P}_2^{(2)} &= -\frac{16}{15}\tilde{c}_j^2\tilde{r}^2+\frac{1}{15}\tilde{c}_j^2\tilde{r}^4, && (5.47) \end{aligned}$$

$$\begin{aligned} \tilde{\Phi}_0^{(2)} &= \begin{cases} -\frac{24}{5}\tilde{c}_j^2 & (\tilde{r}<\tilde{r}_\mathrm{s}) \\ -\frac{24\sqrt{6}}{5}\frac{\tilde{c}_j^2}{\tilde{r}} & (\tilde{r}>\tilde{r}_\mathrm{s}) \end{cases}, && (5.48) \\ \tilde{\Phi}_2^{(2)} &= \begin{cases} \frac{2}{5}\tilde{c}_j^2\tilde{r}^2 & (\tilde{r}<\tilde{r}_\mathrm{s}) \\ \frac{72\sqrt{6}}{5}\frac{\tilde{c}_j^2}{\tilde{r}^3} & (\tilde{r}>\tilde{r}_\mathrm{s}) \end{cases}, && (5.49) \end{aligned}$$

$$\begin{aligned} \tilde{\xi}_0^{(2)} &= \frac{4\sqrt{6}}{5}\tilde{c}_j^2, && (5.50) \\ \tilde{\xi}_2^{(2)} &= -2\sqrt{6}\tilde{c}_j^2. && (5.51) \end{aligned}$$

Using the last result, we can find the value of ellipticity in the way

$$\text{ellipticity} = -\frac{3}{2}\frac{\xi_2^{(2)}}{R} = 3\tilde{c}_j^2 = \frac{25}{2}\frac{\mu^2}{M^2R^2}. \tag{5.52}$$

In general cases, we can write the potentials $\tilde{\Phi}_0^{(2)}$ and $\tilde{\Phi}_2^{(2)}$ as

$$\begin{aligned} \tilde{\Phi}_0^{(2)} &= \begin{cases} \frac{c_{1\Phi}}{\tilde{r}} & (\tilde{r}>\tilde{r}_\mathrm{s}) \\ -\delta\tilde{P}_0^{(2)}+\frac{2}{3}\tilde{c}_j\tilde{a}_{\phi1}+c_{2\Phi} & (\tilde{r}<\tilde{r}_\mathrm{s}) \end{cases}, && (5.53) \\ \tilde{\Phi}_2^{(2)} &= \begin{cases} \frac{d_{1\Phi}}{\tilde{r}^3} & (\tilde{r}>\tilde{r}_\mathrm{s}) \\ -d_{2\Phi}\delta\tilde{P}_{2H}^{(2)}-\delta\tilde{P}_{2P}^{(2)}-\frac{2}{3}\tilde{c}_j\tilde{a}_{\phi1} & (\tilde{r}<\tilde{r}_\mathrm{s}) \end{cases}, && (5.54) \end{aligned}$$

where $\delta\tilde{P}_{2H}^{(2)}$ and $\delta\tilde{P}_{2P}^{(2)}$ are homogeneous and particular solutions for $\delta\tilde{P}_2^{(2)}$, respectively. Considering the junctions at the stellar surface, we derive the equations

$$\begin{aligned} -\frac{c_{1\Phi}}{\tilde{r}_\mathrm{s}}+c_{2\Phi} &= \delta\tilde{P}_0^{(2)}(\tilde{r}_\mathrm{s})-\frac{2}{3}\tilde{c}_j\tilde{a}_{\phi1}(\tilde{r}_\mathrm{s}), && (5.55) \\ \frac{c_{1\Phi}}{\tilde{r}_\mathrm{s}^2} &= \delta\tilde{P}_0^{\prime(2)}(\tilde{r}_\mathrm{s})-\frac{2}{3}\tilde{c}_j\tilde{a}_{\phi1}^{\prime}(\tilde{r}_\mathrm{s})-\tilde{\xi}_0^{(2)}A, && (5.56) \end{aligned}$$

$$\begin{aligned} \frac{d_{1\Phi}}{\tilde{r}_\mathrm{s}^3}+\delta\tilde{P}_{2H}^{(2)}(\tilde{r}_\mathrm{s})d_{2\Phi} &= -\delta\tilde{P}_{2P}^{(2)}(\tilde{r}_\mathrm{s})-\frac{2}{3}\tilde{c}_j\tilde{a}_{\phi1}(\tilde{r}_\mathrm{s}), && (5.57) \\ \frac{3}{\tilde{r}_\mathrm{s}^4}d_{1\Phi}+\left[-\delta\tilde{P}_{2H}^{\prime(2)}(\tilde{r}_\mathrm{s})+\tilde{\xi}_{2H}^{(2)}A\right]d_{2\Phi} &= \delta\tilde{P}_{2P}^{\prime(2)}(\tilde{r}_\mathrm{s})+\frac{2}{3}\tilde{c}_j\tilde{a}_{\phi1}^{\prime}(\tilde{r}_\mathrm{s})-\tilde{\xi}_{2P}^{(2)}A. && (5.58) \end{aligned}$$

In these equations, we have used

$$\begin{aligned}
\xi_0^{(2)} &= -\left(\frac{1}{\rho}\frac{dp}{dr}\right)^{-1} \delta P_0^{(2)}\bigg|_{\xi^{(0)}}, && (5.59)\\
\xi_{2H}^{(2)} &= -\left(\frac{1}{\rho}\frac{dp}{dr}\right)^{-1} \delta P_{2H}^{(2)}\bigg|_{\xi^{(0)}}, && (5.60)\\
\xi_{2P}^{(2)} &= -\left(\frac{1}{\rho}\frac{dp}{dr}\right)^{-1} \delta P_{2P}^{(2)}\bigg|_{\xi^{(0)}}, && (5.61)\\
A &= \left(\tilde{\Phi}_{\rm in}''^{(0)} - \tilde{\Phi}_{\rm ext}''^{(0)}\right)\Big|_{\xi^{(0)}}. && (5.62)
\end{aligned}$$

The solution of the above algebraic equations is given by

$$\begin{aligned}
c_{1\Phi} &= -\frac{\tilde{r}_{\rm s}^2}{3}\left(2\tilde{c}_j\tilde{a}_{\phi 1}'(\tilde{r}_{\rm s}) - 3\delta\tilde{P}_0'^{(2)}(\tilde{r}_{\rm s}) + 3\tilde{\xi}_0^{(2)}A\right), && (5.63)\\
c_{2\Phi} &= \frac{1}{3}\left(-2\tilde{c}_j\tilde{a}_{\phi 1}(\tilde{r}_{\rm s}) + 3\delta\tilde{P}_0^{(2)}(\tilde{r}_{\rm s}) - 2\tilde{r}_{\rm s}\tilde{c}_j\tilde{a}_{\phi 1}'(\tilde{r}_{\rm s}) + 3\tilde{r}_{\rm s}\delta\tilde{P}_0'^{(2)}(\tilde{r}_{\rm s}) - 3\tilde{r}_{\rm s}\tilde{\xi}_0^{(2)}A\right), && (5.64)
\end{aligned}$$

$$\begin{aligned}
d_{1\Phi} &= -\left(\frac{2}{3}\tilde{c}_j\tilde{a}_{\phi 1}(\tilde{r}_{\rm s}) + \delta\tilde{P}_{2P}^{(2)}(\tilde{r}_{\rm s})\right)\tilde{r}_{\rm s}^3 \\
&\quad + \frac{\delta\tilde{P}_{2H}^{(2)}(\tilde{r}_{\rm s})\tilde{r}_{\rm s}^3\left(6\tilde{c}_j\tilde{a}_{\phi 1}(\tilde{r}_{\rm s}) + 9\delta\tilde{P}_{2P}^{(2)}(\tilde{r}_{\rm s}) + 2\tilde{r}_{\rm s}\tilde{c}_j\tilde{a}_{\phi 1}'(\tilde{r}_{\rm s}) + 3\tilde{r}_{\rm s}\delta\tilde{P}_{2P}'^{(2)}(\tilde{r}_{\rm s}) - 3\tilde{r}_{\rm s}\tilde{\xi}_{2P}^{(2)}A\right)}{3\left(3\delta\tilde{P}_{2H}^{(2)}(\tilde{r}_{\rm s}) + \tilde{r}_{\rm s}\delta\tilde{P}_{2H}'^{(2)}(\tilde{r}_{\rm s}) - \tilde{r}_{\rm s}\tilde{\xi}_{2H}^{(2)}A\right)}, \\
d_{2\Phi} &= -\frac{6\tilde{c}_j\tilde{a}_{\phi 1}(\tilde{r}_{\rm s}) + 9\delta\tilde{P}_{2P}^{(2)}(\tilde{r}_{\rm s}) + 2\tilde{r}_{\rm s}\tilde{c}_j\tilde{a}_{\phi 1}'(\tilde{r}_{\rm s}) + 3\tilde{r}_{\rm s}\delta\tilde{P}_{2P}'^{(2)}(\tilde{r}_{\rm s}) - 3\tilde{r}_{\rm s}\tilde{\xi}_{2P}^{(2)}A}{3\left(3\delta\tilde{P}_{2H}^{(2)}(\tilde{r}_{\rm s}) + \tilde{r}_{\rm s}\delta\tilde{P}_{2H}'^{(2)}(\tilde{r}_{\rm s}) - \tilde{r}_{\rm s}\tilde{\xi}_{2H}^{(2)}A\right)}. && (5.65)
\end{aligned}$$

Using these, we can obtain numerical solutions. We show $\delta\tilde{P}_0^{(2)}$, $\delta\tilde{P}_0^{(2)}$, $\tilde{\Phi}_0^{(2)}$ and $\tilde{\Phi}_2^{(2)}$ as a function of $\tilde{r}$ in Figs. 5.1, 5.2, 5.3 and 5.4, respectively, for several polytropic stellar models.

In the same way as the case of rotational flattening, ellipticity can also be calculated as

$$\text{ellipticity} = -\frac{3}{2}\frac{\tilde{\xi}_2^{(2)}}{\tilde{r}_{\rm s}} = -\frac{3}{2}\frac{\tilde{\xi}_2^{(2)}\tilde{m}(\tilde{r}_{\rm s})^2\tilde{r}_{\rm s}}{\tilde{\mu}^2}\frac{\mu^2}{M^2R^2}. \qquad (5.66)$$

Figure 5.5 displays the numerical results obtained for several polytropic stellar models. From this figure, we can find that the value of ellipticity becomes large with the polytropic index n for fixed $\mu^2/(M^2R^2)$.

5.2 General relativistic stars

5.2.1 Formulation

Next, we discuss magnetic deformation of a star in the context of general relativity. The quadrupole deformation of the star endowed with a dipole magnetic field can be treated in

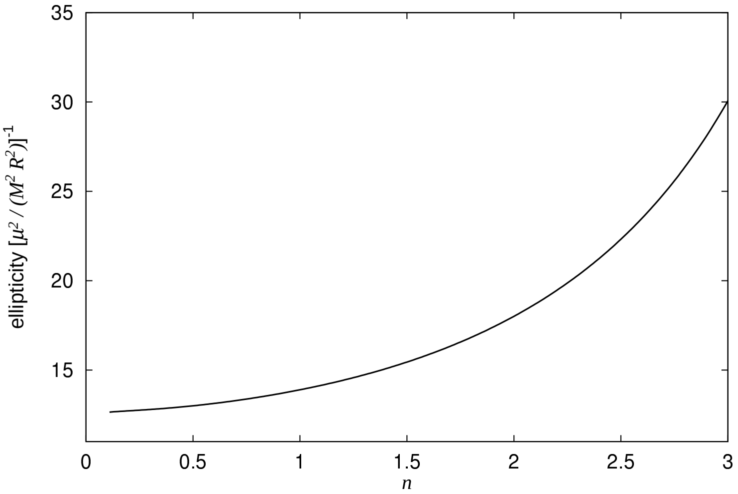

Figure 5.5: Dependence of ellipticity on the polytropic index n.

the very similar way as the rotational case. The space-time of such a star can be described by the line element

$$\begin{aligned} ds^2 &= -e^{\nu}\left[1+2\left(h_0(r)+h_2(r)P_2\right)\right]dt^2+e^{\lambda}\left[1+\frac{2e^{\lambda}}{r}\left(m_0(r)+m_2(r)P_2\right)\right]dr^2 \\ &\quad +r^2\left[1+2k_2(r)P_2\right]\left(d\theta^2+\sin^2\theta d\phi^2\right), \end{aligned} \tag{5.67}$$

where h_0, h_2, m_0, m_2 and k_2 are second-order quantities in ε_B.

The stress-energy tensor of the perfect fluid body endowed with a dipole magnetic field is given by

$$T^{\mu}_{\ \nu}=\left(\rho+p\right)u^{\mu}u_{\nu}+p\delta^{\mu}_{\ \nu}+\frac{1}{4\pi}\left(F^{\mu\lambda}F_{\nu\lambda}-\frac{1}{4}F_{\sigma\lambda}F^{\sigma\lambda}\delta^{\mu}_{\ \nu}\right), \tag{5.68}$$

where the pressure p and the energy density ρ are expanded again in the forms

$$p = p^{(0)}+\left(p_0^{(2)}+p_2^{(2)}P_2\right), \tag{5.69}$$

$$\rho = \rho^{(0)}+\left(\rho_0^{(2)}+\rho_2^{(2)}P_2\right). \tag{5.70}$$

Here, the superscript '(0)' will be abbreviated in most parts. Furthermore, the Faraday tensor $F_{\mu\nu}$ is given by the four-potential $A_{\mu}=(0,0,0,A_{\phi})$ which was dealt with in the last Chapter.

The equations which govern the configuration of the magnetized star can be obtained from the Einstein equations $G^{\mu}_{\ \nu}=8\pi T^{mu}_{\ \nu}$ and the equation of motion $T^{\mu}_{\ \nu;\mu}=0$. First, from the Einstein equation, we obtain

$$\frac{dm_0}{dr} = 4\pi r^2\frac{\rho'}{p'}p_0^{(2)}+\frac{1}{3}\left[e^{-\lambda}\left(a'_{\phi 1}\right)^2+\frac{2}{r^2}a_{\phi 1}^2\right], \tag{5.71}$$

$$\frac{dh_0}{dr} = 4\pi re^{\lambda}p_0^{(2)}+\frac{1}{r}\nu'e^{\lambda}m_0+\frac{1}{r^2}e^{\lambda}m_0+\frac{e^{\lambda}}{3r}\left[e^{-\lambda}\left(a'_{\phi 1}\right)^2-\frac{2}{r^2}a_{\phi 1}^2\right], \tag{5.72}$$

$$\begin{aligned}
\frac{dh_2}{dr}+\frac{dk_2}{dr} &= h_2\left(\frac{1}{r}-\frac{\nu'}{2}\right)+\frac{e^{\lambda}}{r}m_2\left(\frac{1}{r}+\frac{\nu'}{2}\right)+\frac{4}{3r^2}a_{\phi 1}a'_{\phi 1}, &(5.73)\\
h_2+\frac{e^{\lambda}}{r}m_2 &= \frac{2}{3}e^{-\lambda}\left(a'_{\phi 1}\right)^2, &(5.74)\\
\frac{dh_2}{dr}+\left(1+\frac{r\nu'}{2}\right)\frac{dk_2}{dr} &= 4\pi r e^{\lambda}p_2^{(2)}+\frac{1}{r^2}e^{\lambda}m_2+\frac{1}{r}\nu' e^{\lambda}m_2+\frac{3}{r}e^{\lambda}h_2+\frac{2}{r}e^{\lambda}k_2\\
&\quad -\frac{1}{3r}e^{\lambda}\left[e^{-\lambda}\left(a'_{\phi 1}\right)^2+\frac{4}{r^2}a_{\phi 1}^2\right]. &(5.75)
\end{aligned}$$

Second, we obtain the following equations from the equation of motion:

$$\begin{aligned}
\frac{dp_0^{(2)}}{dr} &= -\frac{\nu'}{2}\left(\frac{\rho'}{p'}+1\right)p_0^{(2)}-(\rho+p)\,h'_0+\frac{2}{3r^2}a'_{\phi 1}j_{\phi 1}, &(5.76)\\
\frac{dp_2^{(2)}}{dr} &= -\frac{\nu'}{2}\left(\frac{\rho'}{p'}+1\right)p_2^{(2)}-(\rho+p)\,h'_2-\frac{2}{3r^2}a'_{\phi 1}j_{\phi 1}, &(5.77)\\
p_2^{(2)} &= -(\rho+p)\,h_2-\frac{2}{3r^2}a_{\phi 1}j_{\phi 1}. &(5.78)
\end{aligned}$$

As in the Newtonian case, we derive the general relativistic version of the integrability condition from Eqs. (5.76) and (5.77) in the form [103]

$$\frac{j_{\phi 1}}{r^2(\rho+p)}=c_j=\text{const.} \tag{5.79}$$

Under this condition, we can actually derive Eq. (5.78) from Eq. (5.77). From Eq. (5.76), we now derive the relation

$$\frac{p_0^{(2)}}{(\rho+p)}=-h_0+\frac{2}{3r^2(\rho+p)}a_{\phi 1}j_{\phi 1}+c_{p_0}, \tag{5.80}$$

where c_{p_0} is a constant of integration. Here, we define $\delta P_0^{(2)}$ and $\delta P_2^{(2)}$ as

$$\begin{aligned}
\delta P_0^{(2)} &= \frac{p_0^{(2)}}{\rho+p}, &(5.81)\\
\delta P_2^{(2)} &= \frac{p_2^{(2)}}{\rho+p}. &(5.82)
\end{aligned}$$

Using these quantities, we consequently derive the relations

$$\begin{aligned}
\delta P_0^{(2)} &= -h_0+\frac{2}{3}c_j a_{\phi 1}+c_{p_0}, &(5.83)\\
\delta P_2^{(2)} &= -h_2-\frac{2}{3}c_j a_{\phi 1}. &(5.84)
\end{aligned}$$

From Eq. (5.71) and (5.72), we now have two coupled equations

$$\frac{dm_0}{dr} = -4\pi r^2\frac{\rho'}{p'}(\rho+p)(h_0-c_{p_0})+\frac{1}{3}e^{-\lambda}\left(a'_{\phi 1}\right)^2+\frac{2}{3r^2}a_{\phi 1}^2+\frac{8\pi}{3}\frac{\rho'}{p'}a_{\phi 1}j_{\phi 1}, \tag{5.85}$$

$$\begin{aligned}\frac{dh_0}{dr} &= \left(\frac{1}{r^2}+\frac{\nu'}{r}\right)e^{\lambda}m_0 - 4\pi r e^{\lambda}\left(\rho+p\right)\left(h_0-c_{p_0}\right)\\ &+ \frac{1}{3r}\left(a'_{\phi1}\right)^2 - \frac{2}{3r^3}e^{\lambda}{a_{\phi1}}^2 + \frac{8\pi}{3r}e^{\lambda}a_{\phi1}j_{\phi1}, \end{aligned} \tag{5.86}$$

or

$$\frac{dm_0}{dr} = 4\pi r^2\left(\rho+p\right)\frac{\rho'}{p'}\delta P_0^{(2)} + \frac{1}{3}e^{-\lambda}\left(a'_{\phi1}\right)^2 + \frac{2}{3r^2}a_{\phi1}^2, \tag{5.87}$$

$$\begin{aligned}\frac{d\delta P_0^{(2)}}{dr} &= -\left(\frac{1}{r^2}+\frac{\nu'}{r}\right)e^{\lambda}m_0 - 4\pi r\left(\rho+p\right)e^{\lambda}\delta P_0^{(2)}\\ &- \frac{1}{3r}\left(a'_{\phi1}\right)^2 + \frac{2}{3r^3}e^{\lambda}{a_{\phi1}}^2 + \frac{2}{3}c_j a'_{\phi1}. \end{aligned} \tag{5.88}$$

It is convenient to use Eqs. (5.85) and (5.86) outside the star, while Eqs. (5.87) and (5.88) should be used inside the star. Furthermore, from Eqs. (5.73), (5.74) and (5.75), we can derive the differential equations for $\upsilon_2(\equiv h_2+k_2)$ and h_2,

$$\frac{d\upsilon_2}{dr} = -\nu' h_2 + \frac{2}{3}e^{-\lambda}\left(\frac{1}{r}+\frac{\nu'}{2}\right)\left(a'_{\phi1}\right)^2 + \frac{4}{3r^2}a_{\phi1}a'_{\phi1}, \tag{5.89}$$

$$\begin{aligned}\frac{dh_2}{dr} &= -\frac{4e^{\lambda}}{r^2\nu'}\upsilon_2 + \left[8\pi\frac{e^{\lambda}}{\nu'}\left(\rho+p\right) + \frac{2}{r^2\nu'}\left(1-e^{\lambda}\right) - \nu'\right]h_2\\ &+ \frac{8}{3r^4\nu'}e^{\lambda}a_{\phi1}^2 + \frac{8}{3r^3\nu'}\left(1+\frac{r\nu'}{2}\right)a_{\phi1}a'_{\phi1}\\ &+ \left(\frac{1}{3}\nu' e^{-\lambda} + \frac{2}{3r^2\nu'}\right)\left(a'_{\phi1}\right)^2 + \frac{16\pi}{3r^2\nu'}e^{\lambda}a_{\phi1}j_{\phi1}. \end{aligned} \tag{5.90}$$

The remaining function m_2 can be derived from Eq. (5.74) using the solution of h_2. Therefore, two sets of differential equations (5.85)-(5.86) or (5.87)-(5.88) and (5.89)-(5.89) and one algebraic equation (5.74) govern the structure of the relativistic magnetized star.

Boundary and junction conditions

The boundary and junction conditions which should be imposed take the same forms as in the rotational case, i.e.

- $r \to \infty$

$$h_0, h_2 \to 0, \tag{5.91}$$

$$m_0, m_2 \to \text{finite}, \tag{5.92}$$

$$k_2 \to \frac{1}{r^{\alpha}} \quad \left(\alpha \geq 3\right), \tag{5.93}$$

- $r = R$

$$\begin{aligned} g_{\mu\nu}|_{-\xi} &= g_{\mu\nu}|_{+\xi} \quad (\mu, \nu = t, r, \theta, \phi), & (5.94) \\ g_{ab,r}|_{-\xi} &= g_{ab,r}|_{+\xi} \quad (a, b = t, \theta, \phi), & (5.95) \end{aligned}$$

- $r \to 0$

$$\begin{aligned} h_0, \delta P_0^{(2)} &\to \text{finite}, & (5.96) \\ m_0, m_2, h_2, v_2 &\to 0. & (5.97) \end{aligned}$$

In the case of $n = 0$, we have to pay attention to the junction conditions. In this case, we have the conditions

$$(\lambda'_{\text{in}} - \lambda'_{\text{ext}})|_{\xi^{(0)}} \, \xi_a^{(2)} + \frac{2e^{\lambda}}{r} \left(m_{a\,\text{in}} - m_{a\,\text{ext}}\right)\Big|_{\xi^{(0)}} = 0, \qquad (5.98)$$

$$(\nu''_{\text{in}} - \nu''_{\text{ext}})|_{\xi^{(0)}} \, \xi_a^{(2)} + 2 \left(h'_{a\,\text{in}} - h'_{a\,\text{ext}}\right)|_{\xi^{(0)}} = 0, \qquad (5.99)$$

where a takes 0 or 2. Numerical solutions for the metric functions should be derived following these conditions.

Normalized equations

Here, we summarize the normalized forms of the above equations. First, we derive

$$\begin{aligned} \zeta \delta \tilde{P}_0^{(2)} &= -h_0 + \frac{2\zeta}{3} \tilde{c}_j \tilde{a}_{\phi 1} + c_{p_0}, & (5.100) \\ \zeta \delta \tilde{P}_2^{(2)} &= -h_2 - \frac{2\zeta}{3} \tilde{c}_j \tilde{a}_{\phi 1}. & (5.101) \end{aligned}$$

Next, outside the star, the equations for m_0 and h_0 are written as

$$\begin{aligned} \frac{d\tilde{m}_0}{d\tilde{r}} &= \frac{\zeta}{3} e^{-\lambda} \left(\tilde{a}'_{\phi 1}\right)^2 + \frac{2\zeta}{3\tilde{r}^2} \tilde{a}^2_{\phi 1}, & (5.102) \\ \frac{dh_0}{d\tilde{r}} &= \zeta \left(\frac{1}{\tilde{r}^2} + \frac{\nu'}{\tilde{r}}\right) e^{\lambda} \tilde{m}_0 + \frac{\zeta^2}{3\tilde{r}} \left(\tilde{a}'_{\phi 1}\right)^2 - \frac{2\zeta^2}{3\tilde{r}^3} e^{\lambda} \tilde{a}^2_{\phi 1}. & (5.103) \end{aligned}$$

Inside the star, we derive

$$\begin{aligned} \frac{d\tilde{m}_0}{d\tilde{r}} &= \tilde{r}^2 \left(\tilde{\rho} + \zeta \tilde{p}\right) \frac{\tilde{\rho}'}{\tilde{p}'} \delta \tilde{P}_0^{(2)} + \frac{\zeta}{3} e^{-\lambda} \left(\tilde{a}'_{\phi 1}\right)^2 + \frac{2\zeta}{3\tilde{r}^2} \tilde{a}^2_{\phi 1}, & (5.104) \\ \frac{d\delta \tilde{P}_0^{(2)}}{d\tilde{r}} &= -\left(\frac{1}{\tilde{r}^2} + \frac{\nu'}{\tilde{r}}\right) e^{\lambda} \tilde{m}_0 - \zeta \tilde{r} \left(\tilde{\rho} + \zeta \tilde{p}\right) e^{\lambda} \delta \tilde{P}_0^{(2)} \\ &\quad - \frac{\zeta}{3\tilde{r}} \left(\tilde{a}'_{\phi 1}\right)^2 + \frac{2\zeta}{3\tilde{r}^3} e^{\lambda} \tilde{a}^2_{\phi 1} + \frac{2}{3} \tilde{c}_j \tilde{a}'_{\phi 1}. & (5.105) \end{aligned}$$

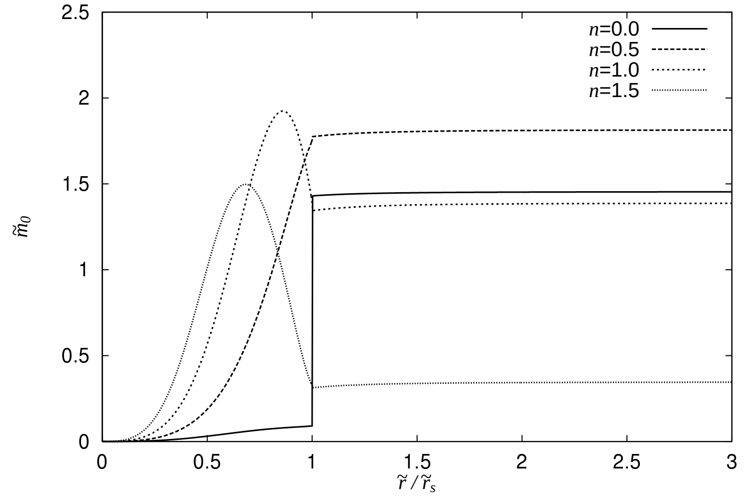

Figure 5.6: The function $\tilde{m}_0(\tilde{r})$ under the boundary condition $\delta P_0^{(2)}(0) = 0$. We adopted stellar models with $M/R = 0.2$.

The equations for v_2 and h_2 are written in the forms

$$\frac{dv_2}{d\tilde{r}} = -\nu' h_2 + \frac{2\zeta^2}{3} e^{-\lambda} \left(\frac{1}{\tilde{r}} + \frac{\nu'}{2} \right) \left(\tilde{a}'_{\phi 1} \right)^2 + \frac{4\zeta^2}{3\tilde{r}^2} \tilde{a}_{\phi 1} \tilde{a}'_{\phi 1}, \tag{5.106}$$

$$\begin{aligned} \frac{dh_2}{d\tilde{r}} = & -\frac{4e^{\lambda}}{\tilde{r}^2 \nu'} v_2 + \left[2\zeta \frac{e^{\lambda}}{\nu'} \left(\tilde{\rho} + \zeta \tilde{p} \right) + \frac{2}{\tilde{r}^2 \nu'} \left(1 - e^{\lambda} \right) - \nu' \right] h_2 \\ & + \frac{8\zeta^2}{3\tilde{r}^4 \nu'} e^{\lambda} \tilde{a}_{\phi 1}^2 + \frac{8\zeta^2}{3\tilde{r}^3 \nu'} \left(1 + \frac{\tilde{r}\nu'}{2} \right) \tilde{a}_{\phi 1} \tilde{a}'_{\phi 1} \\ & + \zeta^2 \left(\frac{1}{3} \nu' e^{-\lambda} + \frac{2}{3\tilde{r}^2 \nu'} \right) \left(\tilde{a}'_{\phi 1} \right)^2 + \frac{4\zeta^2}{3\tilde{r}^2 \nu'} e^{\lambda} \tilde{a}_{\phi 1} \tilde{j}_{\phi 1}. \end{aligned} \tag{5.107}$$

Moreover, the function m_2 can be derived by

$$\tilde{m}_2 = \frac{\tilde{r}}{\zeta e^{\lambda}} \left[-h_2 + \frac{2\zeta^2}{3} e^{-\lambda} \left(\tilde{a}'_{\phi 1} \right)^2 \right]. \tag{5.108}$$

These normalized equations are very useful in numerical calculations.

5.2.2 Solutions for stellar configurations

The functions m_0, $\delta P_0^{(2)}$ and h_0

First, we deal with the metric functions m_0, $\delta P_0^{(2)}$ and h_0. Outside the star, the differential equations (5.102) and (5.103) can easily be integrated. The exterior solution which satisfies the boundary conditions at infinity is given by

$$m_0 = \frac{3\mu^2}{8M^4 r} \left(r^2 - M^2 \right) + \frac{3\mu^2}{8M^5} \left(r^2 - Mr - M^2 \right) \ln \left(1 - \frac{2M}{r} \right)$$

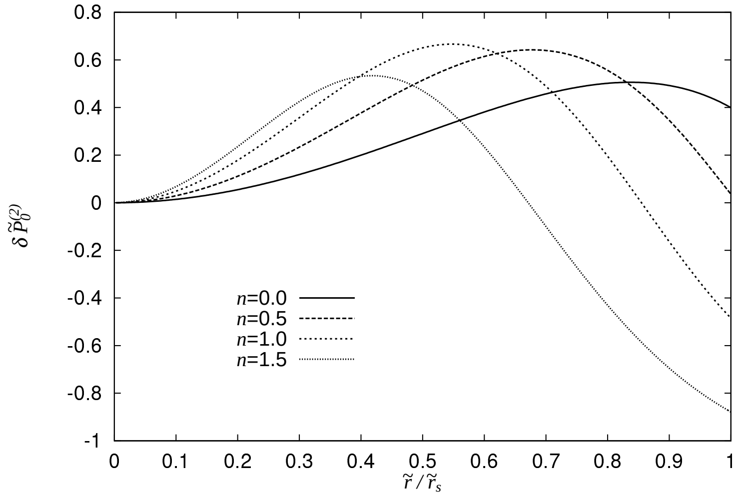

Figure 5.7: The function $\delta\tilde{P}_0^{(2)}(\tilde{r})$ under the boundary condition $\delta P_0^{(2)}(0) = 0$. We adopted stellar models with $M/R = 0.2$.

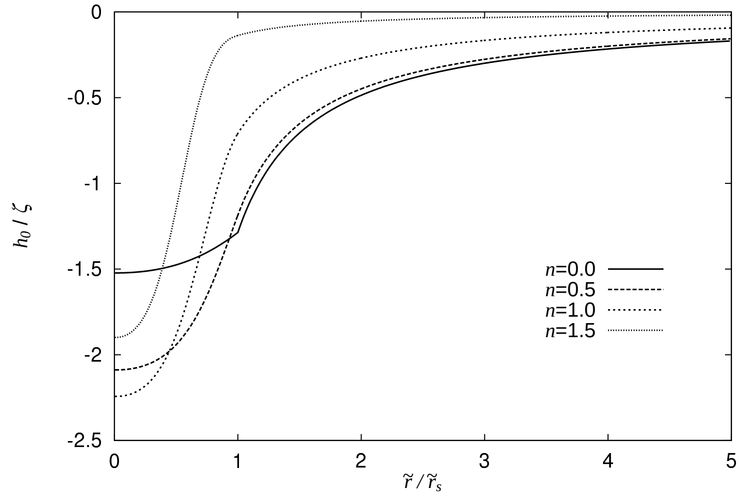

Figure 5.8: The function $h_0(\tilde{r})$ under the boundary condition $\delta P_0^{(2)}(0) = 0$. We adopted stellar models with $M/R = 0.2$.

$$+\frac{3\mu^2}{32M^6}r^2\left(r-2M\right)\left[\ln\left(1-\frac{2M}{r}\right)\right]^2+c_{\rm m}, \tag{5.109}$$

$$\begin{aligned} h_0 \;=\; & -\frac{3\mu^2}{8M^3}\frac{4r-M}{r\left(r-2M\right)}+\frac{3\mu^2}{8M^5}\frac{(r-M)(r-3M)}{r-2M}\ln\left(1-\frac{2M}{r}\right) \\ & +\frac{3\mu^2}{32M^6}r^2\left[\ln\left(1-\frac{2M}{r}\right)\right]^2-\frac{c_{\rm m}}{r-2M}+\frac{3\mu^2}{8M^4}, \end{aligned} \tag{5.110}$$

where $c_{\rm m}$ is a constant corresponding to mass shift.

Interior solutions can be obtained by numerical integration. Figures 5.6, 5.7 and 5.8 display the numerical results of the functions $\tilde{m}_0$, $\delta\tilde{P}_0^{(2)}$ and h_0, respectively, in the case that $\delta P_0^{(2)}$ vanishes at the stellar center. In this case, the mass shift $c_{\rm m}$ is written as

$$\tilde{c}_{\rm m} \;=\; \tilde{m}_{0{\rm in}}-\tilde{m}_{0{\rm out}}+\frac{\tilde{r}e^{-\lambda}}{2\zeta}A_\lambda\tilde{\xi}_0^{(2)}, \tag{5.111}$$

where $\tilde{m}_{0{\rm out}}$ is given by

$$\begin{aligned} \tilde{m}_{0{\rm out}} \;=\; & \zeta\left\{\frac{3\tilde{\mu}^2}{8\zeta^4\tilde{m}(\tilde{r}_{\rm s})^4\tilde{r}_{\rm s}}\left(\tilde{r}_{\rm s}^2-\zeta^2\tilde{m}(\tilde{r}_{\rm s})^2\right)\right. \\ & +\frac{3\tilde{\mu}^2}{8\zeta^5\tilde{m}(\tilde{r}_{\rm s})^5}\left(\tilde{r}_{\rm s}^2-\zeta\tilde{m}(\tilde{r}_{\rm s})\tilde{r}_{\rm s}-\zeta^2\tilde{m}(\tilde{r}_{\rm s})^2\right)\ln\left(1-\frac{2\zeta\tilde{m}(\tilde{r}_{\rm s})}{\tilde{r}_{\rm s}}\right) \\ & \left.+\frac{3\tilde{\mu}^2}{32\zeta^6\tilde{m}(\tilde{r}_{\rm s})^6}\tilde{r}_{\rm s}^2\left(\tilde{r}_{\rm s}-2\zeta\tilde{m}(\tilde{r}_{\rm s})\right)\left[\ln\left(1-\frac{2\zeta\tilde{m}(\tilde{r}_{\rm s})}{\tilde{r}_{\rm s}}\right)\right]^2\right\}, \end{aligned} \tag{5.112}$$

and A_λ is defined as

$$A_\lambda = \left(\lambda'_{\rm in}-\lambda'_{\rm ext}\right)\big|_{\xi^{(0)}}. \tag{5.113}$$

Furthermore, in Figs. 5.9, 5.10 and 5.11, we show the functions $\tilde{m}_0$, $\delta\tilde{P}_0^{(2)}$ and h_0 which are obtained under a different condition, that is, the condition that the mass shift equals to zero. The interior solution can now be written as

$$\tilde{m}_0 \;=\; c_0\tilde{m}_{0{\rm H}}+\tilde{m}_{0{\rm P}}, \tag{5.114}$$

$$\delta\tilde{P}_0^{(2)} \;=\; c_0\delta\tilde{P}_{0{\rm H}}^{(2)}+\delta\tilde{P}_{0{\rm P}}^{(2)}. \tag{5.115}$$

Associated with these expressions, we can write down $\tilde{\xi}_0^{(2)}$ as

$$\tilde{\xi}_0^{(2)} = c_0\tilde{\xi}_{0{\rm H}}^{(2)}+\tilde{\xi}_{0{\rm P}}^{(2)}, \tag{5.116}$$

where

$$\tilde{\xi}_{0{\rm H}}^{(2)} \;=\; -\left(\frac{1}{\tilde{\rho}+\zeta\tilde{p}}\frac{d\tilde{p}}{d\tilde{r}}\right)^{-1}\delta\tilde{P}_{0{\rm H}}^{(2)}\Bigg|_{\xi^{(0)}}, \tag{5.117}$$

$$\tilde{\xi}_{0{\rm P}}^{(2)} \;=\; -\left(\frac{1}{\tilde{\rho}+\zeta\tilde{p}}\frac{d\tilde{p}}{d\tilde{r}}\right)^{-1}\delta\tilde{P}_{0{\rm P}}^{(2)}\Bigg|_{\xi^{(0)}}. \tag{5.118}$$

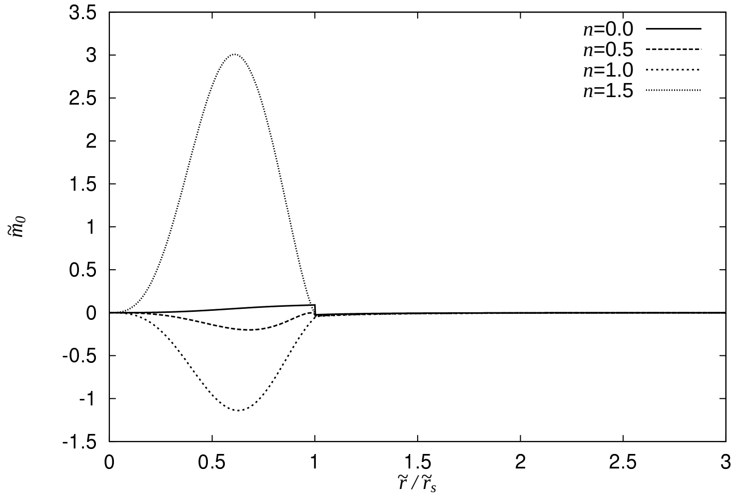

Figure 5.9: The function $\tilde{m}_0(\tilde{r})$ in the case of $c_{\rm m}=0$. We adopted stellar models with $M/R=0.2$.

Using these quantities, c_0 is given by

$$c_0 = \frac{\tilde{m}_{\rm 0out} - \tilde{m}_{\rm 0P}(\tilde{r}_{\rm s}) - \frac{\tilde{r}_{\rm s}e^{-\lambda}}{2\zeta}A_\lambda\tilde{\xi}^{(2)}_{\rm 0P}}{\tilde{m}_{\rm 0H}(\tilde{r}_{\rm s}) + \frac{\tilde{r}_{\rm s}e^{-\lambda}}{2\zeta}A_\lambda\tilde{\xi}^{(2)}_{\rm 0H}}. \tag{5.119}$$

Using this expression, we can find numerical solutions.

The functions v_2, h_2, k_2, m_2 and $\delta P_2^{(2)}$

Next, we consider the functions v_2, h_2, k_2, m_2 and $\delta P_2^{(2)}$.

First, in order to integrate Eqs. (5.106) and (5.107) outside the star, it is useful to introduce the variable z

$$z = \frac{r}{M} - 1 = \frac{\tilde{r}}{\zeta\tilde{m}(\tilde{r}_{\rm s})} - 1 \tag{5.120}$$

as in the rotational case. Using this variable, we derive the differential equations

$$\begin{aligned}
\frac{dv_2}{dz} &= -\frac{1}{(z+1)(z-1)}h_2 + \frac{2z}{3(z+1)^2}\frac{1}{\tilde{m}(\tilde{r}_{\rm s})^2}\left(\frac{d\tilde{a}_{\phi1}}{dz}\right)^2 + \frac{4}{3(z+1)^2}\frac{1}{\tilde{m}(\tilde{r}_{\rm s})^2}\tilde{a}_{\phi1}\frac{d\tilde{a}_{\phi1}}{dz}, \qquad (5.121)\\
\frac{dh_2}{dz} &= -2v_2 - \frac{2z}{z^2-1}h_2 + \frac{4}{3(z+1)^2}\frac{1}{\tilde{m}(\tilde{r}_{\rm s})^2}\tilde{a}_{\phi1}^2\\
&\quad + \frac{4z}{3(z+1)^2}\frac{1}{\tilde{m}(\tilde{r}_{\rm s})^2}\tilde{a}_{\phi1}\frac{d\tilde{a}_{\phi1}}{dz} + \frac{z^2+1}{3(z+1)^2}\frac{1}{\tilde{m}(\tilde{r}_{\rm s})^2}\left(\frac{d\tilde{a}_{\phi1}}{dz}\right)^2. \qquad (5.122)
\end{aligned}$$

The exterior solution which vanishes at infinity can be obtained in the forms

$$v_2 = \frac{2c_1}{\sqrt{z^2-1}}Q_2^1(z) - \frac{3\mu^2}{4M^4\sqrt{z^2-1}}P_2^1(z) + \frac{9\mu^2}{4M^4}z + \frac{3\mu^2}{8M^4}\frac{7z^2-4}{z^2-1}$$

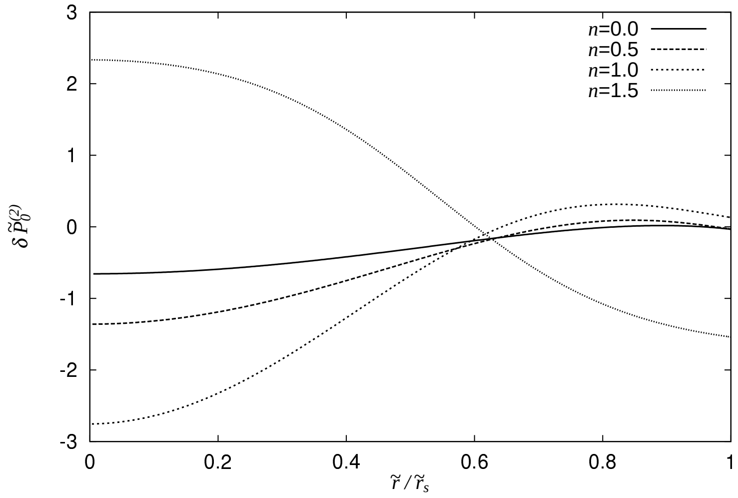

Figure 5.10: The function $\delta\tilde{P}_0^{(2)}(\tilde{r})$ in the case of $c_{\mathrm{m}} = 0$. We adopted stellar models with $M/R = 0.2$.

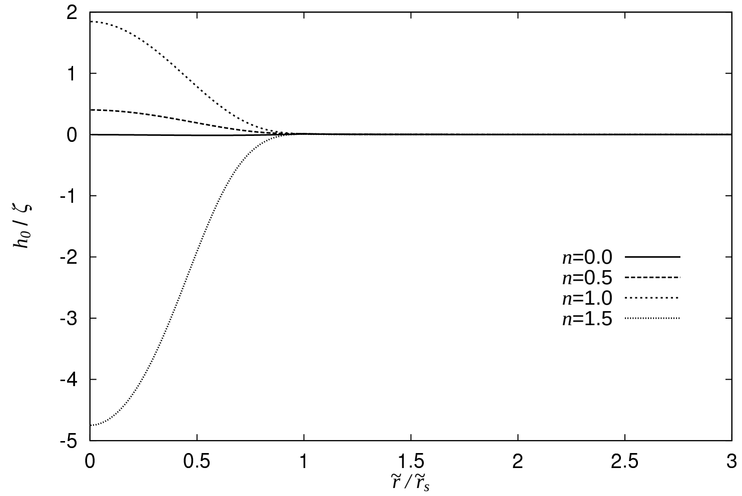

Figure 5.11: The function $h_0(\tilde{r})$ in the case of $c_{\mathrm{m}} = 0$. We adopted stellar models with $M/R = 0.2$.

$$
+\frac{3\mu^2}{16M^4}\frac{z\left(11z^2-7\right)}{z^2-1}\ln\frac{z-1}{z+1}+\frac{3\mu^2}{16M^4}\left(2z^2+1\right)\left(\ln\frac{z-1}{z+1}\right)^2, \tag{5.123}
$$

$$
\begin{aligned}
h_2 &= c_1Q_2^2(z)-\frac{3\mu^2}{8M^4}P_2^2(z)-\frac{3\mu^2}{16M^4}\left[6z^2+3z-6-\frac{4z^2+2z}{z^2-1}\right] \\
&\quad -\frac{3\mu^2}{32M^4}\left[3z^2-8z-3-\frac{8}{z^2-1}\right]\ln\frac{z-1}{z+1}+\frac{3\mu^2}{16M^4}\left(z^2-1\right)\left(\ln\frac{z-1}{z+1}\right)^2, \qquad (5.124)
\end{aligned}
$$

where c_1 is a constant of integration, and P_2^1, Q_2^1, P_2^2 and Q_2^2 are the associated Legendre functions. In the normalized forms, we have

$$
\begin{aligned}
v_2 &= \frac{2c_1}{\sqrt{z^2-1}}Q_2^1(z)-\frac{3\tilde{\mu}^2}{4\zeta^2\tilde{m}_{\rm s}^4\sqrt{z^2-1}}P_2^1(z)+\frac{9\tilde{\mu}^2}{4\zeta^2\tilde{m}_{\rm s}^4}z+\frac{3\tilde{\mu}^2}{8\zeta^2\tilde{m}_{\rm s}^4}\frac{7z^2-4}{z^2-1} \\
&\quad +\frac{3\tilde{\mu}^2}{16\zeta^2\tilde{m}_{\rm s}^4}\frac{z\left(11z^2-7\right)}{z^2-1}\ln\frac{z-1}{z+1}+\frac{3\tilde{\mu}^2}{16\zeta^2\tilde{m}_{\rm s}^4}\left(2z^2+1\right)\left(\ln\frac{z-1}{z+1}\right)^2, \qquad (5.125) \\
h_2 &= c_1Q_2^2(z)-\frac{3\tilde{\mu}^2}{8\zeta^2\tilde{m}_{\rm s}^4}P_2^2(z)-\frac{3\tilde{\mu}^2}{16\zeta^2\tilde{m}_{\rm s}^4}\left[6z^2+3z-6-\frac{4z^2+2z}{z^2-1}\right] \\
&\quad -\frac{3\tilde{\mu}^2}{32\zeta^2\tilde{m}_{\rm s}^4}\left[3z^2-8z-3-\frac{8}{z^2-1}\right]\ln\frac{z-1}{z+1}+\frac{3\tilde{\mu}^2}{16\zeta^2\tilde{m}_{\rm s}^4}\left(z^2-1\right)\left(\ln\frac{z-1}{z+1}\right)^2. \qquad (5.126)
\end{aligned}
$$

Let us now rewrite the exterior solution as

$$
\begin{aligned}
v_2 &= c_1u_1(z)+u_2(z), \qquad (5.127) \\
h_2 &= c_1w_1(z)+w_2(z). \qquad (5.128)
\end{aligned}
$$

An interior solution can also be written as

$$
\begin{aligned}
v_2 &= c_2v_{2\,\rm H}+v_{2\,\rm P}, \qquad (5.129) \\
h_2 &= c_2h_{2\,\rm H}+h_{2\,\rm P}, \qquad (5.130)
\end{aligned}
$$

where c_2 is a constant. The junction conditions determine the constants c_1 and c_2 as

$$
\begin{aligned}
c_1 &= \frac{v_{2\,\rm P}h_{2\,\rm H}-v_{2\,\rm H}h_{2\,\rm P}-u_2h_{2\,\rm H}+w_2v_{2\,\rm H}}{h_{2\,\rm H}u_1-v_{2\,\rm H}w_1}, \qquad (5.131) \\
c_2 &= \frac{-v_{2\,\rm P}w_1+h_{2\,\rm P}u_1+u_2w_1-u_1w_2}{-h_{2\,\rm H}u_1+v_{2\,\rm H}w_1}, \qquad (5.132)
\end{aligned}
$$

where we use the surface values in these equations.

Figures 5.12 and 5.13 display the numerical results of these metric functions. Furthermore, we show the other functions k_2, $\tilde{m}_2$ and $\delta\tilde{P}_2^{(2)}$ derived by using algebraic relations in Figs. 5.14, 5.15 and 5.16.

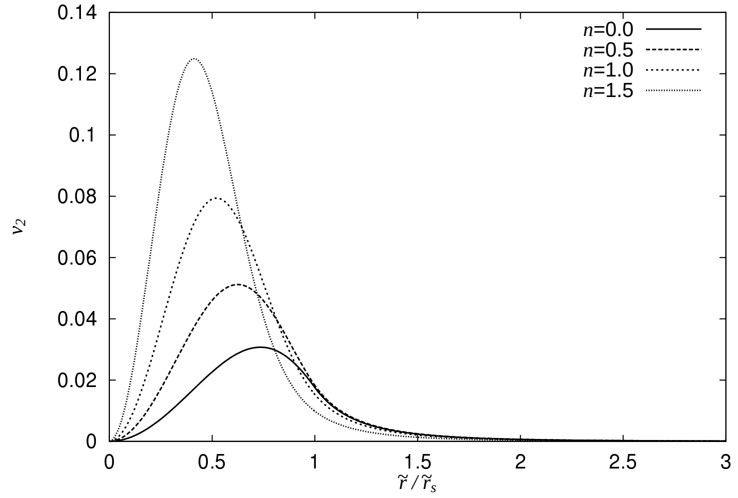

Figure 5.12: The metric function $v_2(\tilde{r})$, which is obtained for polytropic stellar models with $M/R = 0.2$.

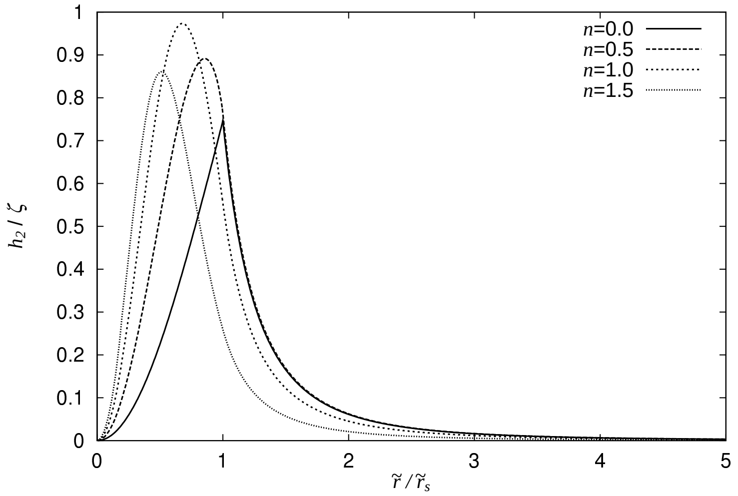

Figure 5.13: The metric function $h_2(\tilde{r})$, which is obtained for polytropic stellar models with $M/R = 0.2$.

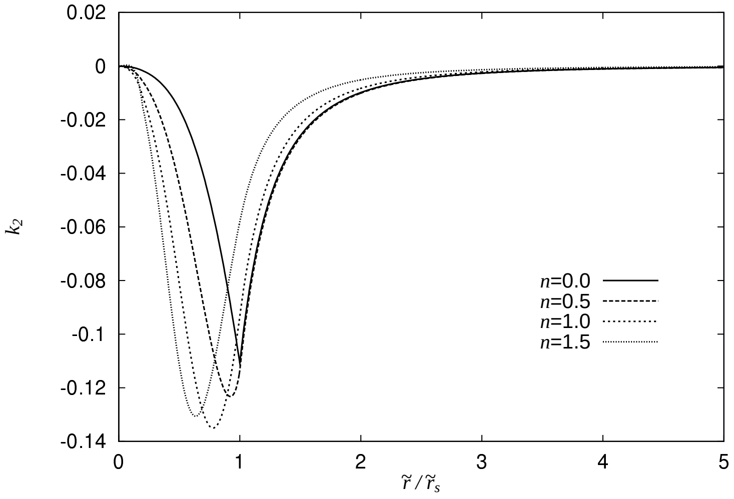

Figure 5.14: The metric function $k_2(\tilde{r})$, which is obtained for polytropic stellar models with $M/R = 0.2$.

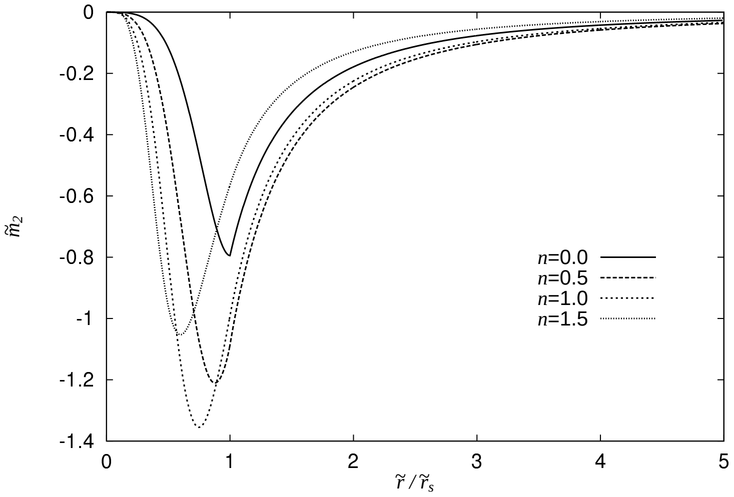

Figure 5.15: The metric function $\tilde{m}_2(\tilde{r})$, which is obtained for polytropic stellar models with $M/R = 0.2$.

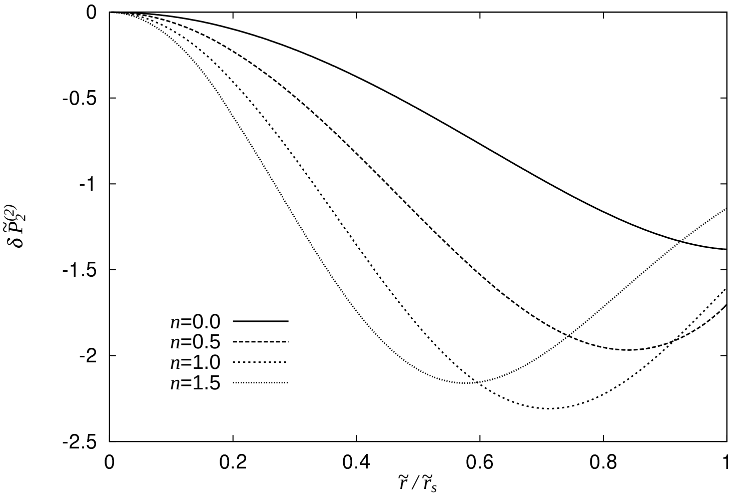

Figure 5.16: The metric function $\delta\tilde{P}_2^{(2)}(\tilde{r})$, which is obtained for polytropic stellar models with $M/R = 0.2$.

5.2.3 Ellipticity

After deriving the solutions for the metric functions, we can calculate the values of ellipticity using the definition

$$\text{ellipticity} = -\frac{3}{2}\left(\frac{\xi_2^{(2)}}{r_\mathrm{s}} + k_2(r_\mathrm{s})\right). \tag{5.133}$$

Figure 5.17 displays dependence of ellipticity on the general relativistic factor M/R. From this figure, we can find that the values of ellipticity slightly become large with the general relativistic factor M/R in each polytropic stellar model for fixed $\mu^2/(M^2R^2)$.

Finally, we show the comparison between flattening by rotation and that by a dipole magnetic field in Fig. 5.18. This figure displays the critical line on which $\varepsilon_\Omega = \varepsilon_B$ and the two regions divided by this line in B-Ω space, where B denotes the typical magnetic field strength defined by $B = \mu/R^3$. We plotted only one representative line of $n = 1$. However, we can also derive very close results for the other indices. In the region I, the magnetic effect dominates the rotational effect, whereas in the region II vice versa. From this figure, we see that objects having magnetic field strength $B \sim 10^{14}$–10^{15}G and a period $T \sim 1\,\mathrm{s}$ such as SGRs and AXPs belong to the region I. Thus, the magnetic effect overwhelms the rotational effect for such observed candidates of magnetars.

Chapter 6

Moments of Inertia of Magnetically Deformed Stars

In this chapter, we consider the moments of inertia of magnetically deformed stars, which are dealt with in the last chapter. In Newtonian gravity, once we have the the mass distribution of an object $\rho(\boldsymbol{x})$, the moment of inertia with respect to any axis can be calculated from $I = \int \rho(\boldsymbol{x})\chi^2 d^3x$, where χ denotes the length from the axis. In general relativity, only for axisymmetric objects, the moment of inertia with respect to the symmetric axis can be well defined. For this definition, we need the slow rotation of the objects. The slow rotation ensures that the angular momentum J is linearly related to the angular velocity Ω, i.e. $J = I\Omega$. Here, I defines the general relativistic version of the moment of inertia. The moments of inertia of relativistic, spherically symmetric stars were already calculated in Chapter 2 (see also Refs. [110,125,132]).

The formulation of the configuration of a rotating, magnetically deformed star is given in §6.1. The general expression for the principal moment of inertia with respect to the symmetry axis is derived. The numerical estimates are obtained for several stellar models in §6.2. In §6.3, we discuss the other principal moments of inertia.

6.1 Rotating magnetically deformed stars

We now consider the slowly rotating star which is subject to quadrupole deformation owing to a dipole magnetic field. We assume that the star slowly rotates on the magnetic axis with a uniform angular velocity $\Omega \sim O(\varepsilon_\Omega)$. In this chapter, we take into account the rotational corrections up to first order in ε_Ω. The metric describing such a star can be given by

$$\begin{aligned} ds^2 &= -e^\nu \left[1+2\left(h_0+h_2P_2\right)\right]dt^2 + e^\lambda \left[1+\frac{2e^\lambda}{r}\left(m_0+m_2P_2\right)\right]dr^2 + r^2\left(1+2k_2P_2\right)d\theta^2 \\ &\quad + r^2\sin^2\theta\left(1+2k_2P_2\right)\left[d\phi - \left(W_1(r) - \frac{W_3(r)}{\sin\theta}\frac{dP_3(\cos\theta)}{d\theta}\right)dt\right]^2 . \end{aligned} \tag{6.1}$$

If we replace W_1 and W_3 with zero in Eq. (6.1), this expression reduces to the metric already investigated in the last chapter. The newly appeared functions W_1 and W_3 lead to frame dragging due to the rotating, magnetically deformed star. In order to involve the effect of deformation, let these functions include corrections up to order of $\varepsilon_\Omega\varepsilon_B^2$. Showing order explicitly, we can write down W_1 and W_3 in the forms

$$W_1 = \omega + W_1^{(2)}, \tag{6.2}$$

$$W_3 = W_3^{(2)}, \tag{6.3}$$

where $\omega \sim O(\varepsilon_\Omega)$ and $(W_1^{(2)}, W_3^{(2)}) \sim O(\varepsilon_\Omega\varepsilon_B^2)$. The form of the terms including W_1 and W_3 in Eq. (6.1) corresponds to the quadrupole deformation of the star. These functions are very analogous to the rotational corrections up to third order in ε_Ω [133, 134].

In this case, the non-vanishing components of four-velocity u^μ appearing in the stress-energy tensor are given by

$$u^t = e^{-\frac{\nu}{2}}\left[1-\left(h_0+h_2P_2\right)\right], \tag{6.4}$$

$$u^\phi = \Omega u^t. \tag{6.5}$$

Furthermore, the Faraday tensor $F_{\mu\nu}$ is given by the 4-potential A_μ [116, 117],

$$A_\mu = \left(a_{t0}(r) + a_{t2}(r)P_2, 0, 0, a_{\phi 1}(r)\sin\theta\frac{dP_1}{d\theta}\right). \tag{6.6}$$

The differential equations which W_1 and W_3 obey can be obtained from the $(t\phi)$-component of the Einstein equation,

$$\frac{1}{r^4}\frac{d}{dr}\left[r^4\mathcal{J}\frac{d\overline{W}_1}{dr}\right] + \frac{4}{r}\frac{d\mathcal{J}}{dr}\overline{W}_1 = -\mathcal{J}\left(S_1 - \frac{S_2}{5}\right), \tag{6.7}$$

$$\frac{1}{r^4}\frac{d}{dr}\left[r^4\mathcal{J}\frac{dW_3}{dr}\right] + \left(\frac{4}{r}\frac{d\mathcal{J}}{dr} - \frac{10}{r^2}e^{\frac{\lambda-\nu}{2}}\right)W_3 = \mathcal{J}\frac{S_2}{5}, \tag{6.8}$$

where $\overline{W}_1$ are defined as

$$\overline{W}_1 = \Omega - W_1 = \varpi - W_1^{(2)}. \tag{6.9}$$

These differential equations are solved order by order. The differential equation for ϖ of order ε_Ω, in which both S_1 and S_2 vanish, was solved in Chapter 3. We are now interested in the differential equations of order of $\varepsilon_\Omega \varepsilon_B^2$. The functions S_1 and S_2 appearing in the source terms in Eqs. (6.7) and (6.8), in general, include W_1 and W_3. However, when we consider S_1 and S_2 up to the order of our interest, these functions include Ω and ω only as shown below. The source terms of order of $\varepsilon_\Omega \varepsilon_B^2$ are given by

$$\begin{aligned} S_1 &= \varpi' \left(-h_0 - \frac{e^\lambda}{r} m_0\right)' - \frac{4}{r^2} e^\lambda (\nu' + \lambda') \varpi m_0 - 16\pi e^\lambda \varpi \left(\rho_0^{(2)} + p_0^{(2)}\right) \\ &\quad + \frac{16 e^\lambda}{3r^4} a_{\phi 1}^2 \omega + \frac{8}{3r^2} \left(a_{\phi 1}'\right)^2 \omega + \frac{8e^\lambda}{r^4} a_{\phi 1} a_{t2} - \frac{4}{r^2} a_{\phi 1}' a_{t0}', \qquad (6.10) \\ S_2 &= \varpi' \left(4k_2 - h_2 - \frac{e^\lambda}{r} m_2\right)' - \frac{4}{r^2} e^\lambda (\nu' + \lambda') \varpi m_2 - 16\pi e^\lambda \varpi \left(\rho_2^{(2)} + p_2^{(2)}\right) \\ &\quad + \frac{32 e^\lambda}{3r^4} a_{\phi 1}^2 \omega - \frac{8}{3r^2} \left(a_{\phi 1}'\right)^2 \omega + \frac{16 e^\lambda}{r^4} a_{\phi 1} a_{t2} - \frac{4}{r^2} a_{\phi 1}' a_{t2}'. \qquad (6.11) \end{aligned}$$

These can be calculated by using the functions already discussed.

The differential equations (6.7) and (6.8) can be solved numerically by imposing boundary and junction conditions. The boundary conditions are summarized as

$$W_1 \to \text{const}, \quad W_3 \to 0 \quad \text{as} \quad r \to 0, \qquad (6.12)$$

$$W_1, W_3 \to \frac{1}{r^\beta} \, (\beta \geq 3) \quad \text{as} \quad r \to \infty. \qquad (6.13)$$

Furthermore, we impose the junction conditions at the stellar surface which is given by

$$\begin{aligned} W_a|_{+\xi^{(0)}} &= W_a|_{-\xi^{(0)}}, \qquad (6.14) \\ W_a'|_{+\xi^{(0)}} &= W_a'|_{-\xi^{(0)}}, \qquad (6.15) \end{aligned}$$

where a takes 1 or 3 (see Eqs. (5.94) and (5.95)).

Before deriving numerical solutions, it is worthwhile to investigate the behavior of W_1 and W_3 at large r in detail using Eqs. (6.7), (6.8), (6.10) and (6.11), because this inspection gives the expressions for the angular momentum and the moment of inertia of the star.

At large r, we have

$$\lambda, \nu \to 0, \quad \text{i.e.} \quad \mathcal{J} \to 1. \qquad (6.16)$$

From Eqs. (6.10) and (6.11), we derive the asymptotic behaviors

$$S_1 \propto \frac{1}{r^8}, \quad S_2 \propto \frac{1}{r^7}. \qquad (6.17)$$

Using these expressions, from Eqs. (6.7), (6.8) and (6.13), we obtain

$$W_1^{(2)} \propto \frac{1}{r^3}, \quad W_3^{(2)} \propto \frac{1}{r^5}. \tag{6.18}$$

Hence, we can put

$$\overline{W}_1 = \Omega - \frac{2J}{r^3} - W_{1p}^{(2)}, \tag{6.19}$$

where J is the angular momentum of the deformed star, and $W_{1p}^{(2)} \sim O(1/r^6)$ is a function of order $\varepsilon_\Omega \varepsilon_B^2$. We now integrate Eq. (6.7) after multiplying both sides by r^4. Using the above expression (6.19), we can obtain the general expression for the principal moment of inertia

$$\begin{aligned} I_z &= \frac{J}{\Omega} \\ &= -\frac{2}{3}\int_0^R r^3 \frac{dj}{dr}\frac{\varpi}{\Omega} dr - \frac{R^4}{6\Omega}\left(\frac{dW_{1p}^{(2)}}{dr}\right)_R + \frac{2}{3}\int_0^R r^3 \frac{dj}{dr}\frac{W_1^{(2)}}{\Omega} dr - \frac{1}{6\Omega}\int_0^R r^4 \mathcal{J}\left(S_1 - \frac{S_2}{5}\right) dr. \end{aligned} \tag{6.20}$$

The moment of inertia of the background, spherically symmetric star $I^{(0)}$ is given by [110,132]

$$I^{(0)} = -\frac{2}{3}\int_0^R r^3 \frac{dj}{dr}\frac{\varpi}{\Omega} dr. \tag{6.21}$$

Therefore, we obtain

$$I_z^{(2)} = -\frac{R^4}{6\Omega}\left(\frac{dW_{1p}^{(2)}}{dr}\right)_R + \frac{2}{3}\int_0^R r^3 \frac{dj}{dr}\frac{W_1^{(2)}}{\Omega} dr - \frac{1}{6\Omega}\int_0^R r^4 \mathcal{J}\left(S_1 - \frac{S_2}{5}\right) dr, \tag{6.22}$$

where we have used the decomposition $I_z = I^{(0)} + I_z^{(2)}$. The magnetic modification of the principal moment of inertia $I_z^{(2)}$ is the second order quantity in ε_B. Numerical estimates of $I_z^{(2)}$ for several stellar models are given in the next section.

6.2 Numerical estimates of the moment of inertia

Using the boundary and junction conditions mentioned in the last section, we can derive the numerical solutions for W_1 and W_3 for any stellar models. The numerical results for the magnetic correction of the principal moment of inertia $I_z^{(2)}$ can also be obtained by using Eq. (6.22). We now show the results of $I_z^{(2)}$ obtained for several polytropic stellar models. In these calculations, in order to clarify the correspondence between non-magnetized and magnetized stars having same mass, we use the condition in which the total mass of the star does not change through the perturbative approach. This is also because the moment of

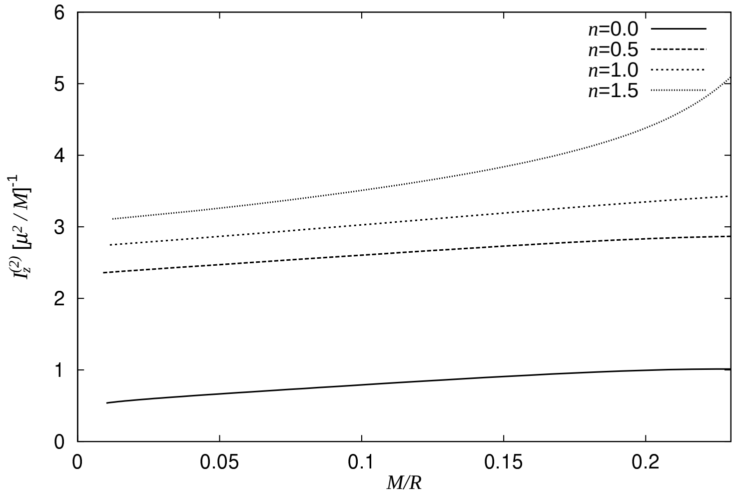

Figure 6.1: The magnetic correction of the principal moment of inertia $I_z^{(2)}$ plotted as a function of M/R. The values are normalized by μ^2/M, and the polytropic index is denoted by n.

inertia can be modified significantly by the mass shift rather than the magnetic deformation. In our formulation, this condition is accomplished by imposing the boundary condition that m_0 vanishes at infinity.

Figure 6.1 displays the magnetic correction $I_z^{(2)}$ as a function of the general-relativistic factor M/R. The values are normalized by the typical value μ^2/M. As a simple example, we now discuss quadrupole deformation of a fluid body in the Newtonian limit. If the deformed body has constant density, which corresponds to $n = 0$, then we can derive the result $I_z^{(2)} = 10\mu^2/(3M)$ from the estimate of ellipticity $25\mu^2/(2M^2R^2)$ (see Chapter 5 and Refs. [100,111]). However, as seen in Fig. 6.1, our numerical result for $n = 0$ is different from this simple estimate. This is because the perturbed star does not have constant effective density by the added perturbation, even though we assume the background star with constant density. This reason can be understood by seeing the differential equation for m_0, i.e. Eq. (5.87). The derivative of m_0 is related to the effective density including electromagnetic energy. In the case of $n = 0$, although the first term on the right-hand side in Eq. (5.87) vanishes, the remaining terms do not vanish and are non-trivial functions. It follows that the effective density is not a constant. Thus, our results include the inertia of electromagnetic fields as well as mass. Therefore, our result shown in Fig. 6.1 cannot be compared with the above simple estimate.

Concentrating on the general relativistic effects on the magnetic correction $I_z^{(2)}$, we can find from Fig. 6.1 that the values of $I_z^{(2)}$ for each stellar model become large with the general relativistic factor M/R. The increments are 50% at most. However, the rates of increase may be neglected except for the case of $n = 1.5$.

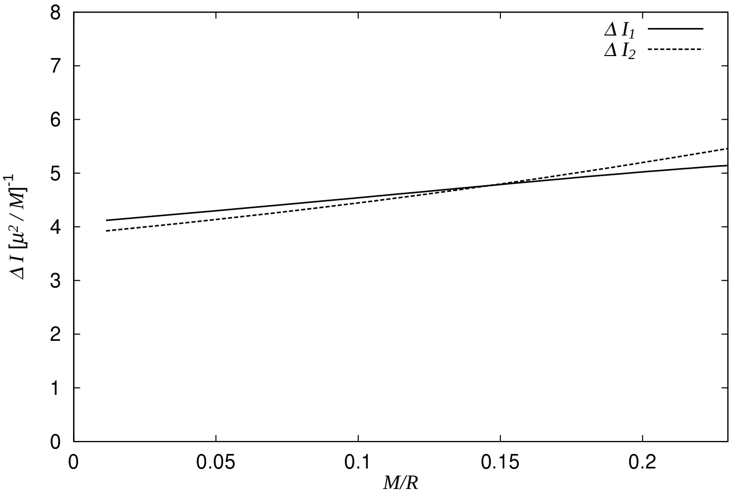

Figure 6.2: Comparison between ΔI_1 and ΔI_2 for $n = 1$. ΔI_1 and ΔI_2 are normalized by μ^2/M and plotted as a function of M/R.

6.3 The other components of moments of inertia

Next, we discuss the other principal moments of inertia, i.e. $I_x^{(2)}$ and $I_y^{(2)}$. In the context of general relativity, the definition of these quantities is associated with a difficulty in the concept. As seen from Eqs. (6.19) and (6.20), the notion of moments of inertia is related with quantities at infinity (see also Refs. [135,136]). If we consider the rotation of the star on the x-axis or the y-axis, it produces the radiation of electromagnetic and gravitational fields. Thus, the exterior space-time is not stationary, but radiative. There is no rigorous way to define the moments of inertia in such a radiative space-time. The concept of $I_x^{(2)}$ and $I_y^{(2)}$ itself may be meaningless to a considerable extent.

Therefore, only approximate expressions are available. It would be useful to extend Newtonian expressions, since it seems that most of Newtonian features still survive for neutron stars specified by the general relativistic factor $M/R \sim 0.2$. We cannot prove the validity mathematically, but will test some empirical relations. For this purpose, let us recall relations using the principal moments of inertia and the ellipticity which hold for an incompressible fluid in the context of Newtonian gravity. These are helpful in seeking the other principal moments of inertia. First, if the fluid body is subject to quadrupole deformation, then the relation between the principal moments of inertia exists

$$I_x^{(2)} = I_y^{(2)} = -\frac{1}{2} I_z^{(2)}. \tag{6.23}$$

Using this relation, the difference between the principal moments of inertia $I_z^{(2)}$ and $I_x^{(2)}$ is given by

$$\Delta I_1 = I_z^{(2)} - I_x^{(2)} = \frac{3}{2} I_z^{(2)}. \tag{6.24}$$

In the different way, this difference can be expressed also by using the ellipticity, which is defined by the difference between the equatorial radius and the polar radius [106, 111, 125], in the form

$$\Delta I_2 = I^{(0)} \times (\text{ellipticity}). \tag{6.25}$$

Thus, the difference is derived by the two methods. There is no reason that the two expressions coincide, but empirically the agreement is good. Note that these expressions (6.24) and (6.25) coincide exactly in this case.

If we assume that the relation (6.23) is applicable to general relativistic cases, it seems that we should simply apply the relation (6.23) to the results shown in Fig. 6.1 and derive $I_x^{(2)}$ and $I_y^{(2)}$. However, in order to utilize this relation, the magnetic corrections must be purely quadrupole contributions. As seen from the metric (6.1), the magnetic deformation includes monopole parts as well as quadrupole parts. Thus, our results in Fig. 6.1 also include monopole parts. Hence, we have to subtract monopole contributions from $I_z^{(2)}$ to derive $I_x^{(2)}$ and $I_y^{(2)}$. It is, nevertheless, not so easy to extract monopole contributions accurately from these magnetically deformed stars.

However, there is no guarantee that all the results in Fig. 6.1 include monopole contributions dominantly. If there is the case in which the monopole part can be neglected, then we can estimate $I_x^{(2)}$ and $I_y^{(2)}$ in the case, by assuming that the relation (6.23) holds approximately. That case would also provide some extrapolation for general relativistic effects on $I_x^{(2)}$ and $I_y^{(2)}$ in the other cases. In order to seek such a case, we now compare ΔI_1 derived by simply using the results in Fig. 6.1 with ΔI_2 calculated from the ellipticity, which was already estimated for several stellar models. In the case that ΔI_1 is almost consistent with ΔI_2 about the values and tendency, it seems that the monopole part can be neglected, and we may use the relation (6.23). From the comparison, we find that ΔI_1 is almost consistent with ΔI_2 in the case of $n = 1$. Figure 6.2 displays the comparison between ΔI_1 and ΔI_2 in this stellar model. The two curves coincide within 10%. Hence, we can estimate $I_x^{(2)}$ and $I_y^{(2)}$ using Eq. (6.23) in this stellar model. Since the values of $I_x^{(2)}$ and $I_y^{(2)}$ are simply given by multiplying $I_z^{(2)}$ by a factor of $-1/2$, the changes of the absolute values of $I_x^{(2)}$ and $I_y^{(2)}$ due to general relativistic effects are specified by the same factor as in the case of $I_z^{(2)}$ (see Fig. 6.3). Consequently, we derive very similar result to that of $I_z^{(2)}$. However, $I_x^{(2)}$ and $I_y^{(2)}$ decrease with the general relativistic factor M/R, while $I_z^{(2)}$ increases. We expect that similar features exist also in the other stellar models.

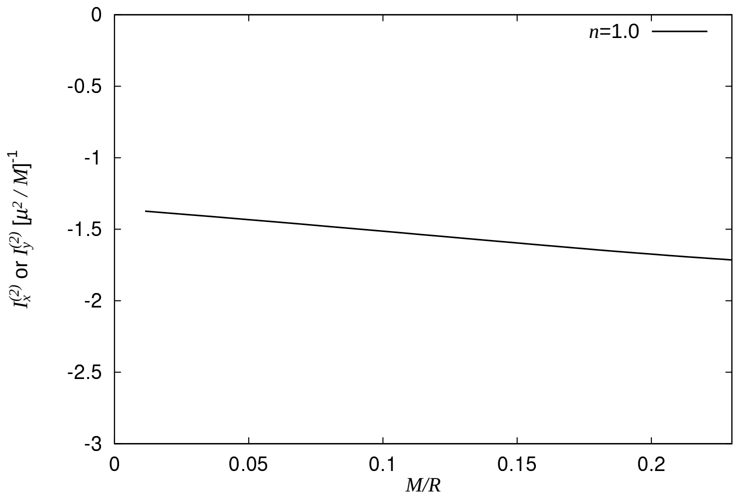

Figure 6.3: The other components of the principal moments of inertia $I_x^{(2)}$ and $I_y^{(2)}$, which are derived for $n = 1$.

Chapter 7

Summary and Conclusion

The discovery of the new classes of objects such as SGRs and AXPs, which are the candidates of magnetars, has inspired us to investigate magnetized stars in the context of general relativity. In particular, we have focused on stellar equilibrium configurations of magnetized stars. For this purpose, we first reviewed spherically symmetric stars in the context of both Newtonian gravity and general relativity, which are background in the perturbation method. In these calculations, we adopted polytropic stellar models. Second, we reviewed rotating configurations of stars, following Refs. [122,123] in the Newtonian case and following Refs. [110,125] in the general relativistic case. This formulation of rotating stars was very helpful to develop the formulation of magnetically deformed stars. Third, we discussed stellar magnetic field, based on Ref. [117]. In this discussion, we restricted ourselves to a dipole magnetic field. From the comparison between the Newtonian results and the general relativistic results, we found that the magnetic field strength is enhanced by the general relativistic effect for fixed magnetic dipole moment. Moreover, we considered the electric field induced by stellar rotation in the case of an aligned dipole rotator. We found that the coupling between the magnetic field and frame dragging induces an electric field in the general relativistic case. This is a purely general relativistic effect. As to the induced electric field strength, it is also enhanced by the general relativistic effect along with the magnetic field strength. This may be an interesting consequence, because the enhancement leads to higher energy radiation. Although the observed energy would be shifted to a lower value owing to the red-shift effect, it is not clear whether or not all these general relativistic effects are canceled exactly. Forth, following Refs. [106,111], we discussed stellar magnetic deformation due to the magnetic stress. Based on the fact that even the magnetic energy of magnetars is smaller than the gravitational energy, we developed a perturbative approach in contrast with the previous studies [103–105]. The simplicity of our formulation makes the results transparent for physical interpretation. From the results for the metric functions, we further calculated ellipticity for several polytropic stellar models. From the numerical estimates, we found that there is a general relativistic modification about 10% for each polytropic stellar model for fixed ratio of the magnetic energy to the gravitational energy. Furthermore, we compared the rotational effect with the magnetic effect on stellar structure for various pulsars. As a result, we saw that the magnetic effect overwhelms the rotational effect for the candidates of magnetars such as SGRs and AXPs, while magnetic deformation can be neglected as compared with the rotational flattening for well-known typical pulsars and millisecond pulsars. Finally, we discussed the moments of inertia of the magnetically deformed stars, considering the rotational configuration on the magnetic axis. From the consideration, we obtained the general expression for the magnetic correction of the moment of inertia. Furthermore, we found the general relativistic modifications about the magnetic correction by numerical calculations. In these calculations, we have adopted polytropic EOS only. However, our method can be extended to more general cases of realistic EOS and various current distributions, in which current exists in some domains of the star. Such calculations will be required to analyze the dynamics of realistic neutron stars including SGRs and AXPs. Thereby, the observed irregular spin-down of AXPs may be disclosed. Therefore, this will be the subject of further investigations.

Bibliography

[1] J.R. Oppenheimer, G.M. Volkoff, Phys. Rev. **56**, 455(1939)

[2] A. Hewish et al., Nature **217**, 709(1968)

[3] R. Giaconni et al., Astrophys. J. **167**, L67(1971)

[4] E. Schreier et al., Astrophys. J. **172**, L79(1972)

[5] H. Tananbaum et al., Astrophys. J. **174**, L143(1972)

[6] S.L. Shapiro, S.A. Teukolsky, *Black Holes, White Dwarfs, and Neutron Stars* (John Wiley & Sons, USA, 1983)

[7] P. Mészáros, *High-Energy Radiation from Magnetized Neutron Stars* (University of Chicago Press, USA, 1992)

[8] A.C. Phillips, *The Physics of Stars* (John Wiley & Sons, England, 1994)

[9] P. Goldreich, W. H. Julian, Astrophys. J. **157**, 869(1969)

[10] A.K. Harding, I. Contopoulos, D. Kazanas, Astrophys. J. **525**, L125(1999)

[11] R.C. Duncan, C. Thompson, Astrophys. J. **392**, L9(1992)

[12] B. Pacyński, Acta Astron. **42**, 145(1992)

[13] V.V. Usov, Nature **357**, 472(1992)

[14] C. Thompson, R.C. Duncan, Astrophys. J. **408**, 194(1993)

[15] C. Thompson, R.C. Duncan, Mon. Not. R. Astron. Soc. **275**, 255(1995)

[16] C. Thompson, R.C. Duncan, Astrophys. J. **473**, 322(1996)

[17] K. Ioka, astro–ph/0009327

[18] R.C. Duncan, astro–ph/0002442

[19] C. Thompson, astro–ph/0010016

[20] B. Cheng et al., Nature **382**, 518(1996)

[21] C. Barat et al., Astron. Astrophys. **79**, L24(1979)

[22] E.P. Mazets et al., Nature **282**, 587(1979)

[23] D.J. Helfand, K.S. Long, Nature **282**, 589(1979)

[24] S.V. Golenetskii et al., Sov. Astron. Lett. **5**, 340(1979)

[25] T.L. Cline et al., Astrophys. J. **237**, L1(1980)

[26] T.L. Cline et al., Astrophys. J. **255**, L45(1982)

[27] S.V. Golenetskii, V.N. Ilyinskii, E.P. Mazets, Nature **307**, 41(1984)

[28] R.E. Rothschild, S.R. Kulkarni, R.E. Lingenfelter, Nature **368**, 432(1994)

[29] J.R. Dickel et al., Astrophys. J. **448** 623(1995)

[30] E.P. Mazets, S.V. Golenetskii, Yu.A. Gur'yan, Sov. Astron. Lett. **5**, 343(1979)

[31] C. Kouveliotou et al., Nature **362**, 728(1993)

[32] K. Hurley et al., Astrophys. J. **431**, L31(1994)

[33] G. Vasisht, S.R. Kulkarni, Astrophys. J. **431**, L35(1994)

[34] K. Hurley et al., Astrophys. J. **463**, L13(1996)

[35] F.J. Vrba et al., Astrophys. J. **468**, 225(1996)

[36] P. Li et al., Astrophys. J. **490**, 823(1997)

[37] J. Sylwester et al., Acta Astron. **48**, 819(1998)

[38] K. Hurley, et al., Astrophys. J. **510**, L107(1999)

[39] K. Hurley et al., Astrophys. J. **510**, L111(1999)

[40] C. Kouveliotou, et al., Astrophys. J. **510**, L115(1999)

[41] T. Murakami et al., Astrophys. J. **510**, L119(1999)

[42] M. Feroci et al., Astrophys. J. **515**, L9(1999)

[43] P.M. Woods et al., Astrophys. J. **518**, L103(1999)

[44] D. Marsden et al., Astrophys. J. **520**, L107(1999)

[45] P.M. Woods, et al., Astrophys. J. **524**, L55(1999)

[46] E. Göğüş et al., Astrophys. J. **526**, L93(1999)

[47] P.M. Woods et al., Astrophys. J. **527**, L47(1999)

[48] K. Hurley et al., Nature **397**, 41(1999)

[49] D.A. Frail, S.R. Kulkarni, J.S. Bloom, Nature **398**, 127(1999)

[50] F.J. Vrba et al., Astrophys. J. **533**, L17(2000)

[51] T.E. Strohmayer, A.I. Ibrahim, Astrophys. J. **537**, L111(2000)

[52] S.S. Eikenberry, D.H. Dror, Astrophys. J. **537**, 429(2000)

[53] A.I. Ibrahim et al., astro–ph/0007043

[54] M. Feroci, K. Hurley, R.C. Duncan, C. Thompson, astro–ph/0010494

[55] J.G. Laros et al., Nature **322**, 152(1986)

[56] J.-L. Atteia et al., Astrophys. J. **320**, L105(1987)

[57] J.G. Laros et al., Astrophys. J. **320**, L111(1987)

[58] C. Kouveliotou et al., Astrophys. J. **322**, L21(1987)

[59] S.R. Kulkarni, D.A. Frail, Nature **365**, 33(1993)

[60] C. Kouveliotou et al., Nature **368**, 125(1994)

[61] T. Murakami et al., Nature **368**, 127(1994)

[62] S.R. Kulkarni et al., Nature **368**, 129(1994)

[63] G. Vasisht, D.A. Frail, S.R. Kulkarni, Astrophys. J. **440**, L65(1995)

[64] S. Corbel et al., Astrophys. J. **478**, 624(1997)

[65] D.A. Frail, G. Vasisht, S.R. Kulkarni, Astrophys. J. **480**, L129(1997)

[66] C. Kouveliotou et al., Nature **393**, 235(1998)

[67] D.M. Palmer, Astrophys. J. **512**, L113(1999)

[68] K. Hurley et al., Astrophys. J. **523**, L37(1999)

[69] E. Göğüş et al., Astrophys. J. **532**, L121(2000)

[70] P.M. Woods et al., Astrophys. J. **535**, L55(2000)

[71] P.M. Woods et al., Astrophys. J. **519**, L139(1999)

[72] K. Hurley et al., Astrophys. J. **519**, L143(1999)

[73] D.A. Smith, H.V. Bradt, A.M. Levine, Astrophys. J. **519**, L147(1999)

[74] E.P. Mazets et al., Astrophys. J. **519**, L151(1999)

[75] S. Corbel et al., Astrophys. J. **526**, L29(1999)

[76] K. Hurley et al., Astrophys. J. **528**, L21(2000)

[77] T. Cline et al., Astrophys. J. **531**, 407(2000)

[78] N.E. White et al., Mon. Not. R. Astron. Soc. **226**, 645(1987)

[79] G.L. Israel, S. Mereghetti, L. Stella, Astrophys. J. **433**, L25(1994)

[80] S. Mereghetti, L. Stella, Astrophys. J. **442**, L17(1995)

[81] C.A. Wilson et al., Astrophys. J. **513**, 464(1999)

[82] B. Paul et al., Astrophys. J. **537**, 319(2000)

[83] G.G. Fahlman, P.C. Gregory, Nature **293**, 202(1981)

[84] A. Baykal, J. Swank, Astrophys. J. **460**, 470(1996)

[85] A. Baykal et al., Astron. Astrophys. **336**, 173(1998)

[86] A. Baykal et al., astro–ph/0009480

[87] F.D. Seward, P.A. Charles, A.P. Smale, Astrophys. J. **305**, 814(1986)

[88] S. Mereghetti, Astrophys. J. **455**, 598(1995)

[89] T. Oosterbroek, Astron. Astrophys. **334**, 925(1998)

[90] G.L. Israel et al., Astrophys. J. **518**, L107(1999)

[91] V.M. Kaspi, J.R. Lackey, D. Chakrabarty, astro–ph/0005326

[92] G. Vasisht, E.V. Gotthelf, Astrophys. J. **486**, L129(1997)

[93] K. Torii et al., Astrophys. J. **503**, 843(1998)

[94] B.M. Gaensler, E.V. Gotthelf, G. Vasisht, Astrophys. J. **526**, L37(1999)

[95] G. Vasisht et al., Astrophys. J. **542**, L49(2000)

[96] F. Haberl et al., Astron. Astrophys. **326**, 662(1997)

[97] A. Melatos, Astrophys. J. **519**, L77(1999)

[98] A. Melatos, Mon. Not. R. Astron. Soc. **313**, 217(2000)

[99] S. Chandrasekhar, E. Fermi, Astrophys. J. **118**, 116(1953)

[100] V.C.A. Ferraro, Astrophys. J. **119**, 407(1954)

[101] D.V. Gal'tsov, V.P. Tsvetkov, Phys. Lett. **103A**, 193(1984)

[102] D.V. Gal'tsov, V.P. Tsvetkov, A.N. Tsirulev, Sov. Phys. JETP **59**, 472(1984)

[103] S. Bonazzola, E. Gourgoulhon, M. Salgado, J.A. Marck, Astron. Astrophys. **278**, 421(1993)

[104] M. Bocquet, S. Bonazzola, E. Gourgoulhon, J. Novak, Astron. Astrophys. **301**, 757(1995)

[105] S. Bonazzola, E. Gourgoulhon, Astron. Astrophys. **312**, 675(1996)

[106] K. Konno, T. Obata, Y. Kojima, Astron. Astrophys. **352**, 211(1999)

[107] R.P. Feynman, R.B. Leighton, M. Sands, *The Feynman Lectures on Physics* (Addison-Wesley, USA, 1964)

[108] T.-C.E. Ma, Am. J. Phys. **54**, 949(1986)

[109] A.S. de Castro, Am. J. Phys. bf 59, 180(1991)

[110] J.B. Hartle, Astrophys. J., **150**, 1005(1967)

[111] K. Konno, T. Obata, Y. Kojima, Astron. Astrophys. **356**, 234(2000)

[112] L. Davis, M. Goldstein, Astrophys. J. **159**, L81(1970)

[113] P. Goldreich, Astrophys. J. **160**, L11(1970)

[114] B. Bertotti, A.M. Anile, Astron. Astrophys. **28**, 429(1973)

[115] C. Cutler, D.I. Jones, preprint: gr-qc/0008021

[116] A.G. Muslimov, A.I. Tsygan, Sov. Astron. **30**, 567(1986)

[117] K. Konno, Y. Kojima, Prog. Theor. Phys. **104**, 1117(2000)

[118] S. Weinberg, *Gravitation and Cosmology* (John Wiley & Sons, USA, 1972)

[119] B.F. Schutz, *A First Course in General Relativity* (Cambridge University Press, England, 1988)

[120] R.M. Wald, *General Relativity* (The University of Chicago Press, USA, 1984)

[121] R.F. Tooper, Astrophys. J. **140**, 434(1964)

[122] S. Chandrasekhar, Mon. Not. R. Astron. Soc. **93**, 390(1933)

[123] S. Chandrasekhar, Mon. Not. R. Astron. Soc. **93**, 539(1933)

[124] S. Chandrasekhar, Astrophys. J. **138**, 801(1963)

[125] S. Chandrasekhar, J.C. Miller, Mon. Not. R. Astron. Soc. **167**, 63(1974)

[126] J. Lense, H. Thirring, Phys. Z. **19**, 156(1918)

[127] J.D. Jackson, *Classical Electrodynamics* (John Wiley & Sons, USA, 1975)

[128] S. Chandrasekhar, K.H. Prendergast, Proc. Natl. Acad. Sci. **42**, 5(1956)

[129] V.L. Ginzburg, L.M. Ozernoĭ, Sov. Phys. JETP **20**, 689(1965)

[130] J.A. Petterson, Phys. Rev. **D10**, 3166(1974)

[131] I. Wasserman, S.L. Shapiro, Astrophys. J. **265**, 1036(1983)

[132] D.G Ravenhall, C.J. Pethick, Astrophys. J. **424**, 846(1994)

[133] H. Quintana, Astrophys. J. **207**, 279(1976)

[134] Y. Kojima, M. Hosonuma, Astrophys. J. **520**, 788(1999)

[135] R. Geroch, J. Math. Phys. **11**, 2580(1970)

[136] R.O. Hansen, J. Math. Phys. **15**, 46(1974)

公表論文

(1) Deformation of Relativistic Magnetized Stars
Kohkichi Konno, Tomohiro Obata, Yasufumi Kojima
Astronomy and Astrophysics, **352**(1999) 211-216

(2) Flattening Modulus of A Neutron Star by Rotation and Magnetic Field
Kohkichi Konno, Tomohiro Obata, Yasufumi Kojima
Astronomy and Astrophysics, **356**(2000) 234-237

(3) General Relativistic Modification of a Pulsar Electromagnetic Field
Kohkichi Konno, Yasufumi Kojima
Progress of Theoretical Physics, **104**(2000) 1117-1127

公表論文(1)

Astron. Astrophys. 352, 211–216 (1999)

ASTRONOMY
AND
ASTROPHYSICS

Deformation of relativistic magnetized stars

K. Konno, T. Obata, and Y. Kojima

Department of Physics, Hiroshima University, Higashi-Hiroshima 739-8526, Japan

Received 9 August 1999 / Accepted 4 October 1999

Abstract. We formulate deformation of relativistic stars due to the magnetic stress, considering the magnetic fields to be perturbations from spherical stars. The ellipticity for the dipole magnetic field is calculated for some stellar models. We have found that the ellipticity becomes large with increase of a relativistic factor for the models with the same energy ratio of the magnetic energy to the gravitational energy.

Key words: relativity – stars: magnetic fields – stars: neutron – methods: analytical

1. Introduction

There is a growing interest in new classes of objects: soft-gamma repeaters (SGRs) and anomalous X-ray pulsars (AXPs). Until now, four identified SGRs are reported observationally. Their associations with supernova remnants strongly suggest that the SGRs are young neutron stars (see e.g. Kulkarni & Frail 1993; Murakami et al. 1994). Furthermore, recent measurements (see e.g. Kouveliotou et al. 1998, 1999) of the period and period derivative, yield evidence for these pulsars to be ultramagnetized neutron stars with field strength ($\sim 10^{15}$G) in excess of $B_{\rm cr} \sim 10^{13}$G, i.e., *magnetars* (Duncan & Thompson 1992; Thompson & Duncan 1993, 1995, 1996). Some classes of X-ray pulsars also suggest the magnetic fields with 10^{14}–10^{15}G (see e.g. Mereghetti & Stella 1995). Such magnetic fields are much stronger than those of known pulsars (10^{8}–10^{13}G; see e.g. Taylor et al. 1993). Though the relation between the SGRs and the AXPs is not yet clear, there exist neutron stars with very strong magnetic fields. In these ultramagnetized stars, the magnetic influence becomes important along with the relativistic effects. If we assume that a long-lived electric current flows in highly conductive neutron-star matter, the magnetic pressure corresponding to the Lorentz force comes into play. Hence, it induces deformation of stars. In this paper, we study such deformation from spherical stars within a general relativistic framework.

The quadrupole deformation of magnetized Newtonian stars was discussed by Chandrasekhar & Fermi (1953) and Ferraro (1954), in which incompressible fluid body with a dipole magnetic field is assumed. This deformation has been discussed also in relation to the gravitational radiation (Gal'tsov et al. 1984; Gal'tsov & Tsetkov 1984). The general relativistic approach by Bocquet et al. (1995) and Bonazzola & Gourgoulhon (1996) has appeared recently. However, their approach is fully numerical. In this paper, we develop almost an analytical treatment by assuming weak magnetic fields compared with gravity. This assumption is valid even in the magnetars. Our formulation is regarded as a general relativistic version of Chandrasekhar & Fermi (1953) and Ferraro (1954). In our method, we can easily include realistic equations of state (EOS) and construct relativistic magnetized stars. Furthermore, this method gives simple calculations of ellipticity of deformed stars etc.

Since the observed ultramagnetized neutron stars have long periods ($T \sim$ several sec), we may neglect the rotation of the magnetized stars, that is, we discuss static cases. We take non-rotating, spherical relativistic stars as backgrounds, and consider the magnetic fields as the perturbation. In particular, we consider only axisymmetric, poloidal magnetic fields produced by long-lived (toroidal) electric currents, because toroidal magnetic fields would break the symmetric property (see also Bocquet et al. 1995 and reference therein). Furthermore, we assume a perfectly conducting interior. Since we now consider non-rotating configurations, this implies that the electric field inside the stars must be zero. Hence, there is no electric charge inside the stars. From this, we can write the 4-current as $J_\mu = (0, 0, 0, J_\phi)$ (Bocquet et al. 1995). Furthermore, the surface charge should be absent, since the total charge should vanish in astrophysical situations. Otherwise, the electromagnetic field itself would have the angular momentum due to the non-vanishing electric field produced by the charge (Feynman et al. 1964; Ma 1986; de Castro 1991). This is not the purely static case.

The current distribution is introduced as the first-order quantity with respect to the perturbation. The corresponding magnetic field is solved by the Maxwell equation. We shall investigate deformation of stars due to the resulting magnetic stress, which arises as the second-order correction to the background field. This perturbation method is very similar to that of slowly rotating stars developed by Hartle (1967), in which the rotation is regarded as a small parameter. Our formalism can be applied to any configurations of the magnetic fields. However, we

---

Send offprint requests to: K. Konno

restrict ourselves to dipole magnetic fields because the dipole fields are important in many astrophysical situations.

The plan of this paper is as follows. In Sect. 2, the magnetic fields are investigated in the background space-time. The effect arising from the magnetic stress on equilibrium of stars is considered in Sect. 3. The solution corresponding to the quadrupole deformation of the stars will be given. To evaluate the deformation quantitatively, the ellipticity is discussed in Sect. 4. Finally, Sect. 5 is devoted to the discussion. Throughout this paper, we use the units in which $c = G = 1$, and the Gaussian system of units for electromagnetic fields.

2. Magnetic fields in spherically symmetric space-time

We now consider an axisymmetric, poloidal magnetic field created by a 4-current $J_\mu = (0,0,0,J_\phi)$ in a non-rotating, spherical star. We suppose that the magnetic field is weak, i.e., $B_\mu \sim O(\varepsilon)$. The line element of the spherically symmetric space-time is given by

$$ds^2 = -e^{\nu(r)}dt^2 + e^{\lambda(r)}dr^2 + r^2d\theta^2 + r^2\sin^2\theta d\phi^2, \tag{1}$$

where ν and λ are functions of the radial coordinate r only. Since we do not consider electric fields, we can assume that the electromagnetic 4-potential A_μ has only the ϕ-component, i.e., $A_\mu = (0,0,0,A_\phi)$ (see also Bocquet et al. 1995). In this case, the Maxwell equation is reduced to

$$\begin{aligned} e^{-\lambda}\frac{\partial^2 A_\phi}{\partial r^2} + \frac{1}{2}(\nu' - \lambda')e^{-\lambda}\frac{\partial A_\phi}{\partial r} \\ + \frac{1}{r^2}\frac{\partial^2 A_\phi}{\partial\theta^2} - \frac{1}{r^2}\cot\theta\frac{\partial A_\phi}{\partial\theta} &= -4\pi J_\phi, \end{aligned} \tag{2}$$

where the prime denotes the differentiation with respect to r.

We expand the potential A_ϕ and the current J_ϕ as follows (Regge & Wheeler 1957):

$$A_\phi = \sum_{l=1}^{\infty} a_l(r)\sin\theta\frac{dP_l(\cos\theta)}{d\theta}, \tag{3}$$

$$J_\phi = \sum_{l=1}^{\infty} j_l(r)\sin\theta\frac{dP_l(\cos\theta)}{d\theta}, \tag{4}$$

where P_l is the Legendre's polynomial of degree l. Substituting these forms into Eq. (2), we have

$$e^{-\lambda}\frac{d^2a_l}{dr^2} + \frac{1}{2}(\nu' - \lambda')e^{-\lambda}\frac{da_l}{dr} - \frac{l(l+1)}{r^2}a_l = -4\pi j_l. \tag{5}$$

For a given current j_l, we can obtain the potential a_l and, therefore, the magnetic field. From now on, we only consider a dipole magnetic field, i.e., $l = 1$. The potential outside the star is easily solved (Ginzburg & Ozernoĭ 1965; Petterson 1974; Wasserman & Shapiro 1983) in the form

$$a_1 = -\frac{3\mu}{8M^3}r^2\left[\ln\left(1 - \frac{2M}{r}\right) + \frac{2M}{r} + \frac{2M^2}{r^2}\right], \tag{6}$$

where μ is a constant corresponding to the magnetic dipole moment with respect to an observer at infinity, and M is the total mass of the background star. In order to describe the magnetic field inside the star, we require the current distribution j_1. The current j_1 is not arbitrary but subject to an integrability condition (Ferraro 1954; Chandrasekhar & Prendergast 1956; Bonazzola et al. 1993). As will be shown in Eq. (25), this current is given, up to the first order in ε, by

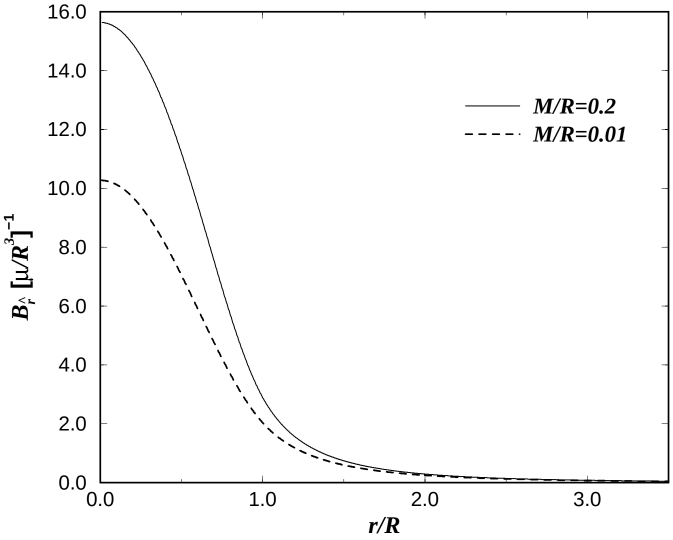

Fig. 1. The tetrad component of the magnetic fields, $B_{\hat{r}}$ on the symmetry axis ($\theta = 0$), plotted against r/R. The solid line denotes a relativistic case ($M/R = 0.2$), while the dashed line corresponds to a Newtonian case ($M/R = 0.01$). The magnetic fields are normalized by the typical field strength μ/R^3.

$$j_1(r) = c_0 r^2(\rho_0(r) + p_0(r)), \tag{7}$$

where c_0 is an arbitrary constant, and ρ_0 and p_0 denote the density and pressure, respectively, of the background star. By requiring that a_1 behaves as a regular function at the center of the star, we now obtain the potential a_1 in the vicinity of the center:

$$a_1 \simeq \alpha_0 r^2 + O(r^4), \tag{8}$$

where α_0 is a constant, which is fixed by the boundary condition at the surface. In this way, we can construct the magnetic field in the whole space-time.

Fig. 1 displays the tetrad component of the magnetic field,

$$B_{\hat{r}} = -\frac{1}{r^2\sin\theta}\partial_\theta A_\phi = \frac{2\cos\theta}{r^2}a_1 \tag{9}$$

on the symmetry axis (i.e., $\theta = 0$), and Fig. 2 displays the tetrad component

$$B_{\hat{\theta}} = \frac{e^{-\frac{\lambda}{2}}}{r\sin\theta}\partial_r A_\phi = -\frac{e^{-\frac{\lambda}{2}}\sin\theta}{r}a_1' \tag{10}$$

on the equatorial plane (i.e., $\theta = \pi/2$) with respect to the radial coordinate r. We have normalized them by the typical magnetic field strength μ/R^3, where R is the radius of the star. The solid lines denote a relativistic case, whereas the dashed lines correspond to a Newtonian case. In these calculations, we have used

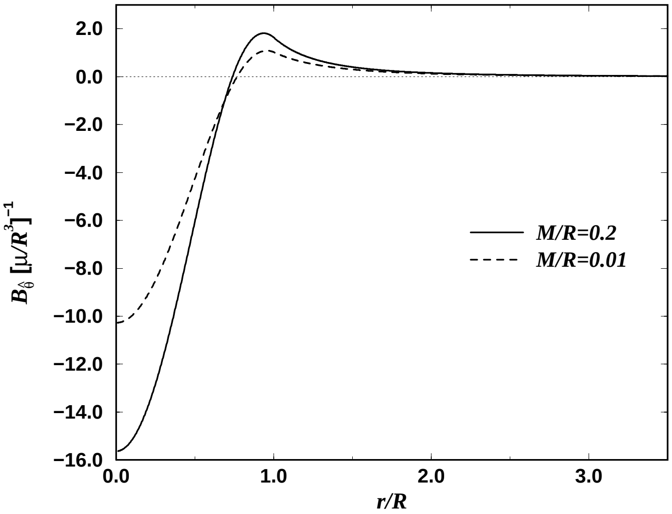

Fig. 2. The tetrad component of the magnetic fields, $B_{\hat{\theta}}$ on the equatorial plane ($\theta = \pi/2$), plotted against r/R. The solid line denotes a relativistic case ($M/R = 0.2$), while the dashed line corresponds to a Newtonian case ($M/R = 0.01$). The magnetic fields are normalized by the typical field strength μ/R^3.

the polytropic EOS: $p_0 = \kappa\rho_0^\gamma$ $(\gamma = 2)$. From these figures, we see that the intensity of the magnetic field increases as r becomes closer to the center. Furthermore, these two figures show that despite the same magnetic moment with respect to an observer at infinity, the central magnetic field of the relativistic star is stronger than that of the Newtonian star by about 50% of the Newtonian case. Therefore, it follows that the relativistic effect strengthens the internal magnetic fields.

3. Equilibrium configurations of magnetized stars

Next, we consider deformation of magnetized stars due to the magnetic stress, which is regarded as the second-order effect. We formulate the deformation of the star and space-time, following Hartle (1967).

3.1. Equations of equilibrium

The metric can be expanded in multipoles around the spherically symmetric space-time. In particular, when we deal only with a dipole field, i.e., $l = 1$ in Eqs. (3) and (4), the metric can be written in the form (see also Hartle 1967; Chandrasekhar & Miller 1974)

$$\begin{aligned} ds^2 &= -e^{\nu(r)}\left[1 + 2\left(h_0(r) + h_2(r)P_2(\cos\theta)\right)\right]dt^2 \\ &\quad + e^{\lambda(r)}\left[1 + \frac{2e^{\lambda(r)}}{r}\left(m_0(r) + m_2(r)P_2(\cos\theta)\right)\right]dr^2 \\ &\quad + r^2\left[1 + 2k_2(r)P_2(\cos\theta)\right]\left(d\theta^2 + r^2\sin^2\theta d\phi^2\right), \end{aligned} \tag{11}$$

where h_0, h_2, m_0, m_2 and k_2 are the corrections of the second order in ε.

The total energy-momentum tensor is the sum of the perfect-fluid part ${T_{(\mathrm{m})}}^{\mu}{}_{\nu}$ and the electromagnetic part ${T_{(\mathrm{em})}}^{\mu}{}_{\nu}$:

$$T^\mu_\nu = {T_{(\mathrm{m})}}^{\mu}{}_{\nu} + {T_{(\mathrm{em})}}^{\mu}{}_{\nu}, \tag{12}$$

where

$$\begin{aligned} {T_{(\mathrm{m})}}^{\mu}{}_{\nu} &= (\rho + p)\, u^\mu u_\nu + p\delta^\mu_\nu, &(13)\\ {T_{(\mathrm{em})}}^{\mu}{}_{\nu} &= \frac{1}{4\pi}\left(F^{\mu\lambda}F_{\nu\lambda} - \frac{1}{4}F_{\sigma\lambda}F^{\sigma\lambda}\delta^\mu_\nu\right). &(14) \end{aligned}$$

In Eq. (14), $F_{\mu\nu}$ is the Faraday tensor. The pressure p and the energy density ρ can also be expanded in multipoles as

$$\begin{aligned} p(r,\theta) &= p_0 + \left(\delta p_{(l=0)} + \delta p_{(l=2)}P_2\right), &(15)\\ \rho(r,\theta) &= \rho_0 + \frac{\rho_0'}{p_0'}\left(\delta p_{(l=0)} + \delta p_{(l=2)}P_2\right), &(16) \end{aligned}$$

where $\delta p_{(l=0)}$ and $\delta p_{(l=2)}$ depend on r only, and we have assumed a barotropic case.

From the Einstein equation, we can obtain

$$m_0' = 4\pi r^2\frac{\rho_0'}{p_0'}\delta p_{(l=0)} + \frac{1}{3}\left[e^{-\lambda}\left(a_1'\right)^2 + \frac{2}{r^2}a_1^2\right], \tag{17}$$

$$\begin{aligned} h_0' &= 4\pi r e^\lambda \delta p_{(l=0)} + \frac{1}{r}\nu' e^\lambda m_0 + \frac{1}{r^2}e^\lambda m_0 \\ &\quad + \frac{e^\lambda}{3r}\left[e^{-\lambda}\left(a_1'\right)^2 - \frac{2}{r^2}a_1^2\right], \end{aligned} \tag{18}$$

$$\begin{aligned} h_2' + k_2' &= h_2\left(\frac{1}{r} - \frac{\nu'}{2}\right) + \frac{e^\lambda}{r}m_2\left(\frac{1}{r} + \frac{\nu'}{2}\right) \\ &\quad + \frac{4}{3r^2}a_1 a_1', \end{aligned} \tag{19}$$

$$h_2 + \frac{e^\lambda}{r}m_2 = \frac{2}{3}e^{-\lambda}\left(a_1'\right)^2, \tag{20}$$

$$\begin{aligned} &h_2' + k_2' + \frac{1}{2}r\nu' k_2' \\ &\quad = 4\pi r e^\lambda \delta p_{(l=2)} + \frac{1}{r^2}e^\lambda m_2 + \frac{1}{r}\nu' e^\lambda m_2 \\ &\qquad + \frac{3}{r}e^\lambda h_2 + \frac{2}{r}e^\lambda k_2 - \frac{1}{3r}e^\lambda\left[e^{-\lambda}\left(a_1'\right)^2 + \frac{4}{r^2}a_1^2\right]. \end{aligned} \tag{21}$$

Furthermore, from the conservation law of the total energy-momentum tensor, we obtain

$$\begin{aligned} \delta p'_{(l=0)} &= -\frac{1}{2}\nu'\left(\frac{\rho_0'}{p_0'} + 1\right)\delta p_{(l=0)} \\ &\quad - \left(\rho_0 + p_0\right)h_0' + \frac{2}{3r^2}a_1' j_1, &(22)\\ \delta p_{(l=2)} &= -\left(\rho_0 + p_0\right)h_2 - \frac{2}{3r^2}a_1 j_1, &(23)\\ \delta p'_{(l=2)} &= -\frac{1}{2}\nu'\left(\frac{\rho_0'}{p_0'} + 1\right)\delta p_{(l=2)} \\ &\quad - \left(\rho_0 + p_0\right)h_2' - \frac{2}{3r^2}a_1' j_1. &(24) \end{aligned}$$

The integrability condition for Eqs. (22) and (24) leads to

$$\frac{j_1}{r^2\left(\rho_0 + p_0\right)} = \text{const.}\left(\equiv c_0\right). \tag{25}$$

This is consistent with Eq. (5.29) of Bonazzola et al. (1993) up to the first order in ε. Using this current distribution, Eq. (22) can also be integrated as

$$\delta p_{(l=0)} = -\left(\rho_0 + p_0\right) h_0 + \frac{2}{3r^2} a_1 j_1 + c_1 \left(\rho_0 + p_0\right), \tag{26}$$

where c_1 is a constant of integration.

Consequently, we have two sets of differential equations,

$$\begin{aligned} m_0' &= -4\pi r^2 \frac{\rho_0'}{p_0'} \left(\rho_0 + p_0\right)\left(h_0 - c_1\right) \\ &\quad + \frac{1}{3} e^{-\lambda} \left(a_1'\right)^2 + \frac{2}{3r^2} a_1^2 + \frac{8\pi}{3} \frac{\rho_0'}{p_0'} a_1 j_1, \end{aligned} \tag{27}$$

$$\begin{aligned} h_0' &= \left(\frac{1}{r^2} + \frac{\nu'}{r}\right) e^{\lambda} m_0 - 4\pi r e^{\lambda} \left(\rho_0 + p_0\right)\left(h_0 - c_1\right) \\ &\quad + \frac{1}{3r} \left(a_1'\right)^2 - \frac{2}{3r^3} e^{\lambda} {a_1}^2 + \frac{8\pi}{3r} e^{\lambda} a_1 j_1, \end{aligned} \tag{28}$$

and

$$v_2' = -\nu' h_2 + \frac{2}{3} e^{-\lambda} \left(\frac{1}{r} + \frac{\nu'}{2}\right) \left(a_1'\right)^2 + \frac{4}{3r^2} a_1 a_1', \tag{29}$$

$$\begin{aligned} h_2' &= -\frac{4e^{\lambda}}{r^2 \nu'} v_2 + \left[8\pi \frac{e^{\lambda}}{\nu'} \left(\rho_0 + p_0\right) + \frac{2}{r^2 \nu'} \left(1 - e^{\lambda}\right) - \nu'\right] h_2 \\ &\quad + \frac{8}{3r^4 \nu'} e^{\lambda} a_1^2 + \frac{8}{3r^3 \nu'} \left(1 + \frac{r\nu'}{2}\right) a_1 a_1' \\ &\quad + \left(\frac{1}{3} \nu' e^{-\lambda} + \frac{2}{3r^2 \nu'}\right) \left(a_1'\right)^2 + \frac{16\pi}{3r^2 \nu'} e^{\lambda} a_1 j_1, \end{aligned} \tag{30}$$

where $v_2 \equiv h_2 + k_2$. These equations govern the relativistic magnetized star. We have to solve four differential equations (27)–(30) and one algebraic equation (20) for the unknown functions $(m_0, m_2, h_0, h_2, v_2)$. Furthermore, we can derive $\delta p_{(l=0)}$ and $\delta p_{(l=2)}$ by substituting the solution of h_0 and h_2 into Eqs. (26) and (23).

In order to solve Eqs. (27) and (28) inside the star, it is also convenient to introduce a quantity

$$\delta P_0 \equiv \frac{\delta p_{(l=0)}}{\rho_0 + p_0}. \tag{31}$$

From Eq. (26), we have

$$\delta P_0 + h_0 - \frac{2}{3} \frac{j_1}{r^2 \left(\rho_0 + p_0\right)} a_1 = c_1. \tag{32}$$

Moreover, Eqs. (27) and (28) are rewritten as

$$m_0' = 4\pi r^2 \frac{\rho_0'}{p_0'} \left(\rho_0 + p_0\right) \delta P_0 + \frac{1}{3} e^{-\lambda} \left(a_1'\right)^2 + \frac{2}{3r^2} a_1^2, \tag{33}$$

$$\begin{aligned} \delta P_0' &= -\left(8\pi p_0 + \frac{1}{r^2}\right) e^{2\lambda} m_0 - 4\pi r e^{\lambda} \left(\rho_0 + p_0\right) \delta P_0 \\ &\quad - \frac{1}{3r} \left(a_1'\right)^2 + \frac{2}{3r^3} e^{\lambda} {a_1}^2 + \frac{2}{3} \frac{j_1}{r^2 \left(\rho_0 + p_0\right)} a_1'. \end{aligned} \tag{34}$$

In the next subsection, we solve these differential equations for the metric functions.

3.2. *The exterior solution and boundary condition*

First, we consider the solution outside of the star, in which $\rho_0 = p_0 = 0$ and $j_1 = 0$.

The solution of m_0 and h_0 is given by

$$\begin{aligned} m_0 &= \frac{3\mu^2}{8M^4 r} \left(r^2 - M^2\right) \\ &\quad + \frac{3\mu^2}{8M^5} \left(r^2 - Mr - M^2\right) \ln\left(1 - \frac{2M}{r}\right) \\ &\quad + \frac{3\mu^2}{32M^6} r^2 \left(r - 2M\right) \left[\ln\left(1 - \frac{2M}{r}\right)\right]^2 + c_2, \end{aligned} \tag{35}$$

$$\begin{aligned} h_0 &= -\frac{3\mu^2}{8M^3} \frac{4r - M}{r\left(r - 2M\right)} \\ &\quad + \frac{3\mu^2}{8M^5} \frac{(r - M)(r - 3M)}{r - 2M} \ln\left(1 - \frac{2M}{r}\right) \\ &\quad + \frac{3\mu^2}{32M^6} r^2 \left[\ln\left(1 - \frac{2M}{r}\right)\right]^2 - \frac{c_2}{r - 2M} + c_3, \end{aligned} \tag{36}$$

where c_2 and c_3 are constants of integration. At large r, m_0 and h_0 behave as

$$m_0 \simeq c_2 - \frac{\mu^2}{3r^3} + O\left(\frac{1}{r^4}\right), \tag{37}$$

$$h_0 \simeq c_3 - \frac{3\mu^2}{8M^4} - \frac{c_2}{r} + O\left(\frac{1}{r^2}\right). \tag{38}$$

Since h_0 must vanish at infinity, we obtain

$$c_3 = \frac{3\mu^2}{8M^4}. \tag{39}$$

The constant c_2 corresponds to the mass shift, which is fixed by matching with the interior solution at the surface.

On the other hand, the differential equations for v_2 and h_2 is rather complicated, but analytically solved. The solution of v_2 is

$$v_2(z) = \frac{2K}{\sqrt{z^2 - 1}} Q_2^1(z) - \frac{3\mu^2}{4M^4 \sqrt{z^2 - 1}} P_2^1(z) + v_{2p}(z), \tag{40}$$

where z is defined as $z \equiv r/M - 1$, K is a constant of integration, P_2^1 and Q_2^1 are the associated Legendre functions, and v_{2p} is

$$\begin{aligned} v_{2p} &= \frac{9\mu^2}{4M^4} z + \frac{3\mu^2}{8M^4} \frac{7z^2 - 4}{z^2 - 1} \\ &\quad + \frac{3\mu^2}{16M^4} \frac{z\left(11z^2 - 7\right)}{z^2 - 1} \ln\frac{z - 1}{z + 1} \\ &\quad + \frac{3\mu^2}{16M^4} \left(2z^2 + 1\right) \left(\ln\frac{z - 1}{z + 1}\right)^2. \end{aligned} \tag{41}$$

Furthermore, h_2 is given by

$$h_2(z) = K Q_2^2(z) - \frac{3\mu^2}{8M^4} P_2^2(z) + h_{2p}(z), \tag{42}$$

where P_2^2 and Q_2^2 are the associated Legendre functions, and h_{2p} is written as

$$h_{2p} = -\frac{3\mu^2}{16M^4} \left[6z^2 + 3z - 6 - \frac{4z^2 + 2z}{z^2 - 1}\right]$$

$$\begin{aligned}&-\frac{3\mu^2}{32M^4}\left[3z^2-8z-3-\frac{8}{z^2-1}\right]\ln\frac{z-1}{z+1}\\&+\frac{3\mu^2}{16M^4}\left(z^2-1\right)\left(\ln\frac{z-1}{z+1}\right)^2.\end{aligned}\tag{43}$$

In Eqs. (40) and (42), we have used the boundary condition at infinity. The remaining constant K will be fixed by the boundary condition at the surface. Thus we have obtained the analytical solution outside the star.

We turn our attention to the interior solution. For a given EOS, we can obtain the solution numerically. For the actual numerical work, we investigate the behavior of the metric functions in the vicinity of the center.

First, we consider the metric functions m_0 and δP_0. The solution in which both m_0 and δP_0 vanish at the center (see also Chandrasekhar & Miller 1974) is given by

$$m_0 \simeq \frac{2}{3}{\alpha_0}^2 r^3+\cdots,\tag{44}$$

$$\delta P_0 \simeq -\frac{2}{3}\left({\alpha_0}^2-c_0\alpha_0\right)r^2+\cdots,\tag{45}$$

where α_0 is defined in Eq. (8).

Next, we consider v_2 and h_2. The regular solution at the center is

$$\begin{aligned}v_2 &\simeq \beta_1 r^4+\cdots,\\ h_2 &\simeq \beta_2 r^2+\cdots,\end{aligned}\tag{46}$$

where constants β_1 and β_2 are not independent by the regularity condition at the center.

Finally, we can obtain the metric functions by imposing the junction conditions (O'Brien & Synge 1952) at the surface:

$$g_{\mu\nu}|_{+R} = g_{\mu\nu}|_{-R} \quad (\mu,\nu=t,r,\theta,\phi),\tag{47}$$

$$g_{ij,r}|_{+R} = g_{ij,r}|_{-R} \quad (i,j=t,\theta,\phi),\tag{48}$$

where $g_{\mu\nu}$ denotes the metric components. From these conditions, the integration constants c_2, K, β_1 and β_2 are fixed.

4. Ellipticity of magnetized stars

We consider the magnetic field on the stellar shape of the equilibrium. The additional Lorentz force $\boldsymbol{J}\times\boldsymbol{B}$ mainly acts on it in the perpendicular direction to the symmetry axis ($\theta=\pi/2$), that is, flattens the star. The flattening effect is also recognized by considering the (r,r) component of the magnetic stress tensor,

$${T_{(\mathrm{em})}}^r{}_r = \frac{1}{8\pi}\left(B_\theta B^\theta - B_r B^r\right).\tag{49}$$

Along the symmetry axis, B_θ must vanish owing to the axisymmetry. Hence, the stress ${T_{(\mathrm{em})}}^r{}_r$ is negative on this axis. On the other hand, on the equatorial plane, since B_r is zero at any r, the stress ${T_{(\mathrm{em})}}^r{}_r$ has the opposite sign. This indicates that the spherical star is shrunk in the parallel direction to the symmetry axis ($\theta=0$) and expanded in the perpendicular direction ($\theta=\pi/2$) by the magnetic effect. Thus we can see the flattening effect.

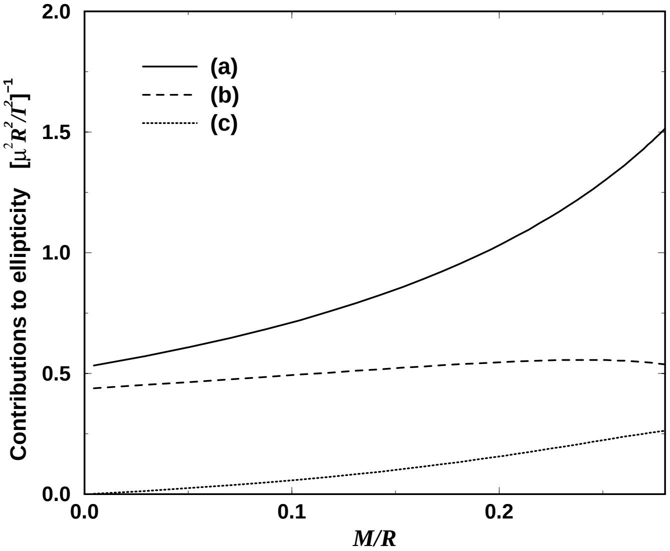

Fig. 3. The three contributions to ellipticity: (a) the effect of the 'Lorentz force', (b) the effect of the perturbation of the 'gravitational potential', and (c) the 'purely relativistic effect' (see text). These are plotted against M/R. We have used the polytropic EOS ($\gamma=2$).

Next, in order to evaluate the deformation quantitatively, let us introduce the ellipticity, which is defined as

$$\text{ellipticity} \equiv \frac{(\text{equatorial radius})-(\text{polar radius})}{(\text{mean radius})},\tag{50}$$

where these radii denote the circumferential radii under general relativistic situations. From this definition, ellipticity is given by (Chandrasekhar & Miller 1974)

$$\text{ellipticity} = \frac{2c_0}{r\nu'}a_1+\frac{3h_2}{r\nu'}-\frac{3}{2}k_2.\tag{51}$$

The first term of the right-hand side in Eq. (51) corresponds to, in a sense, the effect of the 'Lorentz force', the second term represents the effect of the perturbation of the 'gravitational potential' induced by the magnetic effect, and the third term is a 'purely relativistic term' which arises from a definition of the radius, that is, the circumferential radius. These contributions to the ellipticity are shown in Fig. 3 as a function of the relativistic factor M/R. We have normalized them by μ^2R^2/I^2 (I is the moment of inertia, which is well defined also in the relativistic case), and we have used a polytropic EOS ($\gamma=2$). From this figure, we can see that the term due to the 'gravitational potential' does not change significantly, while the term concerning the 'Lorentz force' increases with the relativistic factor M/R as known from Figs. 1 and 2.

Fig. 4 displays the (total) ellipticity for different polytropic models ($\gamma=5/3$ and $\gamma=2$). From this figure, we find that the ellipticity becomes large as the relativistic factor M/R increases, in each case of $\gamma=5/3$ and $\gamma=2$. The common feature of the monotonic increase shows the effect of the 'Lorentz force term' to be effective. An important thing is that the relativistic calculation leads to much larger ellipticity for a fixed value of μ^2R^2/I^2. Finally, we give a comment concerning the previous general-relativistic studies. The quantity plotted in Fig. 4 is

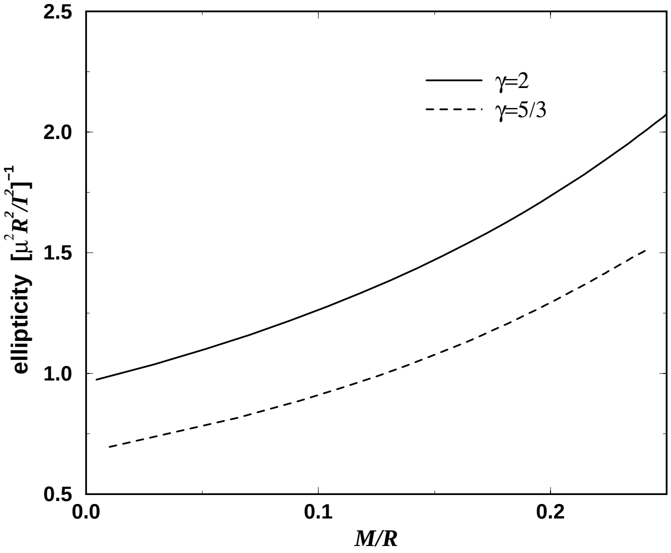

Fig. 4. The variation of the ellipticity with respect to M/R. The solid line denotes the case of the polytropic EOS with $\gamma = 2$, and the dashed line corresponds to the case of $\gamma = 5/3$.

exactly the *magnetic distortion factor* β introduced by Bonazzola & Gourgoulhon (1996). It is noticed that although the EOS which we have used is different from that of Bonazzola & Gourgoulhon (1996), both calculations give the same results (see Fig. 2 of their paper), that is, β takes the values very close to 1.

5. Discussion

Recent observations suggest that some classes of neutron stars have strong magnetic fields. These may promote a new branch with magnetized stars. As a simple approach to the models, we have formulated the structure of the magnetized stars within a general relativistic framework, considering the perturbation from a spherical star. In particular, a dipole magnetic field has been dealt with. We have showed the current distribution which yields equilibrium configurations up to the second order in ε. Furthermore, the ellipticity of the star has been estimated as a simple example. We have found that the ellipticity becomes large as the relativistic factor M/R increases, for the same energy ratio of the magnetic energy to the gravitational energy. Our analytical approach have made the calculations much simpler than that of the previous work. This method can be extended to more general cases of realistic EOS and general current distribution, in which the current exists in some domains of the star. Therefore, this can be applied to wider range of astrophysical situations.

Another extension of this work is to incorporate rotation of stars. The stationary configurations, in which the rotation axis is aligned with the magnetic axis, make the calculations complex because of appearance of non-vanishing electric fields. However, this can be managed. Since the rotational effect deforms the star as well as the magnetic effect, we are also interested in seeing which of them is effective. This will be the subject of further investigations.

Acknowledgements. We would like to thank M. Hosonuma for providing us with a numerical code for rotating stars and useful discussions.

References

Bocquet M., Bonazzola S., Gourgoulhon E., Novak J., 1995, A&A 301, 757
Bonazzola S., Gourgoulhon E., Salgado M., Marck J.A., 1993, A&A 278, 421
Bonazzola S., Gourgoulhon E., 1996, A&A 312, 675
Chandrasekhar S., Fermi E., 1953, ApJ 118, 116
Chandrasekhar S., Miller J.C., 1974, MNRAS 167, 63
Chandrasekhar S., Prendergast K.H., 1956, Proc. Natl. Acad. Sci. 42, 5
de Castro A.S., 1991, Am. J. Phys. 59, 180
Duncan R.C., Thompson C., 1992, ApJ 392, L9
Ferraro V.C.A., 1954, ApJ 119, 407
Feynman R.P., Leighton R.B., Sands M., 1964, The Feynman Lectures on Physics. Vol. 2 Addison-Wesley, Reading, §17-4.
Gal'tsov D.V., Tsvetkov V.P., Tsirulev A.N., 1984, Sov. Phys. JETP 59, 472
Gal'tsov D.V., Tsetkov V.P., 1984, Phys. Lett. 103A, 193
Ginzburg V.L., Ozernoĭ L.M., 1965, Sov. Phys. JETP 20, 689
Hartle J.B., 1967, ApJ 150, 1005
Kouveliotou C., et al., 1998, Nat 393, 235
Kouveliotou C., et al., 1999, ApJ 510, L115
Kulkarni S., Frail D., 1993, Nat 365, 33
Ma T.-C.E., 1986, Am. J. Phys. 54, 949
Mereghetti S., Stella L., 1995, ApJ 442, L17
Murakami T., et al., 1994, Nat 368, 127
O'Brien S., Synge J.L., 1952, Comm. Dublin Inst. Advanced Studies, A no. 9
Petterson J.A., 1974, Phys. Rev. D10, 3166
Regge T., Wheeler J.A., 1957, Phys. Rev. 108, 1063
Taylor J.H., Manchester R.N., Lyne A.G., 1993, ApJS 88, 529
Thompson C., Duncan R.C., 1993, ApJ 408, 194
Thompson C., Duncan R.C., 1995, MNRAS 275, 255
Thompson C., Duncan R.C., 1996, ApJ 473, 322
Wasserman I., Shapiro S.L., 1983, ApJ 265, 1036

公表論文(2)

Astron. Astrophys. 356, 234–237 (2000)

ASTRONOMY
AND
ASTROPHYSICS

Flattening modulus of a neutron star by rotation and magnetic field

K. Konno, T. Obata, and Y. Kojima

Department of Physics, Hiroshima University, Higashi-Hiroshima 739-8526, Japan

Received 28 October 1999 / Accepted 12 January 2000

Abstract. We calculated the ellipticity of the deformed star due to the rotation or magnetic field. These two effects are compared to each other within general relativity. It turned out that the magnetic distortion is important for recently observed candidates of magnetars, while the magnetic effect can be neglected for well-known typical pulsars.

Key words: relativity – stars: neutron – stars: rotation – stars: magnetic fields – methods: analytical

1. Introduction

Observations of pulsars have been accumulated since the first discovery by Hewish et al. (1968), and several new types of pulsars appeared with great surprise. These observations have partially revealed the structure and evolution of rotating neutron stars. Their rotation periods range from 1.5 ms to several seconds. The surface magnetic fields range from 10^8 to 10^{15}G. The upper limit was recently raised by a factor 10^3 by the discovery of the soft gamma-ray repeaters (SGRs) and anomalous X-ray pulsars (AXPs) (see e.g. Kouveliotou et al. 1998, 1999; Mereghetti & Stella 1995). The new class of pulsars with the very strong magnetic field ($B \sim 10^{14}$–10^{15}G) are most likely candidates of *magnetars* (e.g. Thompson & Duncan 1996) and may be worth studying further. In the future, we may find a more extreme case, that is, a rapidly rotating relativistic star with a strong magnetic field.

Most stars have spherically symmetric structure. They are however deformed due to the rapid rotation and the strong magnetic field. It is well known that both effects produce a flattening equilibrium star. We will examine them within general relativity. These effects are assumed to be small and treated as perturbations to spherically symmetric stars. The rotational axis of pulsars does not in general coincide with the axis of the dipole magnetic field. The relativistic treatments for the case is a complicated task, because the situation is not stationary. In this paper, however, we assume that the rotational effect decouples from the magnetic effect. Thus we consider the deformation arising from each perturbation separately and estimate the ellipticity. The estimate is important to judge which effect dominates in the rotating magnetized stars, whose rotation rate and the magnetic field are in a wide range. Our treatment is beyond the classical estimate in the Newtonian gravity, and give better comparison of the rotational effect and the magnetic effect on star deformation for various pulsars. When either of them is huge, our estimate breaks down, and sophisticated numerical codes are required (see e.g. Bocquet et al. 1995; Bonazzola & Gourgoulhon 1996).

The paper is organized as follows. In Sect. 2, we briefly review deformation of stars due to the rotation (Chandrasekhar 1933; Chandrasekhar & Roberts 1963) and the magnetic field (Chandrasekhar & Fermi 1953; Ferraro 1954; Gal'tsov et al. 1984; Gal'tsov & Tsvetkov 1984) within Newtonian gravity. The quadrupole deformation can be evaluated by the ellipticity of the equilibrium shape. In Sect. 3, we also calculate the ellipticity based on the general relativistic perturbation theory (see also Hartle (1967) and Chandrasekhar & Miller (1974) for the rotational cases and Konno et al. (1999) for the magnetic cases). The ellipticity can be summarized in the same form as the Newtonian cases, but with different numerical factors. In Sect. 4, using the ellipticity, we compare the rotational effect with the magnetic effect on star deformation numerically. In this comparison, we keep the parameter range of known pulsars in mind. Finally, we give concluding remarks in Sect. 5. Throughout the paper, we use the units in which $c = G = 1$.

2. Simple estimate of deformation

Quadrupole deformation of an equilibrium body is characterized by the ellipticity ε, which is defined by

$$\varepsilon = \frac{\text{equatorial radius} - \text{polar radius}}{\text{mean radius}}. \tag{1}$$

For the gravitational equilibrium with uniform rotation, the value is essentially related to the ratio of the rotational energy to the gravitational energy. In the slow rotation of a homogeneous star, we have a well-known result (see e.g. Chandrasekhar 1969):

$$\varepsilon_\Omega = \frac{5}{4}\frac{R^3\Omega^2}{M}, \tag{2}$$

where R, M and Ω denote the radius, mass and angular velocity, respectively. For other stellar model, the numerical factor $5/4$

Send offprint requests to: K. Konno

should be replaced by an appropriate one. For example, the factor is 0.76 for the model with the polytropic equation of state (EOS) $p = \kappa\rho^{(n+1)/n}$ with index $n = 1$ (see Table 1 in Chandrasekhar & Roberts 1963). We therefore generalize the expression with a dimensionless factor f as

$$\varepsilon_\Omega = f\frac{R^3\Omega^2}{M}, \tag{3}$$

and will discuss how the factor f depends on the stellar models.

In a similar way, the effect of the magnetic stress is also expressed by the energy ratio of the magnetic field to the gravitational field. Introducing a dimensionless factor g, we have the ellipticity ε_B arising from magnetic field as

$$\varepsilon_B = g\frac{\mu^2}{M^2R^2}, \tag{4}$$

where μ is the magnetic dipole moment. The dimensionless factor g, in general, depends on both the magnetic field configurations and the EOS. For example, in the case of an incompressible fluid body with a dipole magnetic field treated by Ferraro (1954), we derive $g = 25/2$.

3. Relativistic calculation of deformation

In this section, we will review quadrupole deformation due to the slow rotation and weak dipole magnetic field. The deformation can be expressed by the second-order quantities with respect to the rotation rate or the magnetic field strength. In order to calculate the shape, we also have to calculate the space-time metric, which is axisymmetric stationary or static one. The line element can be written in the form

$$\begin{aligned} ds^2 \;=\; & -e^{\nu(r)}\left[1 + 2\left\{h_0(r) + h_2(r)P_2(\cos\theta)\right\}\right]dt^2 \\ & + e^{\lambda(r)}\left[1 + \frac{2e^{\lambda(r)}}{r}\left\{m_0(r) + m_2(r)P_2(\cos\theta)\right\}\right]dr^2 \\ & + r^2\left(1 + 2k_2(r)P_2(\cos\theta)\right) \\ & \quad \times \left[d\theta^2 + \sin^2\theta(d\phi - \omega(r)dt)^2\right], \end{aligned} \tag{5}$$

where P_2 is the Legendre's polynomial of degree 2, and $(h_0, h_2, m_0, m_2, k_2)$ are the second-order quantities for the rotation rate or the magnetic field strength. The quantity ω is the angular velocity acquired by an observer falling freely from infinity to a point r, and is equal to zero for the static magnetic field deformation.

The stress-energy tensor of the perfect fluid body is described by

$$T_{(\mathrm{m})}{}^{\mu}{}_{\nu} = (\rho + p)\,u^\mu u_\nu + p\delta^\mu_{\ \nu}. \tag{6}$$

When we consider the magnetic field deformation, we further take into account the stress-energy tensor arising from the magnetic field, i.e.,

$$T_{(\mathrm{em})}{}^{\mu}{}_{\nu} = \frac{1}{4\pi}\left(F^{\mu\lambda}F_{\nu\lambda} - \frac{1}{4}F_{\sigma\lambda}F^{\sigma\lambda}\delta^\mu_{\ \nu}\right). \tag{7}$$

Solving the Einstein-Maxwell equations, we can obtain the second-order metric functions mentioned above.

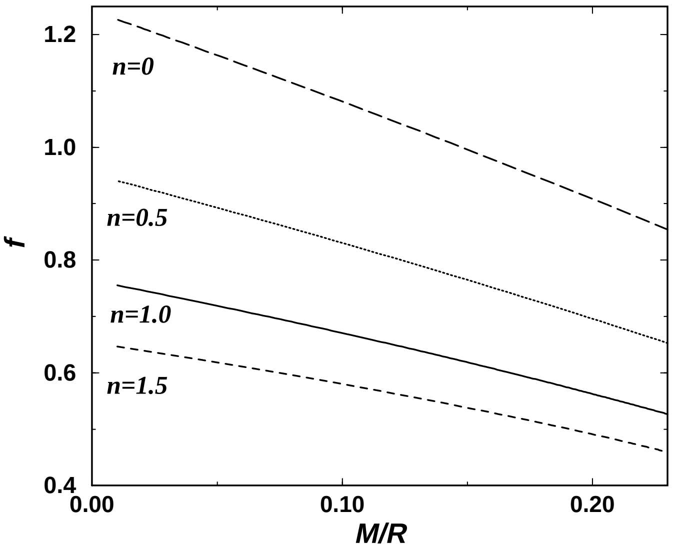

Fig. 1. The dimensionless factor f, that is, the ellipticity of the rotational cases normalized by $R^3\Omega^2/M$, which is plotted against M/R.

The ellipticity of the relativistic star can be calculated from the definition (1) as

$$\varepsilon = -\frac{3}{2}\left(\frac{\xi_2}{r} + k_2\right), \tag{8}$$

where ξ_2 represents the displacement of quadrupole deformation.

Since the displacement of the surface can be determined by the hydrostatic equilibrium condition, the ellipticity of the slowly rotating star is expressed as (Chandrasekhar & Miller 1974)

$$\varepsilon_\Omega = \frac{3}{r\nu'}h_2 + \frac{r}{\nu'}e^{-\nu}(\Omega - \omega)^2 - \frac{3}{2}k_2. \tag{9}$$

In order to compare it with the Newtonian results, we normalize the ellipticity in the same form as Eq. (3). There are several possibilities of the normalization factors for M and R in the relativistic calculation. We use natural choices, i.e., gravitational mass for M and circumferential radius for R in this paper. This normalization is useful to extrapolate from the Newtonian results. Chandrasekhar & Miller (1974) used a different normalization, which causes a prominent peak (see Fig. 5 in their paper). We note that the peak is due merely to a less convenient choice of the normalization. The resultant dimensionless factor f is calculated for the polytropic EOS with $n = 0,\ 0.5,\ 1,\ 1.5$. Fig. 1 displays the variation of the dimensionless quantity f with respect to the relativistic factor M/R. This figure shows that the correct relativistic calculations give smaller values of the ellipticity than those of the Newtonian calculations with fixed $R^3\Omega^2/M$. The factor in the typical relativistic case decreases down to 0.7 of the Newtonian case.

As for the weakly magnetized star, the Lorentz force plays a role on the equilibrium. The rotational term $\Omega - \omega$ is replaced

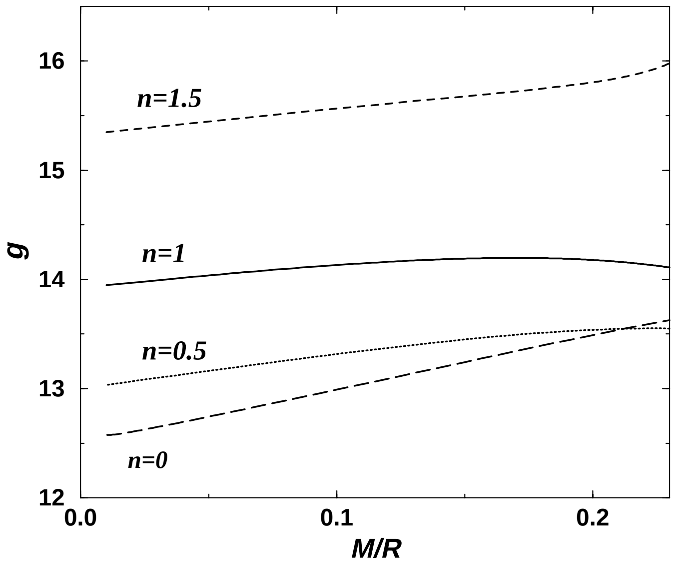

Fig. 2. The dimensionless factor g, that is, the ellipticity of the magnetic case normalized by $\mu^2/(M^2R^2)$, which is plotted against M/R. (Note that the normalization of this figure is different from that of Konno et al. (1999).)

by the magnetic term in the ellipticity. From the hydrostatic condition, we have (Konno et al. 1999)

$$\varepsilon_B = \frac{3}{r\nu'}h_2 + \frac{2r}{\nu'(\rho_0+p_0)}J^\phi A^\phi - \frac{3}{2}k_2, \tag{10}$$

where the subscript ‘0’ denotes the background quantities, and J^ϕ and A^ϕ are the ϕ-components of the 4-current and 4-potential respectively. The ellipticity can also be written in the form of Eq. (4). We also use the gravitational mass M and circumferential radius R. Fig. 2 displays the variation of the ellipticity with respect to the relativistic factor M/R. In these calculations, we have used the current distribution

$$J^\phi \propto \rho_0 + p_0, \tag{11}$$

which is a simplest case derived by the integrability condition (see e.g. Ferraro 1954) and gives the direct general-relativistic extension of Ferraro (1954). Using the normalization, the residual factor g is almost independent of the relativistic factor M/R.

4. The comparison

In order to compare the rotational effect with the magnetic effect on star deformation, we now consider the ratio of ε_Ω to ε_B,

$$\frac{\varepsilon_\Omega}{\varepsilon_B} = \frac{f}{g}\left(\frac{R^3\Omega^2}{M}\right)\left(\frac{\mu^2}{M^2R^2}\right)^{-1}. \tag{12}$$

First, we investigate the dependence of the ratio of the two dimensionless factors, f/g, on the relativistic factor M/R. Fig. 3 displays this ratio. From this figure, we can see that the true relativistic calculations with $M/R \sim 0.2$ give smaller values of the ratio than those obtained by the Newtonian calculations. This fact means that the approach using the Newtonian gravity overestimates the rotational effect. The curves f/g are approximately reproduced within 10% if we use

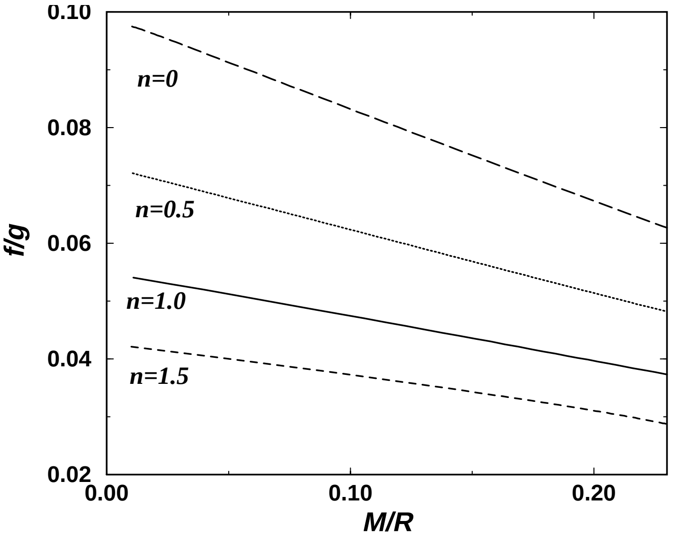

Fig. 3. The ratio of the two dimensionless factors, f/g, plotted against M/R.

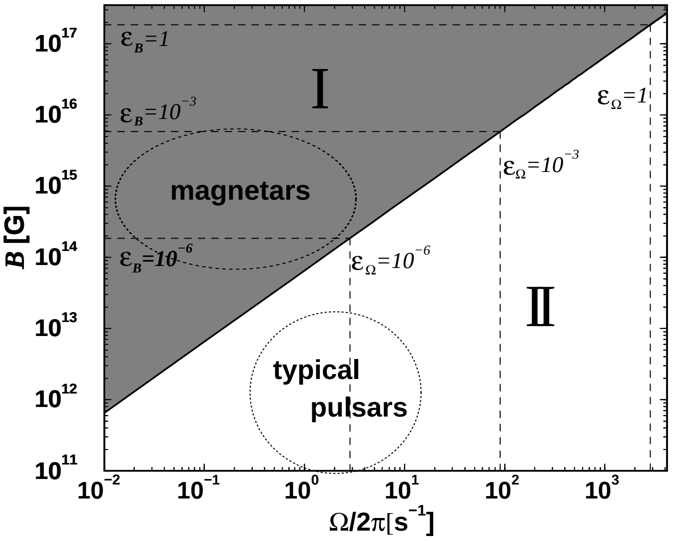

Fig. 4. The critical line on which $\varepsilon_\Omega = \varepsilon_B$ in B-Ω space for $M/R = 0.2$. This line divides the B-Ω space into two regions. In the region I, the magnetic effect dominates the rotational effect, while in the region II vice versa.

$$\frac{f}{g} \approx \frac{1 - 1.4M/R}{10 + 8n}. \tag{13}$$

Next, we consider the comparison including other parameters Ω and μ of stars. We use the stellar model with $M = 1.4M_\odot$ and $R = 10\mathrm{km}$. Fig. 4 displays a critical line on which $\varepsilon_\Omega = \varepsilon_B$ and the two regions divided by this line in B-Ω space, where B denotes the typical magnetic field strength on the surface, which is defined by $B = \mu/R^3$. We have plotted only one representative line of $n = 1$. We can also derive very close results for other indices. The critical line, in general, can be written from Eq. (12) as

$$B[\mathrm{G}] \approx 5.3 \times 10^{13} \sqrt{\frac{f}{g}} \left(\frac{M/1.4M_{\odot}}{R/10\mathrm{km}} \right)^{1/2} \Omega \, [\mathrm{sec}^{-1}], \qquad (14)$$

where it is useful to use the fitting formula Eq. (13) for f/g. In the region I, the magnetic effect dominates the rotational effect, i.e., $\varepsilon_B > \varepsilon_\Omega$, whereas in the region II vice versa, i.e., $\varepsilon_\Omega > \varepsilon_B$. From this figure, we find that objects having magnetic field strength $B \sim 10^{14}$–10^{15}G and period $T \sim 1$ sec such as SGRs and AXPs belong to the region I. Thus, the magnetic effect overwhelms the rotational effect for such observed candidates of magnetars.

On the other hand, well-known typical pulsars with magnetic field strength $B \sim 10^{11}$–10^{13}G and the period $T \sim 10^{-1}$–1 sec (see e.g. Taylor et al. 1993) obviously belong to the region II. Millisecond pulsars also belong to the region II. The magnetic deformation is neglected.

5. Concluding remarks

The new classes of objects, which are candidates of magnetars, have inspired us to investigate the relation between the rotational effect and the magnetic effect on deformation of stars. We have briefly reviewed the quadrupole deformation due to the rotation and that due to the magnetic field based on previous studies, and compared the rotational effect with the magnetic effect for various pulsars reported observationally. From our investigation, we have found that the new classes of objects such as SGRs and AXPs belong to the region in which the magnetic effect dominates the rotational effect, while well-known typical pulsars with magnetic field strength 10^{11}–10^{13}G and millisecond pulsars vice versa. Thus, the critical line on which the ellipticity arising from the rotation equals to that arising from the magnetic field divides the new classes and the well-known pulsars. Once we obtain the parameters Ω, B, R and M of a pulsar, we can see whether the magnetic effect is dominant or the rotational effect is dominant using Eqs. (13) and (14) and Fig. 4. The deformation due to the magnetic field may come into play in the spin-down of the magnetars. The spin-down history of the AXPs is rather irregular. Recently, Melatos (1999) ascribed the irregularity to the radiative precession produced by the deformation. At present, the fit to the observational data is not so good, but will be improved by detailed models. Theoretical models for the deformed stars will be required there.

As discussed by Bonazzola & Gourgoulhon (1996), the non-axisymmetric distortion is also important for the gravitational emission. The deformation can be calculated from the magnetic field, which is estimated from the observed pulsar period and the period derivative. The inferred amplitudes of the gravitational waves are too small for the present known pulsars. In the future, we might find more extreme case such as the early stage of rapidly rotating magnetars.

Acknowledgements. We would like to thank Dr. A.Y. Potekhin for fruitful comments and suggestions.

References

Bocquet M., Bonazzola S., Gourgoulhon E., Novak J., 1995, A&A 301, 757
Bonazzola S., Gourgoulhon E., 1996, A&A 312, 675
Chandrasekhar S., 1933, MNRAS 93, 539
Chandrasekhar S., 1969, Ellipsoidal Figures of Equilibrium. Yale University Press, New Haven
Chandrasekhar S., Fermi E., 1953, ApJ, 118, 116
Chandrasekhar S., Miller J.C., 1974, MNRAS 167, 63
Chandrasekhar S., Roberts P.H., 1963, ApJ 138, 801
Ferraro V.C.A., 1954, ApJ 119, 407
Gal'tsov D.V., Tsvetkov V.P., 1984, Phys. Lett. 103A, 193
Gal'tsov D.V., Tsvetkov V.P., Tsirulev A.N., 1984, Zh. Eksp. Teor. Fiz. 86, 809; Sov. Phys. JETP 59, 472
Hartle J.B., 1967, ApJ 150, 1005
Hewish A., Bell S.J., Pilkington J.D.H., et al., 1968, Nat 217, 709
Konno K., Obata T., Kojima Y., 1999, A&A 352, 211
Kouveliotou C., Dieters S., Strohmayer T., et al., 1998, Nat 393, 235
Kouveliotou C., Strohmayer T., Hurley K., et al., 1999, ApJ 510, L115
Melatos A., 1999, ApJ 519, L77
Mereghetti S., Stella L., 1995, ApJ 442, L17
Taylor J.H., Manchester R.N., Lyne A.G., 1993, ApJS 88, 529
Thompson C., Duncan R.C., 1996, ApJ 473, 322

公表論文(3)

Progress of Theoretical Physics, Vol. 104, No. 6, December 2000

General Relativistic Modification of a Pulsar Electromagnetic Field

Kohkichi KONNO*) and Yasufumi KOJIMA**)

Department of Physics, Hiroshima University, Higashi-Hiroshima 739-8526, Japan

(Received September 4, 2000)

We consider an exterior electromagnetic field surrounding a rotating star endowed with a dipole magnetic field in the context of general relativity. The analytic solution for a stationary configuration is obtained, and the general relativistic modifications and the implications for pulsar radiation are investigated in detail. We find that the general relativistic corrections of both the electric field strength and the curvature radii of magnetic field lines tend to enhance the curvature radiation photon energy.

§1. Introduction

In recent years, new aspects of rotating neutron stars have been revealed in about 1000 pulsars. Eleven X-ray pulsars 1) and eight γ-ray pulsars 2) have been detected in the past several years. Among these new objects, some exhibit quite different behavior in their pulse periods. 3) The measurement of the period and its time derivative yields evidence of ultra-magnetized stars, possibly representing magnetars. 4) Motivated by the recent observational situation, theoretical models have been studied. As for high-energy pulsars, two general classes of models have been proposed. One is the polar cap model 5) and the other is the outer gap model. 6) The main difference between these two models is in the assumed region of the acceleration of charged particles responsible for the radiation. Both models partially explain some observational features of the γ-rays. They will be discriminated after including more detailed radiation processes. Future observation may determine their validity.

An important element to be included in theoretical models is general relativistic effects, which are in particular crucial for polar cap models, since acceleration occurs under strong gravity near the surface of neutron stars. Gonthier and Harding 7) considered the effects on the magnetic field configuration only. Their concern is the curvature radiation and the attenuation of pair production in a strong magnetic field. These processes result in a pair cascade and explain some aspects of pulsar radiation, including high-energy pulses in the γ-ray range. In addition to the magnetic fields, rotationally induced electric fields play an important role in the polar cap region (see, e.g., Ref. 8)). Charged particles are ripped off the surface and accelerated along the magnetic field lines by the electric fields. The magnetosphere is thereby eventually filled with charges. The accelerated particles may be seeds of subsequent curvature radiation. Muslimov and Tsygan 9) discussed general relativistic effects not only in the case of magnetic fields but also electric fields. They derived general expressions

---

*) E-mail: konno@theo.phys.sci.hiroshima-u.ac.jp

**) E-mail: kojima@theo.phys.sci.hiroshima-u.ac.jp

including multipoles of arbitrary order using hypergeometric functions, assuming a vacuum outside the star. Their work, however, is limited to only analytic forms, and therefore not easy, e.g., to compare with the standard results in flat space-time. Order estimates of general relativistic effects are also lacking. In this paper, we derive analytic solutions again for both the electric and magnetic fields around a rotating star endowed with an aligned dipole magnetic field. The resultant expressions are rather cumbersome, and for this reason approximate expressions are also given. Such forms provide an estimate of the corrections to the results in flat space-time, as well as a concise, practical application. We also give detailed discussion concerning the difference between our results and those in Minkowski space-time. This discussion may become important in the future, with progress in observational technology.

As shown in Ref. 10), the deviation from spherical space-time is less than 10^{-3} if the rotation period is longer than 10 msec and the magnetic field at the surface is less than 10^{16} gauss. Therefore, the electric and magnetic fields are determined by solving the Maxwell equations in a fixed background space-time. The appropriate space-time metric is that for an external field surrounding a slowly rotating star. We can neglect the second-order rotational effects, except in the case of rapidly rotating stars. We also restrict ourselves to a stationary configuration, that is, the case in which the magnetic dipole moment $\boldsymbol{\mu}$ is aligned with the angular velocity $\boldsymbol{\Omega}$. This leads to the following form $A_\mu = (A_t, 0, 0, A_\phi)$ for the four-potential (see Ref. 11) and references therein), where A_t is related to the rotationally induced electric field, and therefore $A_t \sim O(\Omega) \times A_\phi$. Detailed calculations to solve the Maxwell equations are given in §2. Approximate expressions of these solutions are discussed in §3. Implications of the general relativistic effects with regard to the acceleration of charged particles and radiation in vacuum gaps are investigated in §4. Finally, we give discussion in §5. Throughout the paper, we use units in which $c = G = 1$.

§2. The general relativistic solution for an exterior stellar electromagnetic field

We now derive expressions for an electromagnetic field surrounding a rotating, magnetized star using a general relativistic treatment. We solve the Maxwell equations in a fixed metric, assuming that the field is in a vacuum. The background metric outside the star with total mass M and angular momentum J is specified up to first order in the slow rotation approximation as

$$ds^2 = -e^{-\lambda(r)}dt^2 - 2\omega(r)r^2\sin^2\theta dt d\phi + e^{\lambda(r)}dr^2 + r^2 d\theta^2 + r^2\sin^2\theta d\phi^2, \quad (2\cdot1)$$

where

$$e^\lambda = \left(1 - \frac{2M}{r}\right)^{-1}, \quad (2\cdot2)$$

$$\omega = \frac{2J}{r^3}. \quad (2\cdot3)$$

In the non-rotating limit, a poloidal magnetic field can be described by the A_ϕ

component only. In the slowly rotating case, the four-potential is given by $A_\mu = (A_t, 0, 0, A_\phi)$. The A_t component is rotationally induced as $A_t \sim O(\Omega) \times A_\phi$. The Maxwell equations for A_t and A_ϕ are given as

$$e^{-\lambda}\frac{\partial^2 A_\phi}{\partial r^2} - \lambda' e^{-\lambda}\frac{\partial A_\phi}{\partial r} + \frac{1}{r^2}\frac{\partial^2 A_\phi}{\partial \theta^2} - \frac{1}{r^2}\cot\theta\frac{\partial A_\phi}{\partial \theta} = 0, \tag{2·4a}$$

$$\begin{aligned} &e^{-\lambda}\frac{\partial^2 A_t}{\partial r^2} + \frac{2e^{-\lambda}}{r}\frac{\partial A_t}{\partial r} + \frac{1}{r^2}\frac{\partial^2 A_t}{\partial \theta^2} + \frac{1}{r^2}\cot\theta\frac{\partial A_t}{\partial \theta} \\ &+ \left[\left(\lambda' + \frac{2}{r}\right)\omega + \omega'\right] e^{-\lambda}\frac{\partial A_\phi}{\partial r} + \frac{2}{r^2}\omega\cot\theta\frac{\partial A_\phi}{\partial \theta} = 0, \end{aligned} \tag{2·4b}$$

where the prime here denotes differentiation with respect to r. Note that the last two terms on the left-hand side of Eq. (2·4b) represent the coupling between the frame-dragging and the stellar magnetic field, and that these terms originate from a purely general relativistic effect.

From this point, we restrict our discussion to the case of a dipole magnetic field, so that Eq. (2·4a) can be solved in the form

$$A_\phi(r,\theta) = -a_\phi(r)\sin^2\theta. \tag{2·5}$$

In a similar way, the potential A_t can be written as

$$A_t(r,\theta) = a_{t0}(r) + a_{t2}(r)P_2(\cos\theta), \tag{2·6}$$

where P_2 is the Legendre polynomial of degree 2.

The solution for a_ϕ can easily be derived in the form [12)]

$$a_\phi = \frac{3\mu}{8M^3}r^2\left[\ln\left(1-\frac{2M}{r}\right) + \frac{2M}{r} + \frac{2M^2}{r^2}\right], \tag{2·7}$$

where μ is the magnetic dipole moment with respect to an observer at infinity. The resulting dipole magnetic field in the local frame is given by

$$B_{(r)} = -\frac{3\mu}{4M^3}\left[\ln\left(1-\frac{2M}{r}\right) + \frac{2M}{r} + \frac{2M^2}{r^2}\right]\cos\theta, \tag{2·8a}$$

$$B_{(\theta)} = \frac{3\mu}{4M^3}\left[\sqrt{1-\frac{2M}{r}}\ln\left(1-\frac{2M}{r}\right) + \frac{2M(r-M)}{r\sqrt{r(r-2M)}}\right]\sin\theta. \tag{2·8b}$$

Next, we discuss the electric field induced by the rigid rotation of the star. The solution for a_{t0} and a_{t2} can be obtained analytically as

$$a_{t0} = \frac{c_0}{r} + \frac{J\mu}{2M^3r^2}(3r-M) + \frac{J\mu}{4M^4r}(3r-4M)\ln\left(1-\frac{2M}{r}\right), \tag{2·9a}$$

$$\begin{aligned} a_{t2} = &\frac{c_1}{M^2}(r-M)(r-2M) \\ &+c_2\left[\frac{2}{Mr}\left(3r^2-6Mr+M^2\right) + \frac{3}{M^2}\left(r^2-3Mr+2M^2\right)\ln\left(1-\frac{2M}{r}\right)\right] \end{aligned}$$

$$-\frac{J\mu}{2M^6r^2}\left(9r^4-3Mr^3-30M^2r^2+8M^3r+2M^4\right)$$
$$-\frac{J\mu}{2M^6r}\left(12r^3-36Mr^2+24M^2r+M^3\right)\ln\left(1-\frac{2M}{r}\right), \qquad (2\cdot 9\text{b})$$

where c_0, c_1 and c_2 are constants of integration. Since c_0 is understood as the net charge of the star, we set $c_0=0$. Furthermore, we derive

$$c_1=\frac{9J\mu}{2M^4}, \qquad (2\cdot 10)$$

from the regularity condition at infinity. The constant c_2 is fixed by the junction condition at the surface of the star. If we impose the assumption of a perfectly conducting interior, the magnetic field is frozen into the the fluid motion, i.e. $u^\mu F_{\mu\nu}=0$, where $u^\mu=(u^t,0,0,\Omega u^t)$ is the four-velocity of the fluid. From this condition at the surface, we have

$$\begin{aligned} c_2=&\left\{\frac{\mu J}{M^5R^2}\left(12R^3-24MR^2+4M^2R+M^3\right)\right.\\ &+\frac{\mu J}{2M^6R}\left(12R^3-36MR^2+24M^2R+M^3\right)\log\left(1-\frac{2M}{R}\right)\\ &\left.-\frac{\mu\Omega}{4M^3}\left[2MR+2M^2+R^2\log\left(1-\frac{2M}{R}\right)\right]\right\}\\ &\bigg/\left[\frac{2}{MR}\left(3R^2-6MR+M^2\right)\right.\\ &\left.\quad+\frac{3}{M^2}\left(R^2-3MR+2M^2\right)\log\left(1-\frac{2M}{R}\right)\right], \qquad (2\cdot 11)\end{aligned}$$

where R denotes the radius of the star. Consequently, using the above c_2, the induced electric field in the local frame can be written as

$$\begin{aligned} E_{(r)}=\frac{1}{2M^6r^3}&\left\{c_2\left[4M^5r\left(6r^2-3Mr-M^2\right)\right.\right.\\ &\left.+6M^4r^3\left(2r-3M\right)\ln\left(1-\frac{2M}{r}\right)\right]\\ &-2MJ\mu\left(24r^3-12Mr^2-4M^2r-3M^3\right)\\ &\left.-3rJ\mu\left(8r^3-12Mr^2-M^3\right)\ln\left(1-\frac{2M}{r}\right)\right\}P_2(\cos\theta),\end{aligned} \qquad (2\cdot 12\text{a})$$

$$\begin{aligned} E_{(\theta)}=&-\frac{3}{M^6r^3\sqrt{r(r-2M)}}\\ &\times\left\{c_2\left[2M^5r^2\left(3r^2-6Mr+M^2\right)\right.\right.\\ &\left.+3M^4r^3\left(r^2-3Mr+2M^2\right)\ln\left(1-\frac{2M}{r}\right)\right]\\ &-MJ\mu\left(12r^4-24Mr^3+4M^2r^2-M^4\right)\\ &\left.-6r^3J\mu\left(r^2-3Mr+2M^2\right)\ln\left(1-\frac{2M}{r}\right)\right\}\sin\theta\cos\theta. \qquad (2\cdot 12\text{b})\end{aligned}$$

The discussion of the quantitative nature of the electromagnetic field strength is given in the next section.

§3. Comparison with results in flat space-time

In the previous section, we obtained expressions for the electromagnetic field in the general relativistic framework. However, these expressions are somewhat cumbersome. They are reduced to standard expressions given in textbooks[8] when the gravitational terms are neglected, i.e. when we take the limits $M, J \to 0$. It is important to compare our expressions with the standard expressions and to examine the differences. From this point of view, we now derive the simpler approximate expressions by expanding in powers of $1/r$. The lowest-order forms give the standard results, and the next terms give their corrections. As an approximation, we use the radius r in the Schwarzschild coordinates as the radius in the flat space-time. The

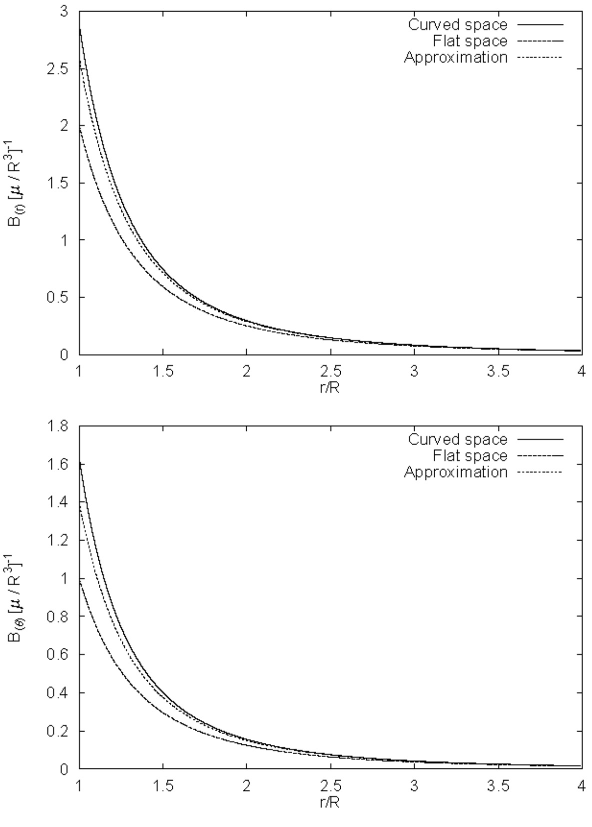

Fig. 1. Radial parts of the magnetic field components $B_{(r)}$ and $B_{(\theta)}$ are plotted as functions of the radius. The field strength is normalized by the typical value μ/R^3. The solid, dashed and dotted curves denote the curved space-time, flat space-time and approximate expressions, respectively.

magnetic and electric fields can be expanded in the forms

$$B_{(r)} \simeq \frac{2\mu}{r^3}\left[1+\frac{3M}{2r}\right]\cos\theta, \qquad (3\cdot1\text{a})$$

$$B_{(\theta)} \simeq \frac{\mu}{r^3}\left[1+\frac{2M}{r}\right]\sin\theta, \qquad (3\cdot1\text{b})$$

$$E_{(r)} \simeq -\frac{2\mu R^2 \Omega}{r^4}\left[1-\left(\frac{1}{2}-\frac{8R}{3r}\right)\frac{M}{R}+\left(1-\frac{2R}{r}\right)\frac{I}{R^3}\right]P_2(\cos\theta), \quad (3\cdot2\text{a})$$

$$E_{(\theta)} \simeq -\frac{2\mu R^2 \Omega}{r^4}\left[1-\left(\frac{1}{6}-\frac{R}{r}\right)\frac{M}{R}+\left(1-\frac{3R}{r}\right)\frac{I}{R^3}\right]\sin\theta\cos\theta, \quad (3\cdot2\text{b})$$

where the terms following the first ones in each of the square brackets are the first-order corrections due to the curved space-time. In Eq. (3·2), the moment of the inertia $I = J/\Omega$ is used. These corrections can be estimated easily for stars with uniform density, in which $I \sim 2MR^2/5$ and $M/R \leq 4/9$. The correction terms

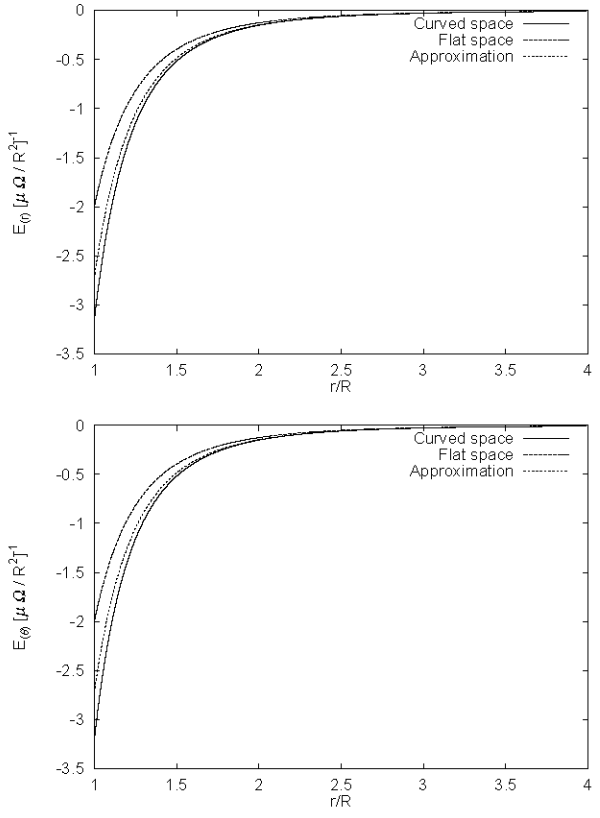

Fig. 2. Radial parts of the magnetic field components $E_{(r)}$ and $E_{(\theta)}$ are plotted as functions of the radius. The field strength is normalized by the typical value $\mu\Omega/R^2$. The solid, dashed and dotted curves denote the curved space-time, flat space-time and approximate expressions, respectively.

become larger with the relativistic factor M/R, but they are less than 1. Thus we see that the expressions obtained in the flat space-time are accurate to within a factor of 2.

In Figs. 1 and 2, we explicitly display the results in the flat and curved space-times as functions of the radius. These figures display the normalized values of the radial parts of the magnetic and electric fields, respectively. We have adopted a polytropic stellar model with $M/R = 0.2$, which is a plausible value for neutron stars. The solid curves here denote the exact values in the curved space-time, while the dashed curves correspond to the standard results in the flat space-time. From these figures, we find that the standard expressions in the flat space-time give values deviating from the curved space-time values by 50% at most. The maximum error is roughly estimated as $2M/r$. Therefore, the standard expressions are useful for arguments within this order of the magnitude.

§4. Implications for the acceleration of charged particles and the radiation in vacuum gaps

In this section, the results for the electromagnetic field in curved space-time are applied to analysis of the pulsar emission mechanism, that is, quantities relevant to the acceleration of charged particles and radiation in vacuum gaps above the polar caps. The gravitational force is much less than the electrostatic force, but gravity affects space-time, whose effects on the electromagnetic field are considered here. We explicitly derive the electric field along the magnetic field lines, curvature radii of the field lines, and size of polar cap regions. They are important to evaluate the available potential energy, curvature radiation, and so on. They significantly depend on the global shape of magnetic field lines, so that deviation from the standard results in flat space-time is not estimated using some local positions, although the overall error is not expected to be large.

First, we investigate the electric field component along the magnetic field lines. This plays a direct, important role in the acceleration of charged particles. The component is derived from Eqs. (2·8) and (2·12) as

$$E_{||} = \frac{E_{(r)}B_{(r)} + E_{(\theta)}B_{(\theta)}}{\sqrt{B^2_{(r)} + B^2_{(\theta)}}}. \tag{4·1}$$

Figure 3 displays $E_{||}$ normalized by the typical value $\mu\Omega/R^2$ as a function of the proper distance l from the stellar surface along a field line. The dashed curve denotes the Minkowskian case, and the solid curve denotes the general relativistic case of $M/R = 0.2$. This figure shows that the electric field component is strengthened by the general relativistic effect with respect to the same value of $\mu\Omega/R^2$. The result in the curved case is about 1.5 times as large as that in the flat case near the surface. A similar kind of enhancement can be seen in the stellar interior due to the general relativistic effect.[10] These enhancements may be regarded as having a common origin.

The configurations of the magnetic field lines are also modified by the general

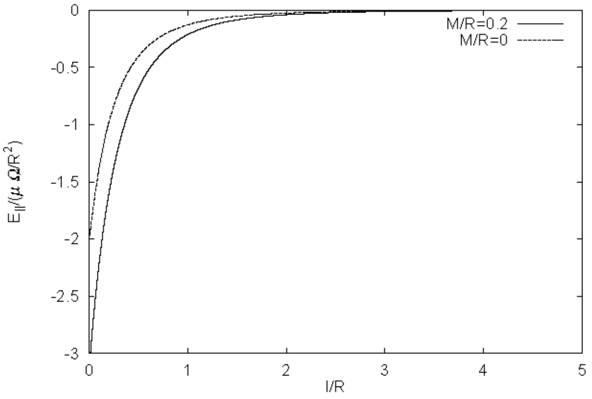

Fig. 3. The electric field component along a magnetic field line that flows from the stellar surface with $\theta = 1^\circ$. The field strength, which is normalized by the typical value $\mu\Omega/R^2$, is calculated for the Minkowskian case $M/R = 0$ (dashed) and the relativistic case $M/R = 0.2$ (solid). The proper distance l from the stellar surface is normalized by R.

relativistic effect. In general, a magnetic field line is described by an ordinary differential equation:[13)]

$$\frac{dr}{d\theta} = \frac{B_r}{B_\theta}. \tag{4·2}$$

The solution of this equation is

$$A_\phi = \text{const}\,(\equiv \tilde{c})\,. \tag{4·3}$$

Each field line is labeled by a constant $\tilde{c}$. Figure 4 displays the magnetic field lines embedded in the z-x plane, where $(z, x) = (r\cos\theta, r\sin\theta)$, both in the Minkowskian case and in the general relativistic case. As easily seen from this figure, the magnetic field lines are moderately modified by the general relativistic effect. Owing to this change, curvature radii of the field lines are also modified by the general relativistic effect.

Mathematically, the radius is defined as

$$\tilde{\rho} = \left(\frac{d\theta}{dl}\right)^{-1}, \tag{4·4}$$

where l denotes the proper distance along a field line. In the Minkowskian case, the field line is simply specified as $\tilde{c}r = \sin^2\theta$, so that the curvature radius along the line labeled by $\tilde{c}$ is given by

$$\tilde{\rho} = \frac{\sin\theta}{\tilde{c}}\sqrt{1 + 3\cos^2\theta}. \tag{4·5}$$

The general relativistic counterpart should be obtained numerically. Figure 5 displays the curvature radii $\tilde{\rho}$ of magnetic field lines which start from the stellar surface with an angle of $\theta = 1^\circ$. From Fig. 5, we find that the general relativistic effect causes the curvature radius to become smaller for a fixed magnetic moment. The

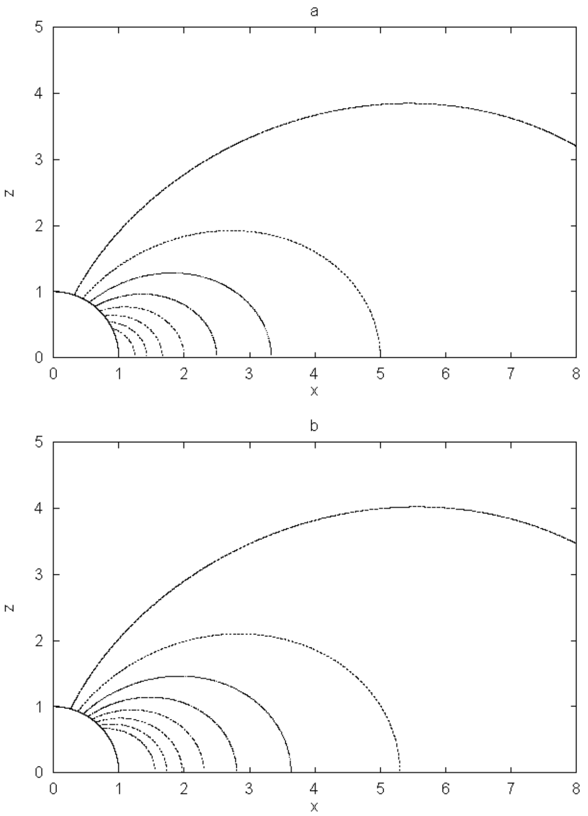

Fig. 4. Magnetic field lines for the Minkowskian case ($M/R = 0$) (a) and the general relativistic case with $M/R = 0.2$ (b), plotted in the z-x plane, where $(z, x) = (r \sin\theta, r \cos\theta)$. Both cases have the same magnetic moment. The surface of the star is denoted by the circle of radius 1.

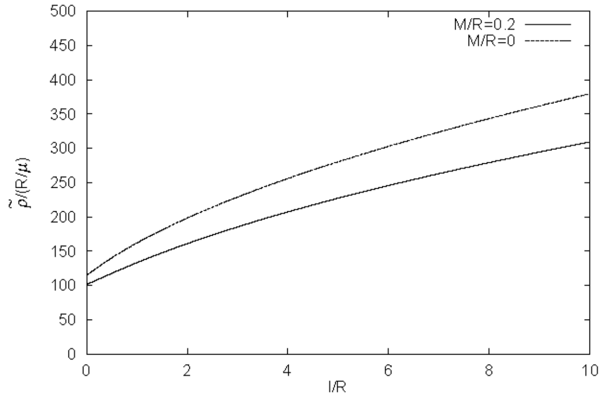

Fig. 5. Curvature radii of magnetic field lines that flow from the stellar surface with $\theta = 1°$. The radii are plotted as functions of the proper distance l along the field line. The solid line denotes the general relativistic case with $M/R = 0.2$, while the dashed line denotes the Minkowskian case $M/R = 0$. The radii $\tilde{\rho}$ and the proper distance l are normalized by R/μ and R, respectively.

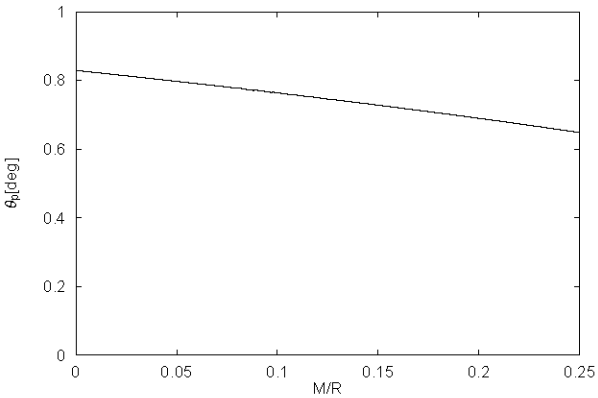

Fig. 6. Polar cap angles plotted as functions of the general relativistic factor M/R for $R_L \simeq 5 \times 10^3 R$.

curvature radiation is produced by charged particles moving along the magnetic field lines. The resulting curvature radiation photon energy is proportional to $\tilde{\rho}^{-1}$. The correct treatment in curved space-time implies an increase of the photon energy. Although we have displayed only one comparison between the flat and curved cases, almost the same results were obtained for all small values of θ.

A modification of the field lines, further, leads to a change of the polar cap radius. The polar cap angle θ_p is given by

$$\theta_p = \sin^{-1} \sqrt{\frac{a_\phi(R_L)}{a_\phi(R)}}, \tag{4·6}$$

where R_L is the radius of the light cylinder. To derive the polar cap angle explicitly, we have assumed

$$R_L = \frac{c}{\Omega} \simeq 5 \times 10^3 R \tag{4·7}$$

for any value of M/R. Figure 6 displays the dependence of the polar cap angle θ_p on the general relativistic factor M/R. From this figure, we see that the polar cap angle is reduced by about 15% due to the curved nature.

§5. Discussion

Recent observations of compact stars have given remarkable results that demand the refinement of theoretical models. Inspired by this, we have reconsidered an exterior electromagnetic field surrounding a rotating star endowed with an aligned dipole magnetic field in the context of general relativity. The electromagnetic fields were derived in analytic and approximate forms. We found that the expressions calculated in the flat space-time are accurate within a factor of approximately 2. We have not calculated the emission and propagation of radiation from polar caps of pulsars, but rather have discussed the implications for the underlining physical processes. We have found that the general relativistic effects increase the strength of electric fields and decrease the curvature radii of the magnetic field lines. Both of these factors contribute to increase the photon energy emitted from charged particles. The magnitude of the correction is of order M/R. Another important general relativistic effect, which has not been considered here, is the redshift factor. The observed energy is shifted to a lower value by a factor of M/R. It is not clear whether or not all these general relativistic effects are canceled. It is important to construct detailed models of pulsar radiation, taking these factors into account.

Although we have restricted our investigation to a rotating star in a vacuum, it seems that actual neutron stars are surrounded by plasma. Hence, it is important to investigate the acceleration of charged particles and the radiation taking into account the plasma distributions around stars. A general relativistic analysis using a certain pulsar model which specifies the plasma distribution has been given by Muslimov and Tsygan.$^{14)}$ The general relativistic effects in pulsar models are not yet clear, since the magnitude of the effects significantly depends on the plasma distribution. It is necessary to discuss the effects in a more general framework. This will be the subject of future investigation.

Acknowledgements

This work was supported in part by a Grant-in-Aid for Scientific Research Fellowship of the Ministry of Education, Science, Sports and Culture of Japan (No. 12001146).

References

1) W. Becker and J. Trümper, Astron. Astrophys. **341** (1999), 803.
2) D. J. Thompson et al., Astrophys. J. **516** (1999), 297.
3) See, e.g., C. Kouveliotou et al., Nature **393** (1998), 235.
C. Kouveliotou et al., Astrophys. J. **510** (1999), L115.
S. Mereghetti and L. Stella, Astrophys. J. **442** (1995), L17.
4) R. C. Duncan and C. Thompson, Astrophys. J. **392** (1992), L9.
5) See, e.g., S. J. Sturner, C. D. Dermer and F. C. Michel, Astrophys. J. **445** (1995), 736.
J. K. Daugherty and A. K. Harding, Astrophys. J. **458** (1996), 278.
B. Zhang and A. K. Harding, Astrophys. J. **532** (2000), 1150.
6) See, e.g., K. S. Cheng, C. Ho and M. Ruderman, Astrophys. J. **300** (1986), 500, 522.
R. W. Romani, Astrophys. J. **470** (1996), 469.
7) P. L. Gonthier and A. K. Harding, Astrophys. J. **425** (1994), 767.
8) P. Mészáros, *High-Energy Radiation from Magnetized Neutron Stars* (The University of Chicago Press, USA, 1992).
9) A. G. Muslimov and A. I. Tsygan, Sov. Astron. **30** (1986), 567.
10) K. Konno, T. Obata and Y. Kojima, Astron. Astrophys. **352** (1999), 211; **356** (2000), 234.
11) S. Bonazzola, E. Gourgoulhon, M. Salgado and J. A. Marck, Astron. Astrophys. **278** (1993), 421.
12) V. L. Ginzburg and L. M. Ozernoĭ, Sov. Phys. -JETP **20** (1965), 689.
13) M. Dovčiak, V. Karas and A. Lanza, astro-ph/0005216.
14) A. G. Muslimov and A. I. Tsygan, Sov. Astron. **34** (1990), 133; Mon. Not. R. Astron. Sci. **255** (1992), 61.
A. I. Tsygan, Astron. Lett. **19** (1993), 268.

参考論文

(1) General Relativistic Effects of Gravity in Quantum Mechanics
— A Case of Ultra-Relativistic, Spin 1/2 Particles —
Kohkichi Konno, Masumi Kasai
Progress of Theoretical Physics, **100**(1998) 1145-1157

(2) Asymmetry in Microlensing-Induced Light Curves
Kohkichi Konno, Yasufumi Kojima
Progress of Theoretical Physics, **101**(1999) 885-901

参考論文(1)

Progress of Theoretical Physics, Vol. 100, No. 6, December 1998

General Relativistic Effects of Gravity in Quantum Mechanics

—— *A Case of Ultra-Relativistic, Spin 1/2 Particles* ——

Kohkichi KONNO*) and Masumi KASAI

Faculty of Science and Technology, Hirosaki University, Hirosaki 036-8561, Japan

(Received June 9, 1998)

We present a general relativistic framework for studying gravitational effects in quantum mechanical phenomena. We concentrate our attention on the case of ultra-relativistic, spin-1/2 particles propagating in Kerr spacetime. The two-component Weyl equation with general relativistic corrections is obtained in the case of a slowly rotating, weak gravitational field. Our approach is also applied to neutrino oscillations in the presence of a gravitational field. The relative phase of two different mass eigenstates is calculated in radial propagation, and the result is compared with those of previous works.

§1. Introduction

It had been thought that physical phenomena in which gravitational effects and quantum effects appear simultaneously are far beyond our reach, before Colella, Overhauser and Werner 1) conducted an elegant experiment using a neutron interferometer. (This kind of experiment is called a COW experiment.) The COW experiment was the first experiment that measures the Newtonian gravitational effect on a wave function. This effect and its detectability were first suggested by Overhauser and Colella, 2) and the next year the effect was verified by Colella et al. 1) Although their analysis, which was based on inserting the Newtonian gravitational potential into the Schrödinger equation, was very simple, this experiment is conceptually very important in the history of quantum theory.

Recently, gravitational effects on another physical phenomenon, neutrino oscillations, have been much discussed. 3)-8) The COW experiment and this phenomenon have the common aspect that gravitational effects appear in the quantum interference. However, there are some differences between the two. In the former case, the spatial spread of the wave function plays a significant role, whereas in the latter case, the existence of different mass eigenstates and linear superposition are important. Another important difference is that the particle is non-relativistic in the former case, whereas it is ultra-relativistic in the latter case.

It seems that a controversy concerning gravitationally induced neutrino oscillation phases has arisen. Ahluwalia and Burgard 3) state that the phases amount to roughly 20% of the kinematic counterparts in the vicinity of a neutron star. Nevertheless, the definition of neutrino energy and the derivation of the phases are not clear in their original paper. 3) On the other hand, other groups 4), 5), 7), 8) have obtained similar results for radially propagating neutrinos (the results seem to be

---

*) Present address: Department of Physics, Hiroshima University, Higashi-Hiroshima 739-8526, Japan.

different from that in Ref. 3)). However, the authors of Ref. 4) assume that different mass eigenstates are produced at different times. This assumption seems to be of questionable validity, because the relative phase between the two different mass eigenstates initially becomes arbitrary. All of these papers, except Ref. 7), are based on a previous work,[9)] in which the classical action is taken as a quantum phase. Therefore, effects arising from the spin of the particle are not considered in these papers. On the other hand, the authors of Ref. 7) use the covariant Dirac equation, but they also calculate the classical action along the particle trajectory in the end.

We provide another framework, different from those of previous works, for studying general relativistic gravitational effects on spin-1/2 particles with non-vanishing mass, such as massive neutrinos. (Experimental confirmation demonstrating that neutrinos have nonzero mass has not yet been obtained. However, recent experimental reports[10)] seem to suggest neutrinos to be massive.) We do not merely calculate the classical action along the particle trajectory, but start from the covariant Dirac equation. Our approach allows us to discuss the effects of the coupling between the spin and the gravitational field. In particular, we consider the propagation of the particle in the Kerr geometry, by which the external field of a rotating star can be described. We perform our calculations in a slowly rotating, weak gravitational field, and derive the two-component Weyl equations with corrections arising from the non-vanishing mass and the gravitational field. Furthermore, we discuss neutrino oscillations in the presence of the gravitational field.

The organization of this paper is as follows. In §2, we assume that the external field of a rotating object is described by the Kerr metric and discuss the covariant Dirac equation in this field. In §3, we derive the Weyl equations with general relativistic corrections for an ultra-relativistic particle. The application to neutrino oscillations in the presence of the gravitational field is discussed in §4. Finally, we give a summary and conclusion in §5.

§2. Covariant Dirac equation in Kerr geometry

In this section, we consider the covariant Dirac equation in the presence of a gravitational field arising from a rotating object. We derive an equation for the time evolution of spinors, which describe particles with spin-1/2, in the last part of this section.

2.1. *Cavariant Dirac equation*

To begin, we briefly review the covariant Dirac equation.[11)-13)]

The natural generalization of the Dirac equation into curved space-time gives

$$\left[i\hbar\gamma^{\mu}\left(\frac{\partial}{\partial x^{\mu}}-\Gamma_{\mu}\right)-mc\right]=0, \tag{2·1}$$

where γ^{μ} are the covariant Dirac matrices connected with space-time through the relations

$$\gamma^{\mu}\gamma^{\nu}+\gamma^{\nu}\gamma^{\mu}=2g^{\mu\nu}, \tag{2·2}$$

and Γ_μ is the spin connection. The spin connection is determined by the condition

$$\frac{\partial \gamma_\nu}{\partial x^\mu} - \Gamma^{\lambda}{}_{\nu\mu}\gamma_\lambda - \Gamma_\mu \gamma_\nu + \gamma_\nu \Gamma_\mu = 0. \tag{2·3}$$

We now introduce the constant Dirac matrices $\gamma^{(a)}$ defined by

$$\gamma^{(a)} = e^{(a)}{}_{\mu}\gamma^\mu, \tag{2·4}$$

where $e^{(a)}{}_{\mu}$ is the orthogonal tetrad satisfying the relation

$$g_{\mu\nu} = \eta_{ab} e^{(a)}{}_{\mu} e^{(b)}{}_{\nu} \tag{2·5}$$

($\eta_{ab} = \mathrm{diag}\,(c^2, -1, -1, -1)$). Using these constant Dirac matrices, the spin connection is expressed as

$$\Gamma_\mu = -\frac{1}{8}\left[\gamma^{(a)}, \gamma^{(b)}\right] g_{\nu\lambda}\, e_{(a)}{}^{\nu} \nabla_\mu e_{(b)}{}^{\lambda}, \tag{2·6}$$

where the square brackets denote the usual commutator.[*]

2.2. *Space-time*

Here, we discuss the gravitational field arising from a rotating object. We now assume that the external field of the rotating object is described by the Kerr metric. If we restrict ourselves to a slowly rotating, weak gravitational field up to the first order in the angular velocity, which is related to the Kerr parameter a, and the Newtonian gravitational potential $\phi = -GM/r$, respectively, the line element is given by

$$\begin{aligned} ds^2 \simeq \left(1 + 2\,\frac{\phi}{c^2}\right) c^2 dt^2 + \frac{4GMa}{c^2 r^3}\,(xdy - ydx)\,dt \\ - \left(1 - 2\,\frac{\phi}{c^2}\right)\left(dx^2 + dy^2 + dz^2\right), \end{aligned} \tag{2·7}$$

where a is expressed in terms of the mass M and the angular momentum J of the gravitational source:

$$a \equiv \frac{J}{M}. \tag{2·8}$$

Assuming that the rotating object is a sphere of radius R with uniform density, we have

$$a \equiv \frac{J}{M} = \frac{2}{5}\,R^2\omega, \tag{2·9}$$

where ω denotes the angular velocity of this object. (If the rotating object deviates from a sphere, or has an inhomogeneous density distribution, then the numerical factor 2/5 might be changed by a factor of order unity.)

---

[*] We have ignored a term proportional to the unit matrix.

2.3. *Equation for time evolution of spinors*

Next, we turn our attention to time evolution of spinors. The covariant Dirac equation (2·1) has beautiful space-time symmetry. However, in order to investigate the time evolution of spinors, we must break the symmetrical form of this equation. For this purpose, we now use the (3+1) formalism. In the (3+1) formalism, the metric $g_{\alpha\beta}$ is split as

$$g_{00} = N^2 - \gamma_{ij}N^iN^j, \tag{2·10a}$$
$$g_{0i} = -\gamma_{ij}N^j \equiv -N_i, \tag{2·10b}$$
$$g_{ij} = -\gamma_{ij}, \tag{2·10c}$$

where N is the lapse function, N^i the shift vector, and γ_{ij} the spatial metric on the 3D hypersurface. Furthermore, we define γ^{ij} as the inverse matrix of γ_{ij}. Using the metric (2·7) derived in the last section, we can write the lapse function, the shift vector and the spatial metric in the following way:

$$N = c\left(1 + \frac{\phi}{c^2}\right), \tag{2·11}$$

$$N^x = \frac{4GMR^2}{5c^2r^3}\omega y, \tag{2·12a}$$
$$N^y = -\frac{4GMR^2}{5c^2r^3}\omega x, \tag{2·12b}$$
$$N^z = 0, \tag{2·12c}$$

$$\gamma_{ij} = \left(1 - 2\frac{\phi}{c^2}\right)\delta_{ij}. \tag{2·13}$$

Furthermore, we choose the tetrad as

$$e_{(0)}^{\ \ \mu} = c\left(\frac{1}{N}, -\frac{N^i}{N}\right), \tag{2·14}$$
$$e_{(k)}^{\ \ \mu} = \left(0, e_{(k)}^{\ \ i}\right), \tag{2·15}$$

where the spatial triad $e_{(k)}^{\ \ i}$ is defined as

$$\gamma_{ij}\, e_{(k)}^{\ \ i}\, e_{(l)}^{\ \ j} = \delta_{kl}. \tag{2·16}$$

From Eqs. (2·11)–(2·13), we derive

$$e_{(0)}^{\ \ 0} = 1 - \frac{\phi}{c^2}, \tag{2·17a}$$
$$e_{(0)}^{\ \ 1} = -\frac{4GMR^2}{5c^2r^3}\omega y, \tag{2·17b}$$
$$e_{(0)}^{\ \ 2} = \frac{4GMR^2}{5c^2r^3}\omega x, \tag{2·17c}$$
$$e_{(0)}^{\ \ 3} = 0, \tag{2·17d}$$

$$e_{(j)}^{\ \ i} = \left(1+\frac{\phi}{c^2}\right)\delta_j^{\ i}. \tag{2·18}$$

Using our choice of the tetrad, the covariant Dirac matrices γ^α are written as

$$\gamma^0 = \gamma^{(a)} e_{(a)}^{\ \ 0} \;=\; \gamma^{(0)}\frac{c}{N}, \tag{2·19}$$

$$\gamma^i = \gamma^{(a)} e_{(a)}^{\ \ i} \;=\; -\gamma^{(0)}\frac{c}{N}N^i + \gamma^{(j)} e_{(j)}^{\ \ i}. \tag{2·20}$$

Hence the covariant Dirac equation (2·1) can be written as

$$\begin{aligned} i\hbar\frac{\partial}{\partial t}\Psi &= H\Psi \\ &= \left[\left(\gamma^{(0)}\gamma^{(j)}cNe_{(j)}^{\ \ i} - N^i\right)(\overline{p}_i + i\hbar\Gamma_i) + i\hbar\Gamma_0 + \gamma^{(0)}mc^2N\right]\Psi, \end{aligned} \tag{2·21}$$

where $\overline{p}_i$ is the momentum operator in flat space-time. This equation describes the time evolution of spinors. If we adopt the Weyl representation as the constant Dirac matrices in this equation, then for massless particles in flat space-time we derive the well-known Weyl equations

$$i\hbar\frac{\partial}{\partial t}\psi = \pm c\boldsymbol{\sigma}\cdot\overline{\boldsymbol{p}}\psi, \tag{2·22}$$

where ψ denotes two-component spinors.

§3. Ultra-relativistic limit

We now restrict our attention to the ultra-relativistic limit, which means that the rest energy of the particle is much smaller than the kinetic energy in the observer's frame. In particular, we expand the energy of the particle itself up to $O\left(m^2c^4/pc\right)$.

Here, we obtain the ultra-relativistic Hamiltonian up to the order of interest by performing a unitary transformation similar to the Foldy-Wouthuysen-Tani (FWT) transformation.[15),16)]

First, following the discussion of Ref. 14), we redefine the spinor and the Hamiltonian according to

$$\Psi' = \gamma^{1/4}\Psi, \quad H' = \gamma^{1/4}H\gamma^{-1/4}, \tag{3·1}$$

where γ is the determinant of the spatial metric:

$$\gamma = \det\left(\gamma_{ij}\right). \tag{3·2}$$

Since the invariant scalar product is

$$(\psi,\varphi) \equiv \int \overline{\psi}\varphi\sqrt{\gamma}d^3x, \tag{3·3}$$

under this redefinition the scalar product comes to assume the same form as in flat space-time:

$$\langle\psi',\varphi'\rangle \equiv \int \overline{\psi'}\varphi' d^3x. \tag{3·4}$$

It is sometimes convenient to adopt this definition of the scalar product.

Next, we perform a unitary transformation to derive the ultra-relativistic Hamiltonian which is the "even" operator up to the order of our interest. From this, we have

$$\begin{aligned}\tilde{H}' &= UH'U^{\dagger} \\ &= \begin{pmatrix} H_R & 0 \\ 0 & H_L \end{pmatrix} + \left[O\left(\frac{m^3c^6}{p^2c^2}\right) \text{ or } O\left(\frac{\phi^2}{c^4}, \omega^2\right)\right] .\end{aligned} \tag{3·5}$$

The Dirac spinor is also divided into each of two-component spinors as

$$\tilde{\Psi}' = \begin{pmatrix} \psi_R \\ \psi_L \end{pmatrix} , \tag{3·6}$$

where the subscript R and L denote the right-handed and the left-handed components, respectively.

We consider the left-handed component. We find that the equation for this component is given by

$$\begin{aligned} i\hbar\frac{\partial}{\partial t}\psi_L &= H_L\psi_L \\ &= -\Bigg[\left\{1+\frac{1}{c^2}\left(\phi+\bar{\boldsymbol{p}}\cdot\phi\bar{\boldsymbol{p}}\frac{1}{\bar{p}^2}+2\frac{GM}{r^3}\boldsymbol{L}\cdot\boldsymbol{S}\frac{1}{\bar{p}^2}\right)\right\}c\bar{p}\,\frac{\boldsymbol{\sigma}\cdot\bar{\boldsymbol{p}}}{\bar{p}} \\ &\quad -\frac{1}{c^2}\left(\frac{4GMR^2}{5r^3}\boldsymbol{\omega}\cdot(\boldsymbol{L}+\boldsymbol{S})+\frac{6GMR^2}{5r^5}\boldsymbol{S}\cdot[\boldsymbol{r}\times(\boldsymbol{r}\times\boldsymbol{\omega})]\right) \\ &\quad +\Bigg\{1+\frac{1}{4c^2}\Bigg(\phi-\frac{1}{\bar{p}^2}\phi\bar{p}^2+\frac{1}{\bar{p}^2}\bar{\boldsymbol{p}}\cdot\phi\bar{\boldsymbol{p}}-\bar{\boldsymbol{p}}\cdot\phi\bar{\boldsymbol{p}}\frac{1}{\bar{p}^2} \\ &\qquad\qquad +2\frac{1}{\bar{p}^2}\frac{GM}{r^3}\boldsymbol{L}\cdot\boldsymbol{S}-2\frac{GM}{r^3}\boldsymbol{L}\cdot\boldsymbol{S}\frac{1}{\bar{p}^2}\Bigg)\Bigg\}\frac{m^2c^3}{2\bar{p}}\,\frac{\boldsymbol{\sigma}\cdot\bar{\boldsymbol{p}}}{\bar{p}} \\ &\quad +\frac{1}{8}m^2c^2\,\frac{1}{c^2}\left(A\frac{1}{\bar{p}^2}-2\frac{\boldsymbol{\sigma}\cdot\bar{\boldsymbol{p}}}{\bar{p}^2}A\frac{\boldsymbol{\sigma}\cdot\bar{\boldsymbol{p}}}{\bar{p}^2}+\frac{1}{\bar{p}^2}A\right)\Bigg]\psi_L, \end{aligned} \tag{3·7}$$

where

$$A=\frac{4GMR^2}{5r^3}\boldsymbol{\omega}\cdot(\boldsymbol{L}+\boldsymbol{S})+\frac{6GMR^2}{5r^5}\boldsymbol{S}\cdot[\boldsymbol{r}\times(\boldsymbol{r}\times\boldsymbol{\omega})] . \tag{3·8}$$

The details of the calculations are given in Appendix A. From this, we find how the spin-orbit coupling, the coupling between the spin and the rotation of the gravitational source, or the coupling between the total angular momentum and the rotation is coupled to the non-vanishing mass.

In radial propagation, the orbital angular momentum vanishes. Therefore, in this case, only spin effects coupled to the rotation appear. If we set $\boldsymbol{\omega} = \boldsymbol{0}$, then there is no spin effect in radial propagation. This consequence is consistent with the results of previous work.[11)]

§4. An application

In this section, we consider an application of the two-component equation derived in the last section to neutrino oscillations in the presence of a gravitational field. In neutrino oscillations (see, e.g., Refs. 17)–19) for analysis in flat space-time), the most important point is the phase difference of the two different mass eigenstates. Hence we now concentrate on the phase shift of the particle.

4.1. *Neutrino oscillation in Kerr space-time*

We derive the phase shift directly from the two-component equation derived in the last section. Furthermore, for simplicity, we consider the radial propagation (r-direction), in which the spin-orbit coupling vanishes.

We now regard terms arising from the non-vanishing mass and the gravitational field as perturbations. Then Eq. (3·7) for the left-handed component is considered to be

$$i\hbar\frac{\partial}{\partial t}\psi_L = \left(H_{0L} + \Delta H_L\right)\psi_L, \tag{4·1}$$

where H_{0L} denotes the unperturbed Hamiltonian $H_{0L} = -c\boldsymbol{\sigma}\cdot\overline{\boldsymbol{p}}$, and ΔH_L the corrections arising from the non-vanishing mass and the gravitational field.

Here we assume that the spinor ψ_L is given by

$$\psi_L(\boldsymbol{x},t) = e^{i\Phi(t)}\psi_{0L}(\boldsymbol{x},t), \tag{4·2}$$

where ψ_{0L} satisfies the equation

$$i\hbar\frac{\partial}{\partial t}\psi_{0L}(\boldsymbol{x},t) = H_{0L}\psi_{0L}(\boldsymbol{x},t). \tag{4·3}$$

Substituting Eq. (4·2) into Eq. (4·1) and using Eq. (4·3), we obtain

$$\Phi = -\frac{1}{\hbar}\int^t \Delta H_L dt. \tag{4·4}$$

In order to derive the gravitationally induced phases practically, we assume that corresponding to the left-handed component, ψ_{0L} satisfies the relation

$$\frac{\boldsymbol{\sigma}\cdot\overline{\boldsymbol{p}}}{\overline{p}}\psi_{0L}(\boldsymbol{x},t) = -\psi_{0L}(\boldsymbol{x},t). \tag{4·5}$$

Furthermore, we here replace the q-numbers in ΔH_L with c-numbers. This is a kind of semi-classical approximation. From this, excluding spin effects, we derive the phase

$$\Phi = -\frac{1}{\hbar}\int_{t_A}^{t_B}\left(2\frac{\phi}{c^2}cp + \frac{m^2c^3}{2p}\right)dt, \tag{4·6}$$

where we have considered the case that the neutrino is produced at a space-time point $A(t_A, r_A)$ and detected at a space-time point $B(t_B, r_B)$. We now concentrate on the term related to m^2, because neutrino oscillations take place as a result of the mass square difference. Let the two different mass eigenstates have common momentum p and propagate along the same path. Then the relative phase $\Delta\Phi_{ij}$ of the two different mass eigenstates, $|\nu_i\rangle$ and $|\nu_j\rangle$, is given by

$$\Delta\Phi_{ij} = \frac{\Delta m_{ij}^2 c^3}{2\hbar}\int_{t_A}^{t_B}\frac{1}{p}dt. \tag{4·7}$$

Next, we discuss the spin-rotation coupling. In a similar way, we replace the q-numbers in terms concerning the spin of the particle in Eq. (3·7) with c-numbers again. From this kind of semi-classical approximation, we find that the spin-rotation term coupled to m^2 vanishes. However, the spin-rotation effects in higher order terms may survive. This fact implies that there is no influence of the spin-rotation coupling on neutrino oscillations, at least up to the order related to m^2.

Consequently, in a radially propagating case, we obtain the phase difference (4·7) between the two different mass eigenstates as a final result.

4.2. *Comparison with previous works*

Finally, we compare the result obtained above with those of previous works. For this purpose, we consider the Schwarzschild limit (i.e., $\omega \to 0$), which leads to the result (4·7) again.

First, we assume the "background" neutrino trajectory as that of radial null geodesics:

$$0 = ds^2 = \left(1 + 2\frac{\phi}{c^2}\right) c^2 dt^2 - \left(1 - 2\frac{\phi}{c^2}\right) dr^2. \tag{4·8}$$

Then we obtain

$$dt \simeq \frac{1}{c}\left(1 - 2\frac{\phi}{c^2}\right) dr. \tag{4·9}$$

Hence, if we transform the integral (4·7) with respect to t to that with respect to r, the relative phase $\Delta\Phi_{ij}$ is given by

$$\Delta\Phi_{ij} = \frac{\Delta m_{ij}^2 c^3}{2\hbar} \int_{r_A}^{r_B} \frac{1}{pc}\left(1 - 2\frac{\phi}{c^2}\right) dr. \tag{4·10}$$

The second term in the round brackets corresponds to the gravitational correction as indicated by Ahluwalia and Burgard.[3] Indeed, under the assumption that the tetrad component of the radial momentum $p_{(r)} = e_{(r)}{}^{r} p_r$ is constant along the trajectory, we can obtain the same expression as in Ref. 3). (Note that Ahluwalia and Burgard[3] assume $p_{(r)}c$ as the energy of the neutrino.)

Next, let us see whether our result (4·7) reproduces the other form of the results.[5],[7],[8] From the mass shell condition $g^{\mu\nu}p_\mu p_\nu = m^2c^2$, p is related with the energy $E (\equiv p_t c)$ in the following way:

$$pc = \left(1 - 2\frac{\phi}{c^2}\right) E + \left[O\left(m^2\right) \text{ or } O\left(\phi^2\right)\right]. \tag{4·11}$$

Under the assumption that E is constant along the trajectory, we finally obtain

$$\begin{aligned} \Delta\Phi_{ij} &= \frac{\Delta m_{ij}^2 c^3}{2\hbar} \int_{r_A}^{r_B} \frac{dr}{E} \\ &= \frac{\Delta m_{ij}^2 c^3}{2\hbar E} \left(r_B - r_A\right), \end{aligned} \tag{4·12}$$

which is the same as the result obtained in previous works.[5],[7],[8] In this sense, our result Eq. (4·7) contains both of the previous expressions. Our analysis here clearly shows that the controversy arising due to the discrepancy between the results of Ahluwalia and Burgard[3] and other authors[5),7),8] is simply due to different assumptions concerning constancy along the neutrino trajectory.

§5. Summary and conclusion

We have studied the general relativistic effects of gravity on spin-1/2 particles with non-vanishing mass. In particular, we have considered particles propagating in the Kerr geometry in the slowly rotating, weak field approximation. By performing a unitary transformation similar to the FWT transformation, we have obtained the two-component Weyl equations with the corrections arising from the non-vanishing mass and the gravitational field from the covariant Dirac equation. The Hamiltonian clearly shows how the spin-orbit coupling, the spin-rotation coupling or the coupling between the total angular momentum and the rotation is coupled to the non-vanishing mass.

Furthermore, we have discussed an application of the two-component equations to neutrino oscillations in the presence of a gravitational field, and we have derived the phase difference of the two different mass eigenstates in radial propagation. It is worth mentioning that our result contains both of the previous expressions. We have shown that the controversy arising from the discrepancy between the results of Ahluwalia and Burgard[3] and other authors[5),7),8] is simply due to different assumptions regarding constancy along the neutrino trajectory. Moreover, as seen in the transformation of the integral variable, the gravitationally induced neutrino oscillation phases arise from the modification of the propagating distance. Indeed, we found that the gravitational correction term comes out in this variable transformation.

We have not applied our approach to a non-radially propagating case in detail in this paper. However, it is of interest whether the spin-orbit coupling affects the neutrino oscillations. This will be the subject of further investigation.

Although it seems difficult to provide verification of these effects with current experimental detectability, we believe that investigation of systems in which both quantum effects and gravitational effects come into play is important. Progress in technology may make the verification of such effects possible.

Acknowledgements

We would like to thank H. Asada and T. Futamase for useful suggestions and discussions and Y. Kojima for valuable comments.

Appendix A

—— *Derivation of Ultra-Relativistic Hamiltonian* ——

A.1. *Components of spin connection*

The spin connection is given by Eq. (2·6):

$$\Gamma_\mu = -\frac{1}{8}\left[\gamma^{(a)}, \gamma^{(b)}\right] g_{\lambda\sigma}\, e_{(a)}^{\ \lambda} \nabla_\mu e_{(b)}^{\ \sigma}. \tag{A·1}$$

It is convenient to introduce the following 4 × 4 matrices similar to the Pauli spin matrices:

$$\rho_1 = \begin{pmatrix} 0 & I \\ I & 0 \end{pmatrix}, \quad \rho_2 = \begin{pmatrix} 0 & -iI \\ iI & 0 \end{pmatrix}, \quad \rho_3 = \begin{pmatrix} I & 0 \\ 0 & -I \end{pmatrix}, \tag{A·2}$$

where I is the 2 × 2 unit matrix. These matrices satisfy the relations

$$\rho_i \rho_j = \delta_{ij} + i\varepsilon_{ijk}\rho_k, \tag{A·3}$$

where ε_{ijk} is the Levi-Civita antisymmetric tensor ($\varepsilon_{123} = +1$). If we adopt the Weyl representation as the constant Dirac matrices, then we have

$$\gamma^{(0)} = \frac{1}{c}\rho_1, \quad \gamma^{(i)} = -i\rho_2\sigma_i, \tag{A·4}$$

where σ are the Pauli spin matrices.

Using the above quantities, the components of spin connection, up to the order of interest, are given by

$$\begin{aligned} i\hbar\Gamma_0 = {} & \frac{1}{2c}\,\rho_3\,\boldsymbol{\sigma}\cdot(\overline{\boldsymbol{p}}\phi) \\ & + \frac{1}{c^2}\left[\frac{4GMR^2}{5r^3}\boldsymbol{\omega}\cdot\boldsymbol{S} + \frac{6GMR^2}{5r^5}\boldsymbol{S}\cdot[\boldsymbol{r}\times(\boldsymbol{r}\times\boldsymbol{\omega})]\right], \end{aligned} \tag{A·5}$$

$$\begin{aligned} i\hbar\Gamma_1 = {} & -\frac{\hbar}{2c^2}\left(\phi_{,2}\,\sigma_3 - \phi_{,3}\,\sigma_2\right) \\ & + \frac{i\hbar}{c^3}\,\rho_3\frac{3GMR^2}{5r^5}\omega\left[-2xy\,\sigma_1 + \left(x^2 - y^2\right)\sigma_2 - yz\,\sigma_3\right], \end{aligned} \tag{A·6}$$

$$\begin{aligned} i\hbar\Gamma_2 = {} & -\frac{\hbar}{2c^2}\left(\phi_{,3}\,\sigma_1 - \phi_{,1}\,\sigma_3\right) \\ & + \frac{i\hbar}{c^3}\,\rho_3\frac{3GMR^2}{5r^5}\omega\left[\left(x^2 - y^2\right)\sigma_1 + 2xy\,\sigma_2 + zx\,\sigma_3\right], \end{aligned} \tag{A·7}$$

$$\begin{aligned} i\hbar\Gamma_3 = {} & -\frac{\hbar}{2c^2}\left(\phi_{,1}\,\sigma_2 - \phi_{,2}\,\sigma_1\right) \\ & + \frac{i\hbar}{c^3}\,\rho_3\frac{3GMR^2}{5r^5}\omega\left[-yz\,\sigma_1 + zx\,\sigma_2\right]. \end{aligned} \tag{A·8}$$

A.2. *Unitary transformation*

The Hamiltonian defined in Eq. (2·21) is given by

$$H = \rho_3 c\boldsymbol{\sigma}\cdot\overline{\boldsymbol{p}} + \rho_3\left[-\frac{1}{2}c\boldsymbol{\sigma}\cdot\left(\overline{\boldsymbol{p}}\frac{\phi}{c^2}\right) + 2\frac{\phi}{c^2}\,c\boldsymbol{\sigma}\cdot\overline{\boldsymbol{p}}\right]$$

$$+\frac{1}{c^2}\left[\frac{4GMR^2}{5r^3}\boldsymbol{\omega}\cdot(\boldsymbol{L}+\boldsymbol{S})+\frac{6GMR^2}{5r^5}\boldsymbol{S}\cdot[\boldsymbol{r}\times(\boldsymbol{r}\times\boldsymbol{\omega})]\right]+\rho_1 mc^2+\rho_1 mc^2\frac{\phi}{c^2}. \tag{A·9}$$

Moreover, the Hamiltonian redefined by Eq. (3·1) is then

$$\begin{aligned}H' &= \rho_3 c\boldsymbol{\sigma}\cdot\overline{\boldsymbol{p}}+\rho_3\left(c\boldsymbol{\sigma}\cdot\overline{\boldsymbol{p}}\,\frac{\phi}{c^2}+\frac{\phi}{c^2}\,c\boldsymbol{\sigma}\cdot\overline{\boldsymbol{p}}\right)\\ &\quad+\frac{1}{c^2}\left[\frac{4GMR^2}{5r^3}\boldsymbol{\omega}\cdot(\boldsymbol{L}+\boldsymbol{S})+\frac{6GMR^2}{5r^5}\boldsymbol{S}\cdot[\boldsymbol{r}\times(\boldsymbol{r}\times\boldsymbol{\omega})]\right]+\rho_1 mc^2+\rho_1 mc^2\frac{\phi}{c^2},\end{aligned} \tag{A·10}$$

where terms proportional to ρ_1 and ρ_2 are "odd", and those proportional to ρ_3 are "even".

Next, by performing a unitary transformation similar to the FWT transformation, let us derive the ultra-relativistic Hamiltonian for the left-handed component. Here we divide the unitary transformation into several steps. First, we use the unitary operator

$$U_1=\exp\left(i\rho_2\frac{1}{2}mc^2\frac{c\boldsymbol{\sigma}\cdot\overline{\boldsymbol{p}}}{c^2\overline{\boldsymbol{p}}^2}\right), \tag{A·11}$$

which is introduced to eliminate the odd term $\rho_1 mc^2$. Using the useful formula

$$e^{iS}He^{-iS}=H+i\,[S,H]+\frac{i^2}{2!}\,[S,[S,H]]+\frac{i^3}{3!}\,[S,[S,[S,H]]]+\cdots \tag{A·12}$$

and the relation (A·3), we obtain the transformed Hamiltonian

$$\begin{aligned}&U_1H'U_1^{\dagger}\\ &=\rho_3 c\boldsymbol{\sigma}\cdot\overline{\boldsymbol{p}}+\rho_3\left(c\boldsymbol{\sigma}\cdot\overline{\boldsymbol{p}}\,\frac{\phi}{c^2}+\frac{\phi}{c^2}\,c\boldsymbol{\sigma}\cdot\overline{\boldsymbol{p}}\right)+\frac{1}{c^2}A+\rho_1 mc^2\frac{\phi}{c^2}\\ &\quad-\rho_1\frac{1}{2}mc^2\left[c\boldsymbol{\sigma}\cdot\overline{\boldsymbol{p}}\left(\frac{c\boldsymbol{\sigma}\cdot\overline{\boldsymbol{p}}}{c^2\overline{\boldsymbol{p}}^2}\,\frac{\phi}{c^2}+\frac{\phi}{c^2}\,\frac{c\boldsymbol{\sigma}\cdot\overline{\boldsymbol{p}}}{c^2\overline{\boldsymbol{p}}^2}\right)+\left(\frac{c\boldsymbol{\sigma}\cdot\overline{\boldsymbol{p}}}{c^2\overline{\boldsymbol{p}}^2}\,\frac{\phi}{c^2}+\frac{\phi}{c^2}\,\frac{c\boldsymbol{\sigma}\cdot\overline{\boldsymbol{p}}}{c^2\overline{\boldsymbol{p}}^2}\right)c\boldsymbol{\sigma}\cdot\overline{\boldsymbol{p}}\right]\\ &\quad+i\rho_2\frac{1}{2}mc^2\left(\frac{c\boldsymbol{\sigma}\cdot\overline{\boldsymbol{p}}}{c^2\overline{\boldsymbol{p}}^2}\frac{A}{c^2}-\frac{A}{c^2}\frac{c\boldsymbol{\sigma}\cdot\overline{\boldsymbol{p}}}{c^2\overline{\boldsymbol{p}}^2}\right)+\rho_3\frac{1}{2}m^2c^4\frac{c\boldsymbol{\sigma}\cdot\overline{\boldsymbol{p}}}{c^2\overline{\boldsymbol{p}}^2}\\ &\quad-\rho_3\frac{1}{8}m^2c^4\left[\frac{1}{c^2\overline{\boldsymbol{p}}^2}\frac{\phi}{c^2}c\boldsymbol{\sigma}\cdot\overline{\boldsymbol{p}}+c\boldsymbol{\sigma}\cdot\overline{\boldsymbol{p}}\frac{\phi}{c^2}\frac{1}{c^2\overline{\boldsymbol{p}}^2}-\left(\frac{c\boldsymbol{\sigma}\cdot\overline{\boldsymbol{p}}}{c^2\overline{\boldsymbol{p}}^2}\frac{\phi}{c^2}+\frac{\phi}{c^2}\frac{c\boldsymbol{\sigma}\cdot\overline{\boldsymbol{p}}}{c^2\overline{\boldsymbol{p}}^2}\right)\right]\\ &\quad-\frac{1}{8}m^2c^4\left(\frac{A}{c^2}\frac{1}{c^2\overline{\boldsymbol{p}}^2}-2\frac{c\boldsymbol{\sigma}\cdot\overline{\boldsymbol{p}}}{c^2\overline{\boldsymbol{p}}^2}\frac{A}{c^2}\frac{c\boldsymbol{\sigma}\cdot\overline{\boldsymbol{p}}}{c^2\overline{\boldsymbol{p}}^2}+\frac{1}{c^2\overline{\boldsymbol{p}}^2}\frac{A}{c^2}\right),\end{aligned} \tag{A·13}$$

where A is given by Eq. (3·8):

$$A=\frac{4GMR^2}{5r^3}\boldsymbol{\omega}\cdot(\boldsymbol{L}+\boldsymbol{S})+\frac{6GMR^2}{5r^5}\boldsymbol{S}\cdot[\boldsymbol{r}\times(\boldsymbol{r}\times\boldsymbol{\omega})]. \tag{A·14}$$

Second, in order to eliminate the second line in Eq. (A·13), we use the unitary operator

$$U_2=\exp\left[-i\rho_2\frac{1}{2}mc^2\left(\frac{c\boldsymbol{\sigma}\cdot\overline{\boldsymbol{p}}}{c^2\overline{\boldsymbol{p}}^2}\frac{\phi}{c^2}+\frac{\phi}{c^2}\frac{c\boldsymbol{\sigma}\cdot\overline{\boldsymbol{p}}}{c^2\overline{\boldsymbol{p}}^2}\right)\right]. \tag{A·15}$$

Using this unitary operator, we obtain

$$\begin{aligned}
&U_2U_1H'U_1^\dagger U_2^\dagger \\
&= \rho_3 c\boldsymbol{\sigma}\cdot\bar{\boldsymbol{p}} + \rho_3\left(c\boldsymbol{\sigma}\cdot\bar{\boldsymbol{p}}\,\frac{\phi}{c^2} + \frac{\phi}{c^2}\,c\boldsymbol{\sigma}\cdot\bar{\boldsymbol{p}}\right) + \frac{1}{c^2}A + \rho_1 mc^2\frac{\phi}{c^2} \\
&\quad + i\rho_2\frac{1}{2}mc^2\left(\frac{c\boldsymbol{\sigma}\cdot\bar{\boldsymbol{p}}}{c^2\bar{\boldsymbol{p}}^2}\frac{A}{c^2} - \frac{A}{c^2}\frac{c\boldsymbol{\sigma}\cdot\bar{\boldsymbol{p}}}{c^2\bar{\boldsymbol{p}}^2}\right) + \rho_3\frac{1}{2}m^2c^4\frac{c\boldsymbol{\sigma}\cdot\bar{\boldsymbol{p}}}{c^2\bar{\boldsymbol{p}}^2} \\
&\quad - \rho_3\frac{1}{8}m^2c^4\left[\frac{1}{c^2\bar{\boldsymbol{p}}^2}\frac{\phi}{c^2}c\boldsymbol{\sigma}\cdot\bar{\boldsymbol{p}} + c\boldsymbol{\sigma}\cdot\bar{\boldsymbol{p}}\frac{\phi}{c^2}\frac{1}{c^2\bar{\boldsymbol{p}}^2} - \left(\frac{c\boldsymbol{\sigma}\cdot\bar{\boldsymbol{p}}}{c^2\bar{\boldsymbol{p}}^2}\frac{\phi}{c^2} + \frac{\phi}{c^2}\frac{c\boldsymbol{\sigma}\cdot\bar{\boldsymbol{p}}}{c^2\bar{\boldsymbol{p}}^2}\right)\right] \\
&\quad - \frac{1}{8}m^2c^4\left(\frac{A}{c^2}\frac{1}{c^2\bar{\boldsymbol{p}}^2} - 2\frac{c\boldsymbol{\sigma}\cdot\bar{\boldsymbol{p}}}{c^2\bar{\boldsymbol{p}}^2}\frac{A}{c^2}\frac{c\boldsymbol{\sigma}\cdot\bar{\boldsymbol{p}}}{c^2\bar{\boldsymbol{p}}^2} + \frac{1}{c^2\bar{\boldsymbol{p}}^2}\frac{A}{c^2}\right). \qquad (\mathrm{A{\cdot}16})
\end{aligned}$$

Finally, we use the two unitary operators $U_3 = e^{iS_3}$ and $U_4 = e^{iS_4}$, where S_3 and S_4 satisfy the relations

$$i\left[S_3, \rho_3 c\boldsymbol{\sigma}\cdot\bar{\boldsymbol{p}}\right] = -\,\rho_1 mc^2\frac{\phi}{c^2}, \qquad (\mathrm{A{\cdot}17})$$

$$i\left[S_4, \rho_3 c\boldsymbol{\sigma}\cdot\bar{\boldsymbol{p}}\right] = -\,i\rho_2\frac{1}{2}mc^2\left(\frac{c\boldsymbol{\sigma}\cdot\bar{\boldsymbol{p}}}{c^2\bar{\boldsymbol{p}}^2}\frac{A}{c^2} - \frac{A}{c^2}\frac{c\boldsymbol{\sigma}\cdot\bar{\boldsymbol{p}}}{c^2\bar{\boldsymbol{p}}^2}\right). \qquad (\mathrm{A{\cdot}18})$$

We here assume the existence of these unitary operators, which make the remaining odd terms vanish. (We need not find the concrete forms of these unitary operators, because extra terms arising from these unitary transformations are higher order terms.) Using these unitary operators, we obtain the transformed Hamiltonian $UH'U^\dagger$ which is even up to the order of our interest,

$$\begin{aligned}
UH'U^\dagger &= \rho_3 c\boldsymbol{\sigma}\cdot\bar{\boldsymbol{p}} + \rho_3\left(c\boldsymbol{\sigma}\cdot\bar{\boldsymbol{p}}\,\frac{\phi}{c^2} + \frac{\phi}{c^2}\,c\boldsymbol{\sigma}\cdot\bar{\boldsymbol{p}}\right) + \frac{1}{c^2}A \\
&\quad + \rho_3\frac{1}{2}m^2c^4\frac{c\boldsymbol{\sigma}\cdot\bar{\boldsymbol{p}}}{c^2\bar{\boldsymbol{p}}^2} \\
&\quad - \rho_3\frac{1}{8}m^2c^4\left[\frac{1}{c^2\bar{\boldsymbol{p}}^2}\frac{\phi}{c^2}c\boldsymbol{\sigma}\cdot\bar{\boldsymbol{p}} + c\boldsymbol{\sigma}\cdot\bar{\boldsymbol{p}}\frac{\phi}{c^2}\frac{1}{c^2\bar{\boldsymbol{p}}^2} - \left(\frac{c\boldsymbol{\sigma}\cdot\bar{\boldsymbol{p}}}{c^2\bar{\boldsymbol{p}}^2}\frac{\phi}{c^2} + \frac{\phi}{c^2}\frac{c\boldsymbol{\sigma}\cdot\bar{\boldsymbol{p}}}{c^2\bar{\boldsymbol{p}}^2}\right)\right] \\
&\quad - \frac{1}{8}m^2c^4\left(\frac{A}{c^2}\frac{1}{c^2\bar{\boldsymbol{p}}^2} - 2\frac{c\boldsymbol{\sigma}\cdot\bar{\boldsymbol{p}}}{c^2\bar{\boldsymbol{p}}^2}\frac{A}{c^2}\frac{c\boldsymbol{\sigma}\cdot\bar{\boldsymbol{p}}}{c^2\bar{\boldsymbol{p}}^2} + \frac{1}{c^2\bar{\boldsymbol{p}}^2}\frac{A}{c^2}\right), \qquad (\mathrm{A{\cdot}19})
\end{aligned}$$

where U is given by $U = U_4U_3U_2U_1$. From this, we can derive Eq. (3·7) by a simple calculation.

References

1) R. Colella, A. W. Overhauser and S. A. Werner, Phys. Rev. Lett. **34** (1975), 1472.
2) A. W. Overhauser and R. Colella, Phys. Rev. Lett. **33** (1974), 1237.
3) D. V. Ahluwalia and C. Burgard, Gen. Relat. Gravit. **28** (1996), 1161; preprint: gr-qc/9606031.
4) T. Bhattacharya, S. Habib and E. Mottola, preprint: gr-qc/9605074.
5) Y. Kojima, Mod. Phys. Lett. **A11** (1996), 2965.
6) Y. Grossman and H. J. Lipkin, Phys. Rev. **D55** (1997), 2760.
7) C. Y. Cardall and G. M. Fuller, Phys. Rev. **D55** (1997), 7960.
8) N. Fornengo, C. Giunti, C. W. Kim and J. Song, Phys. Rev. **D56** (1997), 1895.

9) L. Stodolsky, Gen. Relat. Gravit. **11** (1979), 391.
10) See, e.g., Y. Totsuka (SuperKamiokande Collaboration), in the *Proceedings of the 28th International Symposium on Lepton Photon Interactions, Hamburg, Germany, 1997.*
11) D. R. Brill and J. A. Wheeler, Rev. Mod. Phys. **29** (1957), 465.
12) S. Weinberg, *Gravitation and Cosmology* (John Wiley & Sons, USA, 1972).
13) N. D. Birrel and P. C. W. Davies, *Quantum Fields in Curved Space* (Cambridge University Press, Cambridge, 1984).
14) S. Wajima, M. Kasai and T. Futamase, Phys. Rev. **D55** (1997), 1964.
15) L. L. Foldy and S. A. Wouthuysen, Phys. Rev. **78** (1950), 29.
16) S. Tani, Prog. Theor. Phys. **6** (1951), 267.
17) B. Kayser, Phys. Rev. **D24** (1981), 110.
18) S. M. Bilenky and S. T. Petcov, Rev. Mod. Phys. **59** (1987), 671.
19) J. N. Bahcall, *Neutrino Astrophysics* (Cambridge University Press, USA, 1989).

参考論文(2)

Progress of Theoretical Physics, Vol. 101, No. 4, April 1999

Asymmetry in Microlensing-Induced Light Curves

Kohkichi Konno and Yasufumi Kojima

Department of Physics, Hiroshima University, Higashi-Hiroshima 739-8526, Japan

(Received December 8, 1998)

We discuss distortion in microlensing-induced light curves which are considered to be curves due to single-point-mass lenses at a first glance. As factors of the distortion, we consider close binary and planetary systems, which are the limiting cases of two-point-mass lenses, and the gravitational potential is regarded as the sum of the single point mass and the corrections. In order to quantitatively estimate the asymmetric features of such distorted light curves, we propose a cutoff dependent skewness, and show how to discriminate the similar light curves with it. We also examine as the distortion the general relativistic effect of frame dragging, but the effect coincides with the close binary case in the light curves.

§1. Introduction

Gravitational microlensing (1) is one important probe for studying the nature and distribution of mass in the galaxy. Chang and Refsdal (2) and Gott (3) suggested that even though multiple images by lensing are unresolved, the time variation of the magnitude of the source can still be detected if the lens moves relative to the source. Such light curves caused by the microlensing can be distinguished from curves of intrinsically variable sources, because the change of magnitude by lensing is achromatic, whereas the colors of intrinsically variable stars change in general. Furthermore, microlensing-induced light curves can be distinguished from magnification by bursts, which are likely to appear in sheer shapes. As is well known, microlensing by a point mass has the time-symmetric light curves, provided that the lens and the source have constant relative transverse velocity. Hence, most events are expected to have almost time-symmetric light curves. If the relative velocity is not constant, then of course time-asymmetric light curves will be detected. Gould (4) predicted a parallax effect due to the orbital motion of the Earth, and its effect was indeed detected by Alcock et al. (5) When the time scale of a microlensing event is larger than ~ 100 days, this effect is important. However, if the time scale is of hours to weeks, the parallax effect can be neglected. Then, other factors, such as the non-spherical gravitational potential of the lens, could also produce distortion from the time-symmetric light curves. The effect may be regarded as a higher-order correction to the point-mass lens. The aim of this paper is to evaluate the effect of the intrinsic nature of the lenses, which may slightly distort the light curves. We exclude significantly peculiar light curves, such as double peaks, from which direct information is available without any detailed analyses. We rather restrict our consideration to light curves which are regarded as curves of single-point-mass lenses at a first glance, that is, almost time-symmetric light curves. Since the asymmetric part contains additional information about massive astrophysical compact halo objects (MACHOs), this subject is very important to understanding the nature of MACHOs.

One of the important factors to induce time-asymmetric forms is the binary system of the lensing objects, in which the contribution from both objects to the Newtonian gravitational potential is no longer spherical. The discussion is simplified by considering two-point-mass lenses. In particular, since we consider almost time-symmetric light curves, we hit on two situations: close binary and planetary systems. In a close binary system, the separation distance between the two-point masses is much less than the Einstein radius of the total mass, so that the approximated light curve can be described by the total mass and some corrections to it. The detectability of a close binary system has been discussed in detail by Gaudi and Gould[11)] considering the excess magnification threshold. According to them, the detectability of close binaries with separation less than ~ 0.2 of the Einstein radius is $\sim 10\%$. Therefore, most close binary lenses with such small separation are missed. We consider the possibility of picking up the discarded asymmetry, by which even below the separation of ~ 0.2 of the Einstein radius the binary nature of the lenses may be detected. In a planetary system, the light curve is expected to be described by the contribution from the larger mass and some corrections from the smaller one. Several authors[7)-11)] have discussed planetary systems with remarkable deviations from a single lens. However, we are now interested in planetary events which would be missed due to the special configurations of the lensing geometry. Our new proposal may make the detection of such events possible, in addition to the close binary case. Another factor for the time-asymmetric forms is the asymmetry of the lens object itself. The multipole moment of the lens deviates from gravitational potential of the point mass. The gravitational potential due to the quadrupole never vanishes for the two-point-mass case. Therefore, such a correction term in the gravitational potential can be regarded as the limiting case of the binary. Instead, we shall consider general relativistic effects of dragging of inertial frames due to a rotating object as another factor, which cannot be expressed as corrections to the Newton-like potential. While the Newton-like potential corresponds to the gravitoelectric field, this effect results from the gravitomagnetic field. In this case, corrections up to post-Newtonian order are sufficient. Other post-Newtonian potentials also affect the light curves, but they are neglected here.

This paper is organized as follows. In §2 we discuss the two situations involving two-point-mass lenses and obtain microlensing-induced light curves slightly deviating from the time-symmetric curves. In §3 we discuss the post-Newtonian corrections due to the rotation and obtain time-asymmetric light curves as well. We propose a certain tool to estimate the time-asymmetric features quantitatively in §4. Finally, we give summary and discussion in §5.

§2. Two-point-mass lenses

We investigate two extreme situations involving two-point-mass lenses in order. (The general computational details including critical lines and caustics can be found in Ref. 12).) First, we consider the situation in which the distance l between the two-point masses is much less than the Einstein radius r_E corresponding to the total mass. Next, we consider the situation in which one mass, M_1, is much smaller than the other mass, M_2.

2.1. *Close binary system*

We consider the lens plane on to which the positions of the two-point masses M_1 and M_2 are projected (see Fig. 1). We introduce an angular coordinate system (θ_x, θ_y), in which the two-point masses lie on the θ_x-axis and the origin is chosen as their geometrical center. We also define an angular coordinate system (β_x, β_y) in the source plane, corresponding to the lens plane. We express the distance between the observer and the lens plane, the lens plane and the source plane, and the observer and the source plane by D_L, D_{LS} and D_S, respectively.

If we denote the angular separation between the source and the image by $\boldsymbol{\alpha}$, we have

$$\alpha_x = \frac{4GM_1}{c^2}\frac{D_{LS}}{D_L D_S}\frac{\theta_x - \eta}{(\theta_x - \eta)^2 + \theta_y^2} + \frac{4GM_2}{c^2}\frac{D_{LS}}{D_L D_S}\frac{\theta_x + \eta}{(\theta_x + \eta)^2 + \theta_y^2}, \quad (2\cdot1\text{a})$$

$$\alpha_y = \frac{4GM_1}{c^2}\frac{D_{LS}}{D_L D_S}\frac{\theta_y}{(\theta_x - \eta)^2 + \theta_y^2} + \frac{4GM_2}{c^2}\frac{D_{LS}}{D_L D_S}\frac{\theta_y}{(\theta_x + \eta)^2 + \theta_y^2}, \quad (2\cdot1\text{b})$$

where η is the angular separation of the mass M_1 (or M_2) from the optical axis. Therefore, the lens equation can be written in the form

$$\boldsymbol{\beta} = \boldsymbol{\theta} - \boldsymbol{\alpha}. \quad (2\cdot2)$$

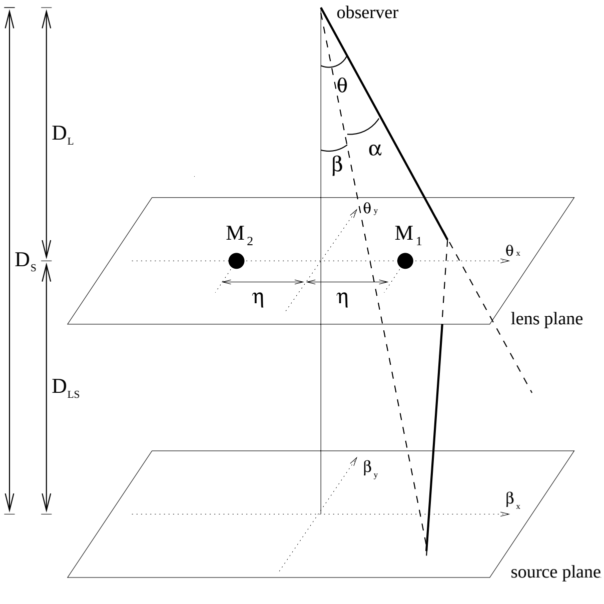

Fig. 1. Geometry of the gravitational lensing considered in §2.1.

We normalize this equation by the Einstein radius for the total mass,

$$\theta_E = \left(\frac{4G\,(M_1+M_2)}{c^2}\,\frac{D_{LS}}{D_L D_S}\right)^{\frac{1}{2}}, \tag{2·3}$$

and introduce normalized quantities

$$\tilde{\boldsymbol{\beta}} \equiv \frac{\boldsymbol{\beta}}{\theta_E}, \qquad \tilde{\boldsymbol{\theta}} \equiv \frac{\boldsymbol{\theta}}{\theta_E}, \qquad \tilde{\eta} \equiv \frac{\eta}{\theta_E}. \tag{2·4}$$

The lens equation is then given by

$$\tilde{\beta}_x = \tilde{\theta}_x - \mu_1 \frac{\tilde{\theta}_x - \tilde{\eta}}{\left(\tilde{\theta}_x - \tilde{\eta}\right)^2 + \tilde{\theta}_y^2} - \mu_2 \frac{\tilde{\theta}_x + \tilde{\eta}}{\left(\tilde{\theta}_x + \tilde{\eta}\right)^2 + \tilde{\theta}_y^2}, \tag{2·5a}$$

$$\tilde{\beta}_y = \tilde{\theta}_y - \mu_1 \frac{\tilde{\theta}_y}{\left(\tilde{\theta}_x - \tilde{\eta}\right)^2 + \tilde{\theta}_y^2} - \mu_2 \frac{\tilde{\theta}_y}{\left(\tilde{\theta}_x + \tilde{\eta}\right)^2 + \tilde{\theta}_y^2}, \tag{2·5b}$$

where μ_1 and μ_2 are defined as

$$\mu_1 = \frac{M_1}{M_1+M_2}, \qquad \mu_2 = \frac{M_2}{M_1+M_2}. \tag{2·6}$$

The separation distance in the projected plane is $l = D_L \cdot 2\eta$, and the Einstein radius for this system $r_E = D_L \cdot \theta_E$. The term 'close binary' in the gravitational lens means $l \ll r_E$. This condition in the astronomical situation is expressed as $l \ll 10^{14}(M/M_\odot)^{1/2}\,(D/(10\,\mathrm{kpc}))^{1/2}$ cm, where we have chosen typical astronomical distances as the scale of the galactic halo, $D_{LS} \sim D_L \sim D_S \sim D$. Therefore, the range of applicability is not so severely limited. The condition of the close binary, $l \ll r_E$, is mathematically expressed as

$$\tilde{\eta} \ll 1. \tag{2·7}$$

Under this condition, we expand the right-hand side of the lens equation with respect to $\tilde{\eta}$. Up to first order in $\tilde{\eta}$, we have

$$\tilde{\beta}_x = \tilde{\theta}_x - \frac{\tilde{\theta}_x}{\tilde{\theta}_x^2 + \tilde{\theta}_y^2} - \tilde{\eta}\,(\mu_1 - \mu_2)\,\frac{\tilde{\theta}_x^2 - \tilde{\theta}_y^2}{\left(\tilde{\theta}_x^2 + \tilde{\theta}_y^2\right)^2}, \tag{2·8a}$$

$$\tilde{\beta}_y = \tilde{\theta}_y - \frac{\tilde{\theta}_y}{\tilde{\theta}_x^2 + \tilde{\theta}_y^2} - \tilde{\eta}\,(\mu_1 - \mu_2)\,\frac{2\tilde{\theta}_x\tilde{\theta}_y}{\left(\tilde{\theta}_x^2 + \tilde{\theta}_y^2\right)^2}, \tag{2·8b}$$

where the last term on each right-hand side represents the deviation from a single-point-mass lens. The first-order corrections vanish for the equal mass case, since $\mu_1 = \mu_2$. It is therefore convenient to express the combination $\tilde{\eta}\,(\mu_1 - \mu_2)$ as one small parameter $\varepsilon \equiv \tilde{\eta}\,(\mu_1 - \mu_2)$.

The inversion of Eq. (2·8), i.e., solving $\tilde{\theta}$ by $\tilde{\beta}$, is possible, but the general form is quite messy. However, under the condition $\varepsilon \ll 1$, the approximate solution, i.e., the first-order solution in ε, is given by the form

$$\tilde{\boldsymbol{\theta}} = \tilde{\boldsymbol{\theta}}_0 + \varepsilon\,\tilde{\boldsymbol{\theta}}_1, \tag{2·9}$$

where $\tilde{\boldsymbol{\theta}}_0$ and $\tilde{\boldsymbol{\theta}}_1$ denote the zeroth-order and the first-order solutions, respectively. Substituting Eq. (2·9) into Eq. (2·8), we can find such solutions. The zeroth-order solution is given by

$$\tilde{\theta}_{0x} = \frac{1}{2}\left(\tilde{\beta}_x \pm \tilde{\beta}_x \sqrt{1 + \frac{4}{\tilde{\beta}_x^2 + \tilde{\beta}_y^2}}\right), \tag{2·10a}$$

$$\tilde{\theta}_{0y} = \frac{1}{2}\left(\tilde{\beta}_y \pm \tilde{\beta}_y \sqrt{1 + \frac{4}{\tilde{\beta}_x^2 + \tilde{\beta}_y^2}}\right). \tag{2·10b}$$

Using this zeroth-order solution, the first-order solution is written in the form

$$\tilde{\theta}_{1x} = \frac{\tilde{\theta}_{0x}^2 - \tilde{\theta}_{0y}^2 - 1}{\left(\tilde{\theta}_{0x}^2 + \tilde{\theta}_{0y}^2\right)^2 - 1}, \tag{2·11a}$$

$$\tilde{\theta}_{1y} = \frac{2\tilde{\theta}_{0x}\tilde{\theta}_{0y}}{\left(\tilde{\theta}_{0x}^2 + \tilde{\theta}_{0y}^2\right)^2 - 1}. \tag{2·11b}$$

Next, we turn our attention to the derivation of magnification. The magnification M is given by

$$\begin{aligned} M &= M_+ + M_- \\ &= \left|\det\left(\frac{\partial\tilde{\beta}_i}{\partial\tilde{\theta}_j}\right)_+\right|^{-1} + \left|\det\left(\frac{\partial\tilde{\beta}_i}{\partial\tilde{\theta}_j}\right)_-\right|^{-1}, \end{aligned} \tag{2·12}$$

where the subscript (+) and (−) correspond to solutions with a plus sign and with a minus sign, respectively, in Eq. (2·10). The inverse of the Jacobian det $\left(\frac{\partial\tilde{\beta}_i}{\partial\tilde{\theta}_j}\right)$ is calculated, up to first order in ε, in the following way:

$$\begin{aligned} \left[\det\left(\frac{\partial\tilde{\beta}_i}{\partial\tilde{\theta}_j}\right)\right]^{-1} &= \left[1 - \frac{1}{\left(\tilde{\theta}_{0x}^2 + \tilde{\theta}_{0y}^2\right)^2} - \varepsilon\frac{4\tilde{\theta}_{0x}}{\left(\tilde{\theta}_{0x}^2 + \tilde{\theta}_{0y}^2\right)^3} + \varepsilon\frac{4\left(\tilde{\theta}_{0x}\tilde{\theta}_{1x} + \tilde{\theta}_{0y}\tilde{\theta}_{1y}\right)}{\left(\tilde{\theta}_{0x}^2 + \tilde{\theta}_{0y}^2\right)^3}\right]^{-1} \\ &= \left(1 - \frac{1}{\left(\tilde{\theta}_{0x}^2 + \tilde{\theta}_{0y}^2\right)^2}\right)^{-1}\left[1 + \varepsilon\frac{4\tilde{\theta}_{0x}}{\left(\tilde{\theta}_{0x}^2 + \tilde{\theta}_{0y}^2 + 1\right)^2\left(\tilde{\theta}_{0x}^2 + \tilde{\theta}_{0y}^2 - 1\right)}\right]. \end{aligned} \tag{2·13}$$

Therefore, using Eqs. (2·10), (2·12) and (2·13), we can derive the magnification as a function of the source position:

$$M = M\left(\beta_x, \beta_y; \varepsilon\right). \tag{2·14}$$

The time variation is produced by the relative change of the positions. The time variation of the magnitude Δm is then given by

$$\Delta m = \Delta m(t) = 2.5\log_{10} M\left(\beta_x(t), \beta_y(t); \varepsilon\right), \tag{2·15}$$

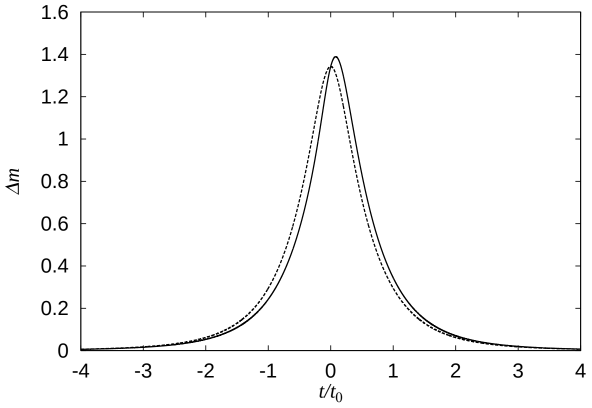

Fig. 2. Microlensing-induced light curves with (solid) and without (dashed) correction for the deviation from a single-point-mass lens. The light curve with the correction is plotted for the small parameter value $\varepsilon = 0.1$. The relative motion of the source to the lens is assumed to be described by $\varphi = 0$ and $p = 0.3$.

where the relative source trajectory is in general described by

$$\tilde{\beta}_x(t) = \frac{t}{t_0}\cos\varphi + p\sin\varphi, \tag{2·16a}$$

$$\tilde{\beta}_y(t) = \frac{t}{t_0}\sin\varphi - p\cos\varphi, \tag{2·16b}$$

where t_0 is the time taken to cross the Einstein radius, φ is the angle of the trajectory from the β_x-axis, and p is the impact parameter normalized by the Einstein radius. From this, we can derive the microlensing-induced light curves, slightly deviating from the time-symmetric curves. An example of the light curves is shown in Fig. 2 for $\varphi = 0$ and $p = 0.3$. The solid line denotes the light curve with the correction for the deviation from a single-point-mass lens, while the dashed line corresponds to the single-point-mass lens. The more general dependence on the angle φ and the impact parameter p is discussed in detail in §4.

2.2. *Planetary system*

In this subsection, we discuss the case that the mass M_1 is much smaller than M_2; that is, the object with smaller mass is regarded as the planet. In this situation, it is convenient to chose the origin of the (θ_x, θ_y) system to be at the position of mass M_2. Furthermore, let the angular separation between the mass M_1 and M_2 be η (see Fig. 3). Then the normalized lens equation is given by

$$\tilde{\beta}_x = \tilde{\theta}_x - \frac{\tilde{\theta}_x}{\tilde{\theta}_x^2 + \tilde{\theta}_y^2} - \mu\frac{\tilde{\theta}_x - \tilde{\eta}}{\left(\tilde{\theta}_x - \tilde{\eta}\right)^2 + \tilde{\theta}_y^2}, \tag{2·17a}$$

$$\tilde{\beta}_y = \tilde{\theta}_y - \frac{\tilde{\theta}_y}{\tilde{\theta}_x^2 + \tilde{\theta}_y^2} - \mu\frac{\tilde{\theta}_y}{\left(\tilde{\theta}_x^2 - \tilde{\eta}\right)^2 + \tilde{\theta}_y^2}, \tag{2·17b}$$

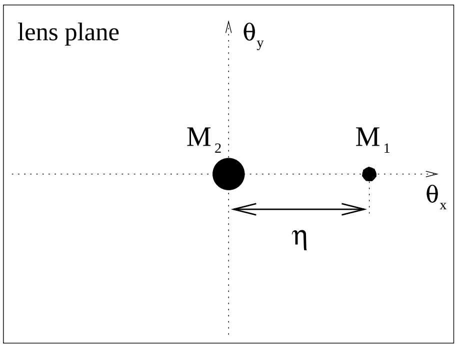

Fig. 3. The lens plane considered in §2.2. The angular separation of the two-point masses is denoted by η.

where $\mu = M_1/M_2\,(\ll 1)$, and we have used for the normalization the Einstein radius of the mass M_2,

$$\theta_E = \left(\frac{4GM_2}{c^2}\,\frac{D_{LS}}{D_L D_S}\right)^{\frac{1}{2}}. \tag{2·18}$$

As in the previous subsection, in the situation $\mu \ll 1$, we approximate the solutions of the lens equation up to first order in μ. Using the zeroth-order solution (2·10), we obtain the first-order solution

$$\tilde{\theta}_{1x} = \frac{\left[\left(\tilde{\theta}_{0x}^2 + \tilde{\theta}_{0y}^2\right)^2 - \left(\tilde{\theta}_{0x}^2 - \tilde{\theta}_{0y}^2\right)\right]\left(\tilde{\theta}_{0x} - \tilde{\eta}\right) - 2\tilde{\theta}_{0x}\tilde{\theta}_{0y}^2}{\left[\left(\tilde{\theta}_{0x}^2 + \tilde{\theta}_{0y}^2\right)^2 - 1\right]\left[\left(\tilde{\theta}_{0x} - \tilde{\eta}\right)^2 + \tilde{\theta}_{0y}^2\right]}, \tag{2·19a}$$

$$\tilde{\theta}_{1y} = \frac{\tilde{\theta}_{0y}\left[\left(\tilde{\theta}_{0x}^2 + \tilde{\theta}_{0y}^2\right)^2 + \left(\tilde{\theta}_{0x}^2 - \tilde{\theta}_{0y}^2\right) - 2\tilde{\theta}_{0x}\left(\tilde{\theta}_{0x} - \tilde{\eta}\right)\right]}{\left[\left(\tilde{\theta}_{0x}^2 + \tilde{\theta}_{0y}^2\right)^2 - 1\right]\left[\left(\tilde{\theta}_{0x} - \tilde{\eta}\right)^2 + \tilde{\theta}_{0y}^2\right]}. \tag{2·19b}$$

Furthermore, we can calculate the magnification by using Eq. (2·12) and the inverse of the Jacobian det $\left(\frac{\partial\tilde{\beta}_i}{\partial\tilde{\theta}_j}\right)$, which is up to first order in μ, given by

$$\begin{aligned}\left[\det\left(\frac{\partial\tilde{\beta}_i}{\partial\tilde{\theta}_j}\right)\right]^{-1} &= \Bigg[1 - \frac{1}{\left(\tilde{\theta}_{0x}^2 + \tilde{\theta}_{0y}^2\right)^2} + \mu\frac{4\left(\tilde{\theta}_{0x}\tilde{\theta}_{1x} + \tilde{\theta}_{0y}\tilde{\theta}_{1y}\right)}{\left(\tilde{\theta}_{0x}^2 + \tilde{\theta}_{0y}^2\right)^3} \\ &\qquad - \mu\frac{2\left(\tilde{\theta}_{0x}^2 - \tilde{\theta}_{0y}^2\right)\left[\left(\tilde{\theta}_{0x} - \tilde{\eta}\right)^2 - \tilde{\theta}_{0y}^2\right] + 8\tilde{\theta}_{0x}\left(\tilde{\theta}_{0x} - \tilde{\eta}\right)\tilde{\theta}_{0y}^2}{\left(\tilde{\theta}_{0x}^2 + \tilde{\theta}_{0y}^2\right)^2\left[\left(\tilde{\theta}_{0x} - \tilde{\eta}\right)^2 + \tilde{\theta}_{0y}^2\right]^2}\Bigg]^{-1} \\ &= \left(1 - \frac{1}{\left(\tilde{\theta}_{0x}^2 + \tilde{\theta}_{0y}^2\right)^2}\right)^{-1}\end{aligned}$$

$$\times \left[1 - \mu \frac{4\left(\tilde{\theta}_{0x}\tilde{\theta}_{1x} + \tilde{\theta}_{0y}\tilde{\theta}_{1y}\right)}{\left(\tilde{\theta}_{0x}^2 + \tilde{\theta}_{0y}^2\right)\left[\left(\tilde{\theta}_{0x}^2 + \tilde{\theta}_{0y}^2\right)^2 - 1\right]} \right.$$
$$\left. + \mu \frac{2\left(\tilde{\theta}_{0x}^2 - \tilde{\theta}_{0y}^2\right)\left[\left(\tilde{\theta}_{0x} - \tilde{\eta}\right)^2 - \tilde{\theta}_{0y}^2\right] + 8\tilde{\theta}_{0x}\left(\tilde{\theta}_{0x} - \tilde{\eta}\right)\tilde{\theta}_{0y}^2}{\left[\left(\tilde{\theta}_{0x}^2 + \tilde{\theta}_{0y}^2\right)^2 - 1\right]\left[\left(\tilde{\theta}_{0x} - \tilde{\eta}\right)^2 + \tilde{\theta}_{0y}^2\right]^2} \right] . \tag{2·20}$$

Therefore, we can also obtain the microlensing-induced light curves

$$\Delta m = \Delta m(t) = 2.5 \log_{10} M\left(\beta_x(t), \beta_y(t); \mu\right) , \tag{2·21}$$

where the relative source trajectory is described by Eq. (2·16) using the angle φ and the impact parameter p. Some examples of the light curves with different values of $\tilde{\eta}$ are shown in Fig. 4 for $\mu = 0.05$, $\varphi = 0$ and $p = 0.3$. As seen in these figures, some light curves tend to have double peaks with certain geometrical configurations. The second peak corresponds to the effect of a planet of mass $0.05 M_2$. The ratio of the height at the peaks is almost determined by the mass ratio μ. Although we have restricted ourselves to the case $\mu \ll 1$ in order to exclude peculiar light curves, light curves with double peaks are still obtained with certain configurations. This is because the correction term $\left[(\theta_{0x} - \tilde{\eta}) + \theta_{0y}^2\right]^{-1}$ becomes effective when θ_{0x} is equal to $\tilde{\eta}$. (More detailed discussions of planetary-binary lensing with dramatic features are given in Refs. 7)–11).)

Furthermore, it is interesting to investigate the configurations in which the Lorentzian curves, i.e., almost time-symmetric light curves arise. For this purpose, we consider the integral of the square of the magnitude difference from the corresponding single-point-mass lens: $\delta \equiv \int_{-\infty}^{+\infty} (\Delta m - \Delta m_0)^2 dt$. The quantity δ indicates the criterion of the deviation from the light curve due to the single-point-mass lens. Figure 5 displays the contours of δ in the $\tilde{\eta}$-φ space for different impact parameters. Of course, as the quantity δ becomes smaller, the light curve moves closer to that due to the single-pint-mass lens. In fact, we can find almost time-symmetric light curves in the domains where δ is smaller than ~ 0.005, as seen in Fig. 4(b). Such domains tend to become larger as the impact parameter p increases. The same tendency can also be derived by making the mass ratio μ small.

§3. Rotating objects

Several relativistic effects also causes corrections to the point-mass lens. We only consider the dragging effect of inertial frames arising from a rotating object, since other spherical post-Newtonian terms never induce asymmetry in light curves. This additional effect is described with the spin angular momentum $\boldsymbol{J}$. We consider the projection of the angular momentum of the rotating object on to the lens plane and define the (θ_x, θ_y) coordinate system so that the θ_y-axis is oriented parallel to

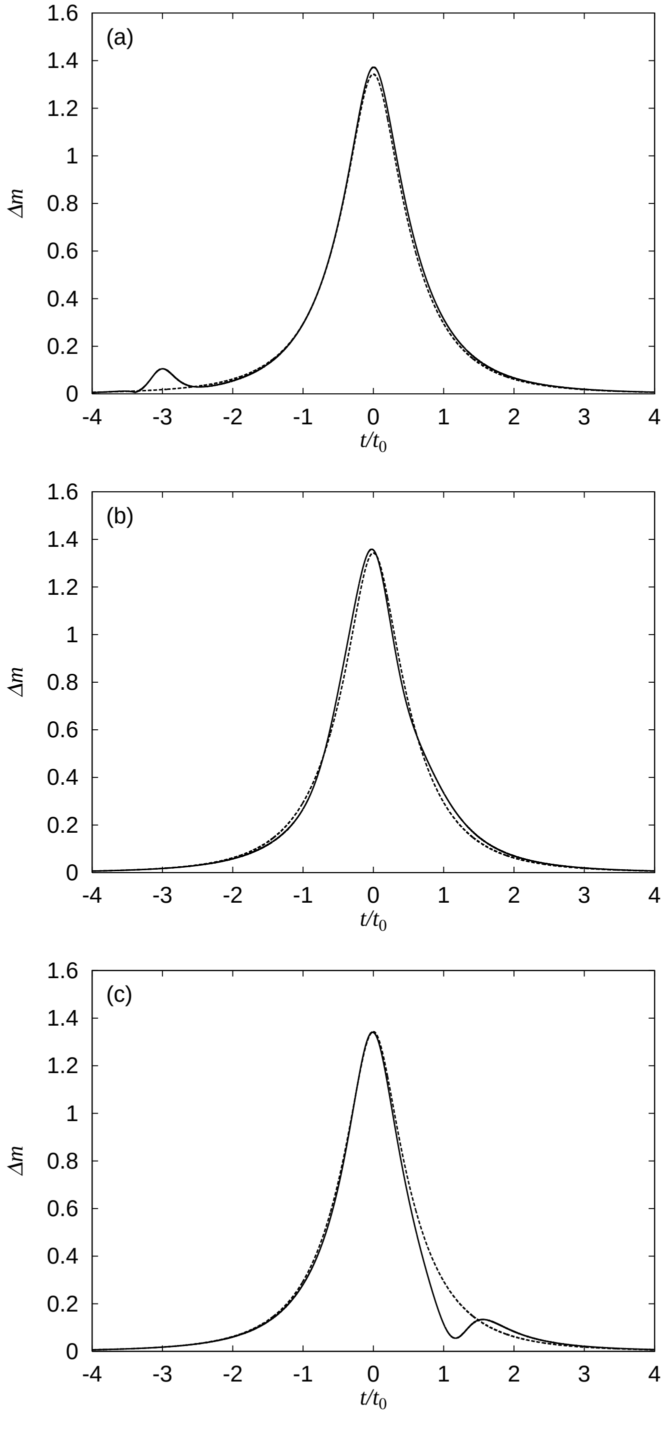

Fig. 4. Microlensing-induced light curves with (solid) and without (dashed) correction for the deviation from a single-point-mass lens. The light curves with the correction are plotted for the case of the small parameter value $\mu = 0.05$ and for angular separations of (a) $\tilde{\eta} = 0.3$, (b) $\tilde{\eta} = 1.0$, and (c) $\tilde{\eta} = 1.7$. The relative motion of the source to the lens is assumed to be described by $\varphi = 0$ and $p = 0.3$.

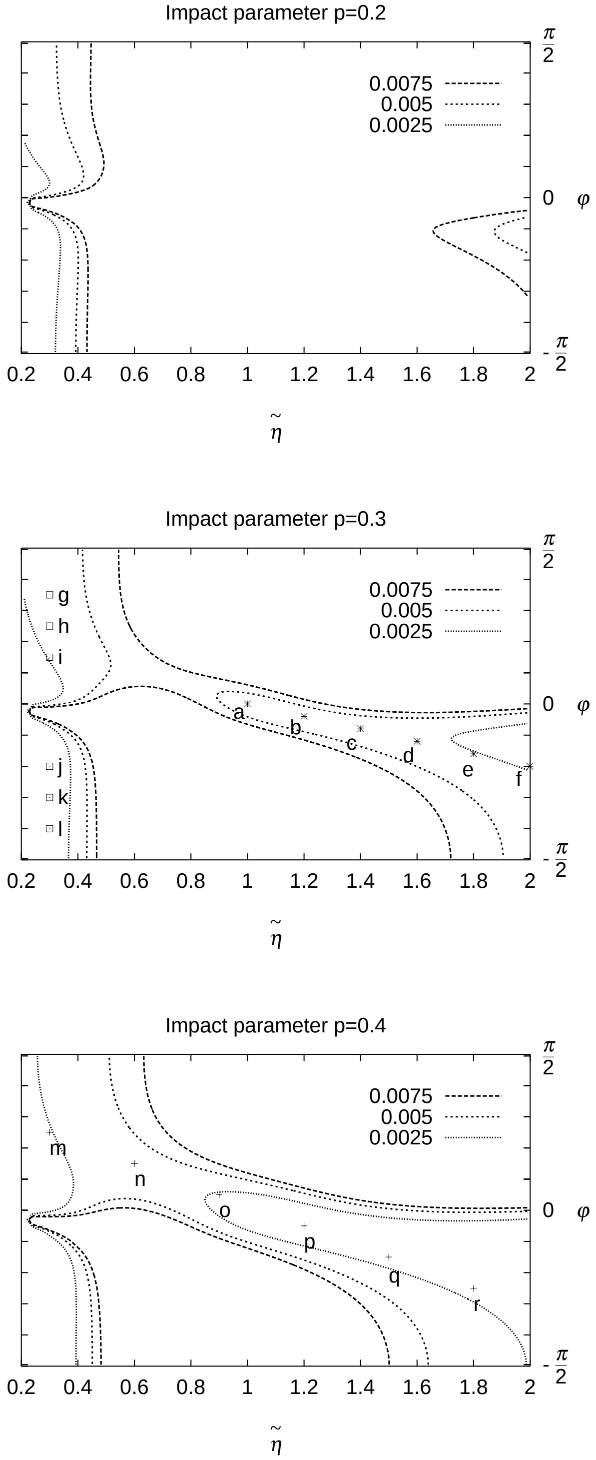

Fig. 5. Contours of δ in $\tilde{\eta}$-φ space for the impact parameters $p = 0.2$, 0.3 and 0.4. The small parameter μ is assumed to be 0.05. The attached labels ‘a’–‘r’ indicate the parameters used in Fig. 10 (see text).

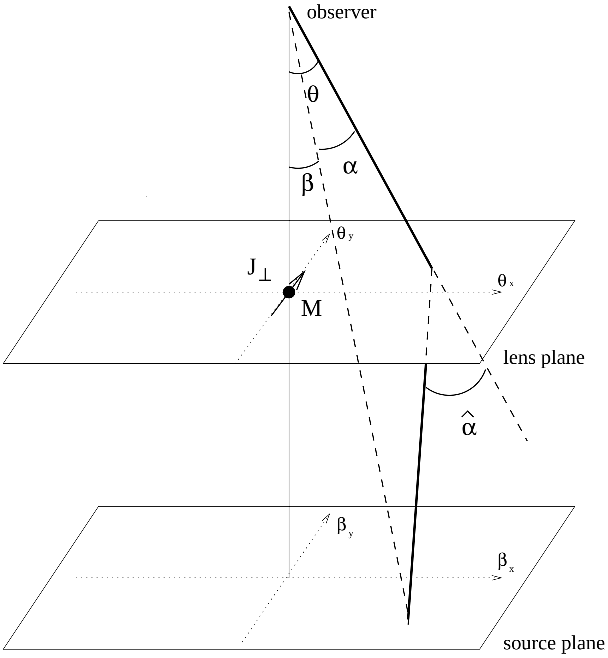

Fig. 6. Geometry of lensing by the rotating object considered in §3.

the projected angular momentum $\boldsymbol{J}_\perp$ (see Fig. 6). The deflection angles $(\hat{\alpha}_x, \hat{\alpha}_y)$ are written as[13)]

$$\hat{\alpha}_x = \frac{4GM}{c^2 D_L}\frac{\theta_x}{\theta_x^2+\theta_y^2} + \frac{4GJ_\perp}{c^3 D_L^2}\frac{\theta_x^2-\theta_y^2}{\left(\theta_x^2+\theta_y^2\right)^2}, \tag{3·1a}$$

$$\hat{\alpha}_y = \frac{4GM}{c^2 D_L}\frac{\theta_y}{\theta_x^2+\theta_y^2} + \frac{4GJ_\perp}{c^3 D_L^2}\frac{2\theta_x\theta_y}{\left(\theta_x^2+\theta_y^2\right)^2}. \tag{3·1b}$$

Hence, we have

$$\alpha_x = \frac{4GM}{c^2}\frac{D_{LS}}{D_L D_S}\frac{\theta_x}{\theta_x^2+\theta_y^2} + \frac{4GJ_\perp}{c^3}\frac{D_{LS}}{D_L^2 D_S}\frac{\theta_x^2-\theta_y^2}{\left(\theta_x^2+\theta_y^2\right)^2}, \tag{3·2a}$$

$$\alpha_y = \frac{4GM}{c^2}\frac{D_{LS}}{D_L D_S}\frac{\theta_y}{\theta_x^2+\theta_y^2} + \frac{4GJ_\perp}{c^3}\frac{D_{LS}}{D_L^2 D_S}\frac{2\theta_x\theta_y}{\left(\theta_x^2+\theta_y^2\right)^2}. \tag{3·2b}$$

Therefore, using the quantities normalized by the Einstein radius, the lens equation becomes

$$\tilde{\beta}_x = \tilde{\theta}_x - \frac{\tilde{\theta}_x}{\tilde{\theta}_x^2+\tilde{\theta}_y^2} - \gamma\frac{\tilde{\theta}_x^2-\tilde{\theta}_y^2}{\left(\tilde{\theta}_x^2+\tilde{\theta}_y^2\right)^2}, \tag{3·3a}$$

$$\tilde{\beta}_y = \tilde{\theta}_y - \frac{\tilde{\theta}_y}{\tilde{\theta}_x^2+\tilde{\theta}_y^2} - \gamma\frac{2\tilde{\theta}_x\tilde{\theta}_y}{\left(\tilde{\theta}_x^2+\tilde{\theta}_y^2\right)^2}, \tag{3·3b}$$

where γ is given by

$$\gamma = \frac{1}{\theta_E} \cdot \frac{J_\perp}{McD_L}. \tag{3·4}$$

It is interesting that this lens equation is the same as that of the two-point-mass lenses for the close binary system, $l \ll r_E$, with the correspondence $\gamma \leftrightarrow \varepsilon$. Hence, the same asymmetric light curves are obtained. Furthermore, it is impossible to distinguish two such corrections. However, the parameter γ is quite small. For example, we consider a Kerr black hole. The angular momentum is $J \sim GM^2/c$, so that we have $\gamma \sim (GMD_S/(c^2 D_L D_{LS}))^{1/2} \ll 1$.

§4. Quantitative estimate

In order to estimate the asymmetry in the light curves quantitatively, we now introduce the notion of 'skewness' from statistics.[14] In statistics, the skewness for any distribution function $f(t)$ is defined as

$$\text{skewness} = \frac{1}{N} \int_{-\infty}^{\infty} \left(\frac{t-\mu}{\sigma} \right)^3 f(t) dt, \tag{4·1}$$

where N is the normalization factor, μ the mean, and σ the standard deviation. However, there is a problem in utilizing the skewness exactly in this form. To see this, we consider a single-point-mass lens. The light curve is then given by

$$\varDelta m = 2.5 \log_{10} \left[\left| \frac{\left(\tilde{\theta}_{x+}^2 + \tilde{\theta}_{y+}^2 \right)^2}{\left(\tilde{\theta}_{x+}^2 + \tilde{\theta}_{y+}^2 \right)^2 - 1} \right| + \left| \frac{\left(\tilde{\theta}_{x-}^2 + \tilde{\theta}_{y-}^2 \right)^2}{\left(\tilde{\theta}_{x-}^2 + \tilde{\theta}_{y-}^2 \right)^2 - 1} \right| \right]. \tag{4·2}$$

If we set $\tilde{\beta}_x = t/t_0$ and $\tilde{\beta}_y = \text{const}$ and consider the case that the time t approaches infinity, then we have

$$\tilde{\theta}_{x+} \to \tilde{\beta}_x = t/t_0 \ (\to \infty), \tag{4·3a}$$

$$\tilde{\theta}_{y+} \to \tilde{\beta}_y = \text{const}, \tag{4·3b}$$

$$\tilde{\theta}_{x-} \to 0, \tag{4·3c}$$

$$\tilde{\theta}_{y-} \to 0. \tag{4·3d}$$

It follows that at large t,

$$\begin{aligned} \varDelta m &\simeq 2.5 \log_{10} \left[\left(1 - \frac{1}{t^4} \right)^{-1} \right] \\ &\simeq \frac{2.5}{\ln 10} \cdot \frac{1}{t^4}. \end{aligned} \tag{4·4}$$

From this, we find that the integral

$$\int_{\mu}^{\infty} t^n \varDelta m(t) dt \tag{4·5}$$

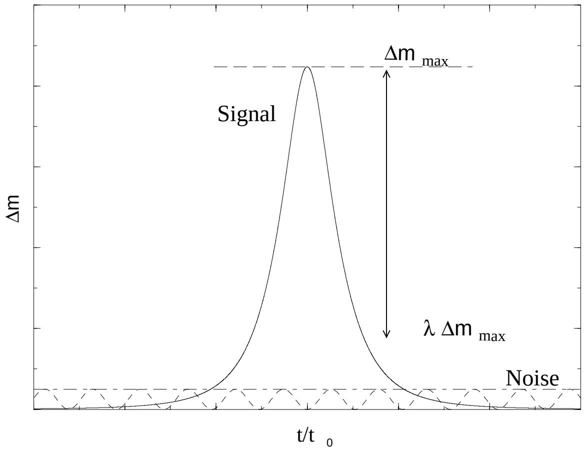

Fig. 7. Illustration of the discussion given in §4. A schematic light curve with noise.

diverges if $n \geq 3$. Therefore, we cannot use Eq. (4·1) itself. Nevertheless, since actually observed light curves necessarily include noise, it seems that the integral to infinity is meaningless. With this consideration, we define the skewness for the restricted region of a light curve $\Delta m > \lambda \Delta m_{\rm max}$, where $\Delta m_{\rm max}$ is the maximum value. Here we have introduced the cutoff λ $(0 < \lambda < 1)$, and the usual skewness corresponds to $\lambda = 0$. The cutoff will naturally appear in the actual data, e.g., the region $\Delta m < \lambda \Delta m_{\rm max}$ may be meaningless due to the noise level (see Fig. 7). In microlensing-induced light curves, the bottom level is constant, but the maximum value may have some uncertainty as $(1 \pm \lambda)\Delta m_{\rm max}$.

We apply this tool to the case of almost identical light curves, which are caused from quite different physical situations, that is, a close binary and a planetary system. The skewness of these light curves is respectively displayed as functions of $1/\lambda$ in Figs. 8–11. Figures 8 and 9 display the dependence of the skewness of the close binary light curves on the angle φ and the impact parameter p, respectively. The light curve given in Fig. 2 corresponds to the curves in Figs. 8 and 9. On the other hand, Figs. 10 and 11 display the skewness of the light curves in the planetary system. In the case of the planetary system, the almost time-symmetric light curves are derived only under certain configurations, as indicated in §2.2. Figure 10 displays the skewness of the light curves under such configurations. The curves labeled by ‘a’–‘r’ correspond to the points labeled by ‘a’–‘r’, respectively, in Fig. 5. Figure 11 displays the impact parameter dependence of the curves corresponding to the point ‘a’. The light curve given in Fig. 4(b) corresponds to the curve ‘a’ in Fig. 10 and a curve in Fig. 11.

As is expected, we have zero skewness when $\varphi = \pm\frac{\pi}{2}$ in Fig. 8. However, when φ is different from $\pm\frac{\pi}{2}$, we have comparable values of the skewness. This demonstrates the useful aspect of the method using the skewness. Nevertheless, the skewness becomes smaller as the impact parameter increases, as seen in Figs. 9 and 11. Thus, the usefulness of the method using the skewness depends mainly on the impact parameter. The skewness with respect to different values of λ fully shows the asymmetric features of the light curves. The absolute values of the skewness

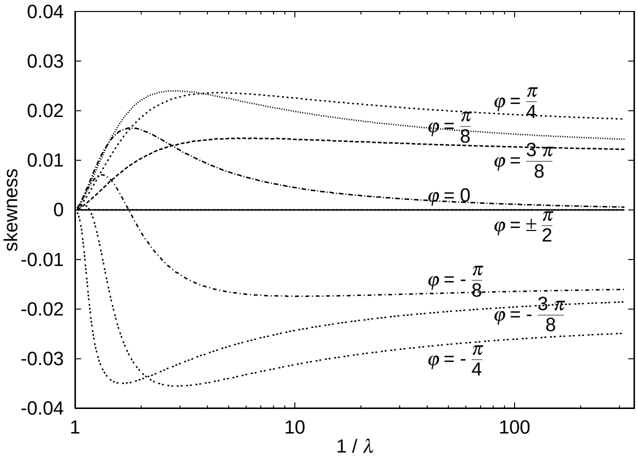

Fig. 8. Dependence of the skewness on the angle φ in the close binary case. The trajectories have the same impact parameter, $p = 0.3$, and the light curves are calculated for the small parameter value $\varepsilon = 0.1$.

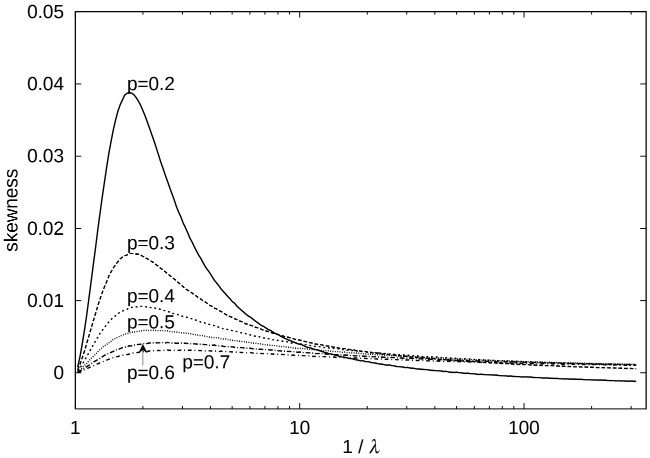

Fig. 9. Dependence of the skewness on the impact parameter p in the close binary case. The trajectories have the same angle, $\varphi = 0$, and the light curves are calculated for the small parameter value $\varepsilon = 0.1$.

depend on the the small parameters ε and μ (i.e., the binary separation and the mass ratio). Furthermore, it should be noted that the absolute values of the skewness have a maximum at $1/\lambda \sim 2$–4 and decrease monotonously in the close binary case, while in the planetary case the skewness indicates different behavior, peaks at larger values of $1/\lambda$, and so on. Therefore, we may discriminate the underlying cases for the asymmetry by the λ-dependent skewness for a good signal-to-noise ratio beyond ~ 10.

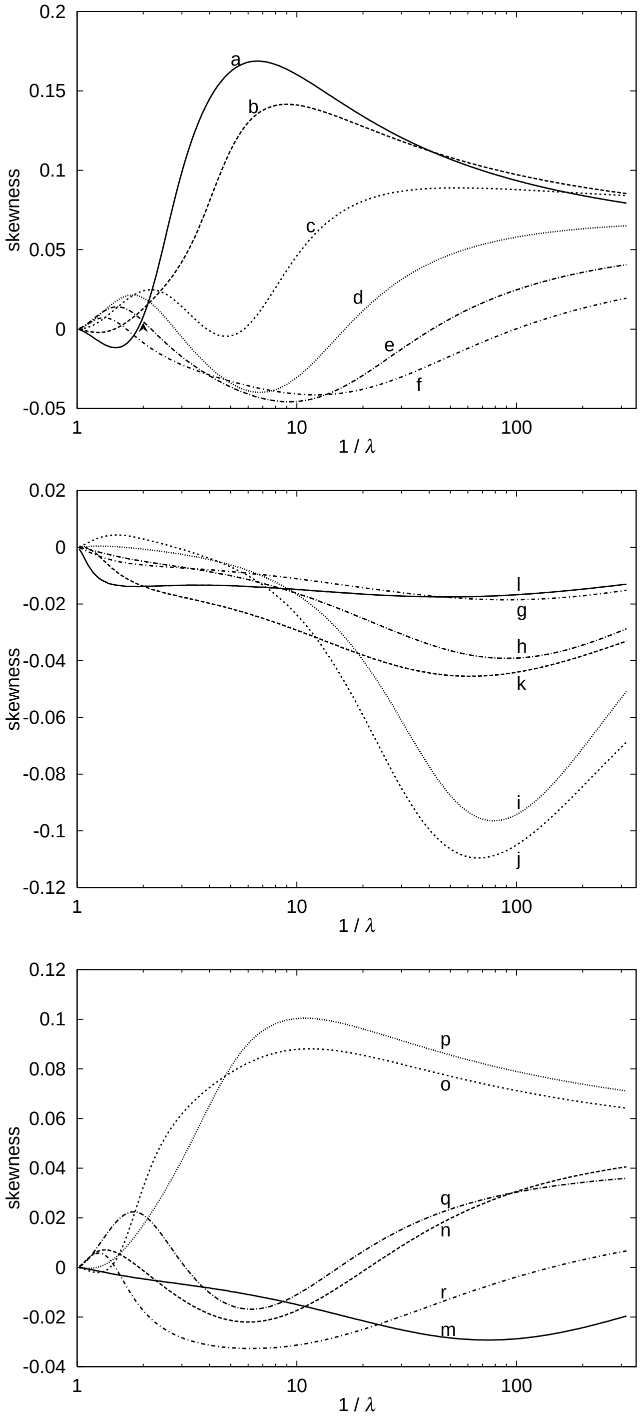

Fig. 10. The skewness of light curves in the planetary system. The curves labeled ‘a’–‘r’ correspond to the points labeled ‘a’–‘r’, respectively, in Fig. 5. The light curves are calculated for the small parameter value $\mu = 0.05$.

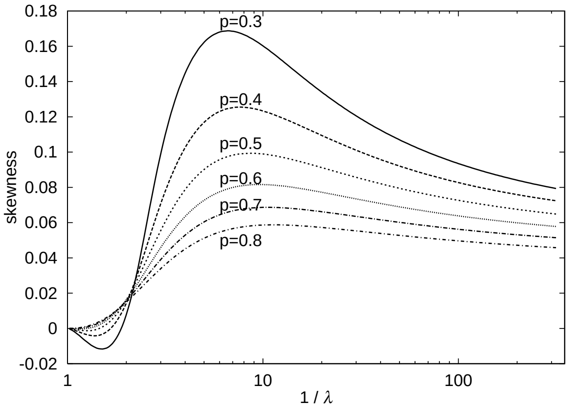

Fig. 11. Dependence of the skewness on the impact parameter p in the planetary case. The light curves correspond to the point ‘a’ in Fig. 5, and are calculated for the small parameter value $\mu = 0.05$.

§5. Summary and discussion

We have studied distortion in microlensing-induced light curves which are considered to be curves of single-point-mass lenses at a first glance. In particular, we have attributed factors inducing the distortion to lenses themselves and considered two sorts of corrections: corrections due to deviation from the Newtonian gravitational potential $\phi = -GM/r$ and corrections due to general relativistic effects of dragging of inertial frames arising from a rotating object. For simplicity, we have discussed two extreme cases in two-point-mass lenses for the corrections of the potential; one is the close binary case in which $l \ll r_E$, and the other is the planetary system case in which $M_1 \ll M_2$. Moreover, we have considered corrections up to the post-Newtonian order for the effect of dragging of inertial frames. From this, we found the same time-asymmetric light curves as in the two-point-mass lenses where $l \ll r_E$. Furthermore, we have introduced the cutoff dependent skewness and estimated the asymmetry in the light curves quantitatively. In particular, we showed the clear difference in the skewness for almost similar light curves.

Here we make a comment on the additional factor for the asymmetry in the binary system. In this paper, we have assumed that the lens systems of the two-point masses are fixed, but each star constituting the binary revolves around the center of mass. Therefore, the rotational effect may also appear. However, if the rotation period $T \sim (l^3/(G(M_1 + M_2)))^{1/2}$ of the binary is much larger than the typical time scale t_0 of a microlensing event, our consideration of the fixed lens systems would be appropriate. For the extreme case $T \ll t_0$, the time-averaged gravitational potential which is projected on to the lens plane may be regarded approximately as that of a single-point-mass lens or a fixed two-point-mass lens with $l \ll r_E$ if the lens is compact. Therefore, more complicated variations of light curves, corresponding to the phase, are expected only if $T \sim t_0$.

It is very interesting whether the time-asymmetric features of light curves discussed in this paper will actually be detected by the projects (MOA, etc.) that are now in progress.

Acknowledgements

This work was supported in part by a Grant-in-Aid for Scientific Research Fund of the Ministry of Education, Science, Sports and Culture of Japan (08640378).

References

1) See, e.g., B. Paczyńsky, Ann. Rev. Astr. Ap. **34** (1996), 419; R. Narayan and M. Bartelmann, astro-ph/9606001.
2) K. Chang and S. Refsdal, Nature **282** (1979), 561.
3) J. R. Gott, Astrophys. J. **243** (1981), 140.
4) A. Gould, Astrophys. J. **392** (1992), 442.
5) C. Alcock, et al., Astrophys. J. **454** (1995), L125.
6) B. S. Gaudi and A. Gould, Astrophys. J. **482** (1997), 83.
7) S. Mao and B. Paczyński, Astrophys. J. **374** (1991), L37.
8) A. Gould and A. Loeb, Astrophys. J. **396** (1992), 104.
9) A. D. Bolatto and E. E. Falco, Astrophys. J. **436** (1994), 112.
10) D. P. Bennett and S. H. Rhie, Astrophys. J. **472** (1996), 660.
11) B. S. Gaudi and A. Gould, Astrophys. J. **486** (1997), 85.
12) P. Schneider and A. Weiss, Astron. Astrophys. **164** (1986), 237.
13) S. O. Sari, Astrophys. J. **462** (1996), 110.
14) See, e.g., W. H. Press et al., *Numerical Recipes in Fortran* (Cambridge University Press, 1992).